Molecular Simulation of DNA Nucleotide-Carbon Nanotube Hybrids

by

Morteza Chehel Amirani

A thesis submitted in partial fulfillment of the requirements for the degree of

Doctor of Philosophy

Department of Mechanical Engineering

University of Alberta

Abstract

Hybrids formed by biological entities and human-made nano-structures have been intensively studied in recent years due to their very interesting properties and applications. DNA-carbon nanotube (CNT) hybrid is one such material and the motivation of this PhD study. The interaction of DNA building blocks (nucleobases and nucleotides) with CNTs was investigated in this study using atomistic classical and quantum mechanical simulations. Depending on the size and complexity of the problem, a pure quantum mechanics (QM), a mixed quantum mechanics and molecular mechanics (QM:MM), or a classical molecular dynamics (MD) approach was employed. The interaction of DNA nucleobases with a CNT in vacuum was studied using QM with density functional theory (DFT). It was shown that the potential energy surface for DNA nucleobase-CNT system is relatively shallow and many local minima corresponding to different configurations can be found. A QM:MM model was developed in order to study the binding of DNA nucleotides with CNTs in aqueous solution. The optimized structure, binding energy, electrostatic potential, and charge transfer for the hybrids were evaluated. Our results indicated properties of DNA nucleotide-CNT hybrids strongly depend on the type of nucleotide and CNT. Finally, a classical MD simulation was performed in order to take dynamics into account. Our results showed that DNA

nucleotides undergo considerable shift along the CNT axis, at a nearly constant separation distance from the CNT surface. Occasional detachment and reattachment of the nucleotides from the CNT were also observed for some systems. Comparing two ways of assigning the partial atomic charges (PAC): (1) PAC obtained from a quantum mechanical calculation for the same optimized DNA nucleotide-CNT hybrid, and (2) PAC obtained based on isolated molecules, the former gave rise to more stable hybrid with less occurrence of detachment and more tightly bound ions. This series of simulations, at different scales, not only allowed us to study the properties of the hybrids, but also provided useful information on how future simulations can be improved to enhance accuracy.

Preface

This dissertation is an original work by Morteza Chehel Amirani. It includes seven chapters to study the interactions of DNA nucleobases and nucleotides with carbon nanotube (CNT). The dissertation was written in the mixed format specified by the Faculty of Graduate Studies and Research at the University of Alberta: Chapters 2 to 5 have been separately published before and Chapter 6 will be submitted for publication soon.

Chapter 1 introduces the physical problem and outlines the structure of the dissertation. Chapter 2 is a comprehensive literature review which was published as "Binding of nucleobases with graphene and carbon nanotube: a review of computational studies" by Morteza Chehel Amirani and Tian Tang in Journal of Biomolecular Structure and Dynamics, 2015, Vol. 33, No. 7, 1567–1597. This review article took nearly two years to finish with many rounds of revisions suggested by Dr. Tang and journal referees. Chapter 3, concerning the binding of DNA nucleobases to CNT in vacuum, was published as "Quantum mechanical treatment of binding energy between DNA nucleobases and carbon nanotube: A DFT analysis" by Morteza Chehel Amirani, Tian Tang, and Javier Cuervo in Physica E, 2013, 54, 65–71. I designed and preformed the simulations, and prepared the manuscript. Dr. Tang was the supervisory author who checked the

results and revised the manuscript. Javier Cuervo assisted me in the interpretation of results and contributed to manuscript edits. Chapter 4, QM:MM simulations on nucleotide-CNT binding, was published as "A QM:MM model for the interaction of DNA nucleotides with carbon nanotubes" by Morteza Chehel Amirani and Tian Tang in Phys. Chem. Chem. Phys., 2015, 17, 7564-7575. I designed and preformed the simulations, and prepared the manuscript. Dr. Tang was the supervisory author who contributed ideas in the investigated problems and data analysis, and revised the manuscript. Chapter 5, evaluating electrostatic potential and charge transfer of the DNA nucleotide-CNT hybrids, was published as “Electrostatics of DNA Nucleotides-Carbon Nanotube Hybrids Evaluated From QM:MM Simulations” by Morteza Chehel Amirani and Tian Tang in Nanoscale, 2015,7, 19586-19595. I carried out the numerical simulations and data analysis, and prepared the manuscript. Dr. Tang was the supervisory author who helped with result interpretation and manuscript revision. Chapter 6, a molecular dynamics study of DNA nucleotide-CNT hybrids, will be submitted for publication. Each chapter has its own bibliography and the reference numbers in each chapter correspond to the list at the end of the corresponding chapter. A complete bibliography containing all references is also given at the end of the dissertation.

Acknowledgements

I would like to express my sincere acknowledgement to my adviser Dr. Tian Tang for her incredible supervision and support during my PhD study. Her constructive comments were absolutely helpful in both guiding my research and writing papers. I learned a lot from Dr. Tang and hope to inherit some of her research characteristics in my future academic life.

Next, I would like to thank Dr. Peter Schiavone whose personality and encouragements were always inspiring. Many thanks to my colleagues including Oxana Malysheva, Tamran Lengyel, Cuiying Jian, Javier Cuervo, Mohammad Koleini, and Professor Gino DiLabio for their helpful comments and discussions.

Thanks to my friends who supported me in many occasions before and during my PhD. I will never forget the help and encouragements from Abdolazim Fadaee, Reza Torabi, Meisam Shakoury, Mohsen Sedeghi, Mehdi Zahed, Eno Damo, Nadine damo, and my beloved teacher Haj Mansour Bagherbeyk.

I would also like to deeply thank my family and in particular my parents whose love and efforts will never be forgotten. I also greatly thank my wife, Fatemeh, who was really patient and supportive while we were far from each other for nearly two years during my PhD. Without her patience, I would have never finished my PhD.

In the end, I must thank all staff in the mechanical engineering department at U of A for the financial and academic supports.

Contents

List of Tables

List of Figures

Abbreviations

A Adenine

AFM Atomic force microscopy

BE Binding energy

BSSE Basis set superposition error

C Cytosine

CCSD(T) Coupled cluster single double (Triple)

CI Configuration interaction

CNT Carbon nanotube

CPCM Conductor polarized continuum model

DCP Dispersion-correcting potential

DFT Density functional theory

DNA Deoxyribonucleic acid

ESP Electrostatic potential

FF Force field

G Guanine

GGA Generalized gradient approximation

HF Hartree-Fock

IC Initial configuration

ITC Isothermal titration calorimetry

LDA Local density approximation

MD Molecular dynamics

MM Molecular mechanics

MWCNT multi-walled CNT

NMP Nucleotide monophosphate

OCS Original charges scheme

ONIOM Our own n-layered integrated molecular orbital and molecular mechanics

PAC Partial atomic charges

PBC Periodic boundary condition

PES Potential energy surface

PW Plane wave

QM Quantum mechanics

RCS Redistributed charges scheme

RESP Restrained electrostatic potential

SCF Self-consistent field

SCS Spin-component scaled

ssDNA Single stranded DNA

SWCNT Single-walled CNT

STM Scanning tunneling microscopy

T Thymine

TDS Thermal desorption spectroscopy

U Uracil

UHV Ultrahigh vacuum

vdW van der Waals

Chapter 1

Introduction

This dissertation is motivated by experiments where single stranded DNA (ssDNA) was found to wrap around single-walled carbon nanotube (CNT) in an electrolyte solution and generate a hybrid structure [1]. The DNA-CNT hybrid has been shown to facilitate the dispersion of CNTs and separation of different CNTs according to their chiralities [1–3]. In addition, many other applications of DNA-CNT hybrids including cancer detection, bio-sensors, and drug delivery have also been introduced [4–7]. In order to better understand the experimental observations and interesting properties of the hybrids, analytical and atomistic models have been proposed to study the interaction between DNA and CNT. At the analytical level, continuum models have been used for ssDNA and CNT to study the hybridization, but they are highly approximate. Atomistic models at classical (e.g., molecular dynamics (MD)) and quantum mechanical (QM) levels have been also introduced to more accurately study the hybrids compared with analytical models. MD provides a fully atomistic description of the system and is more accurate than analytical models, but the current force fields do not properly

take into account the CNT's electronic response. Models based on QM overcome this difficulty, but they are computationally expensive and not feasible for large systems. In this project, atomistic approaches using classical, quantum mechanical, and a mixed quantum and classical method are employed. The objectives of this study are as follows:

- Developing molecular models for the hybrids formed by CNT and DNA building blocks, mainly nucleotides;
- Studying the structure, strength of binding, electrostatic potential, and charge transfer for the hybrids;
- Studying the effect of CNT chirality as well as the nucleobase type in the above properties.

In Chapter 2, a comprehensive review is performed in order to review past studies on the interaction of nucleobases or nucleotides with CNT and graphene. First, experimental works are briefly introduced. Theoretical studies are then comprehensively reviewed and categorized according to the employed approach. A critical review for each work is provided and discussion on the reported results is presented.

In Chapter 3, the interaction of DNA nucleobases with a CNT in vacuum was studied using density functional theory (DFT) as a pure QM approach. From Chapter 2, it was found that the effect of the initial configuration of DNA nucleobase with respect to the CNT is important in the properties of the hybrid and has not been studied in detail. Therefore, a detailed investigation on the effect of the initial configuration is performed in Chapter 3. It is found that different

initial configurations can lead to quite different binding structures with different stability. The most stable structures are then used in the simulations performed in Chapter 4.

In Chapter 4, a new computationally-efficient model is introduced in order to include the electrolyte solution. In this model, a full nucleotide which includes a nucleobase, a sugar ring, and a phosphate group is considered. Furthermore, explicit water molecules and ions are added to the systems to make the model more realistic compared with the past studies. In order to carry out the simulations, a mixed QM:MM approach is introduced. The final structures as well as the strength of binding for DNA nucleotide-CNT hybrids are obtained and analyzed.

Based on the optimized structures obtained in Chapter 4, the electrostatic potential and charge transfer for the DNA nucleotide-CNT hybrids are evaluated and discussed in Chapter 5.

Chapter 6 is a molecular dynamics study of the hybrids obtained in Chapter 4. Specifically, structures optimized from QM:MM simulations are taken and a classical molecular dynamics study is then performed. This allows us to take the dynamics and thermal effects into account.

Chapter 7 includes the concluding remarks and future perspective of this work.

References

[1] M. Zheng, A. Jagota, E. D. Semke, B. A. Diner, R. S. Mclean, S. R. Lustig, R. E. Richardson, and N. G. Tassi, "DNA-assisted dispersion and separation of carbon nanotubes," *Nat Mater*, vol. 2, no. 5, pp. 338–342, 2003.

[2] M. Zheng, A. Jagota, M. S. Strano, A. P. Santos, P. Barone, S. G. Chou, B. A.

Diner, M. S. Dresselhaus, R. S. Mclean, G. B. Onoa, G. G. Samsonidze, E. D. Semke, M. Usrey, and D. J. Walls, "Structure-Based Carbon Nanotube Sorting by Sequence-Dependent DNA Assembly," *Science*, vol. 302, no. 5650, pp. 1545–1548, 2003.

[3] X. Tu, S. Manohar, A. Jagota, and M. Zheng, "DNA sequence motifs for structure-specific recognition and separation of carbon nanotubes," *Nat Mater*, vol. 460, no. 7252, pp. 250–253, 2009.

[4] P. K. Brahman, R. A. Dar, and K. S. Pitre, "DNA-functionalized electrochemical biosensor for detection of vitamin {B1} using electrochemically treated multiwalled carbon nanotube paste electrode by voltammetric methods ," *Sensors and Actuators B: Chemical*, vol. 177, no. 0, pp. 807 – 812, 2013.

[5] S. Wang, R. Wang, P. J. Sellin, and S. Chang, "Carbon nanotube based dna biosensor for rapid detection of anti-cancer drug of cyclophosphamide," *Current Nanoscience*, vol. 5, no. 3, pp. 312–317, 2009.

[6] E. Katz and I. Willner, "Biomolecule-Functionalized Carbon Nanotubes: Applications in Nanobioelectronics," *ChemPhysChem*, vol. 5, no. 8, pp. 1084–1104, 2004.

[7] M. Prato, K. Kostarelos, and A. Bianco, "Functionalized Carbon Nanotubes in Drug Design and Discovery," *Accounts of Chemical Research*, vol. 41, no. 1, pp. 60–68, 2008.

Chapter 2

Literature review[1]

2.1 Introduction

Carbon nanotube (CNT) is among the most interesting nano-materials developed to date and has attracted growing attention since its discovery [1]. It has been extensively studied, used and commercialized during the past two decades, and many unique properties and capabilities have been observed [2–6]. The structure of a CNT can be described by imagining the process of rolling up graphene layers. First, a vector named chiral vector is defined between two carbon atoms (A and B in 2.1(a)) on a graphene. When the graphene is rolled up so that points A and B superimpose each other, a single-walled CNT (SWCNT) is formed. A multi-walled CNT (MWCNT) can be constructed in a similar manner, using more than one graphene layer. The chiral vector, $\mathbf{C}_h$, from point A to point B, can be described by two integer numbers (m, n) called chirality so that $\mathbf{C}_h$ can be

[1] A modified version of an originally published paper in Journal of Biomolecular Structure and Dynamics, Volume 33, Issue 7, Pages 1567-1597, 2015, Morteza Chehel Amirani & Tian Tang, "Binding of nucleobases with graphene and carbon nanotube: a review of computational studies", reprinted with permission.

expressed in terms of the two vectors $\mathbf{a}_1$ and $\mathbf{a}_2$ as $\mathbf{C}_h = m\mathbf{a}_1 + n\mathbf{a}_2$. 2.1(b)-(d) show the structure of three SWCNTs with similar diameter but different chiralities. The chirality determines not only the size of the CNT, but also the alignment of atoms on the CNT. Chirality is a very important structural parameter for CNT, and along with its length and number of walls, determines many of CNT's properties [7]. Mechanical properties such as Young's modulus and Poisson's ratio, thermal properties such as thermal conductivity were shown to depend on CNT's diameter and number of walls [8–14]. Electronic properties were found to have a strong relation to chirality. For example, for a SWCNT, it was shown that if $m - n$ is a multiple of 3, the CNT demonstrates metallic behaviors, otherwise the CNT is a semiconducting material with its band gap depending on the chirality [7].

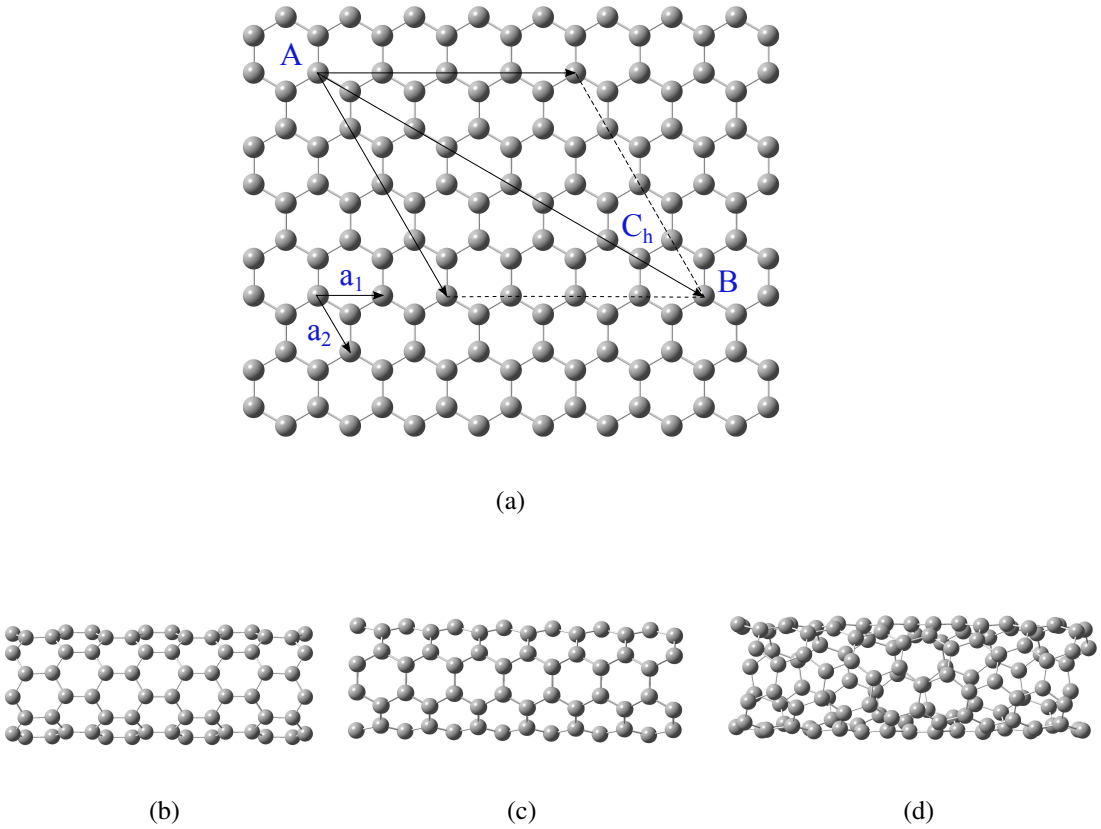

(a)

(b) (c) (d)

Figure 2.1: Molecular structures of (a) graphene and (b)-(d) three CNTs with similar diameter but different chiralities: (b) (7,0), (c) (4,4) and (d) (5,3).

In addition to the intriguing properties of CNTs themselves, their functionalization has been extensively investigated in recent years [15–58]. Both organic and inorganic molecules have been employed to functionalize CNTs through covalent [15–19] and non-covalent interactions [20, 21]. These functionalizations have facilitated development in many different areas such as CNT purification and separation, fabrication of polymer composites, biosensing, drug delivery, etc. For example, chemically modified CNTs have been introduced to control characteristics of neurite outgrowth [15]. CNTs functionalized with carboxyl groups have been used as atomic force microscopy (AFM) tips to provide chemical and

biological discrimination [16].

A special class of molecules widely used for CNT functionalization is DNA [17, 21, 22, 42–52, 59]. Hybrid materials formed by DNA and CNT have shown outstanding potential in drug delivery [53] and biosensing areas [54–57]. For example, DNA can be encapsulated inside CNTs [24], which can be potentially used as a gene delivery vehicle [53]. DNA-SWCNT electrodes have been made by wrapping single-stranded DNA (ssDNA) around CNTs, which offered electrochemical detection of certain biological molecules with high sensitivity [54]. ssDNA molecules have also been used to disperse bundled CNTs in water and to separate them according to their different electronic structures [21, 58]. Although DNA polymers were used in these applications, the interesting properties of the DNA-CNT hybrids, which often depend on the chirality of the CNT as well as the sequence of the DNA, have motivated many studies on the interaction between CNT and nucleobase, nucleoside or nucleotide, the building blocks of DNA polymers (See Figure 2.2 for structure of nucleobases). In those studies, graphene was frequently used as a reference system, which is a CNT with zero curvature.

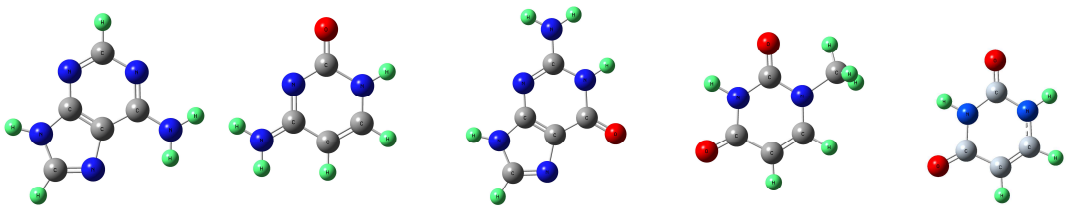

(a) (b) (c) (d) (e)

Figure 2.2: Molecular structures of nucleobases: (a) Adenine (A), (b) Cytosine (C), (c) Guanine (G), (d) Thymine (T), (e) Uracil (U).

Experimentally, adsorption of nucleobases onto graphite has been investigated.

Structural and energetic aspects of the adsorption have been addressed by different groups [60–76]. On the theoretical front, many modeling and simulation studies have been performed on CNT or graphene binding with nucleobases, with different degrees of complexity and accuracy. The calculations in these studies were mainly conducted using quantum mechanical (QM) level methods (e.g., Hartree-Fock (HF), Density Functional Thoery (DFT), etc), with a few recent works adopting hybrid methods that combine QM and molecular mechanics (MM) computations. Despite the different systems studied and different methods used, the main focuses of the past work have been on the nature of the interaction (physisorption or chemisorptions), structure of the hybridization (alignment of nucleobases relative to the CNT or graphene) and strength of the interaction (binding energy (BE)). Most of the studies have attempted to address how the binding is affected by system parameters such as the type of nucleobase and the chirality of the CNT. However, a quick examination of the results obtained in the past reveals the clear discrepancies among them, especially for the BE. Different values for the BE as well as the order of the BE associated with different nucleobases have been reported, even for the same nucleobase-CNT system. In an attempt to understand these discrepancies, in this work, we provide a comprehensive review on the binding of CNT or graphene with nucleic acid (NA) building blocks (nucleobase, nucleoside or nucleotide). Major effort is spent on reviewing simulation work performed in this area, while some experimental data are given at the beginning so that comparison can be made with the simulation results. By reviewing not only the simulation results but also the simulation methods, we identify and discuss several factors that can contribute to the discrepancies existing in literature.

The rest of the chapter is organized as follows. A brief review on experimental

measurements of nucleobase-graphite interaction is presented in Section 2.2. In Section 2.3, computational studies on the binding of CNT or graphene with nucleic acid building blocks are reviewed in detail. Discussion and conclusions are given in Sections 2.4 and 2.5.

2.2 Experimental studies

Several experimental studies have been carried out to characterize the binding between nucelobases and graphite [60–73, 76]. Allen et al. [60] for the first time, performed scanning tunneling microscopy (STM) experiments and showed that aqueous-phase A and T strongly bound to a heated graphite surface and formed ordered surface layers. Heckl et al. [61] used the same STM technique and observed the formation of a two-dimensional ordered structure on graphite after thermal evaporation of an aqueous solution containing G. Formation of purine and pyrimidine monolayers on graphite was subsequently reported in several STM experiments performed in Heckl's group [63, 67, 69–73]. Uchihashi and Okada [74] provided evidence on the deposition of A monolayer on graphite in an ultrahigh vacuum (UHV) using non-contact AFM. Srinivasan et al., using STM, reported the adsorption of G [64] and A [65, 66] on graphite in NaCl solution. In addition [66], condensed A layer was formed in both NaCl and NaI solutions and its structure depended on the applied electric potential. Tao and Shi [62] studied the spontaneous adsorption of G and A monolayers on graphite in NaCl solution. Using both AFM and STM, they confirmed that both G and A formed ordered lattice on the graphite surface.

Although most of the experimental studies focused on addressing the structure

nucleobases form on the graphite, a few works explored quantitative evaluation of the BE between nucleobases and graphite. The BE for A on graphene in vacuum was determined by Freund [77] to be 97.45 kJ/mol using thermal desorption spectroscopy (TDS). Sowerby et al. [73] studied the adsorption of nucleobases on graphite in water and for the first time reported the order of the BE for different nucleobases. Based on adsorption isotherms, the order of the BE was found to be G>A>T>C>U. In a separate study, Varghese et al. [76] used isothermal titration calorimetry (ITC) to study the adsorption of nucleobases and nucleosides with two different samples of graphene in water. Interestingly, they observed different sequence for the BE of the two samples: A>C>T in one case and A>T>C in the other case. On the other hand, a single trend (A>C>T) was found for the BE between nucleosides and both samples. To our knowledge, the only experimental work that evaluated the BE between nucleobases and CNT was done by Das et al. [75] in which ITC was used to determined the BE between nucleobases and a SWCNT in water. The order of the BE was shown to be T>A>C.

2.3 Computational studies

Theoretical studies on the interaction between DNA and CNT have been performed at different levels including QM approaches [78–102], all-atom molecular dynamics (MD) simulations [103–115], coarse-grained MD simulations [116], statistical mechanics simulations [117]and continuum level modeling [118–121], with decreasing computational cost and accuracy. Different methods have different focus and apply different treatment for the molecules. Continuum models typically consider long strand of DNA interacting with CNT and focus on address-

ing the electric field generated by the DNA-CNT hybrid [118]. Usually the DNA is modeled as a charged line or cylinder, the CNT as a bulk metallic or dielectric medium, and the solution is described by the Poisson-Boltzmann equation [122]. While providing some first insights into how the CNT's electronic response may affect the electric field of the hybrid, the description of the electronic response is highly approximate. In addition, other interactions between the DNA and CNT, leading to the binding of the two, are often neglected. MD simulations utilize force field (FF) parameters to describe the interactions between CNT and DNA atoms. These simulations can also handle molecules with moderate length, and were used to study the binding structure, energy and stability of the hybrid. A main drawback in these MD simulations is that the carbon atoms on the CNT are usually modeled as particles that interact with other atoms only via van der Waals (vdW) interactions (e.g., Lennard-Jones potential). While the ongoing development of polarizable FF may improve the accuracy of the simulations, proper description of the CNT's electronic response has been missing from past MD simulations. Aiming at solving for the electron distribution, QM approaches are the most accurate in capturing the electrostatic interactions in the hybrid. However, the great amount of computation required has limited the QM simulations to CNT binding with a short piece of DNA, nucleobase, nucleoside or nucleotide. The solution environment is typically not included. The focuses of these studies have been the binding structure and BE. More recently, there have also been approaches that tried to combine methods at different levels (hybrid method) in order to achieve a balance between accuracy and efficiency.

In the following, a review is conducted for the computational studies. Since the focus of the review is on the interaction of CNT or graphene with nucleobases,

most studies on this topic were performed using QM approaches. These are reviewed in Section 2.3.1. There are also some studies in which MM or semi-empirical QM approach was used. These are reviewed in Section 2.3.2.

Table 1 summarizes the studies reviewed in this work, which are grouped into 3 categories: (1) first-principles studies based on methods lacking dispersion correction, (2) first-principles studies based on dispersion-corrected methods and (3) studies based on semi-empirical and FF methods. For each study, the system simulated, method used and computational details are given. The BE between the CNT or graphene with the DNA fragment, which is an indicator of stability of the formed hybrid, is used to compare these works. Unless otherwise specified, CNTs referred to in this review are SWCNTs, and the unit of BE is kJ/mol. Detailed description of these works and comparison among them are given below.

Table 2.1: Summary of previous computational studies on the binding between nucleobases and CNT or graphene. (Explanation on notation: for example LDA/PW means simulation was performed using LDA approach with plane wave (PW) basis set; MP2//PW91LYP means geometry optimization was performed using PW91LYP and BE calculation was performed using MP2)

Reference	**System**	**Method**	**Calculation details**	**Results on BE**
First-principles studies based on methods lacking dispersion correction				
Gowtham et al. [78]	A, C, G, T and U (attached to a methyl group)-Graphene	LDA/PW and MP2/6-311++G(d,p)	LDA geometry optimization; MP2 BE calculation	LDA: G>A=T=C>U MP2: G>A>T>C>U
Gowtham et al. [79]	A, C, G, T and U (attached to a methyl group)-(5,0)CNT	LDA/PW	LDA geometry optimization; BE calculation	G>A>T>C>U
Meng et al. [80]	A, C, G and T-(10,0)CNT	LDA/PW	MM and LDA geometry optimization; LDA BE calculation	T>G>C>A
Meng et al. [81]	A, C, G and T-(10,0)CNT	Time dependent LDA and FF (CHARMM)	Optical absorbance spectrum from LDA; FF PES scan and BE calculation	G>A>T>C

Continued on next page

Reference	System	Method	Calculation details	Results on BE
Shtogun et al. [82]	A-(6,6) CNT T-(8,0) CNT A-Radical-(6,6) CNT T-Radical-(8,0) CNT	LDA/PW	LDA geometry optimization and BE calculation	A-(6,6)CNT: 34.16 T-(8,0) CNT: 30.49 A-Radical-(6,6) CNT: 49.88 T-Radical-(8,0) CNT: 63.78
Wang and Ceulemans [83]	A (2 adenosine monophosphates)-zigzag and armchair CNTs	LDA/LCAO	LDA geometry optimization and BE calculation	[144.73-366.64]
Wang and Bu [84]	C-zigzag and armchair CNT fragments	PW91LYP/6-311++G(d,p), MPWB1K/cc-pVDZ and MP2/6-311G(d,p)	DFT (PW91LYP and MPWB1K) and MP2 geometry optimization; MP2 BE calculation	MP2//PW91LYP: 27.97 MP2//MPWB1K: 32.78 MP2//MP2: 39.61

Continued on next page

Reference	System	Method	Calculation details	Results on BE
Wang [85]	A, C, G and T-(5,5) and (10,0) CNTs; both gas and aqueous phases	MPWB1K/cc-pVDZ and MP2/6-311++G(d,p)	MPWB1K geometry optimization; MP2 BE calculation	gas phase: G>A>T>C for both CNTs aqueous solution: A>G>T>C for (10,0) CNT and G>A>T>C for (5,5) CNT
First principles studies based on dispersion-corrected methods				
Ortmann et al. [86]	A-Graphene	LDA, PW91, PW91+vdW each with PW basis set	DFT PES scan and BE calculation	LDA: 44.38 PW91: 6.75 PW91+vdW: 105.17
Berland et al. [87]	A-Graphene	vdW-DFT/PW	vdW-DFT PES scan and BE calculation	68.6
Panigrahi et al. [88]	A, C, G, T and U-Graphene	wB97XD/6-31G(d,p)	wB97XD geometry optimization and BE calculation	G>A>C>T>U

Continued on next page

Reference	System	Method	Calculation details	Results on BE
Chandra Shekar and Swathi [89]	A, C, G, T and U-Graphene	wB97XD with 6-31G(d,p) and 6-311+G(d,p) basis sets	wB97XD/6-31G(d,p) geometry optimization; wB97XD/6-311+G(d,p) BE calculation	G>T>A>C>U
Antony and Grimme [90]	A, C, G, T and U-Graphene	B97-D/TZV(d,p)	B97-D geometry optimization and BE calculation	G>A>T>C
Lee et al. [91]	A, C, G and T (attached to a methyl group)-Graphene	LDA, PBE, PBE+vdW each with tier2 basis set	DFT geometry optimization and BE calculation	LDA: G>C>A>T PW91: G>C>T>A PW91+vdW: G>A>T>C
Le et al. [92]	A, C, G, T and U-Graphene	TS, sTS, vdW-DF, vdW-DF2, DFT-D2 and DFT-D3 each with PW basis set	vdW-DF geometry optimization; BE calculation with different methods	G>A>T>C>U

Continued on next page

Reference	System	Method	Calculation details	Results on BE
Cho et al. [93]	A, C, G and T-Graphene	optB86b/PW and PBE+TS/tier2	optB86b and PBE+TS geometry optimization and BE calculation	G>A>T>C
Vovusha et al. [94]	A, C, G, T and U-Graphene	M05-2X and M06-2X with 6-31G(d), 6-31+G(d,p) and 6-311++G(d,p) basis sets	M05-2X/6-31G(d) geometry optimization; M05-2X and M06-2X BE calculation with 6-31+G(d,p) and 6-311++G(d,p) basis sets	M05-2X/6-311++G(d,p): G>C>T>A>U M06-2X/6-311++G(d,p): G>T>C>A>U
Enyashin et al. [95]	A, C, G and T nucleotides-Graphene	Dispersion-corrected DFT tight binding	DFT geometry optimization and BE calculation	G>A>C>T

Continued on next page

Reference	System	Method	Calculation details	Results on BE
Stepanian et al. [96]	C-zigzag CNT	DFT and MP2 each with 6-31++G(d,p), 6-31G(d) and STO-3G basis sets for different atoms	MPWB1K, M05, M05-2X, MPW1B95; MP2 geometry optimization and MP2 BE calculation	MP2//MP2: 50.3 MP2//M05-2X: 49.6 MP2//M05: 45.2 MP2//MPWB1K: 50.3 MP2//MPW1B95: 49.4
Shukla et al. [97]	A, C, G, T and U-(7,0) CNT	M05-2X with 6-31G(d), 6-31G(d,p), 6-31+G(d,p) and cc-PVDZ basis sets	M05-2X/6-31G(d) geometry optimization; M05-2X BE calculation with 6-31G(d,p), 6-31+G(d,p) and cc-PVDZ basis sets	G>C>A>T>U
Chehel Amirani et al. [102]	A, C, G and T-(7,0) CNT	M05-2X/6-31G(d,p)	M05-2X geometry optimization and BE calculation	G>T>A>C

Continued on next page

Reference	System	Method	Calculation details	Results on BE
Akdim et al. [98]	A, C, G, T, U-(6,5), (9,1), (8,3) and (5,0) CNTs	B97-D with 6-31G(d) and Def2-TZVP basis sets and EFP2/6-31G	B97-D/6-31G(d) geometry optimization; BE calculation with B97-D/6-31G(d), B97-D/Def2-TZVP and EFP2/6-31G	(6,5) CNT and (9,1) CNT: G>A>T>C (8,3) CNT: G>A>C>T (5,0) CNT: G>T>C>A
Studies based on semi-empirical and force-field methods				
Edelwirth [123]	A-Graphite	MM (Dreiding II FF)	MM geometry optimization and BE calculation	87.86
Ramraj et al. [99]	A, C, G, T and U-Graphene, (5,0) CNT, (6,6) CNT	PM3-D, and DFT (B97-D, DFT-D, M05-2X, M06-2X) with TZV(2d,2p) basis set	PM3-D geometry optimization; PM3-D and DFT BE calculation	G>A>T>C>U

Continued on next page

Reference	System	Method	Calculation details	Results on BE
Umadevi and Sastry [100]	A, C, G, T and U-(3,3), (4,4) and (5,5) CNT and graphene	DFT (B3LYP-D/6-31G(d)) and ONIOM (M06-2X/6-31G(d):AM1)	ONIOM geometry optimization; B3LYP-D BE calculation	CNT: G>T∼A>C>U Graphene: G>A>T>C>U
Sarmah and Roy [101]	A, C, G, T and U (attached to a methyl group)-(7,5), (7,6), (8,3) and (9,2) CNT	ONIOM (B3LYP/6-31G(d):UFF)	ONIOM geometry optimization and BE calculation	(7,5) CNT: G>A∼T>C>U (7,6) CNT: G>A>T∼C∼U (8,3) CNT: A>T>C>G>U (9,2) CNT: G>T>C>A>U

Continued on next page

Reference	System	Method	Calculation details	Results on BE
Varghese et al. [76]	A, C, G and T-Graphene; both gas and aqueous phases	MM (Amber FF)	MM geometry optimization and BE calculation; implicit solvent	G>A>T>C
Das et al. [75]	A, C, G, T and U-(5,5) CNT; both gas and aqueous phases	HF/6-31G(d,p), MSCFF and AMBER FFs	Geometry optimization and BE calculation using HF and FF ; implicit solvent	Vacuum: G>A>T>C Aqueous: G>T>A>C
Frischknecht and Martin [103]	nucleotide monophospahtes-(6,0) CNT in solution	MD (CHARMM FF)	MD simulation at 298 K with explicit solvent, followed by BE calculation	No salt: A>T>C∼G>U With salt: T>C>U>A>G
Yamazaki and Fenniri [117]	A, C, G, and T-(7,0), (11,0) and (15,0) CNT in solution	3D-RISM	3D-RISM molecular liquid theory and BE calculation	G>A>T>C
Lv [104]	A, C, G, and T-Charged (8,8) CNT in solution	MD (Amber FF)	MD simulation at 300 K and 1 atm with explicit solvent, followed by BE calculation	G>A>T>C

2.3.1 Studies based on First-Principles approaches

Within the QM framework, there are also different methods with different levels of complexity and accuracy, including *ab initio* methods (HF, MP2 and CCSD(T)), DFT and semi-empirical methods. HF, originally named SCF method, is the first *ab initio* method and the basis of post-HF methods. Despite having correct description for the exchange energy, HF does not treat the electron correlation exactly. Post-HF methods including MP2 [124, 125], CI and CCSD(T) have been proposed to properly describe the correlation energy. These *ab initio* methods are usually used for very small atomic systems due to their high computational cost. Semi-empirical QM methods are based on *ab initio* methods but include empirical parameters to speed up the calculations, examples including AM1 [126], PM3 [127–129] and PM6 [130]. Among the QM methods, DFT has been widely used in computational quantum physics and chemistry, due to its relatively low computational cost compared with high level *ab initio* methods and high accuracy compared with semi-empirical methods. In 1964, Hohenberg and Kohn [131] published the first paper on DFT in which they substituted the many electron wavefunction with the electron density and significantly reduced the number of variables. One year later, Kohn and Sham [132] improved Hohenberg and Kohn's theory by introducing effective potential that included external potential, exchange and correlation interactions. A difficult step in the advancement of DFT method is to determine the exchange and correlation functional, since there is not a standard way to specify it. Local density approximation (LDA) approach, based on the uniform electron gas model, was the first scheme to represent the exchange and correlation functional. The functional in LDA depends only on the electron den-

sity itself but not its gradient. The electron density gradient was later included in the exchange and correlation functional, and such an approach was named generalized gradient approximation (GGA) [133]. A number of functionals have been developed since then and many studies have been performed to investigate the performance of those functionals. Readers are encouraged to look at Refs [134] and [135] for more detailed information.

It is worth pointing out that dispersion forces, which are universal and among the most important interactions in molecular systems, were poorly treated in many DFT approaches. Considerable research efforts are still being spent in the computational chemistry community [134–154] on how to accurately include dispersion in the correlation term of DFT. For the system of nucleobase binding to CNT or graphene, there were studies in which dispersion interaction was not taken into account. Specially, some early works used the LDA scheme of DFT, which is well known to lack dispersion correction. More recent studies have adopted either classical FF or dispersion corrected DFTs to incorporate dispersion. Since it is believed that π-π stacking plays a crucial role in the binding of nucleobase to graphene or CNT, dispersion can be important in determining the binding structure and BE. Therefore it is expected that different results may be predicted from different approaches. For this reason, below we separate the past studies into two categories: those performed with methods that do not consider dispersion, and those obtained from dispersion-corrected methods.

2.3.1.1 Studies performed with methods lacking dispersion correction

Gowtham et al. studied the adsorption of nucleobases (A, T, C, G and U) on graphene using LDA and MP2 [78]. Nucleobases in their work were attached to

a methyl group in order to resemble nucleotides. Supercell approach with plane wave basis set was used in the LDA calculations, while in the MP2 calculations, 6-311++G(d,p) basis set was used with the graphene modeled by a finite sheet containing 28 carbon atoms terminated by hydrogen atoms at the edge. For each nucleobase on the graphene, they first performed a force relaxation to determine the preferred orientation and optimum separation distance between nucelobases and the graphene sheet. This was followed by a scan of the potential energy surface (PES) where the nucleobases were kept parallel to the graphene surface at a fixed distance but laterally translated and rotated relative to the graphene to generate a series of configurations. At each configuration, a single point energy calculation using LDA was conducted and the configuration that had the minimum potential energy was determined. This configuration was subjected to a further optimization step in which all atoms were free to move and the final optimized structure was identified. The BE was then calculated for the optimized structure using both LDA and MP2. Table 2.2 shows the values of the obtained BEs. According to their results, MP2 predicted BE values that almost doubled the LDA values. On the other hand, BEs with respect to the different nucleobases almost remained the same order: it was G>A=T=C>U using LDA and G>A>T>C>U using MP2. In all cases, the final optimized nucleobases were found to be parallel to the graphene sheet with the separation distance being 3.5 Å.

Table 2.2: BE (kJ/mol) between nucleobases and graphene in Ref. [78]

Nucleobase	LDA	MP2
G	58.86	103.24
A	47.28	90.70
T	47.28	80.08
C	47.28	77.19
U	42.25	71.40

In a later work, Gowtham et al. extended their study to the adsorption of the same nucleobases on a (5,0) CNT [79], using the same approach except that the BE calculation was only done with LDA, but not with MP2. The order of the BE was found to be the same, i.e., G>A>T>C>U with the values being 47.28, 37.63, 32.81, 27.98 and 27.02 kJ/mol, respectively. Their results showed that the BEs for CNT were much smaller than those for graphene, which was attributed to the larger curvature of the CNT and resulting smaller area of contact. Nevertheless the preferred configuration of all the nucleobases was still parallel to the CNT surface with the separation distance of about 3.2 Å. In both of their works, Gowtham et al. [78, 79] used a multi-step procedure to determine the final optimized structure. An extensive PES scan was performed in each simulation, and higher level energy calculations with MP2 was used in the case of graphene to complement the LDA optimization. Despite these efforts, the inability of LDA to capture dispersion interaction can lead to errors in the optimization step. In addi-

tion, it is generally believed that both LDA and MP2 overestimate the energy of binding driven by vdW-type interactions [84, 140, 155–158] through overestimation of the correlation energy. For example, Hobza et al. [158–160] showed that compared to CCSD(T), MP2 considerably overestimated the stabilization energy for benzene dimers.

While the nucleobases in the work of Gowtham et al. [78, 79] were simply terminated with a methyl group, Meng et al. studied the binding of a (10,0) CNT with nucleosides each composed of a DNA nucleobase (A, T, C, G), a deoxyribose sugar ring and OH groups at the 3' and 5' ends [80]. Both MM and QM methods were employed. Specifically, the binding structures were first optimized using CHARMM FF [161, 162] for nucleosides and an adapted graphitic carbon FF for CNT [163]. They were then re-optimized using LDA with plane wave basis set. Again, the base plane in the nucleosides was found to be parallel to the CNT, but its separation distance from the CNT changed from 3.3 Å after the MM optimizations to around 3 Å after LDA optimization. The BEs evaluated with LDA fell into a narrow range for the different nucleosides (41.49-44.38 kJ/mol), and the order of the BE was given by T>G>C>A, which is quite different from the work of Gowtham et al. [79] on nucleobase-CNT binding. In their approach, Meng et al. [80] initially optimized the structures using CHARMM FF which includes an empirical description of dispersion interaction, but dispersion was neglected again during the re-optimization step using LDA.

Using a different approach, namely time-dependent LDA method, Meng et al. later studied again the binding between DNA nucleosides and a (10,0) CNT [81]. From the simulations, the optical absorbance spectrum for DNA nucleosides were obtained, which was used to determine the preferred orientation of the nucleo-

sides on the CNT. Optimized binding structures were also obtained using MM (CHARMM) calculations, and good agreement was reported between the MM and LDA results. According to their MM calculations, the order of the BE for the most stable structures was G>A>T>C with the BE values of 82.01, 78.15, 74.29 and 67.54 kJ/mol, respectively. Compared with their LDA results earlier [80], not only did the order of the BE change, the BE values were found to be significantly larger and cover a much larger range.

Shtogun et al., using LDA with plane wave basis set, studied the effect of charge on nucleobase-CNT interaction [82]. In particular, they simulated the adsorption of A and A-radical (by removing an H atom from the nucleobase) on a metallic (6,6) CNT, and the adsorption of T and T-radical on a semiconducting (8,0) CNT. Simulations were first performed for A and T where fifteen initial configurations (ICs) for A and five ICs for T were considered. For each IC, the entire system (CNT and nucleobase) was optimized, and the BE was calculated afterwards. According to their results, different optimized structures could be obtained by starting from different ICs. Furthermore, BEs for the optimized structures were very close indicating the shallowness of the PES. The first two rows in Table 2.3 shows the nucleobase-CNT separations for the optimized hybrids that have the highest BEs and the corresponding BE values. To do the simulations for radical-CNT binding, the ICs were adopted from the most stable A-(6,6) CNT and T-(8,0) CNT hybrids, respectively for A-radical and T-radical. Each radical-CNT system was then subjected to an additional optimization step. The introduction of a charge did not cause much change in the nucleobase-CNT separation, but had a profound influence on the BE. Specifically, the BE increased by 46% when A was replaced by A-radical, and the increase was more significant when T was

replaced by T-radical, being 109%. While BE for A-(6,6) CNT is higher than that for T-(8,0) CNT, the value for T-radical-(8,0) CNT is higher than that for A-radical-(6,6) CNT. The higher BE for A-(6,6) CNT compared with T-(8,0) CNT was attributed to the larger diameter of the (6,6) CNT, i.e., 0.81 nm as compared to 0.63 nm for the (8,0) CNT. For the radicals, however, the difference was attributed to the different partial charge distribution, which played a more important role than curvature, since the Coulombic forces were stronger than the vdW forces in this case.

Table 2.3: BE (kJ/mol) and equilibrium distance (Å) in Ref.[82]

Hybrid	BE	Equilibrium distance
A-(6,6) CNT	34.16	3.14
T-(8,0) CNT	30.49	3.10
A-Radical-(6,6) CNT	49.88	3.14
T-Radical-(8,0) CNT	63.78	2.96

The dependence of BE on CNT chirality was investigated by Wang and Ceulemans [83] using LDA. In an effort to better resemble real DNA building blocks, they considered two connected adenosine-monophosphates with the phosphate groups terminated by H atoms. The resulting molecule was neutral and was taken to interact with different CNTs, including five (m,0) zigzag tubes with m = 7,8,9,10,17 and four (n,n) armchair tubes with n = 4,5,6,7. Periodic boundary condition (PBC) was applied using supercell approach and the linear combination of numerical atomic orbitals (LCAO) basis set with double-ζ polarizations. Ge-

ometry optimization for the hybrids was carried out from the initial structure in which the nucleobases were aligned parallel to the CNT surface with a relatively large separation distance of 7.5 Å. BEs were then calculated based on the optimized structure. As shown in Figure 2.3, despite the presence of the phosphate group, the nucleobases were almost parallel to the CNT surface in the optimized structures, with the separation distances being 3 to 3.2 Å. The reported BE values varied from 144.73 kJ/mol to 366.64 kJ/mol for different CNT chiralities, which was much larger than the BE between single nucleobase and CNT reported earlier, likely due to the larger size of the double adenosine-monophosphates. For armchair tubes, the BE was found to increase with increasing CNT diameter, i.e., (7,7) CNT>(6,6) CNT>(5,5) CNT>(4,4) CNT. This was attributed to the increased area of contact between the two entities as the CNT became larger. For zigzag tubes, however, a different dependence was found. Specifically, the order of the BE was determined to be (7,0) CNT>(9,0) CNT>(8,0) CNT>(17,0) CNT>(10,0) CNT. The overall decreasing trend of the BE with increasing CNT diameter (except for (8,0) and (10,0) tubes) was not yet understood.

The above studies all used LDA as the main approach, although some of them incorporated other QM or MM methods. The simplicity of LDA was one of the reasons for the wide usage of DFT. However, it is also known for its inaccuracy. LDA is rarely used nowadays for π-π stacking systems due to availability of many other functionals that have shown better performance compared to LDA.

Attempting to explore the effect of CNT curvature and electronic property, Wang and Bu considered C interacting with small fragments, $C_{24}H_{12}$, of armchair (n,n) (n=5,7,8) and zigzag (m,0) (m=8,10,12) CNTs [84]. The structures were optimized using DFT with PW91LYP and MPWB1K functionals; the BEs

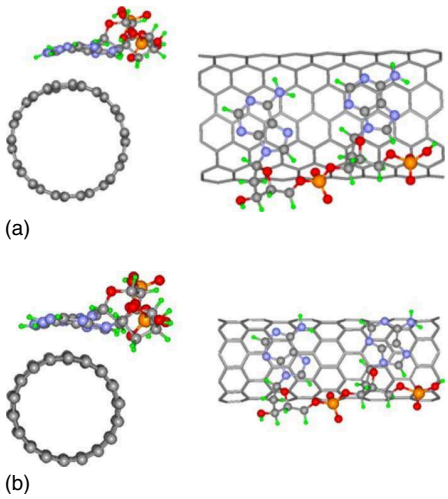

Figure 2.3: Optimized structures of two connected adenosine-monophosphates on (a) (7,7) CNT, (b) (9,0) CNT in Ref. [83] (reproduced with permission from Ref. [83]).

were evaluated not only with DFT, but also with MP2. Seven initial placements of C with respect to the CNT were considered, including two parallel and five perpendicular configurations. Their results showed that the final configurations were parallel if optimized from the parallel configurations and perpendicular if optimized from the perpendicular configurations. For the (5,5) fragment, if both optimization and BE calculation were carried out at the PW91LYP/6-311++G(d,p) level, the BSSE-corrected BE ranged from 7.78 to 15.19 kJ/mol, depending on the initial configuration. In addition, the structures optimized from the perpendicular configurations had larger BE indicating that they were more stable than the ones optimized from the parallel configurations, which is quite counterintuitive. However, results obtained after doing single point energy calculations using MP2 were completely different: structures optimized from the parallel configurations had higher BE than the ones optimized from the perpendicular configurations. Also,

MP2 method predicted much higher BE values. The highest BSSE-corrected BE between C and the (5,5) CNT fragment computed at MP2/6-311G(d,p) level was 27.95 and 32.76 kJ/mol respectively for the structures optimized at PW91LYP/6-311++G(d,p) and MPWB1K/cc-pVDZ levels. These values were considerably larger than those calculated at PW91LYP/6-311++G(d,p) level. The dramatically different or even opposite results obtained from different methods clearly demonstrated how sensitive such calculations can be to the choice of simulation method. The results for other CNT fragments in Wang and Bu's work showed that increasing CNT diameter in general led to higher BE for the parallel configurations while it had little effect on the BE for the perpendicular configurations. This is consistent with the results of Wang and Ceulemans [83] on armchair CNTs, but not on zigzag CNTs. It should be noted that the $C_{24}H_{12}$ fragments considered in this work could not properly reflect the electronic properties of the CNTs, which was confirmed by their HOMO-LUMO orbital energy calculations. Therefore, only one of their goals, i.e., the curvature effect, was achieved and the effect of electronic structure was not captured.

In a later work, Wang considered all four DNA nucleobases interacting with two types of CNTs: (5,5) and (10,0) [85]. Same as his first work [84], for each type of CNT, only a small fragment ($C_{24}H_{12}$) was chosen to interact with the nucleobases. Both DFT and MP2 methods were adopted in the simulations. In particular, geometry optimization was carried out at MPWB1K/cc-pVDZ level where carbon and hydrogen atoms were kept frozen in the $C_{24}H_{12}$ fragments. The optimized structures were then subjected to a single point energy calculation at MP2/6-311++G(d,p) level. Different from the previous work, simulations were performed in both vacuum and aqueous environment. In the latter case, the con-

ductor polarized continuum model (CPCM) [164] was used to model the solution. Table 2.4 shows the values of BEs in all cases. The BSSE-corrected BE for the C-(5,5) CNT hybrid in vacuum was 46.46 kJ/mol which is quite different from Wang's former study [84] in which the BE for the same system was determined to be 32.76 kJ/mol. The order of the BE between nucleobase and CNT in the gas phase was found to be G>A>T>C for both CNTs. This is in agreement with the DFT studies of Gowtham et al. on the interaction of nucleobases with graphene and (5,0) CNT [78, 79], as well as with the MM results of Meng et al. for the interaction of nucleosides with a (10,0) CNT. The inclusion of an aqueous environment was shown to affect the BE. Specifically, in the solution the order of the BE remained for the (5,5) CNT, but was changed to A>G>T>C for the (10,0) CNT. In all cases, the BE was found to decrease upon the introduction of the solution. In some cases, the decrease was significant, for example, for C on both CNTs. Also, in vacuum the BEs between the nucleobases and the (5,5) CNT were smaller than those between the nucleobases and the (10,0) CNT, while in the aqueous environment, BEs for the (5,5) CNT were larger than those for the (10,0) CNT except for C. The observation in vacuum may be understood by recognizing that the (5,5) CNT has a smaller radius and hence a small area of contact with the nucleobases. On the other hand, there was not a clear explanation for the opposite behavior (except for C) observed in the aqueous environment.

Although the model for the solvent was at continuum level and hence was approximate, Wang's work presented an attempt to understand the behavior of the hybrids in solution and how they might differ from those in vacuum. Several limitations do exist in Wang's study. First, the model for CNT was a small fragment that contained only 24 carbon atoms, which may not properly represent

the CNT. Secondly, single neutral DNA nucelobases were simulated without considering phosphate group or sugar ring, whereas DNAs are charged in aqueous environment. In addition, MPWB1K was used for geometry optimization, which is not a dispersion-corrected method, although there was some evidence for its accuracy [138].

Table 2.4: BE (kJ/mol) between nucleobases and CNT in Ref. [85]

Nucleobase	(5,5) CNT		(10,0) CNT	
	Gas	Aqueous	Gas	Aqueous
G	59.86	47.30	61.11	42.28
A	55.67	46.46	57.76	44.79
T	51.90	41.44	52.32	39.77
C	46.46	29.72	47.30	35.58

The simulation works reviewed above are all based on methods that lack correction for dispersion interaction. With the advancement in computational chemistry, more accurate dispersion corrected methods have been introduced, which have been used in most of the recent studies on π-π interacting systems. Such studies on nucleobase-CNT/graphene binding are reviewed below.

2.3.1.2 Studies performed with dispersion-corrected methods

A number of dispersion-corrected methods exist in literature and benchmarking has been performed for some of them [134, 135, 137, 139, 145, 147, 151, 165,

166]. Among these methods, Minnesota density functionals developed by Truhlar's group, e.g., M05, M05-2X, M06, M06-L, M06-2X and M06-HF, are based on meta-GGA approximations [167–171]. The exchange-correlation term in all Minnesota functionals depends on kinetic energy. In the M06 family, M06-2X has shown good performance in several studies where vdW interaction was important [137]. Grimme's method which includes B97-D, DFT-D2 and DFT-D3 is based on an empirical dispersion correction added to the Kohn–Sham DFT [143, 144, 172]. Dion et al. proposed the vdW-DF method to treat dispersion interaction, which is based on non-local correlation [151]. Lee et al. modified Dion's vdW-DF functional and was able to generate more accurate results for equilibrium separations, strength of hydrogen bond and vdW attractions in non-covalently bound complexes [173]. Tkatchenko and Scheffler (TS) developed the TS functional in which the inter-atomic dispersion coefficients were calculated from rescaled atomic dispersion coefficients and polarizabilities using a London-type formula [141]. A series of dispersion-corrected potentials (DCPs) were recently developed by DiLabio's group to be used in combination with the PBE0 (PBE0-DCP) and B3LYP (B3LYP-DCP) functionals. Benchmarking was done for a number of non-covalently interacting systems, which showed excellent performance for predicting the structures and BEs in these systems [174]. M05-2X [168],M06-2X [169], TS [141], vdW-DF [151], vdW-DF2 [173], DFT-D2 [143] and DFT-D3 [144] are some of the dispersion-corrected methods that have been used to study the binding of nucleobases with graphene and CNTs.

Ortmann et al. studied the binding between A and graphene using DFT and plane wave basis set [86]. They employed three different schemes: LDA, GGA with PW91 functional, and GGA with a modified PW91 functional where a Lon-

don dispersion term was added. A PES scan was conducted by changing the position of A with respect to graphene. Based on their investigation, the parallel orientation of A with respect to the graphene surface led to the most stable structures with highest BE values. The separation distances between A and the graphene in the most stable structures were reported to be 3.1, 4 and 3.4 Å respectively using LDA, PW91 and dispersion-corrected PW91. The corresponding BE values were respectively 44.38, 6.75 and 105.17 kJ/mol . Clearly, BE evaluated using the dispersion-corrected PW91 was much larger than the values obtained from PW91 and LDA. In fact, the result from dispersion-corrected PW91 was shown to be in fairly good agreement with the experimental value of 97.45 kJ/mol obtained from TDS [77]. PW91 [175] is the first functional that includes exchange and correlation energy via GGA. It does not contain dispersion correction and has been shown to underestimate the BE for benzene dimers [176]. Therefore it is not surprising that PW91 predicted BE that was more than one order of magnitude smaller than the result from dispersion-corrected method. While usually believed to overestimate the energy of binding caused by vdW type interactions, LDA has also been reported by some studies to underestimate interlayer BE of graphene [177]. In this work, the BE obtained from LDA was larger than the value from PW91, but smaller than the value from dispersion-corrected PW91.

Physisorption of A on graphene was also studied by Berland et al. [87] using vdW-DF [151] with plane wave basis set. A two-step procedure was followed in order to find the optimal alignment of A on the graphene. Firstly, A was placed parallel to the graphene surface and the optimal separation distance was determined via a PES scan. Such distance was found to be 3.5 Å. Then, at this separation distance, A was rotated and translated laterally, and the configuration with

the largest BE was determined to be the final optimal configuration. The BE for the determined configuration was found to be 68.6 kJ/mol, which was less than the one obtained by Ortmann et al. [86] using dispersion-corrected PW91. In this work, a convergence study was also performed for graphenes with different size. The results showed that graphene model containing 96 carbon atoms was sufficient for calculating its BE with A. The BE of two-dimensional crystal overlayer of A on graphene was also determined; the value of 97.06 kJ/mol was in agreement with experiments [77].

Panigrahi et al. employed dispersion-corrected DFT using wB97XD functional to study nucleobase-graphene binding [88]. Nucleobases in their work were attached to a methyl group, similar to the study by Gowtham et al. [78]. Each nucleobase was placed above a square graphene sheet with eight carbon rings in each direction and H atoms at the edges. The IC of the base plane was parallel to the graphene surface with a separation distance of 4 Å, which was subjected to a full optimization at wB97XD/6-31G(d,p) level. The separation distance in the optimized structures was found to be around 3.5 Å. BSSE corrected BE was calculated at the same level and found to be 94.16, 85.03, 79.30, 77.04 and 68.41 kJ/mol respectively for G, A, C, T and U, i.e., G>A>C>T>U. Such order is identical to what was observed by Gowtham et al. [78] on the same system using LDA optimization accompanied by MP2 energy calculation. The BE values are also close to the MP2 results of Gowtham et al. [78] but almost double those obtained using LDA alone.

In another study using the wB97XD functional, Chandra Shekar and Swathi examined physisorption of nucleobases on coronene ($C_{24}H_{12}$) as a model of graphene [89]. Different ICs were considered while the separation distance was set to $\sim$ 3 Å in

all ICs. Geometry optimization was carried out at wB97XD/6-31G(d,p) level followed by a single point energy calculation at wB97XD/6-311+G(d,p). Different from the results of Panigrahi et al. [88], the order of the BSSE corrected BEs was determined to be G>T>A>C>U with the values of 75.73, 66.53, 65.27, 64.43 and 56.48 kJ/mol, respectively. BE values in this work were less than the ones obtained by Panigrahi et al. [88], which may be attributed to the smaller size of graphene in this study compared to that in Panigrahi et al. The separation distance in the optimized structures was found to be 3.24, 3.25, 3.30, 3.22 and 3.20 Å, respectively for G, T, A, C and U. These separation distances were also smaller than the ones obtained by Panigrahi et al. [88].

Antony and Grimme studied the interaction of nucleobases with graphene using DFT-D [90]. Four different sizes of graphene were considered, with 24 ($C_{24}H_{12}$), 54 ($C_{54}H_{18}$), 96 ($C_{96}H_{24}$) and 150 ($C_{150}H_{30}$) carbon atoms respectively. Hybrids were fully optimized at B97-D/TZV(d,p) level. A three dimensional PES scan was also performed for the interaction of nucleobases with the $C_{96}H_{24}$ fragment, and no other minima were found except the one obtained from optimization. Table 2.5 shows the BEs (without counterpoise correction) for the optimized systems. The order of the BEs for all graphene fragments is generally G>A>T>C>U, in agreement with the result from Gowtham [78] using coupled LDA and MP2 method. In addition, it can be seen from Table 2.5 that the BE associated with $C_{96}H_{24}$ is quite close to the BE associated with $C_{150}H_{30}$. This indicates that $C_{96}H_{24}$ is sufficiently large to evaluate the BEs, which is consistent with the convergence test result of Berland et al. [87]. On the other hand, comparing the BE of A with $C_{96}H_{24}$ or $C_{150}H_{30}$ to the results of Berland et al. and Ortmann et al., there is considerable discrepancy: the prediction by Antony and

Grimme (86.67 kJ/mol) is larger than the value obtained by Berland et al.(68.6 kJ/mol) using vdW-DF but smaller than the one (105.17 kJ/mol) obtained by Ortmann et al. using dispersion-corrected PW91. Finally, using spin-component scaled (SCS) MP2 method and a double hybrid density functional that contains empirical dispersion-correction (B2PLYP-D), additional single point energy calculations were conducted for the B97-D/TZV(d,p) optimized structures involving $C_{54}H_{18}$. The results showed that the order of the BE remained the same, as well there was little change in the absolute values of the BE.

Table 2.5: BE (kJ/mol) between nucleobases and graphene fragments in Ref. [90]

Base	$C_{24}H_{12}$	$C_{54}H_{18}$	$C_{96}H_{24}$	$C_{150}H_{30}$
G	79.13	100.90	105.51	107.60
A	60.71	82.90	86.67	87.50
T	65.31	77.04	81.22	82.48
C	59.03	77.03	80.39	80.81
U	56.52	66.15	69.92	71.18

In a comparative study similar to Ortmann et al. [86], Lee et al. [91] investigated the physisorption of DNA nucleobases on graphene using LDA, GGA and a dispersion-corrected GGA approach. PBE functional was used in the GGA and dispersion-corrected GGA approach; in the latter case (PBE+vdW), vdW energy was added to the PBE energy to account for dispersion. Nucleobases were attached to a methyl group and PBC was applied in their study. Full geometry optimization for the hybrid structures was performed but no detailed explanations were given for the ICs. Results for the BE and separation distance obtained using

the three approaches with tier2 basis set are shown in Table 2.6. Similar to the results of Ortmann et al., BEs from the dispersion-corrected approach were higher than the ones obtained using LDA and GGA methods. Also, the order of the BE was found to be different using different methods: G∼C>A>T, G>C>T>A and G>A>T>C, respectively using LDA, PBE and PBE+vdW. Compared with the work of Gowtham et al. [78], the LDA BEs were very close since nucleobases were capped with methyl group in both studies. Compared with the work of Ortmann et al. [86], the LDA BE for A reported by Lee et al. was greater, which may be argued to arise from the presence of methyl group. This, however, cannot explain why the PBE+vdW BE was smaller in Lee et al.

Table 2.6: BE (kJ/mol) and separation distance between nucleobases and graphene in Ref. [91]

Nucleobase	LDA		PBE		PBE+vdW	
	BE	Separation distance	BE	Separation distance	BE	Separation distance
G	69.47	3.08	13.51	3.95	113.85	3.26
A	53.07	3.17	5.79	4.00	96.49	3.29
T	52.10	3.10	7.72	4.02	91.66	3.29
C	54.03	3.12	12.54	3.97	89.73	3.27

Le et al. evaluated the BE of nucleobases with graphene using several dispersion-corrected DFT methods [92]: TS [157], simplified TS (sTS) [92], vdW-DF [151], vdW-DF2 [173], DFT-D2 [143] and DFT-D3 [144], each with plane wave set. The optimal binding structures were determined through a two-step procedure. First,

each nucleobase was aligned parallel to the graphene at a separation of 3.2 Å. It was rotated at an increment of 5° and for each configuration a single point energy calculation was carried out using sTS. The configuration with the highest BE was then subjected to a geometry optimization using vdW-DF. Finally, BE for the optimized structure was computed using all of the mentioned methods. According to their results, the separation distance in the optimized structures varied from 3.13 to 3.53 Å for the five nucleobases. Different functionals gave rise to different BE: the values ranged from 47.86 to 92.53 kJ/mol; the prediction was lowest with vdW-DF2 and highest with vdW-DF. On the other hand, all methods in this work resulted in the same order for the BE, being G>A>T>C>U, which is in agreement with the work of Antony and Grimme [90], but differs slightly from result of Chandra Shekar and Swathi et al. [89]. The two-step optimization procedure employed in this study allowed more accurate determination for the location of the potential energy minimum. A systematic comparison was also made among different methods. However, it is worth noting that although different methods were used in the BE calculations, the optimization was performed using the same approach.

Recently, Cho et al. used optB86b [178] and PBE+TS (PBE with Tkatchenko-Scheffler [157] vdW correction) functionals within DFT to study interaction of DNA nucleobases with graphene [93]. Plane wave and tier2 basis sets were used, respectively for optB86b and PBE+TS. PBC was applied and geometry optimizations based on a basin-hopping procedure were carried out for the nucleobase-graphene system while the graphene was kept fixed during the optimizations. Results for the BE values and separation distances are listed in Table 2.7. According to their results, both methods predicted the same order of the BE, being

G>A>T>C. This trend is in agreement with the ones obtained by Le et al. [92] and also Antony and Grimme [90]. BE values in Table 2.7 are slightly smaller than the results from Antony and Grimme (see data for $C_{150}H_{30}$ in Table 2.5), which may be due to the lack of BSSE correction in the BE calculations in Antony and Grimme, 2008. Cho et al. also studied the interaction of DNA nucleobases with graphene flake (without applying PBC) to investigate the effect of graphene size on the BE. Three models of graphene, $C_{54}H_{18}$, $C_{96}H_{24}$ and $C_{150}H_{30}$, were considered and subjected to full geometry optimizations using PBE+TS and BLYP-D3 methods, respectively with tier 2 and aVTZ basis sets. Compared to the case where PBC was applied, similar optimized geometries were obtained, so was the order for the BE, but as expected BEs for $C_{150}H_{30}$ were closest to the ones obtained from PBC.

Table 2.7: BE (kJ/mol) and separation distance between nucleobases and graphene in Ref. [93]

Nucleobase	optB86b		PBE+TS	
	BE	Separation distance	BE	Separation distance
G	93.3	3.17	90.8	3.27
A	83.3	3.26	82.8	3.27
T	80.3	3.15	82.4	3.23
C	75.3	3.18	77.0	3.23

In another recent publication, interaction of nucleobases with graphene was studied by Vovusha et al. [94] using M05-2X and M06-2X fuctionals. Graphene

model in their study included 54 carbons with 18 hydrogen atoms capping the edge carbons. Geometry optimizations were all performed at M05-2X/6-31G(d) level and BEs were evaluated using both M05-2X and M06-2X methods with 6-31+G(d,p) and 6311++G(d,p) basis sets. The separation distance between nucleobases and graphene in the optimized structures was determined to be 3.2-3.5 Å which is close to previously reported results. Table 2.8 shows BEs evaluated at different levels of theory in their work. Results obtained using M06-2X were considerably larger than the ones obtained using M05-2X method. More specifically, in some cases the difference between BEs evaluated using the same basis set but different methods, i.e., M05-2X and M06-2X, was even greater than the BE itself obtained using the M05-2X. The order of the BE using M05-2X was determined to be G>C=T>A>U and G>C>T>A>U respectively with 6-31+G(d,p) and 6-311++G(d,p) basis sets. When M06-2X was used for the BE calculation, the order was changed to G>T>A>C>U and G>T>C>A>U respectively using 6-31+G(d,p) and 6-311++G(d,p) basis sets. This demonstrates the great effect of method and basis set on the value and order of the BE. In most of the previous results on the BE between nucleobases and graphene, BE of A was only second to G, while this was not obtained by Vovusha et al. It is worth noting that the IC of nucleobases with respect to the graphene was not clearly stated in Vovusha et al.'s work.

Table 2.8: BE (kJ/mol) between nucleobases and graphene in Ref. [94]

Nucleobase	DFT level			
	M05-2X		M06-2X	
	6-31+G(d,p)	6-311++G(d,p)	6-31+G(d,p)	6-311++G(d,p)
G	37.62	27.23	65.08	57.46
A	27.01	16.70	52.19	44.23
T	27.98	19.64	52.93	46.23
C	27.98	20.50	51.02	45.10
U	22.19	13.93	46.36	35.00

Enyashin et al. explored the binding between neutral monophosphate nucleotides and a graphene sheet [95] using self-consistent-charge density functional based tight binding method (SCC-DFTB). Dispersion-corrected SCC-DFTB (DC-SCC-DFTB) was employed to take into account the non-covalent interactions between nucleotides and the graphene sheet. PBC was applied and full geometry optimization was performed. The reported BEs were 115.78, 109.99, 93.59 and 89.73 kJ/mol for G, A, C and T nucleotides, respectively. The order of the BE (G>A>T>C) was the same as the result of Antony and Grimme [90], Le et al. [92] and Cho et al. [93] although phosphate group and sugar ring were not included in the work of Antony and Grimme [90]. To our knowledge, the study of Enyashin et al. was the only one involving binding of nucleotides with graphene, although the nucleotides were not charged and the systems were simulated in vacuum.

While most of the simulations using dispersion-corrected methods focused on the interaction of nucleobases with graphene, Stepanian et al. studied the interaction between C and fragments of a (10,0) CNT by combining DFT and MP2 approaches [96]. Various DFT functionals including MPWB1K, M05, M05-2X and MPW1B95 as well as the MP2 method were used. 6-31++G(d,p) for C, 6-31G(d) for the carbon atoms in CNT and STO-3G for the hydrogen atoms in CNT were the basis sets used for all methods. A benchmarking study was first performed using the MPWB1K functional for CNT fragments with different sizes: $C_{38}H_{16}$, $C_{56}H_{22}$, $C_{68}H_{22}$, $C_{66}H_{22}$, and $C_{120}H_{20}$. Molecular structures of the CNT fragments are shown in Figure 2.4. $C_{38}H_{16}$ was the first simulated CNT fragment. C was kept parallel to the $C_{38}H_{16}$ surface at a separation distance of 3.3 Å and was rotated at the increment of 30° to generate six different ICs. Geometry optimizations were then performed where all carbon atoms in the $C_{38}H_{16}$ fragment were kept frozen, and the BE was calculated for each of the six optimized structures. Both optimization and BE calculation were conducted using MPWB1K. The highest BE among the six optimized structures was found to be 39.9 kJ/mol. The effect of size of the CNT fragment was explored next by calculating the BE of C with $C_{56}H_{22}$, $C_{68}H_{22}$, $C_{66}H_{22}$ and $C_{120}H_{20}$, also using MPWB1K, where the position of C relative to these fragments was adopted from the optimized structure of C on $C_{38}H_{16}$ with the highest BE. The BE was found to increase from 39.9 to 41.1 kJ/mol as the fragment changed from $C_{38}H_{16}$ to $C_{120}H_{20}$. Such a small difference led the authors to choose the smallest fragment, $C_{38}H_{16}$, to study how different methods may affect the binding results. To perform the optimizations at DFT as well as MP2 levels, the ICs were adopted from optimized structure of C on $C_{38}H_{16}$ obtained using MPWB1K. Table 2.9 shows the highest energies

for C-$C_{38}H_{16}$ binding obtained from different methods, where BE (MP2) is the BSSE corrected BE obtained from a further single point energy calculation using MP2. Clearly, BEs obtained from MPWB1K, MPW1B95 and M05 are quite close, and they are much smaller than the values obtained from M05-2X. After the MP2 energy calculation, BEs increase in all cases, but the increase is smallest with M05-2X probably because the correlation energy in M05-2X is closer to the one in MP2 than the other methods.

In the same article, Stepanian et al. also investigated the effect of CNT diameter on the BE. Interaction of C with the $C_{38}H_{16}$ fragment of different zigzag (n, 0) CNTs (n = 8-40) was studied by doing geometry optimizations using MPWB1K followed by single point energy calculations using MP2. The ICs were adopted from the optimized structure of C on $C_{38}H_{16}$ fragment of (10,0) CNT obtained from MPWB1K. Their results showed that the BE increased with increasing tube diameter and approached the BE of C with graphene obtained from the same simulation method (59.1 kJ/mol).

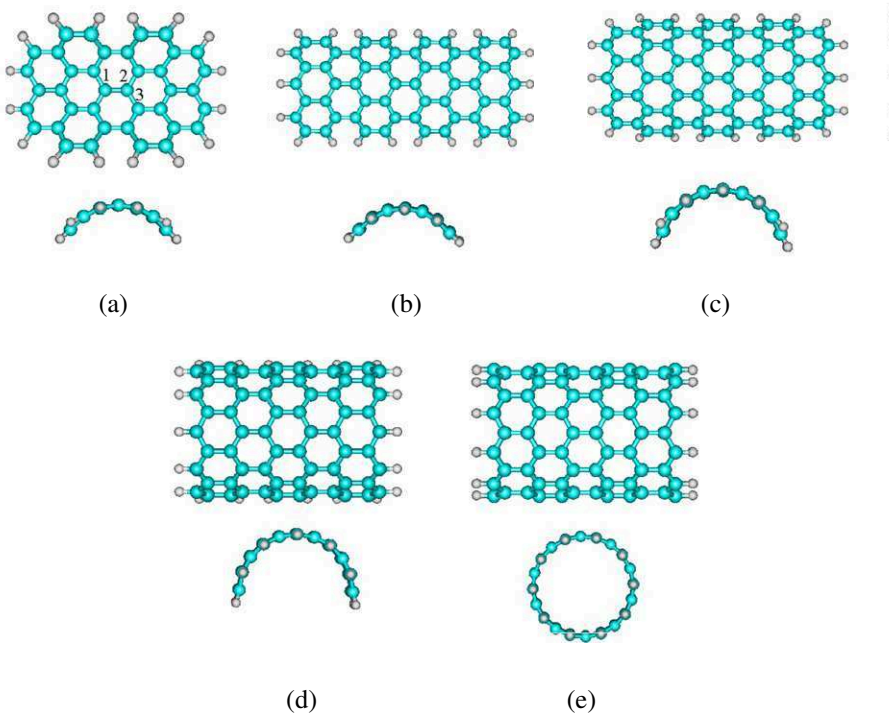

Figure 2.4: CNT fragments simulated in Ref. [96]. (a) $C_{38}H_{16}$, (b) $C_{56}H_{22}$, (c) $C_{68}H_{22}$, (d) $C_{66}H_{22}$, (e) $C_{120}H_{20}$ (reproduced with permission from Ref. [96]).

Table 2.9: BE (kJ/mol) between cytosine and $C_{38}H_{16}$ fragment of a (10,0) CNT in Ref. [96]

	MP2	MPWB1K	MPW1B95	M05	M05-2X
BE	50.3	38.5	39.9	36.4	48.7
BE (MP2)	50.3	49.4	49.6	45.2	49.6

Shukla et al. used M05-2X functional to calculate the BE of nucleobases with a (7,0) CNT [97]. The CNT contained seven carbon rings in the longitudinal direction and was terminated with H atoms at the ends. Geometry optimizations were performed at M05-2X/6-31G(d) level and single point energy calculations

were conducted with 6-31G(d,p), 6-31+G(d,p) and cc-pVDZ basis sets. BSSE corrected BEs are shown in Table 2.10. Different basis sets gave rise to different BE orders: G>A>C>T>U using cc-PVDZ and 6-31G(d,p) but G>C>A>T>U using 6-31+G(d,p). The BE values associated with different nucleobases can be very close. For example, at the M05-2X/6-31G(d) level, the BEs for A and C differ only by 0.1 kJ/mol. Comparing the data in Table 2.10 with the results of Stepanian et al. [96], it can be seen that the BEs reported by Shukla et al. are much smaller. In fact, it was reported that M05-2X functional tend to underestimate the BE for π-π stacking systems and M06-2X has a better performance in describing dispersion [165]. It should also be pointed out that the exact IC used for geometry optimization was not described in this work.

Table 2.10: BE (kJ/mol) between nucleobases and a (7,0) CNT in Ref. [97]

Nucleobase	Basis set		
	6-31G(d,p)	6-31+G(d,p)	cc-pVDZ
G	26.5	32.9	31.3
A	18.2	24.0	23.4
C	18.1	25.1	22.6
T	17.6	23.7	21.4
U	17.1	23.0	20.8

Lacking a systematic discussion in the literature on the role of IC in nucleobase-CNT binding encouraged a detailed study on the effect of IC [102]. A series of DFT calculations for the BE of nucleobases with the same (7,0) CNT studied by Shukla et al. [97] was carried out, for each nucleobase twenty-four ICs with differ-

ent lateral and angular positions relative to the CNT were considered. Geometry optimization and BE calculation were performed using the same method as in Shukla et al. (M05-2X/6-31G(d,p)). Comparison of the results with the work of Shukla et al. showed the importance of IC in the BE calculations. The BE was shown to be very sensitive to the IC both quantitatively and qualitatively. For example, two different ICs for the adsorption of A on the (7,0) CNT are shown in Figure 2.5, along with the optimized structures resulted from these two ICs. The BE for the structure in Figure 2.5(b) (optimized from the IC shown in Figure 2.5(a)) was 17.2 kJ/mol, while the BE for the structure in Figure 2.5(d) (optimized from the IC shown in Figure 2.5(c)) was considerably different, being 29.6 kJ/mol. The ranges of the BE obtained for A, C, G, and T were quite large, being respectively [17.2, 29.6] kJ/mol, [16.4, 27.9] kJ/mol, [24.4, 39.9] kJ/mol and [15.9, 29.8] kJ/mol. The BEs obtained by Shukla et al. for the same system (but without a clearly specified IC) fell into the above ranges. The order of the BE with respect to different nucleobases was shown to change with even small changes in the IC. These results provided a possible explanation for the discrepancies that exist in the literature on the nucleobase-CNT BE.

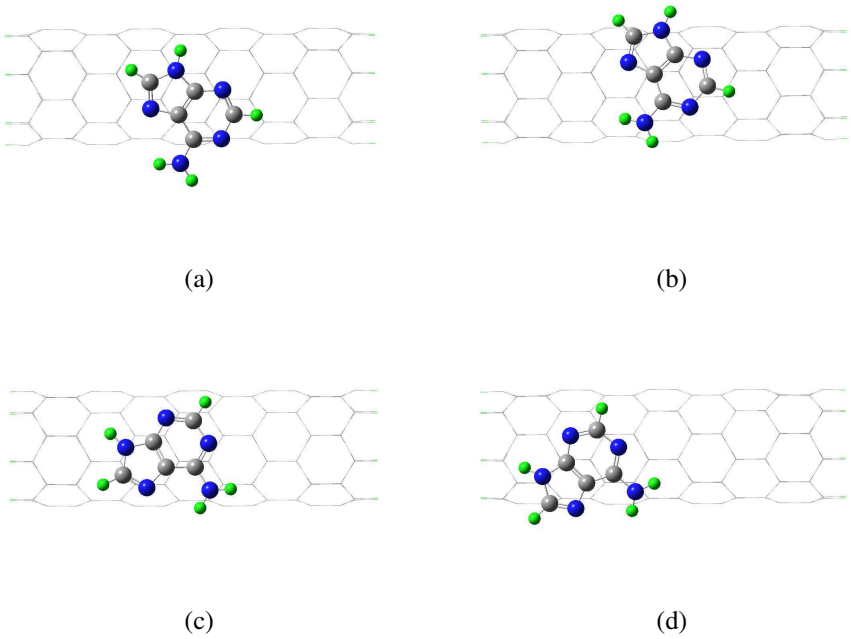

(a) (b)

(c) (d)

Figure 2.5: Adsorption of A on a (7,0) CNT: (a) IC#1, (b) Optimized structure obtained from IC#1 with the BE of 17.2 kJ/mol, (c) IC#2, (d) Optimized structure obtained from IC#2 with the BE of 29.6 kJ/mol.

Akdim et al. calculated BEs for DNA nucleobases with chiral CNTs using B97-D method [98]. Three CNTs were studied with the same diameter but different chiralities of (6,5), (9,1) and (8,3). Each CNT had finite length ($\sim$160 carbon atoms) and was terminated with H atoms at its ends. To generate the ICs, they first performed simulations for 1ps at 330 K using DC-SCC-DFTB method. Geometry optimizations and BE calculations were then carried out at B97-D/6-31G(d) level on the structures obtained from the previous dynamic step. The results are given in Table 2.11, which shows G>A>T>C for both (6,5) CNT and (9,1) CNT but G>A>C>T for the (8,3) CNT. The BEs for all CNTs in this work are larger than the ones obtained by Shukla et al. [97], which could be due to the fact that CNTs modeled by Akdim et al. had larger diameter compared to the (7,0) CNT

studied by Shukla et al. [97]. The authors also carried out a single point energy calculation at B97-D/Def2-TZVP level for the optimized structures and showed that the BEs ranged from 62 to 71 kJ/mol with the same order. In addition, BEs of nucleobases with a zigzag (5,0) CNT were computed using the effective fragment potential (EFP2) method [179], which expressed the BE as a sum of electrostatic, polarization, exchange repulsion, charge transfer and dispersion terms. The dispersion term was found to be considerably larger than the other three terms which shows the importance of dispersion.The values for the BE were found to be 110.91, 109.23, 90.02 and 72.89 kJ/mol with the order of G>T>C>A. These values are more than twice the BEs obtaining by Gowtham et al. [79] on the same CNT, and even larger than the values shown in Table 2.11, although the diameter of the (5,0) CNT is smaller than the three chiral CNTs. In addition, for the (5,0) CNT, the BE for A is the lowest among the four nucleobases. The only other work that reported the same observation was by Meng et al. [80] for nucleosides binding with a (10,0) CNT.

Table 2.11: BE (kJ/mol) between nucleobases and CNTs in Ref. [98]

Base	(6,5) CNT	(9,1) CNT	(8,3) CNT
G	86.75	85.24	87.76
A	71.13	70.30	69.75
C	61.29	59.45	65.72
T	63.56	61.09	62.17

Compared with the works reviewed in Section 2.3.1, the addition of dispersion correction in the above studies is expected to better capture the interaction

between nucleobases and graphene or CNT and generate more accurate results. On the other hand, simulations with dispersion corrected methods are usually computationally more costly. Most of the studies using these methods focused on binding of nucleobases with graphene. Only a few investigations were carried out for CNT. Several simulations also used fragments of graphene or CNT. In addition, all simulations were performed in vacuum; no charges or solution environment were considered. Given the current computing capabilities, in order to simulate larger and more complex systems, some efforts were spent on conducting simulations using lower level methods: MM, semi-empirical, or a combination of MM and QM methods.

2.3.2 Studies based on semi-empirical and force-field methods

Lower level methods used to study the binding of nucleobases with graphene or CNT typically involve classical MM or semi-empirical QM approaches. AM1 [126], PM3 [127–129] and PM6 [130] are the widely used semi-empirical methods. Non-bonded interactions including electrostatic and vdW forces are implemented in classical FFs such as Amber [180] and CHARMM [162]. It has been shown that Amber FF can even be more accurate than some of the semi-empirical QM methods when evaluating the BE for biological systems [136, 137]. These simulation efforts are summarized below.

To our knowledge, work by Edelwirth et al. was the first computational study on the interaction a nucleobase with graphite [123]. Adsorption of A on a graphite composed of 3 layers of 30×30 carbon atoms was studied using Dreiding II FF [181], and PBC was applied on the system. Both A and graphite were consid-

ered to be rigid and geometry optimization was done for several ICs. All simulations, starting from different ICs, led to the same final configuration in which the plane of A was parallel to the graphite surface. The separation distance was found to be 3.40 Å and the BE between A and graphite was determined to be 87.86 kJ/mol which was reported to be close to 97.45 kJ/mol obtained from TDS [77].

Ramraj et al. employed PM3-D, the dispersion-corrected version of the semi-empirical PM3 method, to study the interaction of nucleobases with graphene and CNTs in vacuum [99]. $C_{24}H_{12}$, $C_{54}H_{18}$ and $C_{96}H_{24}$ as three fragments of graphene and two model CNTs with chiralities of (6,6) and (5,0) were considered. Only one IC was used for each system, and it was generated by placing the center of the ring, in the case of pyrimidine bases (C, T and U), or the center of the bridging bond, in the case of purine bases (A and G), above a central carbon atom. Geometry optimizations and BE calculation were performed from such configuration. Table 2.12 shows the BE for all systems. For both graphene and CNT, the order of the BE was determined to be G>A>T>C>U, which is in agreement with results reported by Antony and Grimme [90] and Le et al. [92] on graphene, as well as the results of Gowtham et al. [79] on (5,0) CNT. The effect of curvature is clear from Table 2.12, where the BE is larger for graphene than for CNT, and the smallest CNT, (5,0), has the lowest BE. Such a trend was observed in many earlier QM-level studies and was attributed to the smaller area of contact associated with smaller tubes. In the same work, dispersion-corrected DFT methods were used for $C_{96}H_{24}$ to verify the accuracy of the semi-empirical method. The optimized geometries from the semi-empirical method were used for the DFT BE calculations. The results are shown in Table 2.13 for the four different methods used: M05-2X, M06-2X, B97-D/TZ(2d,2p) and DFT-D. Data

from the PM3-D method were found to be close to those generated using DFT-D and B97-D/TZ(2d,2p), with the same order of BE and similar magnitude for the BE values. M05-2X and M06-2X, on the other hand, predicted much smaller BEs and its order changed to G>T>C>A>U using M05-2X and G>T>A>C>U using M06-2X.

Table 2.12: BE (kJ/mol) between nucleobases and fragments of graphene and CNT using PM3-D method in Ref. [99]

Nucleobase	$C_{24}H_{12}$	$C_{54}H_{18}$	$C_{96}H_{24}$	(6,6) CNT	(5,0) CNT
G	74.94	92.11	95.88	70.34	56.10
A	67.41	84.15	87.92	64.06	54.85
T	66.57	76.20	77.46	56.94	49.40
C	61.55	72.85	72.85	50.24	46.06
U	54.01	61.13	62.80	44.80	39.36

Table 2.13: BE (kJ/mol) between nucleobases and $C_{96}H_{24}$ fragment of graphene in Ref. [99], evaluated using different method.

Nucleobase	B97-D/TZV(2d,2p)	DFT-D	M05-2X	M06-2X
G	101.32	96.30	52.34	74.11
A	84.57	80.39	37.68	57.78
T	79.55	74.94	41.03	58.62
C	77.46	71.18	40.19	56.94
U	68.24	61.96	36.01	51.50

Umadevi and Sastry further explored the effect of the curvature by considering the binding of nucleobases with graphene and a series of armchair (n,n) CNTs where n=3, 4 and 5 [100]. The graphene and CNTs were all finite with H atoms used to saturate the dangling bonds at the boundaries. Each system was optimized using ONIOM method at the (M06-2X/6-31G(d):AM1) level. Atoms in the nucleobases and the "reacting atoms" of CNTs were modeled as the high layer using M06-2X/6-31G(d), although it was not clearly explained what carbon atoms were considered to be reacting. The remaining atoms in CNT were considered as the low layer using semi-empirical AM1. Single point energy calculations were performed for the optimized structures using the dispersion-corrected B3LYP method (B3LYP-D) with the 6-31G(d) basis set. The BE was found to be graphene>(5,5) CNT>(4,4) CNT>(3,3) CNT for all nucleobases except T, for which the order was graphene>(5,5) CNT>(3,3) CNT>(4,4) CNT. The BSSE-corrected BE was 30-51 kJ/mol for CNTs and 50-73 kJ/mol for graphene. The order of the BE with respect to different nucleobases was determined to be G>T∼A>C>U for the CNTs and G>A>T>C>U for the graphene. The order for graphene is in agreement with a number of studies, for example Gowtham et al. [78] using LDA and Ramraj et al. [99] using semi-empirical PM3. It should be noted that the semi-empirical AM1 method used to treat non-interacting carbon atoms in the CNT is not dispersion-corrected. BE between T and (3,3) CNT was found to be greater than that between T and (4,4) CNT, which is contrary to the effect of curvature observed for other nucleobases. The only other work that reported decreasing BE with increasing CNT diameter was by Wang and Ceulemans [83] for the adsorption of adenosine-monophosphates on CNTs. However, in that study, the opposing trend was observed for zigzag (n,0) CNTs; for armchair CNTs BE still increased

with increasing CNT diameter.

In another study performed using ONIOM, Sarmah and Roy [101] studied the interaction of nucleobases with semiconducting CNTs. Similar to the models studied by Gowtham et al. [78, 79], nucleobases were capped with a methyl group. CNTs with different chiralities, (7,5), (7,6), (8,3) and (9,2), were considered, and each had a finite length. The QM region included nucleobase and four hexagonal rings of carbon atoms on CNT; the rest of atoms in CNT were considered as the MM region. Figure 2.6 shows the QM and MM regions on the (7,5) CNT. The CNTs and nucleobases were first independently optimized at B3LYP/6-31G(d) level; then the nucleobase-CNT hybrids were optimized at ONIOM (B3LYP/6-31G(d):UFF) level, after which the BEs were calculated. The optimized binding structures are shown in Figure 2.6, where it is clear that not all the nucleobases formed parallel stacking with the CNT surface. On the other hand, the reported BE values were significantly larger than any other works and covered a range of 38.33 to 2316.30 kJ/mol. The order of the BE with respect to the five nucleobases is shown in Table 2.14. Similar to most other studies, U was found to have the smallest BE and G had the largest BE except for the (8,3) CNT in which G had smaller BE than A, C and T. Among the four types of CNTs, the (8,3) tube was found to have smallest BEs, which was attributed to its smaller diameter compared to other CNTs. However, BEs for the (7,6) CNT were also determined to be smaller than those for (7,5) and (9,2) tubes, although the (7,6) CNT has larger diameter than the other two. Similar behavior was also reported by Umadevi and Sastry [100] as well as Wang and Ceulemans [83], but a clear explanation has not been available. It is worth noting that only a small number of carbon atoms on the CNTs were included in the QM region. More importantly, the functional used

for the QM region, B3LYP, is known to predict unphysical binding structure (e.g., detachment) for systems involving π-π attractions. Also, UFF [182], which was used to treat the MM region, has been reported to be inaccurate FF [183].

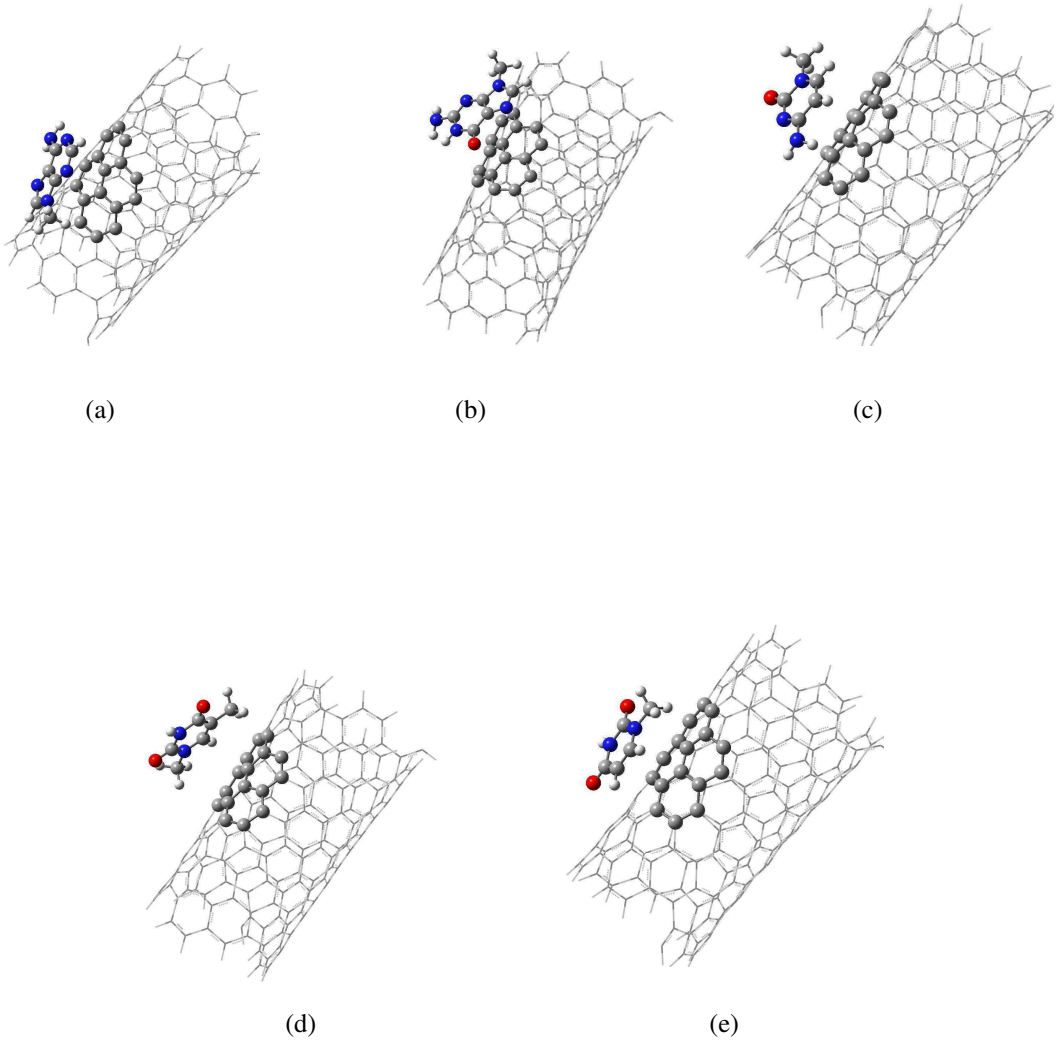

Figure 2.6: Optimized structures in Ref. [101] for the binding of nucleobases to a (7,5) CNT: (a) A, (b) G, (c) C, (d) T, and (e) U (reproduced with permission from Ref. [101]). All atoms in the nucleobases are modeled at the QM level and the CNT atoms in the QM region are highlighted.

Table 2.14: Order of the BE between nucleobases and CNTs in Ref. [101]

Chirality of SWCNT	Order
(7,5)	G>A∼T>C∼U
(7,6)	G>A>T∼C∼U
(8,3)	A>T>C>G>U
(9,2)	G>T>C>A>U

The computational efficiency associated with lower level methods has allowed some studies to be performed in solution. Specifically, Varghese et al. studied the interaction of DNA nucleobases with graphene in vacuum and in solution [76]. A graphene sheet with 20 hexagons was considered without PBC and all nucleobases were aligned parallel to the graphene surface in the ICs. Two completely different methods were used for optimization and BE calculation: HF with 6-31G(d,p) basis set (without dispersion correction) vs. Amber FF calculation (with empirical potential for dispersion). A large difference was observed for the results from the two methods. For example, the BE of A with graphene was found to be 5.78 kJ/mol using HF and 74.32 kJ/mol using Amber FF. 8212 Due to the large contribution of vdW interaction to the BE, only the vdW energy, obtained using Amber, was considered for the BE. The BE calculated this way was found to be 79.97, 74.32, 69.63 and 60.79 kJ/mol respectively for G, A, T and C. The order, G>A>T>C, is in agreement with the ones obtained by Antony and Grimme [90], Le et al. [92] and Cho et al. [93] using dispersion corrected DFT approaches. To evaluate the BEs in solution, no further optimizations were performed. Instead, the BEs in vacuum were adjusted by adding to them the solvation energies calcu-

lated using the Amber Generalized Born (GB) model where the solvent is modeled as a continuum with dielectric properties of water. The BEs in solution were determined to be 63.22, 61.96, 61.76 and 33.20 kJ/mol respectively for G, A, T and C. Hence the BE values decreased after adding the solution and the reduction was most significant for C. On the other hand, the same order for the BE was obtained in solution, i.e., G>A>T>C.

Das et al. calculated the BE between DNA nucleobases and a (5,5) CNT with the finite length of 10 Å in both vacuum and water [75]. Several different approaches were used for the simulations in vacuum. To start, they used restricted open shell Hartree-Fock (ROHF) method with 6-31G(d,p) basis set to perform geometry optimizations for each nucleobase from two different initial configurations: one with the nucleobase parallel to the CNT and the other with the nucleobase perpendicular to the CNT. The final optimized configurations were shown to be the same, which was different from Wang and Bu's result [84]. The ROHF BEs for the optimized structures were 6.75, 3.86, 2.89, 1.93 kJ/mol respectively for C, G, A and T, with the order of C>G>A>T. These values were at least one order of magnitude smaller than the ones obtained in other studies reviewed earlier, proving the inadequate performance of the HF method in modeling π-π stacking systems due to its lack of dispersion interaction. Also, G was found to have lower BE to the CNT compared with C, which was not reported elsewhere. Next, the authors used DFT at B3LYP/6-31G(d,p) level to optimize the structure and calculate the BE of C to the CNT. The same small BE was obtained, i.e., 6.75 kJ/mol, due to the lack of dispersion correction in B3LYP. To include the vdW interaction, optimization at MM level were then performed using MSC [184] and AMBER FFs. The vdW energy was calculated after the optimization and added

to the BE calculated using HF method. According to their results, both MSC and AMBER FFs led to the same values for the vdW energy. The order of the BE obtained using this approach was G>A>T>C with the values of 52.10, 49.21, 45.35 and 37.63 kJ/mol. Comparing these values with those obtained using HF or DFT (B3LYP) reveals the importance of dispersive vdW forces in the interaction of nucleobases with CNT. This order of BE is in agreement with the results for the same (5,5) CNT obtained by Wang [85]. To obtain the BEs in water, an approach similar to that of Varghese et al. was employed. Poisson-Boltzmann continuum model was used for the solvent. Optimized structures obtained in vacuum were adopted without further optimization, and the BE was evaluated at the HF/6-31G(d,p) level in presence of the implicit solvent. Using this approach, the order of the BE changed to G>T>A>C with the values of 55.00, 49.21, 47.28 and 28.95 kJ/mol, which differed from the work of Wang [85] but was shown to be in agreement with their experimental result i.e., T>A>C. The BE for T increased upon the addition of solution, which was opposite to Varghese et al. [76]. For G, A and C, the BE decreased in the aqueous environment, but the extent of reduction was not as severe as in the work of Varghese et al. [76]. In both studies, the BEs in solution were calculated based on structures optimized in vacuum. In addition, the solution was treated using continuum models. Full optimization in explicit solvent may lead to very different binding structures compared with those optimized in vacuum, but such simulations are still too time-consuming at the QM or even semi-empirical level.

In an MD work, Frischknecht and Martin studied the adsorption of nucleotide monophospahtes (NMPs) on a (6,0) CNT in solution [103]. Two simulations were performed for each nucleotide-CNT system: one with only two Na^+ ions for neu-

tralization (Case 1) and the other with 10 Na^+ and 8 Cl^- ions (Case 2). PBC was applied and CHARMM FF with modified parameters was used in order to more accurately describe the non-bonded interactions between water molecules and the CNT [185]. Table 2.15 shows the average BEs. For case 1, the order of the BE was determined to be A>T>C∼G>U while it was completely different for case 2, being T>C>U>A>G. This implies that screening ions may have a large impact on the interactions of charged NMPs with CNT. Interestingly, G was more weakly bound to the CNT compared to other DNA nucleobases, which is drastically different from the results obtained by Enyashin et al. [95] on nucleotide-graphene binding in vacuum.

Table 2.15: BE (kJ/mol) between nucleotides and a (6,0) CNT in Ref. [103]

NMP	BE	
	Case 1	Case 2
A	43.10	20.08
C	20.92	23.43
G	20.92	17.99
T	22.18	28.87
U	1.67	19.66

In a study using statistical mechanical theory of molecular liquids (3D-RISM) [186], Yamazaki and Fenniri evaluated the BEs between nucleobases and CNT in water [117]. Three CNTs with the chiralities of (7,0), (11,0) and (15,0) were considered. Amber FF was employed to model nucleobases. The same order, i.e., G>A>T>C was obtained for all three CNTs. This is in agreement with the re-

sults of Das et al. [75] and Varghese et al. [76] from Amber FF simulations. Not surprisingly, CNTs with larger diameters were found to bind more strongly to the nucleobases.

While graphene or CNTs in all studies reviewed so far were neutral, Lv studied interactions of nucleobases with both neutral and charged (8,8) CNTs in solution using MD [104]. PBC was applied and Amber FF with a modification on the carbon-water vdW potential [187] was used to perform the simulations. Both positively and negatively charged CNTs with charge densities varying from ± 0.01 to ± 0.05 *e*/C were considered and localized partial charges were assigned to each carbon atom. The whole system was then neutralized by adding counterions (Na^+ or Cl^-) to the solution. For the neutral CNT, the order of the binding free energy was found to be G>A>T>C, similar to previously reported results obtained using MM method [75, 76, 117]. For charged CNTs, their results showed that increasing charge density made the adsorption of nucleobases less stable specially when the charge density exceeded 0.03 *e*/C. This was possibly due to the fact that vdW attractive energy decreased as the charge density of the CNT increased and a sharp change was observed at the charge density of 0.03 *e*/C.

2.4 Discussion

Both experimental and computational studies have been carried out on the adsorption of nucleobases on graphene or CNT. This chapter presents a comprehensive review of past computational work, where three categories of methods have been used: (1) first-principles studies based on methods lacking dispersion correction, (2) first-principles studies based on dispersion-corrected methods and (3) studies

based on semi-empirical and FF methods. The reviewed efforts are summarized in Figure 2.7 and categorized based on the method and CNT diameter, where graphene is considered as a CNT with infinite diameter. Studies that included aqueous solution are indicated by *. It is clear from Figure 2.7 that most work has been performed for nucleobase-graphene system using dispersion-corrected first-principles approaches. In addition, the majority did not include solution and were performed in vacuum. Those few studies that considered solution were carried out using either first-principles approaches without dispersion correction, FF or semi-empirical methods.

Diameter	First-principles studies based on methods lacking dispersion correction	First-principles studies based on dispersion-corrected methods	Studies based on force-field and semi-empirical methods
Graphene	Ortmann *et al.*, 2005 Gowtham *et al.*, 2007 Lee *et al.*, 2007	Ortmann *et al.*, 2005 Enyashin *et al.*, 2007 Antony and Grimme, 2008 Berland *et al.*, 2011 Le *et al.*, 2012 Panigrahi *et al.*, 2012 Vovusha *et al.*, 2013 Cho *et al.*, 2013 Lee *et al.*, 2013 Chandara Shekar and Swathi, 2014	Edelwirth *et al.*, 1998 Varghase *et al.*, 2009 * Umadevi and Sastry, 2011
0.7-1.4 nm	Meng *et al.*, 2007a Wang, 2008 * Wang and Ceulemans, 2009 Shtogun *et al.*, 2013	Stepanian *et al.*, 2008 Ramraj *et al.*, 2010 Akdim *et al.*, 2012	Meng *et al.*, 2007b Ramraj *et al.*, 2010 Lv, 2011 * Yamazaki and Feniri, 2012 * Sarmah and Roy, 2013
< 0.7 nm	Wang and Bu, 2007 Gowtham *et al.*, 2008 Wang, 2008 * Wang and Ceulemans, 2009 Shtogun *et al.*, 2013	Stepanian *et al.*, 2008 Shukla *et al.*, 2009 Ramraj *et al.*, 2010 Chehel Amirani *et al.*, 2013	Frischknecht and Martin, 2008 * Das *et al.*, 2008 * Ramraj *et al.*, 2010 Umadevi and Sastry, 2011 Yamazaki and Feniri, 2012 *

Method

Figure 2.7: Categorization of past computational studies based on method and CNT diameter. Graphene can be considered as a CNT with infinite diameter. Works that involve aqueous solution are indicated by *.

In nearly all studies reviewed above, the nucleobases were found to be paral-

lel to the graphene or CNT with the separation distance being around 3 Å, which confirms the π-π stacking nature of the interaction. On the other hand, drastically different results have been reported for the BE. All calculated BEs for nucleobase-graphene system are depicted in Figure 2.8. Results obtained using different categories of methods are shown in different sub-figures. Data reported by the same authors using the same method are connected to show the trends. With the same method, G was typically found to have the largest BE while U had the smallest BE. The order of the BE for the other nucleobases (A, T and C), on the other hand, is not very clear and a universal trend cannot be determined. Since different methods were used, the BE values cover a large range, which is [13.51, 115.78] kJ/mol, [5.79, 109.99] kJ/mol, [7.72, 91.66] kJ/mol, [12.54, 93.59] kJ/mol and [11.92, 71.4] kJ/mol, respectively for G, A, T, C and U. First principle studies based on dispersion-corrected methods tend to predict higher BEs compared to methods in the other two categories.

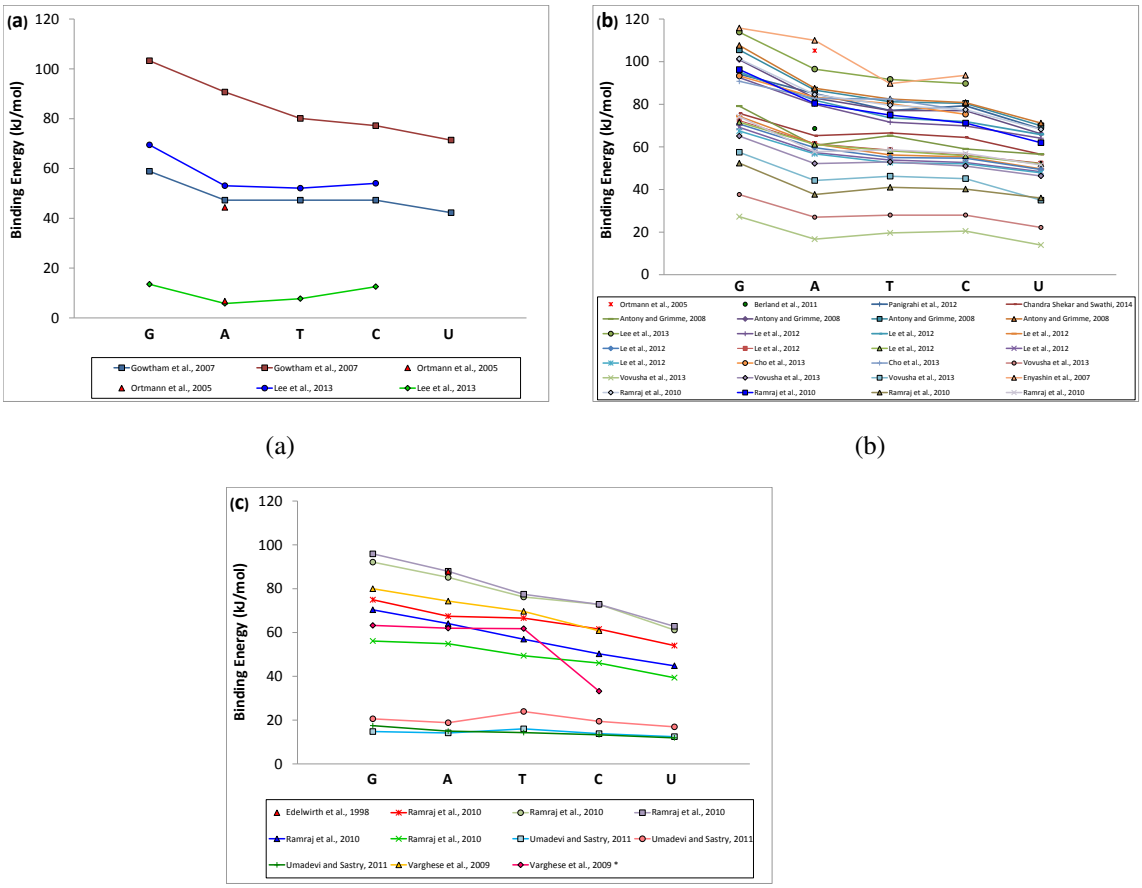

Figure 2.8: Reported BEs for nucleobase-graphene systems: (a) First-principles studies based on methods lacking dispersion correction, (b) First-principles studies based on dispersion-corrected methods and (c) Studies based on force-field and semi-empirical methods. Data reported by the same authors using the same method are connected. There may be multiple curves corresponding to the same reference because the authors of that reference have used different methods to evaluate the BE. Works that involve aqueous solution are indicated by *.

Figure 2.9 shows the reported values for the BE between nucleobases and CNT. Only two references reviewed earlier are excluded from this figure: Wang and Ceulemans, 2009 where two interconnected nucleotides were simulated leading to much larger BE than single nucleobases; and Sarmah and Roy, 2013 where

the reported BEs were significantly higher than other studies. Including these two references would make other data in Figure 2.9 indistinguishable. The horizontal axis corresponds to CNT diameter; and results obtained using different categories of methods are indicted by different symbols. Data from the same work calculated using the same method but on CNTs with different diameters are connected with a line. Most past works simulated CNTs with diameters less than 9 Å. As the CNT diameter increases, higher BEs are usually observed when the same method is used for the calculation, although the opposite trend was shown by Wang [85] in solution. Examining the BE obtained using the same method at the same CNT diameter, again G typically possesses the highest BE among the 5 nucleobases while U has the smallest BE. Compared to graphene, smaller BEs have been generally predicted for nucleobase-CNT system. Similar to graphene, considerably different BEs have been reported. The ranges for the works shown in Figure 2.9 are respectively [3.86, 87.76] kJ/mol, [2.89, 78.15] kJ/mol, [1.93, 74.29] kJ/mol, [5.02, 67.54] kJ/mol and [1.67, 44.8] kJ/mol for G, A, T, C and U, while including the work of Wang and Ceulemans, 2009 as well as Sarmah and Roy, 2013 extended the ranges to [3.86, 2316.30] kJ/mol, [2.89, 1211.44] kJ/mol, [1.93, 1333.65] kJ/mol, [5.02, 1261.35] kJ/mol and [1.67, 1099.72] kJ/mol, respectively for G, A, T, C and U. Unlike graphene, the studies based on dispersion-corrected methods (indicated by $\triangle$) do not necessarily predict higher BEs compared with methods in the other two categories.

According to the BEs summarized in Table 1 and depicted in Figures 2.8 and 2.9, there are discrepancies among the data both qualitatively and quantitatively. Even for the same nucleobase and similar CNTs the BE could be very different (e.g., [80, 81]). Several factors contribute to such discrepancies, such as

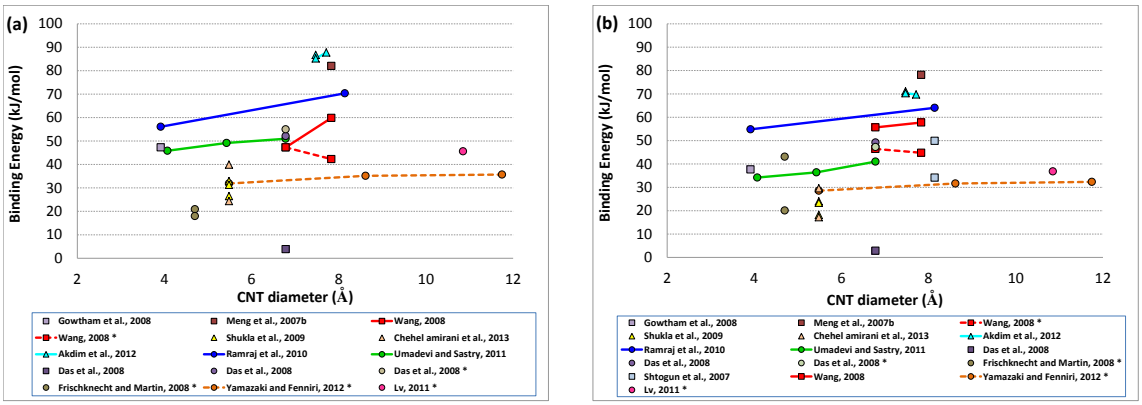

(a) G

(b) A

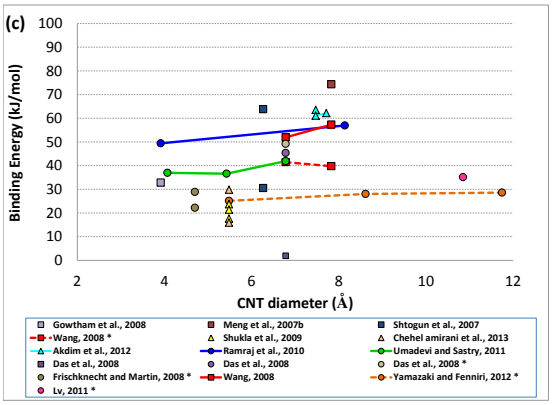

(c) T

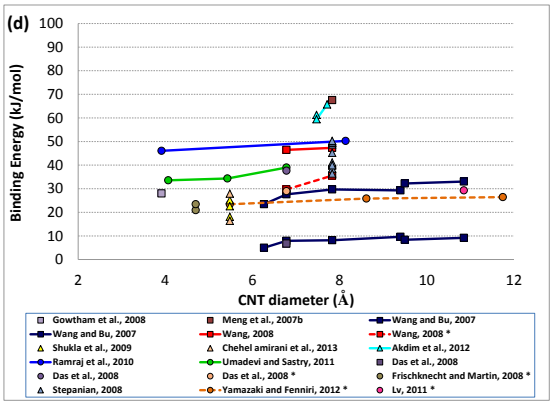

(d) C

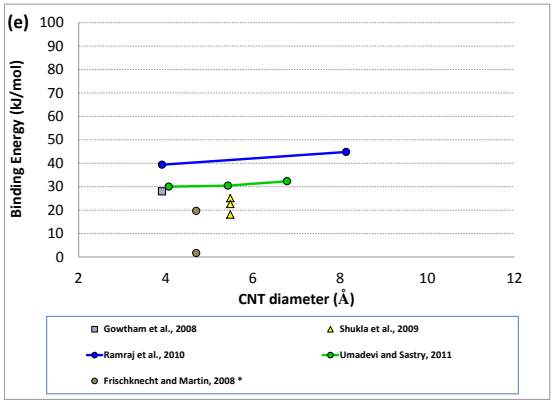

(e) U

Figure 2.9: Reported BEs for nucleobase-CNT systems: (a) G, (b) A, (c) T, (d) C, (e) U; First-principles studies based on methods lacking dispersion correction are indicated by □; First-principles studies based on dispersion-corrected methods are indicated by △; Studies based on force-field and semi-empirical methods are indicated by ◯. BEs in the same study and using the same method but for CNTs with different diameters are connected with lines; works that involve aqueous solution are indicated by *.

the difference in simulated systems, method used for the simulations, optimization procedures, and IC of the nucleobases relative to the graphene or CNT.

The first factor is the difference in simulated systems. In terms of nucleobases, in most cases bare neutral nucleobases were considered, while in some studies a methyl group was attached to the nucleobases [78, 79]. In a few works, nucleotides, nucleobases attached to a sugar ring and phosphate group, were simulated. The addition of methyl or phosphate groups results in structures that are not as flat as nucleobases, which can affect the optimized geometries and BEs. In terms of CNT, it has been clearly shown in many studies that CNT diameter has a direct effect on the BE: larger diameter usually results in higher BE value. Even for CNTs with equal diameter, their BEs can differ due to the different structures (chiralities) they have [85]. CNT length can also affect BE values. While some studies employed PBC, others were done for a short CNT terminated with hydrogen. Edge effect can play a role in determining the optimized structure and BE.

Different methods adopted in previous studies have strong influences on the BE results. Some studies used structures optimized from MM force field to perform BE calculations at the QM level. There can be considerable difference between the structures obtained from MM optimization and those obtained from QM optimization. Earlier QM simulations on this topic typically used DFT without dispersion correction in the optimization step and/or in the BE calculation. LDA approach was one of the most frequently used methods, but no dispersion treatment was done for LDA. B3LYP, as another commonly used functional, has poor performance in treating π-π stacked systems. In fact, it often predicts repulsive behaviour for π-π systems and nucleobases will detach from graphene or

CNT instead of being attracted to it if optimization is done using B3LYP. Recent works using dispersion-corrected DFT also gave rise to different results, possibly due to the different ways in incorporating dispersion interaction in these methods. Even with the same method, the choice of basis sets can affect the BE evaluation [97]. In addition, it has been shown that BSSE can be large and has to be taken into account [188]. Performance of simulation methods and basis set are still being widely evaluated in the computational chemistry community. For instance, GMTKN30 database for general main group thermochemistry, kinetics and noncovalent interactions is being used to carry out benchmarking studies and compare performance of different dispersion-corrected methods [189]. Other methods are also being explored, for example, long-range correction schemes in DFT (LC functional) [190] and joint DFT (JDFT) [191].

Optimization procedure also plays an important role in BE calculations for these weakly bound systems where the PES is expected to be quite flat with many local minima [80, 81]. Direct optimization may lead the system to a nearby local minimum, but not necessarily the global minimum. Therefore, the optimization can be very sensitive to the IC chosen to do the simulation. In fact, it has been shown that different ICs result in very different BE values and can even change the order of the BE corresponding to different nucleobases [102]. On the other hand, the effect of IC was not carefully considered in most of the past works. A majority of them used a single IC to do the optimization, and ICs in many previous studies were not clearly specified or explained. There were only a few works that explored the effect of the ICs by examining the BE associated with different ICs.

One way to reduce the effect of IC is to perform a PES scan, which was done in some past studies. In particular, the PES was scanned by placing the nucleobases

at different positions relative to the graphene or CNT, and the position that resulted in the highest BE was considered the optimal position. Definition of these relative positions is crucial in achieving good quality for the PES scan. Also, in such PES scan, the nucleobases and graphene or CNT are essentially treated as rigid bodies, i.e., the internal degrees of freedom are neglected. This may not be appropriate for larger molecules such as nucleotides and long CNTs. An additional optimization step after the PES scan can help relaxing the internal structures. To reduce computational cost, selected atoms were frozen in some studies (e.g., the CNT), which can introduce error in the optimization.

With the growth in computing power and the development in computing methodology, it is expected that many limitations that we are facing now can be removed or reduced, bringing the simulated DNA-CNT system closer to reality. Of particular interest is the effect of CNT chirality on the properties of the hybrid. Previous QM calculations on BE already showed some effects of CNT chirality [98], however it is not yet clear whether such effects are correlated with the electronic structure of the CNT. When a finite CNT is simulated instead of PBC, the electronic structure of the CNT may not be properly captured.

Another extension of the past studies is the inclusion of electrolytic solution. Due to the high computational cost associated with simulating water, the majority of theoretical studies have been done in vacuum. Solution was only considered in a few works, but with very approximate continuum models. In addition, usually no further optimization was done in solution, structures optimized in vacuum were simply adopted to do BE calculations in solution [75]. Including explicit water and ions in the QM optimization is still a challenge.

All studies reviewed in this work simulated only one or two nucleobases, while

practically it is more interesting to consider the hybridization of DNA polymer with CNT or graphene. When DNA polymer rather than monomer is considered, additional effects can play role in its binding. For example, in the case of homopolymer DNA binding to CNT, the backbone elasticity can influence the wrapping of DNA around CNT. Such elasticity may arise from the intrinsic bending and torsion rigidity of the backbone as well as from the electrostatic repulsion among the charges located on the backbone [21, 58, 108, 119, 192]. Homopolymer-graphene binding can also be affected by backbone elasticity, as well as steric interaction among the nucleobases [193, 194]. In the situation where CNT or graphene binds to a DNA polymer with certain sequence, the hydrogen bonding between complementary nucleobases is an additional factor that can contribute to the stability of the hybridization [113, 195, 196]. Past DNA polymer simulations were almost exclusively based on MD, which included some of the factors mentioned, but at the same time lacked important considerations such as the proper treatment of CNT's electronic structure. More accurate models that represent the DNA-CNT or DNA-graphene systems are still in demand.

Furthermore, it is important to point out that the binding of DNA with CNT or graphene under room temperature is a dynamic process. The thermal motion was completed neglected in QM optimization performed at 0 K. The BE difference between different nucleobases was sometimes found to be on the order of the thermal energy at room temperature (2.5 kJ/mol). Therefore, including dynamics can lead to quite different answers to the relative binding strength, and is worth exploring.

In parallel to theoretical efforts that aim at modeling larger and more realistic systems, it is also important to continue experimental development that can allow

more direct comparison with simulation results. Currently, little such comparison can be made between theoretical and experimental works due to the large discrepancies between the systems studied using the two approaches. Since the majority of reviewed computational works was on nucleobases, it would be helpful to have more experiments on the binding of single nucleobases rather than DNA polymers. Also, considering the computational limitations in simulating binding in solution, it would be favorable to have some experiments performed in vacuum to facilitate the comparison. In addition, as it is more feasible to simulate graphene in the theoretical work, experimental measurement on a single layer graphene sheet instead of graphite would be beneficial.

Finally, we mention that BE has been used as the main parameter for comparisons made in this review. Other properties such as charge transfer and density of states have only been reported in some ($<$50%) of the cited works and hence are not suitable for systematic comparison. Also, the calculation of charge transfer does not only depend on the QM method (e.g., choice of functional and basis set in DFT analysis), but also on the charge distribution scheme (e.g., Mulliken, ESP, RESP, etc) [197], which makes the comparison among different studies more complicated. Exploring the method-dependence of charge evaluation is interesting, but is out of the scope of this review.

2.5 Conclusion

In this work, we performed a thorough review on the theoretical studies, mainly at the QM level, on the binding of nucleobases (and in a few cases, nucleosides or nucleotides) with graphene or CNT. BE, as an indicator for the stability of the bind-

ing, was used to compare different studies. Due to the difference in simulated systems, simulation method and procedure, a large range of BE values were reported, and considerable discrepancies exist among the past investigations. Through the review, we highlight the importance of using dispersion-corrected method and proper design of the optimization procedure to account for the shallow PES wells. Care should always be taken in interpreting the simulations results. In the next chapter, the effect of the initial configuration as one of the reasons of discrepancies in binding structures and energy will be studied in detail.

References

[1] S. Iijima, "Helical microtubules of graphitic carbon," *Nature*, vol. 354, pp. 56–58, 1991.

[2] S. Akita, H. Nishijima, Y. Nakayama, F. Tokumasu, and K. Takeyasu, "Carbon nanotube tips for a scanning probe microscope: their fabrication and properties," *Journal of Physics D: Applied Physics*, vol. 32, no. 9, p. 1044, 1999.

[3] R. H. Baughman, A. A. Zakhidov, and W. A. de Heer, "Carbon Nanotubes–the Route Toward Applications," *Science*, vol. 297, no. 5582, pp. 787–792, 2002.

[4] R. H. Baughman, C. Cui, A. A. Zakhidov, Z. Iqbal, J. N. Barisci, G. M. Spinks, G. G. Wallace, A. Mazzoldi, D. De Rossi, A. G. Rinzler, O. Jaschinski, S. Roth, and M. Kertesz, "Carbon Nanotube Actuators," *Science*, vol. 284, no. 5418, pp. 1340–1344, 1999.

[5] T. Zhang, S. Mubeen, N. V. Myung, and M. A. Deshusses, "Recent progress in carbon nanotube-based gas sensors," *Nanotechnology*, vol. 19, no. 33, p. 332001, 2008.

[6] M. Zhang, S. Fang, A. A. Zakhidov, S. B. Lee, A. E. Aliev, C. D. Williams, K. R. Atkinson, and R. H. Baughman, "Strong, Transparent, Multifunctional, Carbon Nanotube Sheets," *Science*, vol. 309, no. 5738, pp. 1215–1219, 2005.

[7] R. Saito, G. Dresselhaus, and M. Dresselhaus, *Physical Properties of Carbon Nanotube*. Imperial College Press, 1998.

[8] A. Krishnan, E. Dujardin, T. W. Ebbesen, P. N. Yianilos, and M. M. J. Treacy, "Young's modulus of single-walled nanotubes," *Phys. Rev. B*, vol. 58, pp. 14013–14019, 1998.

[9] S. Xiao and W. Hou, "Studies of Size Effects on Carbon Nanotubes' Mechanical Properties by Using Different Potential Functions," *Fullerenes, Nanotubes and Carbon Nanostructures*, vol. 14, no. 1, pp. 9–16, 2006.

[10] B. WenXing, Z. ChangChun, and C. WanZhao, "Simulation of Young's modulus of single-walled carbon nanotubes by molecular dynamics," *Physica B: Condensed Matter*, vol. 352, no. 1–4, pp. 156–163, 2004.

[11] M. Meo and M. Rossi, "Prediction of Young's modulus of single wall carbon nanotubes by molecular-mechanics based finite element modelling," *Composites Science and Technology*, vol. 66, no. 11–12, pp. 1597–1605, 2006.

[12] A. M. Marconnet, M. A. Panzer, and K. E. Goodson, "Thermal conduction phenomena in carbon nanotubes and related nanostructured materials," *Rev. Mod. Phys.*, vol. 85, pp. 1295–1326, 2013.

[13] M. S. Dresselhaus, G. Dresselhaus, J. C. Charlier, and E. Hernández, "Electronic, thermal and mechanical properties of carbon nanotubes," *Philosophical Transactions of the Royal Society of London. Series A: Mathematical, Physical and Engineering Sciences*, vol. 362, no. 1823, pp. 2065–2098, 2004.

[14] A. A. Balandin, "Thermal Properties of Graphene, Carbon Nanotubes and Nanostructured Carbon Materials," *Nature Materials*, vol. 10, pp. 569–581, 2011.

[15] H. Hu, Y. Ni, V. Montana, R. C. Haddon, and V. Parpura, "Chemically Functionalized Carbon Nanotubes as Substrates for Neuronal Growth," *Nano Letters*, vol. 4, no. 3, pp. 507–511, 2004.

[16] C. B. Jacobs, M. J. Peairs, and B. J. Venton, "Review: Carbon nanotube based electrochemical sensors for biomolecules," *Analytica Chimica Acta*, vol. 662, no. 2, pp. 105–127, 2010.

[17] C. Dwyer, M. Guthold, M. Falvo, S. Washburn, R. Superfine, and D. Erie, "DNA-functionalized single-walled carbon nanotubes," *Nanotechnology*, vol. 13, no. 5, p. 601, 2002.

[18] K. Balasubramanian and M. Burghard, "Chemically Functionalized Carbon Nanotubes," *Small*, vol. 1, no. 2, pp. 180–192, 2005.

[19] S. Banerjee, T. Hemraj-Benny, and S. S. Wong, "Covalent Surface Chemistry of Single-Walled Carbon Nanotubes," *Advanced Materials*, vol. 17, no. 1, pp. 17–29, 2005.

[20] R. J. Chen, S. Bangsaruntip, K. A. Drouvalakis, N. Wong Shi Kam, M. Shim, Y. Li, W. Kim, P. J. Utz, and H. Dai, "Noncovalent functionalization of carbon nanotubes for highly specific electronic biosensors," *Proceedings of the National Academy of Sciences*, vol. 100, no. 9, pp. 4984–4989, 2003.

[21] M. Zheng, A. Jagota, E. D. Semke, B. A. Diner, R. S. Mclean, S. R. Lustig, R. E. Richardson, and N. G. Tassi, "DNA-assisted dispersion and separation of carbon nanotubes," *Nat Mater*, vol. 2, no. 5, pp. 338–342, 2003.

[22] E. Katz and I. Willner, "Biomolecule-Functionalized Carbon Nanotubes: Applications in Nanobioelectronics," *ChemPhysChem*, vol. 5, no. 8, pp. 1084–1104, 2004.

[23] F. Fang and H. Choi, "Noncovalent self-assembly of carbon nanotube wrapped carbonyl iron particles and their magnetorheology," *Journal of Applied Physics*, vol. 103, no. 7, pp. 07A301–07A301–3, 2008.

[24] H. Gao, Y. Kong, D. Cui, and C. S. Ozkan, "Spontaneous Insertion of DNA Oligonucleotides into Carbon Nanotubes," *Nano Letters*, vol. 3, no. 4, pp. 471–473, 2003.

[25] J. V. Veetil and K. Ye, "Development of Immunosensors Using Carbon Nanotubes," *Biotechnology Progress*, vol. 23, no. 3, pp. 517–531, 2007.

[26] Y.-B. Zhang, M. Kanungo, A. J. Ho, P. Freimuth, D. van der Lelie, M. Chen, S. M. Khamis, S. S. Datta, A. T. C. Johnson, J. A. Misewich, and S. S. Wong, "Functionalized Carbon Nanotubes for Detecting Viral Proteins," *Nano Letters*, vol. 7, no. 10, pp. 3086–3091, 2007.

[27] A. Hirsch, "Functionalization of Single-Walled Carbon Nanotubes," *Angewandte Chemie International Edition*, vol. 41, no. 11, pp. 1853–1859, 2002.

[28] M. S. Strano, C. A. Dyke, M. L. Usrey, P. W. Barone, M. J. Allen, H. Shan, C. Kittrell, R. H. Hauge, J. M. Tour, and R. E. Smalley, "Electronic Structure Control of Single-Walled Carbon Nanotube Functionalization," *Science*, vol. 301, no. 5639, pp. 1519–1522, 2003.

[29] Y. Wang, Z. Iqbal, and S. Mitra, "Microwave-induced rapid chemical functionalization of single-walled carbon nanotubes," *Carbon*, vol. 43, no. 5, pp. 1015–1020, 2005.

[30] Y.-P. Sun, K. Fu, Y. Lin, and W. Huang, "Functionalized Carbon Nanotubes: Properties and Applications," *Accounts of Chemical Research*, vol. 35, no. 12, pp. 1096–1104, 2002.

[31] M. Prato, K. Kostarelos, and A. Bianco, "Functionalized Carbon Nanotubes in Drug Design and Discovery," *Accounts of Chemical Research*, vol. 41, no. 1, pp. 60–68, 2008.

[32] J. L. Bahr and J. M. Tour, "Highly Functionalized Carbon Nanotubes Using in Situ Generated Diazonium Compounds," *Chemistry of Materials*, no. 11, pp. 3823–3824, 2001.

[33] T. Ramanathan, F. T. Fisher, R. S. Ruoff, and L. C. Brinson, "Amino-Functionalized Carbon Nanotubes for Binding to Polymers and Biological Systems," *Chemistry of Materials*, vol. 17, no. 6, pp. 1290–1295, 2005.

[34] J. L. Bahr, J. Yang, D. V. Kosynkin, M. J. Bronikowski, R. E. Smalley, and J. M. Tour, "Functionalization of Carbon Nanotubes by Electrochemical Reduction of Aryl Diazonium Salts: A Bucky Paper Electrode," *Journal of the American Chemical Society*, vol. 123, no. 27, pp. 6536–6542, 2001.

[35] V. Georgakilas, K. Kordatos, M. Prato, D. M. Guldi, M. Holzinger, and A. Hirsch, "Organic Functionalization of Carbon Nanotubes," *Journal of the American Chemical Society*, vol. 124, no. 5, pp. 760–761, 2002.

[36] J. Chen, H. Liu, W. A. Weimer, M. D. Halls, D. H. Waldeck, and G. C. Walker, "Noncovalent Engineering of Carbon Nanotube Surfaces by Rigid, Functional Conjugated Polymers," *Journal of the American Chemical Society*, vol. 124, no. 31, pp. 9034–9035, 2002.

[37] D. Pantarotto, C. D. Partidos, R. GraffH, J. Hoebeke, J.-P. Briand, M. Prato, and A. Bianco, "Synthesis, Structural Characterization, and Immunological Properties of Carbon Nanotubes Functionalized with Peptides," *Journal of the American Chemical Society*, vol. 125, no. 20, pp. 6160–6164, 2003.

[38] Y. Lin, A. M. Rao, B. Sadanadan, E. A. Kenik, and Y.-P. Sun, "Functionalizing Multiple-Walled Carbon Nanotubes with Aminopolymers," *The Journal of Physical Chemistry B*, vol. 106, no. 6, pp. 1294–1298, 2002.

[39] M. Shim, N. W. Shi Kam, R. J. Chen, Y. Li, and H. Dai, "Functionalization

of Carbon Nanotubes for Biocompatibility and Biomolecular Recognition," *Nano Letters*, vol. 2, no. 4, pp. 285–288, 2002.

[40] P. Qi, O. Vermesh, M. Grecu, A. Javey, Q. Wang, H. Dai, S. Peng, and K. J. Cho, "Toward Large Arrays of Multiplex Functionalized Carbon Nanotube Sensors for Highly Sensitive and Selective Molecular Detection," *Nano Letters*, vol. 3, no. 3, pp. 347–351, 2003.

[41] R. Rastogi, N. Dhindsa, C. R. Suri, B. Pant, S. Tripathi, I. Kaur, and L. M. Bharadwaj, "Interfacing of {DNA} with carbon nanotubes for nanodevice applications ," *Materials Chemistry and Physics*, vol. 135, no. 2–3, pp. 268 – 276, 2012.

[42] S. R. Shin, C. K. Lee, I. S. So, J. H. Jeon, T. M. Kang, C. W. Kee, S. I. Kim, G. M. Spinks, G. G. Wallace, and S. J. Kim, "DNA-Wrapped Single-Walled Carbon Nanotube Hybrid Fibers for supercapacitors and Artificial Muscles," *Advanced Materials*, vol. 20, no. 3, pp. 466–470, 2008.

[43] C. M. Arnett, C. P. Marsh, C. R. Welch, M. S. Strano, J.-H. Han, J. H. Gray, and T. A. Carlson, "Enzyme-Mediated Assimilation of DNA-Functionalized Single-Walled Carbon Nanotubes," *Langmuir*, vol. 26, no. 2, pp. 613–617, 2010.

[44] J. N. Barisci, M. Tahhan, G. G. Wallace, S. Badaire, T. Vaugien, M. Maugey, and P. Poulin, "Properties of Carbon Nanotube Fibers Spun from DNA-Stabilized Dispersions," *Advanced Functional Materials*, vol. 14, no. 2, pp. 133–138, 2004.

[45] R. Yang, Z. Tang, J. Yan, H. Kang, Y. Kim, Z. Zhu, and W. Tan, "Noncovalent Assembly of Carbon Nanotubes and Single-Stranded DNA: An Effective Sensing Platform for Probing Biomolecular Interactions," *Analytical Chemistry*, vol. 80, no. 19, pp. 7408–7413, 2008.

[46] K. A. Williams, P. T. M. Veenhuizen, B. G. de la Torre, R. Eritja, and C. Dekker, "Towards DNA-Mediated Self Assembly of Carbon Nanotube Molecular Devices," *AIP Conference Proceedings*, vol. 633, no. 1, pp. 444–448, 2002.

[47] H. Wang, N. B. Muren, D. Ordinario, A. A. Gorodetsky, J. K. Barton, and C. Nuckolls, "Transducing methyltransferase activity into electrical signals in a carbon nanotube-DNA device," *Chem. Sci.*, vol. 3, pp. 62–65, 2012.

[48] P. K. Brahman, R. A. Dar, and K. S. Pitre, "DNA-functionalized electrochemical biosensor for detection of vitamin {B1} using electrochemically treated multiwalled carbon nanotube paste electrode by voltammetric methods ," *Sensors and Actuators B: Chemical*, vol. 177, no. 0, pp. 807 – 812, 2013.

[49] P. Singh, J. Kumar, F. M. Toma, J. Raya, M. Prato, B. Fabre, S. Verma, and A. Bianco, "Synthesis and characterization of nucleobase-carbon nanotube hybrids," *Journal of the American Chemical Society*, vol. 131, no. 37, pp. 13555–13562, 2009.

[50] D. A. Yarotski, S. V. Kilina, A. A. Talin, S. Tretiak, O. V. Prezhdo, A. V. Balatsky, and A. J. Taylor, "Scanning Tunneling Microscopy of DNA-Wrapped Carbon Nanotubes," *Nano Letters*, vol. 9, no. 1, pp. 12–17, 2009.

[51] X. Qiu, C. Y. Khripin, F. Ke, S. C. Howell, and M. Zheng, "Electrostatically Driven Interactions between Hybrid DNA-Carbon Nanotubes," *Phys. Rev. Lett.*, vol. 111, p. 048301, 2013.

[52] S. S. Kim, C. L. Hisey, Z. Kuang, D. A. Comfort, B. L. Farmer, and R. R. Naik, "The effect of single wall carbon nanotube metallicity on genomic DNA-mediated chirality enrichment," *Nanoscale*, vol. 5, pp. 4931–4936, 2013.

[53] R. Singh, D. Pantarotto, D. McCarthy, O. Chaloin, J. Hoebeke, C. D. Partidos, J.-P. Briand, M. Prato, A. Bianco, and K. Kostarelos, "Binding and Condensation of Plasmid DNA onto Functionalized Carbon Nanotubes: Toward the Construction of Nanotube-Based Gene Delivery Vectors," *Journal of the American Chemical Society*, vol. 127, no. 12, pp. 4388–4396, 2005.

[54] C. Hu, Y. Zhang, G. Bao, Y. Zhang, M. Liu, and Z. L. Wang, "DNA Functionalized Single-Walled Carbon Nanotubes for Electrochemical Detection," *The Journal of Physical Chemistry B*, vol. 109, no. 43, pp. 20072–20076, 2005.

[55] Y. Ma, S. R. Ali, A. S. Dodoo, and H. He, "Enhanced Sensitivity for Biosensors: Multiple Functions of DNA-Wrapped Single-Walled Carbon Nanotubes in Self-Doped Polyaniline Nanocomposites," *The Journal of Physical Chemistry B*, vol. 110, no. 33, pp. 16359–16365, 2006.

[56] P. He and M. Bayachou, "Layer-by-Layer Fabrication and Characterization

of DNA-Wrapped Single-Walled Carbon Nanotube Particles," *Langmuir*, vol. 21, no. 13, pp. 6086–6092, 2005.

[57] Y. Xu, P. E. Pehrsson, L. Chen, R. Zhang, and W. Zhao, "Double-Stranded DNA Single-Walled Carbon Nanotube Hybrids for Optical Hydrogen Peroxide and Glucose Sensing," *The Journal of Physical Chemistry C*, vol. 111, no. 24, pp. 8638–8643, 2007.

[58] M. Zheng, A. Jagota, M. S. Strano, A. P. Santos, P. Barone, S. G. Chou, B. A. Diner, M. S. Dresselhaus, R. S. Mclean, G. B. Onoa, G. G. Samsonidze, E. D. Semke, M. Usrey, and D. J. Walls, "Structure-Based Carbon Nanotube Sorting by Sequence-Dependent DNA Assembly," *Science*, vol. 302, no. 5650, pp. 1545–1548, 2003.

[59] S. Kilina, D. A. Yarotski, A. A. Talin, S. Tretiak, A. J. Taylor, and A. V. Balatsky, "Unveiling Stability Criteria of DNA-Carbon Nanotubes Constructs by Scanning Tunneling Microscopy and Computational Modeling," *Journal of Drug Delivery*, vol. 2011, 2011.

[60] M. Allen, M. Balooch, S. Subbiah, R. Tench, W. Siekhaus, and R. Balhorn, "Scanning Tunneling Microscope Images of Adenine and Thymine at Atomic Resolution," *Scanning Microsc*, vol. 5, no. 3, pp. 625–630, 1991.

[61] W. M. Heckl, D. P. Smith, G. Binnig, H. Klagges, T. W. Hänsch, and J. Maddocks, "Two-Dimensional Ordering of the DNA Base Guanine Observed by Scanning Tunneling Microscopy," *Proc. Natl. Acad. Sci. U. S. A.*, vol. 88, no. 18, pp. 8003–8005, 1991.

[62] N. J. Tao and Z. Shi, "Monolayer Guanine and Adenine on Graphite in NaCl Solution: A Comparative STM and AFM Study," *The Journal of Physical Chemistry*, vol. 98, no. 5, pp. 1464–1471, 1994.

[63] J. E. Freund, M. Edelwirth, P. Kröbel, and W. M. Heckl, "Structure determination of two-dimensional adenine crystals on graphite," *Phys. Rev. B*, vol. 55, pp. 5394–5397, 1997.

[64] R. Srinivasan, J. Murphy, R. Fainchtein, and N. Pattabiraman, "Electrochemical STM of condensed guanine on graphite ," *Journal of Electroanalytical Chemistry and Interfacial Electrochemistry*, vol. 312, no. 1–2, pp. 293 – 300, 1991.

[65] R. Srinivasan, J. Murphy, and N. Pattabiraman, "STM observations of two-dimensional condensed layers on solid electrodes ," *Ultramicroscopy*, vol. 42–44, Part 1, no. 0, pp. 453 – 459, 1992.

[66] R. Srinivasan and P. Gopalan, "Order and stability of an electrochemically condensed adenine layer on graphite," *The Journal of Physical Chemistry*, vol. 97, no. 34, pp. 8770–8775, 1993.

[67] S. Sowerby, W. Heckl, and G. Petersen, "Chiral symmetry breaking during the self-assembly of monolayers from achiral purine molecules," *Journal of Molecular Evolution*, vol. 43, no. 5, pp. 419–424, 1996.

[68] S. J. Sowerby and G. B. Petersen, "Scanning tunneling microscopy of uracil monolayers self-assembled at the solid|liquid interface ," *Journal of Electroanalytical Chemistry*, vol. 433, no. 1–2, pp. 85 – 90, 1997.

[69] S. Sowerby, M. Edelwirth, and W. Heckl, "Molecular mechanics simulation of uracil adlayers on molybdenum disulfide and graphite surfaces," *Applied Physics A*, vol. 66, no. 1, pp. S649–S653, 1998.

[70] S. J. Sowerby, M. Edelwirth, and W. M. Heckl, "Self-Assembly at the Prebiotic Solid-Liquid Interface: Structures of Self-Assembled Monolayers of Adenine and Guanine Bases Formed on Inorganic Surfaces," *The Journal of Physical Chemistry B*, vol. 102, no. 30, pp. 5914–5922, 1998.

[71] S. Sowerby and W. Heckl, "The Role of Self-Assembled Monolayers of the Purine and Pyrimidine Bases in the Emergence of Life," *Origins of life and evolution of the biosphere*, vol. 28, no. 3, pp. 283–310, 1998.

[72] S. Sowerby, P. Stockwell, W. Heckl, and G. Petersen, "Self-programmable, Self-assembling Two-dimensional Genetic Matter," *Origins of life and evolution of the biosphere*, vol. 30, no. 1, pp. 81–99, 2000.

[73] S. J. Sowerby, C. A. Cohn, W. M. Heckl, and N. G. Holm, "Differential adsorption of nucleic acid bases: Relevance to the origin of life," *Proceedings of the National Academy of Sciences*, vol. 98, no. 3, pp. 820–822, 2001.

[74] T. Uchihashi, T. Okada, Y. Sugawara, K. Yokoyama, and S. Morita, "Self-assembled monolayer of adenine base on graphite studied by noncontact atomic force microscopy," *Phys. Rev. B*, vol. 60, pp. 8309–8313, 1999.

[75] A. Das, A. Sood, P. K. Maiti, M. Das, R. Varadarajan, and C. Rao, "Binding of nucleobases with single-walled carbon nanotubes: Theory and experiment," *Chemical Physics Letters*, vol. 453, no. 4–6, pp. 266–273, 2008.

[76] N. Varghese, U. Mogera, A. Govindaraj, A. Das, P. K. Maiti, A. K. Sood, and C. N. R. Rao, "Binding of DNA Nucleobases and Nucleosides with Graphene," *ChemPhysChem*, vol. 10, no. 1, pp. 206–210, 2009.

[77] J. E. Freund, . PhD thesis, Ludwig-Maximilians-Universität, München, 1998.

[78] S. Gowtham, R. H. Scheicher, R. Ahuja, R. Pandey, and S. P. Karna, "Physisorption of nucleobases on graphene: Density-functional calculations," *Phys. Rev. B*, vol. 76, p. 033401, 2007.

[79] S. Gowtham, R. H. Scheicher, R. Pandey, S. P. Karna, and R. Ahuja, "First-principles study of physisorption of nucleic acid bases on small-diameter carbon nanotubes," *Nanotechnology*, vol. 19, no. 12, p. 125701, 2008.

[80] S. Meng, P. Maragakis, C. Papaloukas, and E. Kaxiras, "DNA Nucleoside Interaction and Identification with Carbon Nanotubes," *Nano Letters*, vol. 7, no. 1, pp. 45–50, 2007.

[81] S. Meng, W. L. Wang, P. Maragakis, and E. Kaxiras, "Determination of DNA-Base Orientation on Carbon Nanotubes through Directional Optical Absorbance," *Nano Letters*, vol. 7, no. 8, pp. 2312–2316, 2007.

[82] Y. V. Shtogun, L. M. Woods, and G. I. Dovbeshko, "Adsorption of Adenine and Thymine and Their Radicals on Single-Wall Carbon Nanotubes," *The Journal of Physical Chemistry C*, vol. 111, no. 49, pp. 18174–18181, 2007.

[83] H. Wang and A. Ceulemans, "Physisorption of adenine DNA nucleosides

on zigzag and armchair single-walled carbon nanotubes: A first-principles study," *Phys. Rev. B*, vol. 79, p. 195419, 2009.

[84] Y. Wang and Y. Bu, "Noncovalent Interactions between Cytosine and SWCNT," *The Journal of Physical Chemistry B*, vol. 111, no. 23, pp. 6520–6526, 2007.

[85] Y. Wang, "Theoretical Evidence for the Stronger Ability of Thymine to Disperse SWCNT than Cytosine and Adenine: Self-Stacking of DNA Bases vs Their Cross-Stacking with SWCNT," *The Journal of Physical Chemistry C*, vol. 112, no. 37, pp. 14297–14305, 2008.

[86] F. Ortmann, W. G. Schmidt, and F. Bechstedt, "Attracted by Long-Range Electron Correlation: Adenine on Graphite," *Phys. Rev. Lett.*, vol. 95, p. 186101, 2005.

[87] K. Berland, S. D. Chakarova-Käck, V. R. Cooper, D. C. Langreth, and E. Schröder, "A van der Waals density functional study of adenine on graphene: single-molecular adsorption and overlayer binding," *Journal of Physics: Condensed Matter*, vol. 23, no. 13, p. 135001, 2011.

[88] S. Panigrahi, A. Bhattacharya, S. Banerjee, and D. Bhattacharyya, "Interaction of Nucleobases with Wrinkled Graphene Surface: Dispersion Corrected DFT and AFM Studies," *The Journal of Physical Chemistry C*, vol. 116, no. 7, pp. 4374–4379, 2012.

[89] S. Chandra Shekar and R. S. Swathi, "Stability of nucleobases and base pairs adsorbed on graphyne and graphdiyne," *The Journal of Physical Chemistry C*, vol. 118, no. 8, pp. 4516–4528, 2014.

[90] J. Antony and S. Grimme, "Structures and interaction energies of stacked graphene-nucleobase complexes," *Phys. Chem. Chem. Phys.*, vol. 10, pp. 2722–2729, 2008.

[91] J.-H. Lee, Y.-K. Choi, H.-J. Kim, R. H. Scheicher, and J.-H. Cho, "Physisorption of DNA Nucleobases on h-BN and Graphene: vdW-Corrected DFT Calculations," *The Journal of Physical Chemistry C*, vol. 117, no. 26, pp. 13435–13441, 2013.

[92] D. Le, A. Kara, E. Schröder, P. Hyldgaard, and T. S. Rahman, "Physisorption of nucleobases on graphene: a comparative van der Waals study," *Journal of Physics: Condensed Matter*, vol. 24, no. 42, p. 424210, 2012.

[93] Y. Cho, S. K. Min, J. Yun, W. Y. Kim, A. Tkatchenko, and K. S. Kim, "Noncovalent Interactions of DNA Bases with Naphthalene and Graphene," *Journal of Chemical Theory and Computation*, vol. 9, no. 0, pp. 2090–2096, 2013.

[94] H. Vovusha, S. Sanyal, and B. Sanyal, "Interaction of nucleobases and aromatic amino acids with graphene oxide and graphene flakes," *The Journal of Physical Chemistry Letters*, vol. 4, no. 21, pp. 3710–3718, 2013.

[95] A. N. Enyashin, S. Gemming, and G. Seifert, "DNA-wrapped carbon nanotubes," *Nanotechnology*, vol. 18, no. 24, p. 245702, 2007.

[96] S. Stepanian, M. Karachevtsev, A. Glamazda, V. Karachevtsev, and L. Adamowicz, "Stacking interaction of cytosine with carbon nanotubes: MP2, DFT and Raman spectroscopy study," *Chemical Physics Letters*, vol. 459, no. 1–6, pp. 153–158, 2008.

[97] M. Shukla, M. Dubey, E. Zakar, R. Namburu, Z. Czyznikowska, and J. Leszczynski, "Interaction of nucleic acid bases with single-walled carbon nanotube," *Chemical Physics Letters*, vol. 480, no. 4–6, pp. 269–272, 2009.

[98] B. Akdim, R. Pachter, P. N. Day, S. S. Kim, and R. R. Naik, "On modeling biomolecular–surface nonbonded interactions: application to nucleobase adsorption on single-wall carbon nanotube surfaces," *Nanotechnology*, vol. 23, no. 16, p. 165703, 2012.

[99] A. Ramraj, I. H. Hillier, M. A. Vincent, and N. A. Burton, "Assessment of approximate quantum chemical methods for calculating the interaction energy of nucleic acid bases with graphene and carbon nanotubes," *Chemical Physics Letters*, vol. 484, no. 4–6, pp. 295–298, 2010.

[100] D. Umadevi and G. N. Sastry, "Quantum Mechanical Study of Physisorption of Nucleobases on Carbon Materials: Graphene versus Carbon Nanotubes," *The Journal of Physical Chemistry Letters*, vol. 2, no. 13, pp. 1572–1576, 2011.

[101] A. Sarmah and R. K. Roy, "Understanding the interaction of nucleobases with chiral semiconducting single-walled carbon nanotubes: An alternative theoretical approach based on density functional reactivity theory," *The Journal of Physical Chemistry C*, vol. 117, no. 41, pp. 21539–21550, 2013.

[102] M. Chehel Amirani, T. Tang, and J. Cuervo, "Quantum mechanical treatment of binding energy between DNA nucleobases and carbon nanotube: A

DFT analysis," *Physica E: Low-dimensional Systems and Nanostructures*, vol. 54, pp. 65–71, 2013.

[103] A. L. Frischknecht and M. G. Martin, "Simulation of the adsorption of nucleotide monophosphates on carbon nanotubes in aqueous solution," *The Journal of Physical Chemistry C*, vol. 112, no. 16, pp. 6271–6278, 2008.

[104] W. Lv, "The adsorption of DNA bases on neutral and charged (8, 8) carbon-nanotubes," *Chemical Physics Letters*, vol. 514, no. 4–6, pp. 311 – 316, 2011.

[105] Zhao and J. K. Johnson, "Simulation of Adsorption of DNA on Carbon Nanotubes," *Journal of the American Chemical Society*, vol. 129, no. 34, pp. 10438–10445, 2007.

[106] R. R. Johnson, A. T. C. Johnson, and M. L. Klein, "Probing the Structure of DNA-Carbon Nanotube Hybrids with Molecular Dynamics," *Nano Letters*, vol. 8, no. 1, pp. 69–75, 2008.

[107] R. R. Johnson, A. T. C. Johnson, and M. L. Klein, "The Nature of DNA-Base–Carbon-Nanotube Interactions," *Small*, vol. 6, no. 1, pp. 31–34, 2010.

[108] S. Manohar, T. Tang, and A. Jagota, "Structure of Homopolymer DNA-CNT Hybrids," *The Journal of Physical Chemistry C*, vol. 111, no. 48, pp. 17835–17845, 2007.

[109] D. Roxbury, A. Jagota, and J. Mittal, "Sequence-Specific Self-Stitching Motif of Short Single-Stranded DNA on a Single-Walled Carbon Nan-

otube," *Journal of the American Chemical Society*, vol. 133, no. 34, pp. 13545–13550, 2011.

[110] X. Zhao, "Self-Assembly of DNA Segments on Graphene and Carbon Nanotube Arrays in Aqueous Solution: A Molecular Simulation Study," *The Journal of Physical Chemistry C*, vol. 115, no. 14, pp. 6181–6189, 2011.

[111] Z. Xiao, X. Wang, X. Xu, H. Zhang, Y. Li, and Y. Wang, "Base- and Structure-Dependent DNA Dinucleotide–Carbon Nanotube Interactions: Molecular Dynamics Simulations and Thermodynamic Analysis," *The Journal of Physical Chemistry C*, vol. 115, no. 44, pp. 21546–21558, 2011.

[112] S. Neihsial, G. Periyasamy, P. K. Samanta, and S. K. Pati, "Understanding the Binding Mechanism of Various Chiral SWCNTs and ssDNA: A Computational Study," *The Journal of Physical Chemistry B*, vol. 116, no. 51, pp. 14754–14759, 2012.

[113] D. Roxbury, A. Jagota, and J. Mittal, "Structural Characteristics of Oligomeric DNA Strands Adsorbed onto Single-Walled Carbon Nanotubes," *The Journal of Physical Chemistry B*, vol. 117, no. 1, pp. 132–140, 2013.

[114] A. K. Manna and S. K. Pati, "Theoretical understanding of single-stranded DNA assisted dispersion of graphene," *J. Mater. Chem. B*, vol. 1, pp. 91–100, 2013.

[115] W. Martin, W. Zhu, and G. Krilov, "Simulation Study of Noncovalent Hybridization of Carbon Nanotubes by Single-Stranded DNA in Water," *The Journal of Physical Chemistry B*, vol. 112, no. 50, pp. 16076–16089, 2008.

[116] J. Zou, W. Liang, and S. Zhang, "Coarse-grained molecular dynamics modeling of DNA–carbon nanotube complexes," *International Journal for Numerical Methods in Engineering*, vol. 83, no. 8-9, pp. 968–985, 2010.

[117] T. Yamazaki and H. Fenniri, "Imaging carbon nanotube interaction with nucleobases in water using the statistical mechanical theory of molecular liquids," *The Journal of Physical Chemistry C*, vol. 116, no. 28, pp. 15087–15092, 2012.

[118] O. Malysheva, T. Tang, and P. Schiavone, "Binding Force Between a Charged Wall and a Complex Formed by a Polyelectrolyte and an Electronically Responsive Cylinder," *The Journal of Adhesion*, vol. 87, no. 3, pp. 251–271, 2011.

[119] S. R. Lustig, A. Jagota, C. Khripin, and M. Zheng, "Theory of Structure-Based Carbon Nanotube Separations by Ion-Exchange Chromatography of DNA/CNT Hybrids," *The Journal of Physical Chemistry B*, vol. 109, no. 7, pp. 2559–2566, 2005.

[120] C. Sun and T. Tang, "Structure of a polyelectrolyte around an electronically responsive cylinder," *Journal of Colloid and Interface Science*, vol. 338, no. 1, pp. 276 – 283, 2009.

[121] M. Zheng, K. Eom, and C. Ke, "Calculations of the resonant response of carbon nanotubes to binding of DNA," *Journal of Physics D: Applied Physics*, vol. 42, no. 14, 2009.

[122] P. Debye and E. Hückel, "The theory of electrolytes. i. lowering of freezing

point and related phenomena," *Physikalische Zeitschrift*, vol. 24, pp. 185–206, 1923.

[123] M. Edelwirth, J. Freund, S. Sowerby, and W. Heckl, "Molecular mechanics study of hydrogen bonded self-assembled adenine monolayers on graphite ," *Surface Science*, vol. 417, no. 2–3, pp. 201 – 209, 1998.

[124] C. Møller and M. S. Plesset, "Note on an approximation treatment for many-electron systems," *Phys. Rev.*, vol. 46, pp. 618–622, 1934.

[125] M. Head-Gordon, J. A. Pople, and M. J. Frisch, "{MP2} energy evaluation by direct methods," *Chemical Physics Letters*, vol. 153, no. 6, pp. 503 – 506, 1988.

[126] M. J. S. Dewar, E. G. Zoebisch, E. F. Healy, and J. J. P. Stewart, "Development and use of quantum mechanical molecular models. 76. am1: a new general purpose quantum mechanical molecular model," *Journal of the American Chemical Society*, vol. 107, no. 13, pp. 3902–3909, 1985.

[127] J. J. P. Stewart, "Optimization of parameters for semiempirical methods i. method," *Journal of Computational Chemistry*, vol. 10, no. 2, pp. 209–220, 1989.

[128] J. J. P. Stewart, "Optimization of parameters for semiempirical methods ii. applications," *Journal of Computational Chemistry*, vol. 10, no. 2, pp. 221–264, 1989.

[129] J. J. P. Stewart, "Optimization of parameters for semiempirical methods. iii extension of pm3 to be, mg, zn, ga, ge, as, se, cd, in, sn, sb, te, hg, tl, pb,

and bi," *Journal of Computational Chemistry*, vol. 12, no. 3, pp. 320–341, 1991.

[130] J. Stewart, "Optimization of parameters for semiempirical methods v: Modification of nddo approximations and application to 70 elements," *Journal of Molecular Modeling*, vol. 13, no. 12, pp. 1173–1213, 2007.

[131] P. Hohenberg and W. Kohn, "Inhomogeneous electron gas," *Phys. Rev.*, vol. 136, pp. B864–B871, 1964.

[132] W. Kohn and L. J. Sham, "Self-consistent equations including exchange and correlation effects," *Phys. Rev.*, vol. 140, pp. A1133–A1138, 1965.

[133] J. P. Perdew, K. Burke, and M. Ernzerhof, "Generalized gradient approximation made simple," *Phys. Rev. Lett.*, vol. 77, pp. 3865–3868, 1996.

[134] E. R. Johnson, R. A. Wolkow, and G. A. DiLabio, "Application of 25 density functionals to dispersion-bound homomolecular dimers," *Chemical Physics Letters*, vol. 394, no. 4–6, pp. 334–338, 2004.

[135] E. R. Johnson, I. D. Mackie, and G. A. DiLabio, "Dispersion interactions in density-functional theory," *Journal of Physical Organic Chemistry*, vol. 22, no. 12, pp. 1127–1135, 2009.

[136] L. R. Rutledge, H. F. Durst, and S. D. Wetmore, "Evidence for Stabilization of DNA/RNA Protein Complexes Arising from Nucleobase Amino Acid Stacking and T-Shaped Interactions," *Journal of Chemical Theory and Computation*, vol. 5, no. 5, pp. 1400–1410, 2009.

[137] L. R. Rutledge and S. D. Wetmore, "The assessment of density functionals for DNAprotein stacked and T-shaped complexes," *Canadian Journal of Chemistry*, vol. 88, no. 8, pp. 815–830, 2010.

[138] Y. Zhao and D. G. Truhlar, "Benchmark databases for nonbonded interactions and their use to test density functional theory," *Journal of Chemical Theory and Computation*, vol. 1, no. 3, pp. 415–432, 2005.

[139] Y. Zhao and D. G. Truhlar, "Applications and validations of the Minnesota density functionals," *Chemical Physics Letters*, vol. 502, no. 1–3, pp. 1–13, 2011.

[140] E. Meijer and M. Sprik, "A density-functional study of the intermolecular interactions of benzene," *Journal of Chemical Physics*, vol. 105, no. 19, pp. 8684–8689, 1996.

[141] A. Tkatchenko and M. Scheffler, "Accurate Molecular Van Der Waals Interactions from Ground-State Electron Density and Free-Atom Reference Data," *Phys. Rev. Lett.*, vol. 102, p. 073005, 2009.

[142] S. Grimme, "Accurate description of van der Waals complexes by density functional theory including empirical corrections," *Journal of Computational Chemistry*, vol. 25, no. 12, pp. 1463–1473, 2004.

[143] S. Grimme, "Semiempirical GGA-type density functional constructed with a long-range dispersion correction," *Journal of Computational Chemistry*, vol. 27, no. 15, pp. 1787–1799, 2006.

[144] S. Grimme, J. Antony, S. Ehrlich, and H. Krieg, "A consistent and accurate

ab initio parametrization of density functional dispersion correction (DFT-D) for the 94 elements H-Pu," *The Journal of Chemical Physics*, vol. 132, no. 15, p. 154104, 2010.

[145] S. Ehrlich, J. Moellmann, and S. Grimme, "Dispersion-Corrected Density Functional Theory for Aromatic Interactions in Complex Systems," *Accounts of Chemical Research*, vol. 46, no. 4, pp. 916–926, 2013.

[146] S. Grimme and M. Steinmetz, "Effects of London dispersion correction in density functional theory on the structures of organic molecules in the gas phase," *Phys. Chem. Chem. Phys.*, pp. 16031–16042, 2013.

[147] S. Grimme, "Density functional theory with London dispersion corrections," *Wiley Interdisciplinary Reviews: Computational Molecular Science*, vol. 1, no. 2, pp. 211–228, 2011.

[148] J. Gräfenstein and D. Cremer, "An efficient algorithm for the density-functional theory treatment of dispersion interactions.," *Journal of Chemical Physics*, vol. 130, no. 12, p. 124105, 2009.

[149] J. Seponer, J. Leszczynski, and P. Hobza, "Base stacking in cytosine dimer. A comparison of correlated ab initio calculations with three empirical potential models and density functional theory calculations," *Journal of Computational Chemistry*, vol. 17, no. 7, pp. 841–850, 1996.

[150] N. Kurita and H. Sekino, "Ab initio and {DFT} studies for accurate description of van der Waals interaction between He atoms," *Chemical Physics Letters*, vol. 348, no. 1–2, pp. 139–146, 2001.

[151] M. Dion, H. Rydberg, E. Schröder, D. C. Langreth, and B. I. Lundqvist, "Van der Waals Density Functional for General Geometries," *Phys. Rev. Lett.*, vol. 92, p. 246401, 2004.

[152] P. Jurečka, J. Černý, P. Hobza, and D. R. Salahub, "Density functional theory augmented with an empirical dispersion term. Interaction energies and geometries of 80 noncovalent complexes compared with ab initio quantum mechanics calculations.," *Journal of Computational Chemistry*, vol. 28, no. 2, pp. 555–569, 2007.

[153] O. A. von Lilienfeld, I. Tavernelli, U. Rothlisberger, and D. Sebastiani, "Optimization of Effective Atom Centered Potentials for London Dispersion Forces in Density Functional Theory," *Phys. Rev. Lett.*, vol. 93, p. 153004, 2004.

[154] S. Kristyán and P. Pulay, "Can (semi)local density functional theory account for the London dispersion forces?," *Chemical Physics Letters*, vol. 229, no. 3, pp. 175–180, 1994.

[155] R. O. Jones and O. Gunnarsson, "The density functional formalism, its applications and prospects," *Rev. Mod. Phys.*, vol. 61, pp. 689–746, 1989.

[156] N. Park, S. Lim, G. Kim, and S.-H. Jhi, "Calculation of Hydrogen Physisorption Affinity to Graphene Species with Ab-Intio and Density-Functional Methods ," *Journal of the Korean Physical Society*, vol. 53, no. 23, pp. 691–694, 2008.

[157] A. Tkatchenko, J. Robert A. DiStasio, M. Head-Gordon, and M. Scheffler, "Dispersion-corrected M[o-slash]ller–Plesset second-order perturba-

tion theory," *The Journal of Chemical Physics*, vol. 131, no. 9, p. 094106, 2009.

[158] P. Hobza, H. L. Selzle, and E. W. Schlag, "Potential Energy Surface for the Benzene Dimer. Results of ab Initio CCSD(T) Calculations Show Two Nearly Isoenergetic Structures: T-Shaped and Parallel-Displaced," *The Journal of Physical Chemistry*, vol. 100, no. 48, pp. 18790–18794, 1996.

[159] S. Tsuzuki, T. Uchimaru, K. Matsumura, M. Mikami, and K. Tanabe, "Effects of the higher electron correlation correction on the calculated intermolecular interaction energies of benzene and naphthalene dimers: comparison between {MP2} and CCSD(T) calculations," *Chemical Physics Letters*, vol. 319, no. 5–6, pp. 547–554, 2000.

[160] R. L. Jaffe and G. D. Smith, "A quantum chemistry study of benzene dimer," *The Journal of Chemical Physics*, vol. 105, no. 7, pp. 2780–2788, 1996.

[161] B. Brooks, R. Bruccoleri, D. Olafson, D. States, S. Swaminathan, and M. Karplus, "Charmm: A program for macromolecular energy, minimization, and dynamics calculations," *Journal of Computational Chemistry*, vol. 4, pp. 187–217, 1983.

[162] A. MacKerel Jr., C. Brooks III, L. Nilsson, B. Roux, Y. Won, and M. Karplus, *CHARMM: The Energy Function and Its Parameterization with an Overview of the Program*, vol. 1 of *The Encyclopedia of Computational Chemistry*, pp. 271–277. John Wiley & Sons: Chichester, 1998.

[163] J. H. Walther, R. Jaffe, T. Halicioglu, and P. Koumoutsakos, "Carbon nanotubes in water: Structural characteristics and energetics," *The Journal of Physical Chemistry B*, vol. 105, no. 41, pp. 9980–9987, 2001.

[164] V. Barone and M. Cossi, "Quantum calculation of molecular energies and energy gradients in solution by a conductor solvent model," *The Journal of Physical Chemistry A*, vol. 102, no. 11, pp. 1995–2001, 1998.

[165] E. G. Hohenstein, S. T. Chill, and C. D. Sherrill, "Assessment of the Performance of the M055-2X and M06-2X Exchange-Correlation Functionals for Noncovalent Interactions in Biomolecules," *Journal of Chemical Theory and Computation*, vol. 4, no. 12, pp. 1996–2000, 2008.

[166] Y. Zhao and D. G. Truhlar, "Density functionals with broad applicability in chemistry," *Accounts of Chemical Research*, vol. 41, no. 2, pp. 157–167, 2008.

[167] Y. Zhao, N. E. Schultz, and D. G. Truhlar, "Exchange-correlation functional with broad accuracy for metallic and nonmetallic compounds, kinetics, and noncovalent interactions," *The Journal of Chemical Physics*, vol. 123, no. 16, pp. 1–4, 2005.

[168] Y. Zhao, N. E. Schultz, and D. G. Truhlar, "Design of density functionals by combining the method of constraint satisfaction with parametrization for thermochemistry, thermochemical kinetics, and noncovalent interactions," *Journal of Chemical Theory and Computation*, vol. 2, no. 2, pp. 364–382, 2006.

[169] Y. Zhao and D. Truhlar, "The M06 suite of density functionals for main group thermochemistry, thermochemical kinetics, noncovalent interactions, excited states, and transition elements: two new functionals and systematic testing of four M06-class functionals and 12 other functionals," *Theoretical Chemistry Accounts*, vol. 120, no. 1-3, pp. 215–241, 2008.

[170] Y. Zhao and D. G. Truhlar, "Density Functional for Spectroscopy: No Long-Range Self-Interaction Error, Good Performance for Rydberg and Charge-Transfer States, and Better Performance on Average than B3LYP for Ground States," *The Journal of Physical Chemistry A*, vol. 110, no. 49, pp. 13126–13130, 2006.

[171] Y. Zhao and D. G. Truhlar, "A new local density functional for main-group thermochemistry, transition metal bonding, thermochemical kinetics, and noncovalent interactions," *The Journal of Chemical Physics*, vol. 125, no. 19, p. 194101, 2006.

[172] S. Grimme, S. Ehrlich, and L. Goerigk, "Effect of the damping function in dispersion corrected density functional theory," *Journal of Computational Chemistry*, vol. 32, no. 7, pp. 1456–1465, 2011.

[173] K. Lee, É. D. Murray, L. Kong, B. I. Lundqvist, and D. C. Langreth, "Higher-accuracy van der Waals density functional," *Phys. Rev. B*, vol. 82, p. 081101, 2010.

[174] E. Torres and G. A. DiLabio, "A (nearly) universally applicable method for modeling noncovalent interactions using b3lyp," *The Journal of Physical Chemistry Letters*, vol. 3, no. 13, pp. 1738–1744, 2012.

[175] J. P. Perdew and Y. Wang, "Accurate and simple analytic representation of the electron-gas correlation energy," *Phys. Rev. B*, vol. 45, pp. 13244–13249, 1992.

[176] T. Okada, T. Abe, and M. Kaneko, "Historical overview and fundamental aspects of molecular catalysts for energy conversion," in *Molecular Catalysts for Energy Conversion* (T. Okada and M. Kaneko, eds.), vol. 111 of *Springer Series in Materials Science*, pp. 1–36, Springer Berlin Heidelberg, 2009.

[177] M. Hasegawa and K. Nishidate, "Semiempirical approach to the energetics of interlayer binding in graphite," *Phys. Rev. B*, vol. 70, p. 205431, 2004.

[178] J. c. v. Klimeš, D. R. Bowler, and A. Michaelides, "Van der waals density functionals applied to solids," *Phys. Rev. B*, vol. 83, p. 195131, 2011.

[179] M. S. Gordon, L. Slipchenko, H. Li, and J. H. Jensen, "Chapter 10 the effective fragment potential: A general method for predicting intermolecular interactions," vol. 3 of *Annual Reports in Computational Chemistry*, pp. 177 – 193, Elsevier, 2007.

[180] W. D. Cornell, P. Cieplak, C. I. Bayly, I. R. Gould, K. M. Merz, D. M. Ferguson, D. C. Spellmeyer, T. Fox, J. W. Caldwell, and P. A. Kollman, "A second generation force field for the simulation of proteins, nucleic acids, and organic molecules," *Journal of the American Chemical Society*, vol. 117, no. 19, pp. 5179–5197, 1995.

[181] S. L. Mayo, B. D. Olafson, and W. A. Goddard, "Dreiding: a generic

force field for molecular simulations," *The Journal of Physical Chemistry*, vol. 94, no. 26, pp. 8897–8909, 1990.

[182] A. K. Rappe, C. J. Casewit, K. S. Colwell, W. A. Goddard, and W. M. Skiff, "UFF, a full periodic table force field for molecular mechanics and molecular dynamics simulations," *Journal of the American Chemical Society*, vol. 114, no. 25, pp. 10024–10035, 1992.

[183] M. G. Martin, "Comparison of the AMBER, CHARMM, COMPASS, GROMOS, OPLS, TraPPE and UFF force fields for prediction of vapor–liquid coexistence curves and liquid densities ," *Fluid Phase Equilibria*, vol. 248, no. 1, pp. 50 – 55, 2006.

[184] K. Brameld, S. Dasgupta, and W. A. Goddard, "Distance dependent hydrogen bond potentials for nucleic acid base pairs from ab initio quantum mechanical calculations (lmp2/cc-pvtz)," *The Journal of Physical Chemistry B*, vol. 101, no. 24, pp. 4851–4859, 1997.

[185] T. Werder, J. H. Walther, R. L. Jaffe, T. Halicioglu, and P. Koumoutsakos, "On the water-carbon interaction for use in molecular dynamics simulations of graphite and carbon nanotubes," *The Journal of Physical Chemistry B*, vol. 107, no. 6, pp. 1345–1352, 2003.

[186] F. Hirata, ed., *Molecular Theory of Solvation*, vol. 24 of *Understanding Chemical Reactivity*. Springer, 2003.

[187] G. Hummer, J. Rasaiah, and J. Noworyta, "Water conduction through the hydrophobic channel of a carbon nanotube.," *Nature*, vol. 414, no. 6860, p. 188, 2001.

[188] F. Tournus and J.-C. Charlier, "*Ab initio* study of benzene adsorption on carbon nanotubes," *Phys. Rev. B*, vol. 71, p. 165421, 2005.

[189] L. Goerigk and S. Grimme, "A thorough benchmark of density functional methods for general main group thermochemistry, kinetics, and noncovalent interactions," *Phys. Chem. Chem. Phys.*, vol. 13, pp. 6670–6688, 2011.

[190] H. Iikura, T. Tsuneda, T. Yanai, and K. Hirao, "A long-range correction scheme for generalized-gradient-approximation exchange functionals," *The Journal of Chemical Physics*, vol. 115, no. 8, pp. 3540–3544, 2001.

[191] S. A. Petrosyan, A. A. Rigos, and T. A. Arias, "Joint density-funationl theory: Ab initio study of cr2o3 surface chemistry in solution," *The Journal of Physical Chemistry B*, vol. 109, no. 32, pp. 15436–15444, 2005.

[192] D. Roxbury, S. Manohar, and A. Jagota, "Molecular Simulation of DNA β-Sheet and β-Barrel Structures on Graphite and Carbon Nanotubes," *The Journal of Physical Chemistry C*, vol. 114, no. 31, pp. 13267–13276, 2010.

[193] A. J. Patil, J. L. Vickery, T. B. Scott, and S. Mann, "Aqueous Stabilization and Self-Assembly of Graphene Sheets into Layered Bio-Nanocomposites using DNA," *Advanced Materials*, vol. 21, no. 31, pp. 3159–3164, 2009.

[194] T. Premkumar and K. E. Geckeler, "Graphene–DNA hybrid materials: Assembly, applications, and prospects ," *Progress in Polymer Science*, vol. 37, no. 4, pp. 515 – 529, 2012. Topical Issue on Polymer Physics.

[195] F. Albertorio, M. E. Hughes, J. A. Golovchenko, and D. Branton, "Base dependent DNA–carbon nanotube interactions: activation enthalpies and as-

sembly–disassembly control," *Nanotechnology*, vol. 20, no. 39, p. 395101, 2009.

[196] A. Shankar, A. Jagota, and J. Mittal, "DNA Base Dimers Are Stabilized by Hydrogen-Bonding Interactions Including Non-Watson–Crick Pairing Near Graphite Surfaces," *The Journal of Physical Chemistry B*, vol. 116, no. 40, pp. 12088–12094, 2012.

[197] A. v. d. Vaart and K. M. Merz, Jr., "Charge transfer in biologically important molecules: comparison of high-level ab initio and semiempirical methods," *International Journal of Quantum Chemistry*, vol. 77, no. 1, pp. 27–43, 2000.

Chapter 3

Binding Energy of DNA Nucleobases-Carbon Nanotube Hybrid[1]

3.1 Introduction

Carbon nanotubes (CNTs) are among the most interesting nano-materials and have attracted a growing attention since their discovery [1]. Their intriguing physical properties have made CNT a useful material for many novel applications [2–5]. Several techniques can be used to synthesize CNTs including for example arc discharge, laser ablation and chemical vapor deposition [2, 4, 5]. As-produced CNTs form bundles due to the strong adhesion between them. Therefore, dis-

[1]Reprinted from Physica E: Low-dimensional Systems and Nanostructures Volume 54, December 2013, Pages 65–71, Morteza Chehel Amirani, Tian Tang, and Javier Cuervo, "Quantum mechanical treatment of binding energy between DNA nucleobases and carbon nanotube: A DFT analysis", with permission.

persion, separation and purification of CNTs are often needed before they can be employed in practical applications. This is especially important in electronic applications where the CNT's chirality plays an important role. In an experiment by Zheng *et al.* [6], it was discovered that single-stranded DNA (ssDNA) can bind to CNT and form a hybrid structure where the ssDNA helically wraps around the CNT. The hybrids can be dispersed in an aqueous solution and subsequently be subjected to ion exchange chromatography, leading to the separation of the CNTs into metallic and semiconducting types. More recently, such a method has been shown to be able to separate semiconducting CNTs with only slight difference in their chiralities [7]. Particular ssDNA sequences have been shown to have better capacity in separating the CNTs [8, 9], indicating that the ssDNA-assisted CNT separation is a sequence-dependent process.

Theoretical efforts have been put forward in order to understand the interesting interaction between ssDNA and CNT. Some of these studies were at the continuum level where the spaces inside and outside the DNA/CNT hybrid were simplified and modeled as continuum media [10–13]. Some works used molecular dynamics simulations based on molecular mechanics force fields, and the interaction between the DNA and the CNT was described using empirical van der Waals potentials [14, 15]. While providing useful information on the wrapping geometry, these approaches lack an accurate description of the CNT's electronic structure and therefore cannot distinguish CNTs according to their chiralities. To capture CNT's electronic properties and their effect on ssDNA/CNT hybridization, it is necessary to introduce models at the quantum mechanical (QM) level. Due to the limited computational capacity, the QM simulations performed to date have focused on addressing the interaction of nucleobases (adenine (A), cytosine

(C), guanine (G) and thymine (T)) as the building blocks of DNA with CNT. In particular, the majority of these QM studies are centered around evaluating the binding energy (BE) of nucleobases to graphene or CNT.

Gowtham *et al.* [16] studied the adsorption of nucleobases on graphene using DFT(LDA) and MP2 methods. The BE values that they obtained followed the order of G>A=T=C>U using DFT(LDA) and G>A>T>C>U using MP2 method. Antony and Grimme [17] performed similar study but used the dispersion corrected B97-D method. The order of the BE between nucleobases and graphene was found to be consistent with the results of Gowtham *et al.*, i.e., G>A>T>C>U. Panigrahi *et al.* [18] used wB97XD method and obtained a different result, with the order of the BE following G>A>C>T>U for the nucleobase/graphene hybrid. Gowtham *et al.* [19] later studied the adsorption of nucleobases on a (5,0) metallic CNT using DFT(LDA) method, and found that the BE was in the same order as in the case of a graphene, i.e., G>A>T>C>U, but the absolute values of the BE are smaller for CNT than for graphene. Wang [20] investigated the interaction of nucleobases with (5,5) and (10,0) CNT fragments using DFT and MP2 methods. Simulations were carried out in both vacuum and aqueous environment. The order of the BE in the gas phase was G>A>T>C for both CNTs, and in the aqueous solution it remained to be the same for (5,5) CNT but was changed to A>G>T>C for (10,0) CNT. Das *et al.* [21] calculated the BE between nucleobases and a (5,5) CNT in both vacuum and aqueous environments using restricted open shell Hartree-Fock (ROHF) method and classical force fields. Different from Wang [20], the order of the BE was found to be G>A>T>C in vacuum but changed to G>T>A>C in aqueous solution. Shukla *et al.* [22] used the M05-2X functional to calculate the BE of nucleobases with

a (7,0) zigzag CNT. The order of the BE was determined to be G>A>C>T>U using the 6-31G(d,p) basis set. Ramraj *et al.* [23] employed dispersion corrected PM3 method (PM3-D) as a semi-empirical method to study the interaction of nucleobases with graphene and CNTs. According to their results, the order of the BE was G>A>T>C>U for both graphene and CNTs. Umadevi and Sastry [24] calculated the BE of nucleobases with graphene and CNT using an ONIOM method at the M06-2X/6-31G*:AM1 level and reported G>T∼A>C>U for CNT and G>A>T>C>U for graphene. Akdim *et al.* [25] calculated the BE for the hybridization of G, A, T and C with chiral CNTs using B97-D method. They studied three chiral CNTs (chiralities being (6,5), (9,1) and (8,3)) which all have the same diameter. According to their results, the order of the BE for both (6,5) and (9,1) CNTs was G>A>T>C and it was G>A>C>T for (8,3) CNT. They also computed the BE for a zigzag (5,0) CNT using effective fragment potential (EFP2) method and obtained G>T>C>A for the order of the BE. Clearly, even for the same CNT, discrepancies exist in the order of the BE associated with different nucleobases. G has the largest BE and U has the lowest BE in most cases but there is no agreement on how the BE for the other nucleobases is ordered. The discrepancies become more significant quantitatively, if the absolute values of the BE are compared. Values of the reported BE cover a large range, varying from about less than 10 to higher than 100 kJ/mol [16–25].

Several factors can contribute to the observed discrepancies among previous studies. The first is the method used to conduct the calculations. Many works used DFT without dispersion correction in the optimization step and/or in the BE calculation. LDA approach is the easiest DFT approach and has been used in some works to optimize the nucleobase/CNT hybrid. No dispersion treatment has

been done for the LDA method and BE calculated at this level are usually overestimated [26]. Moreover, recent works using dispersion-corrected DFT also gave rise to different results. For example, Le *et al.* [27] evaluated the BE of nucleobases with graphene using several dispersion-corrected DFT methods, including TS [28], simplified TS (sTS) [27], vdW-DF [29], vdW-DF2 [30], DFT-D2 [31] and DFT-D3 [32]. Although all the methods in that study predicted the same order for the BE, i.e., G>A>T>C>U, the actual BE values were shown to strongly depend on the specific method used. The discrepancy may be because of the different treatments employed in these methods to incorporate dispersion interaction. Performance of these dispersion corrected methods is yet to be examined [33, 34]. Another reason for such discrepancies is the different initial configurations (ICs) used for the geometry optimization of the hybrids. In most of the previous studies, either the initial configuration was not clearly specified or a single initial configuration was adopted for the optimization. Very few works have explored the effect of the ICs by examining the BE associated with different ICs.

In this study, we performed a series of DFT calculations for the BE of the nucleobases with a model CNT and systematically examined the effect of the IC by adopting 24 different ICs with different lateral and angular position of nucleobases with respect to the CNT. M05-2X, a recently developed dispersion corrected DFT method [35], was employed for both the geometry optimization and the BE calculation. Comparison of our results with an earlier work by Shukla *et al.*[22] shows the importance of considering the IC in the BE calculation at the QM level. The rest of the chapter is organized as follows. In Section 3.2, computational details, especially on how the ICs are systematically changed, are described. Results and discussion are presented in Section 3.3 and conclusions are given in Section 3.4.

3.2 Computational details

The model system that we chose to simulate here was adopted from the work of Shukla et al. [22], where the M05-2X functional was used to calculate the BE. In their work, the IC used to perform the optimization was not clearly specified. By examining the same system but with a series of different ICs, the effect of IC on the BE can be clearly demonstrated. Specifically, individual DNA nucleobases, i.e. A, C, G and T shown in Figs. 1(a) to 1(d) respectively, are considered to interact with a semiconducting single-walled carbon nanotube with the chirality of (7,0) and length of 15.57 Å shown in Fig. 1(e). Hydrogen atoms are used at both ends of the tube to saturate the dangling bonds.

Because the nucleobases and the CNT considered here are small, when specifying the ICs, the internal degrees of freedom (DOF) do not need to be considered, i.e., the CNT can be treated as a cylinder and the nucleobase can be treated as a plane. The relative position of the nucleobase to the CNT can therefore be specified by three translational DOF and three rotational DOF. In this work, we focus on varying the ICs using two of the six DOF. One of them is the translational DOF of the nucleobase along the CNT axis and the other is the rotational DOF about the axis perpendicular to the base plane. In all ICs, the nucleobase was placed directly on top of the CNT with its plane being tangential to the CNT surface. The separation distance between the nucleobase and the CNT was set to be 3.3 Å which is close to the separation distance in the optimized configurations reported in the literature [20, 23, 36, 37]. The translational DOF in the lateral direction with respect to the tube was not considered since the tube diameter is small and laterally moving the nucleobase away from the CNT surface will decrease the

contact area, which is energetically unfavored. Similarly, the two other rotational DOF were not considered since parallel orientation of the bases with respect to the tube is preferred in the optimized structures [21, 25, 37]. By varying these two rotational DOF, the orientation of the base will deviate from the favorable parallel configuration, leading to more computation time in the optimization process.

The positions associated with the chosen two DOF were systematically varied according the following procedure to generate different ICs. First, as shown in Figs. 3.1 (a)-(d), we labelled two carbon atoms (C2 and C5) and two nitrogen atoms (N1 and N3) on each base. Using these atoms, two vectors were defined on the base. They are respectively V_1 pointing from C2 to C5 and V_1 pointing from N3 to N1. Similarly, four carbon atoms C1, C2, C3 and C4 in the middle of the tube were used to define two vectors R_1 (from C1 to C2) and R_2 (from C3 to C4), as shown in Fig. 1(e). The first IC was prepared such that atom C2 on each base was above atom C2 on the tube at a separation distance of 3.3 Å and the vectors V_1 and V_2 were parallel to R_1 and R_2, respectively. Subsequently, different ICs were generated by performing the two translational and rotational moves for each base as specified above. For the translational move, four sites were defined on the tube surface (see Site 1 - Site 4 in Fig. 3.1e and the carbon atom C2 on the base was placed above one of those four sites. For the rotational move, each base was rotated about the axis perpendicular to the base plane at an increment of 60 degrees after being placed above one of those four sites. With the four translational positions and six rotational positions, 24 ICs were generated for each base.

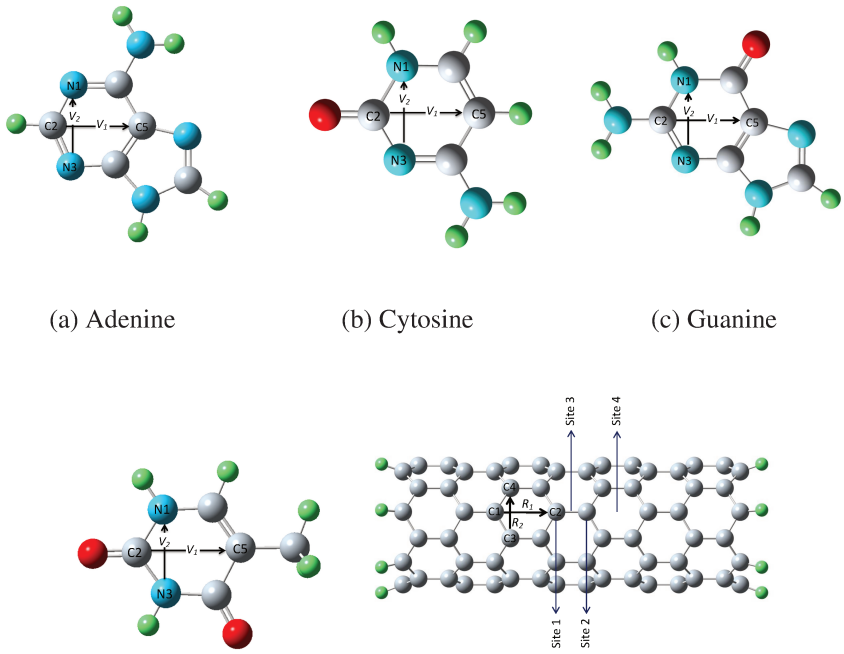

(a) Adenine (b) Cytosine (c) Guanine

(d) Thymine (e) (7,0) CNT

Figure 3.1: Molecular structures of the nucleobases and CNT simulated in this work

To facilitate the discussion, we introduce the following notation for the 24 ICs. Hereafter, IC-m-ϕ refers to the IC in which the atom C2 on the base was placed on site No. m and the base plane was rotated for ϕ degrees. m can have values of 1, 2, 3 and 4 and ϕ can have values of 0, 60, 120, 180, 240 and 300 representing the rotation angles. For example, IC-4-180 refers to the IC in which the C2 atom from the base is placed over site No. 4 on the CNT and the base plane is rotated for 180 degrees. Fig. 3.2 shows the configuration of IC-4-180 for the C base.

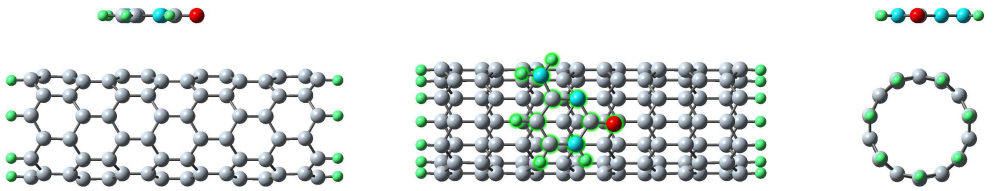

(a) Side view (b) Top view (c) Front view

Figure 3.2: IC-4-180 for C

Even though only two DOF were chosen to vary the IC, with each IC the nucleobase/CNT hybrid was fully optimized, i.e., all atoms in the base and in the CNT were allowed to move freely in the optimization process. The M05-2X functional was employed for all the calculations. Specifically, the geometry optimization was done at M05-2X/6-31G(d) level and for the optimized structure a single point energy calculation was performed using the 6-31G(d,p) basis set. The basis set superposition error (BSSE) correction was done for all BE calculations. M0 family functionals are dispersion corrected methods which have shown good performance in treating π-π stacking interactions [38]. It should be noted that even though M06-2X has shown better performance compared to M05-2X [38, 39], M05-2X was used so that comparison can be made between results obtained in this work and those in Ref. [22] to show the effect of IC. All calculations were carried out using Gaussian 09 program [40].

3.3 Results and discussion

Figs. 3.3(a)-3.3(d) show the optimized structures associated with IC-4-240 for A, IC-1-240 for C, IC-1-60 for G and IC-3-120 for T. These are respectively the most stable structures for each base, gauged by the greatest BE (calculation shown later) among the structures optimized from all ICs. In all cases, the parallel orientation of the bases with respect to the CNT in the optimized structures confirm the stacking interaction between the nucleobases and the CNT which has been reported in previous theoretical studies [20, 21, 25, 36] and experiments [41, 42]. The separation distance between the nucleobase and the CNT in the optimized structures is 3.11, 3.09, 3.00 and 2.82 Å respectively for A, C, G and T. Therefore, compared with the initial separation of 3.3 Å the bases have been slightly attracted to the CNT.

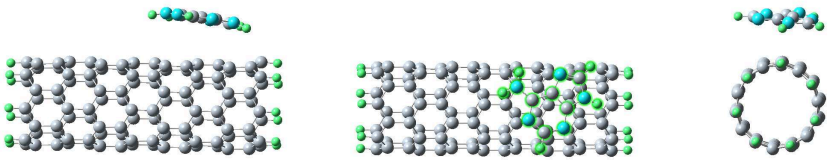

(a) Side View (b) Top view (c) Front view

(a)

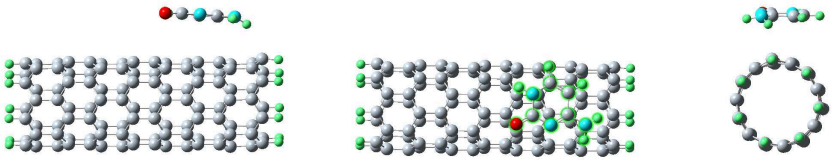

(d) Side View (e) Top view (f) Front view

(b)

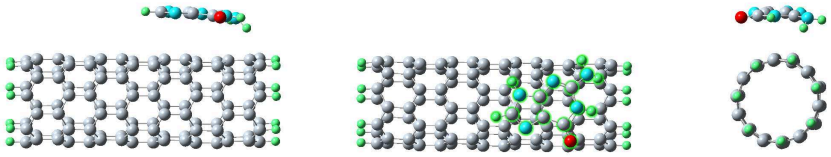

(g) Side View (h) Top view (i) Front view

(c)

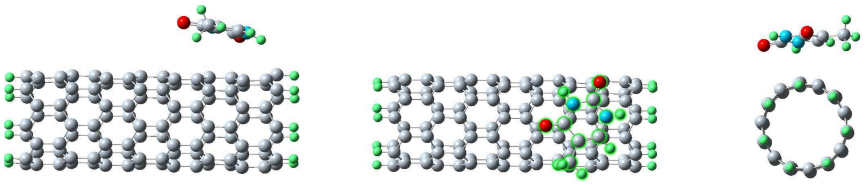

(j) Side View (k) Top view (l) Front view

(d)

Figure 3.3: Optimized Nucleobase/CNT structures: (a) A optimized from IC-4-240, (b) C optimized from IC-1-240, (c) G optimized from IC-1-60 and (d) T optimized from IC-3-120

The separation distance in all optimized structures is shown in Fig. 3.4. Each subfigure corresponds to a particular base, and it contains four curves that are respectively associated with the four site numbers. It can be seen that depending on the IC (site number and rotation angle), the separation distance in the final optimized structure can be different. In fact, the separation distance covers a range of [3.06, 3.18], [2.88, 3.11], [3.00, 3.11] and [2.82, 3.16] for A, C, G and T, respectively. Such variation suggest that the BE between the nucleobases and the CNT can also change with the ICs, which is demonstrated below.

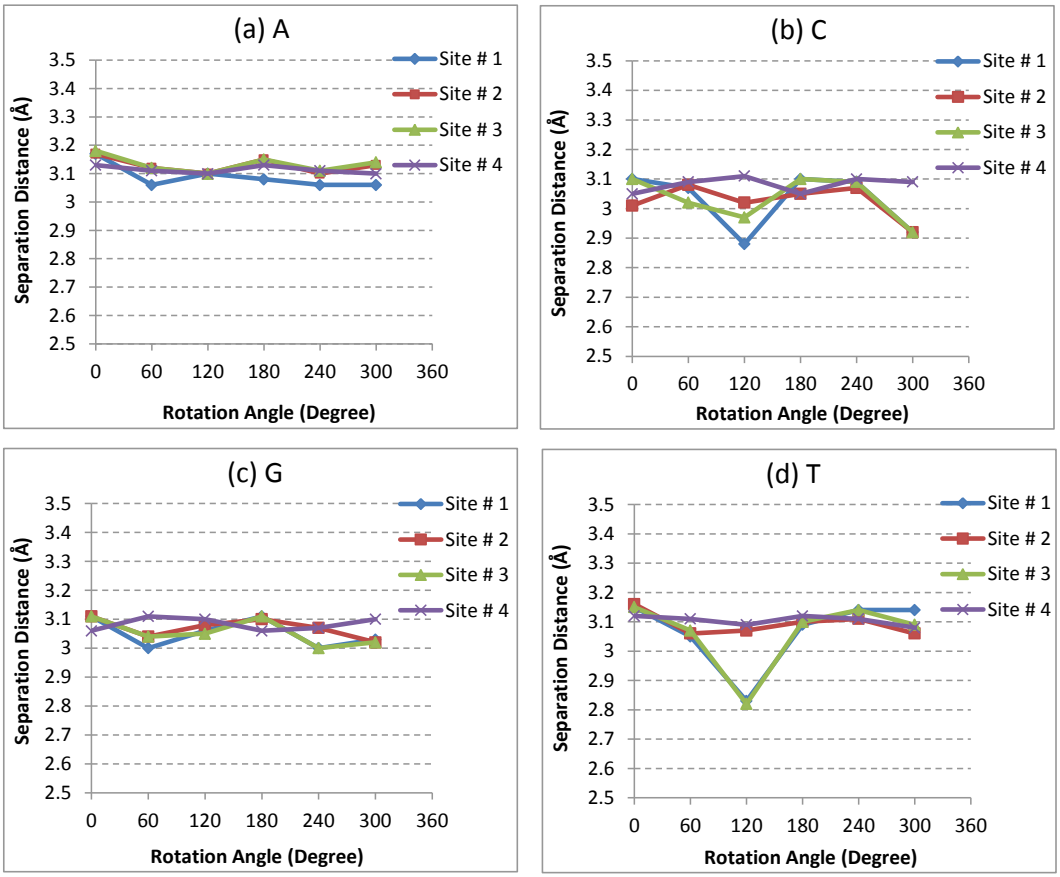

Figure 3.4: Separation distance between (a) A, (b) C, (c) G, (d) T and CNT in the optimized structures obtained from different ICs

The BE of the hybrid is calculated as follows:

$$BE = E^{Hybrid} - E^{Base} - E^{CNT} \tag{3.1}$$

where E^{Hybrid} is the BSSE corrected energy of the optimized hybrid, E^{Base} is the energy of the relaxed base and E^{CNT} is the energy of the relaxed CNT. Because the binding of the nucleobase with the CNT is an energetically favored process, BE calculated from Eq. 3.1 is a negative number. The absolute value of the BE is an indicator of the strength of binding. The larger the absolute value, the stronger the nucleobase binds to the CNT. Therefore the absolute value of the quantity calculated from Eq. 3.1 will be reported throughout this work and referred to as the BE. Fig. 3.5 shows the obtained BE for all bases as a function of rotation angle. (BEs for all 24 simulations are also provided in Figure A.1 of the Appendix A) Each subfigure corresponds to a particular base, and four curves associated with the four site numbers are presented in each subfigure. As shown in these graphs, different BEs can be obtained if the optimization starts from different ICs, and the BE value generally exhibits a non-monotonic change with the translational and rotational positions. Quantitatively, the ranges of the BE for A, C, G and T are respectively [17.2, 29.6] kJ/mol, [16.4, 27.9] kJ/mol, [24.4, 39.9] kJ/mol and [15.9, 29.8] kJ/mol. In other words, the variation of the BE with respect to the IC is large and equals 72%, 70%, 64% and 87% respectively for A, C, G and T. The difference between the minimum BE and the maximum BE is 12.4, 11.5, 15.5 and 13.9 kJ/mol for A, C, G and T respectively, indicating that the magnitude of the change in BE with IC is comparable with the magnitude of the BE itself.

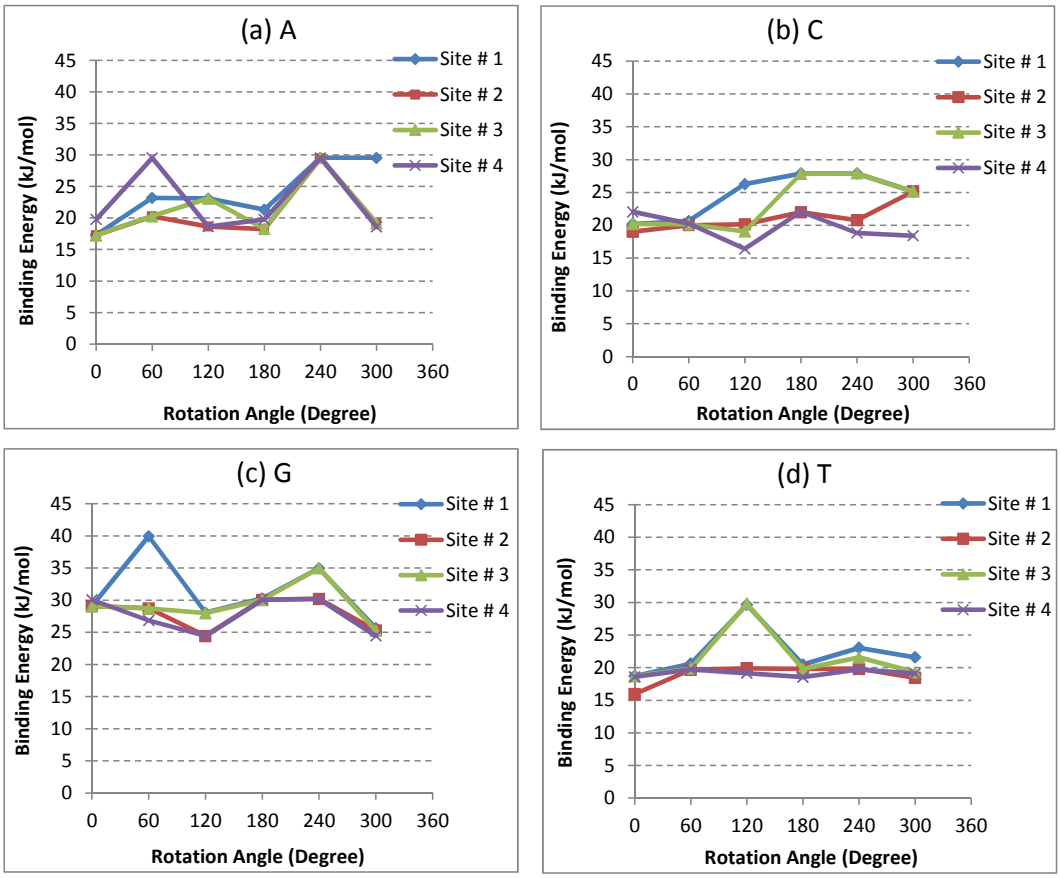

Figure 3.5: Binding energy for (a)A, (b)C, (c)G and (d)T obtained from different initial configurations

Our results also show that performing geometry optimization from different ICs not only leads to different BE values, but also changes the order of the BE associated with the four bases. This is illustrated in Table 3.1, where the order of the BE is listed for all 24 ICs. Here, the notations of IC-1 to IC-4 refer to the ICs in which C2 from a base was placed on top of sites No.1 to 4, respectively. Except for four cases, G displays the highest BE regardless of the ICs, which is in agreement with previous theoretical studies [16–19, 21, 23, 25]. Among all the ICs, the one that results in the highest BE is IC-4-240 for A (29.6 kJ/mol), IC-

Table 3.1: Order of BE for nucleobase-CNT interaction obtained from different ICs

Angle	IC-1	IC-2	IC-3	IC-4
0	G>C>T>A	G>C>A>T	G>C>T>A	G>C>A>T
60	G>A>C>T	G>A>C>T	G>A>C>T	A>G>C>T
120	T>G>C>A	G>C>T>A	T>G>A>C	G>T>A>C
180	G>C>A>T	G>C>T>A	G>C>T>A	G>C>A>T
240	G>A>C>T	G>A>C>T	G>A>C>T	G>A>T>C
300	A>G>C>T	G>C>A>T	G>C>T>A	G>T>A>C

1-240 for C (27.9 kJ/mol), IC-1-60 for G (39.9 kJ/mol) and IC-3-120 for T (29.8 kJ/mol). The structures optimized from these ICs correspond to the most stable hybrids (shown in Fig. 3.3). Taking the optimized hybrids with the highest BEs, the order of the BE is found to be G>T>A>C.

It is of particular interest to compare our results with those in Ref. [22] where the same system was simulated using the same functional and the single point energy calculations were also performed at the M05-2X/6-31G(d,p) level. The comparison is shown in Table 3.2. The BEs in Ref. [22] fall into the range of BEs obtained in this study. This implies that the optimized structure obtained in Ref. [22] corresponds to one of the many local minima in the potential energy surface (PES), which is not necessarily the one with the highest BE. It should also be noted that in Ref. [22] the difference between the BEs for A/CNT and C/CNT hybrids is only 0.1 kJ/mol while our results show that a small change in the IC cause changes in the BE larger than 0.1 kJ/mol. Therefore, care should be exercised in the calculation and interpretation of the BE, and it may be more appropriate to report a range of BE values rather than reporting a single one.

It is important to point out the limitations of this study. First of all, the CNT

Table 3.2: BE (kJ/mol) between nucleobases and CNT: A comparison with Ref. [22]

Hybrid	Ref. [22]	Our Results
CNT-A	18.2	17.2-29.6
CNT-C	18.1	16.4-27.9
CNT-G	26.5	24.4-39.9
CNT-T	17.6	15.9-29.8

simulated here is a short one with hydrogen atoms at the two ends. The free edges can introduce some effects on the BE values. Secondly, only single nucleobases were considered in this work. It will be an interesting study to include the ribose sugar and phosphate group in the system, as it has been shown that the inclusion of ribose-sugar backbone can change the order of the BE [43]. Also, our simulations were done in vacuum whereas experiments on the adsorption of nucleobases to CNT or graphite are typically performed in solution. For instance, based on adsorption isotherms, Sowerby *et al.* [44] reported G>A>T>C>U for the order of the BE with graphite in water. Using isothermal titration calorimetry, Varghese *et al.* [45] observed A>C>T and A>T>C for the binding of nucleobases with two different samples of graphene in water. Including solution and hence the solvation energy can change the order of the BE [21]. In addition, only two DOF are considered to generate the 24 ICs. Changing other DOF or varying the currently considered DOF with smaller increment can result in other optimized structures and hence other BE values. Also, M05-2X was chosen to perform the calculations, which is not the best among the available methods. For example, M06-2X has shown better performance compared to M05-2X and some other dispersion corrected methods for π-π stacking systems [46]. Despite these limitations, it

should be noted that the main purpose of this study is to demonstrate the importance of IC in optimizing nucleobase/CNT hybrid systems and calculating their BEs, which have been missing in many past works. Such purpose is best served by considering a system and method identical to those in a previous work.

3.4 Conclusion

We evaluated the binding energy of DNA nucleobases with a (7,0) CNT using DFT method and examined the effect of the initial configuration on the binding energy. The binding energy is shown to be very sensitive to the initial configuration both quantitatively and qualitatively. Specifically, the ranges of the binding energy obtained for A, C, G, and T are respectively [17.2, 29.6] kJ/mol, [16.4, 27.9] kJ/mol, [24.4, 39.9] kJ/mol and [15.9, 29.8] kJ/mol. That is, the variation of the binding energy with respect to the initial configuration is large, being 72%, 70%, 64% and 87% respectively for A, C, G and T. In addition, the order of the binding energy can change with even small changes in the initial configuration. Binding energy values obtained in a previous study for the same system (but without a clearly specified initial configuration) fall into the range reported here. Our results show that the potential energy surface between the nucleobase and the CNT can have many local minima and reporting a range for the binding energy is more appropriate than reporting a single value.

References

[1] S. Iijima, "Helical microtubules of graphitic carbon," *Nature*, vol. 354, pp. 56–58, 1991.

[2] A. Jorio, G. Dresselhaus, and M. S. Dresselhaus, *Carbon Nanotubes: Advanced Topics in the Synthesis, Structure, Properties and Applications*. , Springer, 2008.

[3] R. H. Baughman, A. A. Zakhidov, and W. A. de Heer, "Carbon Nanotubes–the Route Toward Applications," *Science*, vol. 297, no. 5582, pp. 787–792, 2002.

[4] S. B. Sinnott and R. Andrews, "Carbon Nanotubes: Synthesis, Properties, and Applications," *Critical Reviews in Solid State and Materials Sciences*, vol. 26, no. 3, pp. 145–249, 2001.

[5] J. Prasek, J. Drbohlavova, J. Chomoucka, J. Hubalek, O. Jasek, V. Adam, and R. Kizek, "Methods for carbon nanotubes synthesis-review," *Journal of Materials Chemistry*, vol. 21, pp. 15872–15884, 2011.

[6] M. Zheng, A. Jagota, E. D. Semke, B. A. Diner, R. S. Mclean, S. R. Lustig, R. E. Richardson, and N. G. Tassi, "DNA-assisted dispersion and separation of carbon nanotubes," *Nat Mater*, vol. 2, no. 5, pp. 338–342, 2003.

[7] X. Tu, S. Manohar, A. Jagota, and M. Zheng, "DNA sequence motifs for structure-specific recognition and separation of carbon nanotubes," *Nature Materials*, vol. 460, no. 7252, pp. 250–253, 2009.

[8] M. Zheng, A. Jagota, M. S. Strano, A. P. Santos, P. Barone, S. G. Chou, B. A. Diner, M. S. Dresselhaus, R. S. Mclean, G. B. Onoa, G. G. Samsonidze, E. D. Semke, M. Usrey, and D. J. Walls, "Structure-Based Carbon Nanotube Sorting by Sequence-Dependent DNA Assembly," *Science*, vol. 302, no. 5650, pp. 1545–1548, 2003.

[9] X. Tu and M. Zheng, "A DNA-based approach to the carbon nanotube sorting problem," *Nano Research*, vol. 1, pp. 185–194, 2008.

[10] O. Malysheva, T. Tang, and P. Schiavone, "Binding Force Between a Charged Wall and a Complex Formed by a Polyelectrolyte and an Electronically Responsive Cylinder," *The Journal of Adhesion*, vol. 87, no. 3, pp. 251–271, 2011.

[11] C. Sun and T. Tang, "Structure of a polyelectrolyte around an electronically responsive cylinder," *Journal of Colloid and Interface Science*, vol. 338, no. 1, pp. 276 – 283, 2009.

[12] S. R. Lustig, A. Jagota, C. Khripin, and M. Zheng, "Theory of Structure-Based Carbon Nanotube Separations by Ion-Exchange Chromatography of DNA/CNT Hybrids," *The Journal of Physical Chemistry B*, vol. 109, no. 7, pp. 2559–2566, 2005.

[13] M. Zheng, K. Eom, and C. Ke, "Calculations of the resonant response of carbon nanotubes to binding of DNA," *Journal of Physics D: Applied Physics*, vol. 42, no. 14, 2009.

[14] S. Manohar, T. Tang, and A. Jagota, "Structure of Homopolymer DNA-CNT

Hybrids," *The Journal of Physical Chemistry C*, vol. 111, no. 48, pp. 17835–17845, 2007.

[15] D. Roxbury, A. Jagota, and J. Mittal, "Sequence-Specific Self-Stitching Motif of Short Single-Stranded DNA on a Single-Walled Carbon Nanotube," *Journal of the American Chemical Society*, vol. 133, no. 34, pp. 13545–13550, 2011.

[16] S. Gowtham, R. H. Scheicher, R. Ahuja, R. Pandey, and S. P. Karna, "Physisorption of nucleobases on graphene: Density-functional calculations," *Phys. Rev. B*, vol. 76, p. 033401, 2007.

[17] J. Antony and S. Grimme, "Structures and interaction energies of stacked graphene-nucleobase complexes," *Phys. Chem. Chem. Phys.*, vol. 10, pp. 2722–2729, 2008.

[18] S. Panigrahi, A. Bhattacharya, S. Banerjee, and D. Bhattacharyya, "Interaction of Nucleobases with Wrinkled Graphene Surface: Dispersion Corrected DFT and AFM Studies," *The Journal of Physical Chemistry C*, vol. 116, no. 7, pp. 4374–4379, 2012.

[19] S. Gowtham, R. H. Scheicher, R. Pandey, S. P. Karna, and R. Ahuja, "First-principles study of physisorption of nucleic acid bases on small-diameter carbon nanotubes," *Nanotechnology*, vol. 19, no. 12, p. 125701, 2008.

[20] Y. Wang, "Theoretical Evidence for the Stronger Ability of Thymine to Disperse SWCNT than Cytosine and Adenine: Self-Stacking of DNA Bases vs Their Cross-Stacking with SWCNT," *The Journal of Physical Chemistry C*, vol. 112, no. 37, pp. 14297–14305, 2008.

[21] A. Das, A. Sood, P. K. Maiti, M. Das, R. Varadarajan, and C. Rao, "Binding of nucleobases with single-walled carbon nanotubes: Theory and experiment," *Chemical Physics Letters*, vol. 453, no. 4–6, pp. 266–273, 2008.

[22] M. Shukla, M. Dubey, E. Zakar, R. Namburu, Z. Czyznikowska, and J. Leszczynski, "Interaction of nucleic acid bases with single-walled carbon nanotube," *Chemical Physics Letters*, vol. 480, no. 4–6, pp. 269–272, 2009.

[23] A. Ramraj, I. H. Hillier, M. A. Vincent, and N. A. Burton, "Assessment of approximate quantum chemical methods for calculating the interaction energy of nucleic acid bases with graphene and carbon nanotubes," *Chemical Physics Letters*, vol. 484, no. 4–6, pp. 295–298, 2010.

[24] D. Umadevi and G. N. Sastry, "Quantum Mechanical Study of Physisorption of Nucleobases on Carbon Materials: Graphene versus Carbon Nanotubes," *The Journal of Physical Chemistry Letters*, vol. 2, no. 13, pp. 1572–1576, 2011.

[25] B. Akdim, R. Pachter, P. N. Day, S. S. Kim, and R. R. Naik, "On modeling biomolecular–surface nonbonded interactions: application to nucleobase adsorption on single-wall carbon nanotube surfaces," *Nanotechnology*, vol. 23, no. 16, p. 165703, 2012.

[26] E. J. Meijer and M. Sprik, "A density-functional study of the intermolecular interactions of benzene," *The Journal of Chemical Physics*, vol. 105, no. 19, pp. 8684–8689, 1996.

[27] D. Le, A. Kara, E. Schröder, P. Hyldgaard, and T. S. Rahman, "Physisorption of nucleobases on graphene: a comparative van der Waals study," *Journal of Physics: Condensed Matter*, vol. 24, no. 42, p. 424210, 2012.

[28] A. Tkatchenko and M. Scheffler, "Accurate Molecular Van Der Waals Interactions from Ground-State Electron Density and Free-Atom Reference Data," *Phys. Rev. Lett.*, vol. 102, p. 073005, 2009.

[29] M. Dion, H. Rydberg, E. Schröder, D. C. Langreth, and B. I. Lundqvist, "Van der Waals Density Functional for General Geometries," *Phys. Rev. Lett.*, vol. 92, p. 246401, 2004.

[30] K. Lee, É. D. Murray, L. Kong, B. I. Lundqvist, and D. C. Langreth, "Higher-accuracy van der Waals density functional," *Phys. Rev. B*, vol. 82, p. 081101, 2010.

[31] S. Grimme, "Semiempirical GGA-type density functional constructed with a long-range dispersion correction," *Journal of Computational Chemistry*, vol. 27, no. 15, pp. 1787–1799, 2006.

[32] S. Grimme, J. Antony, S. Ehrlich, and H. Krieg, "A consistent and accurate ab initio parametrization of density functional dispersion correction (DFT-D) for the 94 elements H-Pu," *The Journal of Chemical Physics*, vol. 132, no. 15, p. 154104, 2010.

[33] E. R. Johnson, R. A. Wolkow, and G. A. DiLabio, "Application of 25 density functionals to dispersion-bound homomolecular dimers," *Chemical Physics Letters*, vol. 394, no. 4–6, pp. 334–338, 2004.

[34] E. R. Johnson, I. D. Mackie, and G. A. DiLabio, "Dispersion interactions in density-functional theory," *Journal of Physical Organic Chemistry*, vol. 22, no. 12, pp. 1127–1135, 2009.

[35] Y. Zhao, N. E. Schultz, and D. G. Truhlar, "Design of density functionals by combining the method of constraint satisfaction with parametrization for thermochemistry, thermochemical kinetics, and noncovalent interactions," *Journal of Chemical Theory and Computation*, vol. 2, no. 2, pp. 364–382, 2006.

[36] Y. V. Shtogun, L. M. Woods, and G. I. Dovbeshko, "Adsorption of Adenine and Thymine and Their Radicals on Single-Wall Carbon Nanotubes," *The Journal of Physical Chemistry C*, vol. 111, no. 49, pp. 18174–18181, 2007.

[37] S. Stepanian, M. Karachevtsev, A. Glamazda, V. Karachevtsev, and L. Adamowicz, "Stacking interaction of cytosine with carbon nanotubes: MP2, DFT and Raman spectroscopy study," *Chemical Physics Letters*, vol. 459, no. 1–6, pp. 153–158, 2008.

[38] Y. Zhao and D. G. Truhlar, "Density Functionals with Broad Applicability in Chemistry," *Accounts of Chemical Research*, vol. 41, no. 2, pp. 157–167, 2008.

[39] Y. Zhao and D. G. Truhlar, "Applications and validations of the Minnesota density functionals," *Chemical Physics Letters*, vol. 502, no. 1–3, pp. 1 – 13, 2011.

[40] M. J. Frisch, G. W. Trucks, H. B. Schlegel, G. E. Scuseria, M. A. Robb, J. R. Cheeseman, G. Scalmani, V. Barone, B. Mennucci, G. A. Petersson,

H. Nakatsuji, M. Caricato, X. Li, H. P. Hratchian, A. F. Izmaylov, J. Bloino, G. Zheng, J. L. Sonnenberg, M. Hada, M. Ehara, K. Toyota, R. Fukuda, J. Hasegawa, M. Ishida, T. Nakajima, Y. Honda, O. Kitao, H. Nakai, T. Vreven, J. J. A. Montgomery, J. E. Peralta, F. Ogliaro, M. Bearpark, J. J. Heyd, E. Brothers, K. N. Kudin, V. N. Staroverov, R. Kobayashi, J. Normand, K. Raghavachari, A. Rendell, J. C. Burant, S. S. Iyengar, J. Tomasi, M. Cossi, N. Rega, J. M. Millam, M. Klene, J. E. Knox, J. B. Cross, V. Bakken, C. Adamo, J. Jaramillo, R. Gomperts, R. E. Stratmann, O. Yazyev, A. J. Austin, R. Cammi, C. Pomelli, J. W. Ochterski, R. L. Martin, K. Morokuma, V. G. Zakrzewski, G. A. Voth, P. Salvador, J. J. Dannenberg, S. Dapprich, A. D. Daniels, Ö. Farkas, J. B. Foresman, J. V. Ortiz, J. Cioslowski, and D. J. Fox, "Gaussian 09 Revision A.1." Gaussian Inc. Wallingford CT 2009.

[41] J. E. Freund, M. Edelwirth, P. Kröbel, and W. M. Heckl, "Structure determination of two-dimensional adenine crystals on graphite," *Phys. Rev. B*, vol. 55, pp. 5394–5397, 1997.

[42] R. Srinivasan and P. Gopalan, "Order and stability of an electrochemically condensed adenine layer on graphite," *The Journal of Physical Chemistry*, vol. 97, no. 34, pp. 8770–8775, 1993.

[43] M. Santosh, S. Panigrahi, D. Bhattacharyya, A. K. Sood, and P. K. Maiti, "Unzipping and binding of small interfering RNA with single walled carbon nanotube: A platform for small interfering RNA delivery," *The Journal of Chemical Physics*, vol. 136, no. 6, p. 065106, 2012.

[44] S. J. Sowerby, C. A. Cohn, W. M. Heckl, and N. G. Holm, "Differential adsorption of nucleic acid bases: Relevance to the origin of life," *Proceedings of the National Academy of Sciences*, vol. 98, no. 3, pp. 820–822, 2001.

[45] N. Varghese, U. Mogera, A. Govindaraj, A. Das, P. K. Maiti, A. K. Sood, and C. N. R. Rao, "Binding of DNA Nucleobases and Nucleosides with Graphene," *ChemPhysChem*, vol. 10, no. 1, pp. 206–210, 2009.

[46] L. R. Rutledge and S. D. Wetmore, "The assessment of density functionals for DNAprotein stacked and T-shaped complexes," *Canadian Journal of Chemistry*, vol. 88, no. 8, pp. 815–830, 2010.

Chapter 4

A QM:MM Model for the Interaction of DNA Nucleotides with Carbon Nanotube[1]

4.1 Introduction

Since the discovery of carbon nanotube (CNT) in 1991 [1], extensive studies have been performed to uncover its interesting properties. Theoretical and experimental investigations have shown strong dependence of CNT's properties on its structure [2]. For example, electronic properties of CNT depend strongly on its chirality (n,m): if $n = m$, the CNT has metallic properties and if $n - m$ is a multiple of 3, the CNT is a semi-conducting material with a small band gap [2].

Functionalization of CNT has introduced an exciting area of research and various functional groups have been investigated in recent years. DNA is one type

[1]Reproduced by permission of the PCCP Owner Societies.

of molecule that has exhibited interesting properties when used to functionalize a CNT [3]. The intriguing properties of the hybrids formed by DNA and CNT have led to potential applications such as drug delivery [3–13], biosensing [4–7], CNT dispersion and separation [8, 9] and DNA sequencing [10–13]. Understanding the process of hybrid formation and the properties of these hybrids are essential to the realization and wide usage of such applications. Theoretically, interaction of a DNA polymer with CNT has been widely studied mostly using classical molecular mechanics (MM) simulations. A Classical MM approach is suitable to study these large molecular systems, however, it is inaccurate in describing the electronic response of CNTs because in those simulations, CNTs were completely neutral and only interacted with the DNA through van der Waals (vdW) interactions [14–21]. Quantum mechanics (QM) approaches can precisely model electronic behavior of materials based on the Shrödinger equation. On the other hand, QM approaches are limited to very small systems (typically less than one hundred atoms) due to their high computational cost. Therefore, most QM simulations have been restricted to the interaction of CNT or graphite with small building blocks of DNA including nucleobase, nucleoside or nucleotide. More specifically, binding of individual nucleobases to CNT or graphite constitutes the majority of past studies with QM methods [22–40]. In addition, most studies using QM methods have been carried out in vacuum while in experiments DNA-CNT hybrids have been formed in an electrolyte solution. Only very few studies considered solution, but in those studies the hybrid structures were still optimized in vacuum, and the solvation energy was simply added using a continuum solvent model. A comprehensive review on the interaction of nucleobases with graphene or CNT can be found in Chehel Amirani and Tang[41].

While the dominant majority of the past work focused on the interaction of nucleobases with CNT, there are a few works on nucleotide-CNT interactions. Compared with nucleobases, nucleotides are larger molecules that consist of a nucleobase (base), a sugar ring, and a phosphate group. When residing in a solution, the phosphate group in the nucleotide becomes negatively charged and its electric field may be affected if a CNT (electronically responsive) is nearby. Therefore, to resemble the experimental conditions, it is more appropriate to consider the interaction of nucleotide with CNT in solution at the QM level. Wang and Ceulemans employed density functional theory (DFT) with local density approximation (LDA) to study the interaction of adenosine monophosphates with different CNTs in vacuum and evaluated the binding energy (BE) and charge transfer upon hybridization [42]. In another study also in vacuum, Enyashin *et al* [43] explored the binding between monophosphate nucleotides and a graphene sheet using dispersion-corrected self-consistent-charge density functional based tight binding method (DC-SCC-DFTB) and reported BEs. While attempting to include sugar ring and phosphate group into their simulation, the nucleotides in both works above were kept neutral and no solution was involved. Charged nucleotides were studied by Frischknecht and Martin in an MD work [14]. In their work, the adsorption of nucleotide monophosphates (NMPs) on a (6,0) CNT in solution was studied and BEs were evaluated. Although their model was relatively large, electronic response of the CNT was still lacking. To date, a comprehensive model that takes into account charged nucleotides, solution, and the electronic response of CNT is still missing.

In this study, our goal is to present a more complete model to study the interaction of nucleotides with CNT. Charged nucleotides as well as explicit representa-

tion for water and ion are to be considered, which makes our model considerably larger than what has been simulated before at QM level. Since the electronic structure of CNT is important, a proper QM method should be employed to model CNT and nucleotides. The large number of water molecules can be simulated using classical MM approach in order for the simulation time to be manageable. Hence, a hybrid QM:MM model is developed for the nucleotide-CNT interaction. The rest of the chapter is organized as follows. In Section 4.2, model development and computational details are described. The structural analysis and BE calculations are presented in Section 4.3. Conclusions are given in Section 4.4.

4.2 The QM:MM Model

4.2.1 Simulated systems

Four DNA nucleotides in the form of monophosphates i.e., nucleoside monophosphate (NMP), were considered in this study: adenosine 5'-monophosphates (AMP), cytidine 5'-monophosphates (CMP) , guanosine 5'-monophosphates (GMP) and thymidine 5'-monophosphates (TMP). Figure 4.1(a)-(d) shows the corresponding molecular structure of the NMPs. It has been reported in a number of experimental and theoretical works that under physiological conditions each of the two singly-bond oxygen atoms carries one negative charge and hence each NMP has a net charge of -2 at neutral pH [14, 44–49].

Two CNTs were chosen to interact with NMPs: a zigzag CNT with the chirality of (7,0) and an armchair CNT with the chirality of (4,4). These two CNTs have similar diameters (5.48 and 5.42 Å) and hence the effect of their curvature in

the binding with NMPs is negligible; however, the arrangements of carbon atoms in the two CNTs are different. Figure 4.1(e) and 4.1(f) shows the molecular structures of the two CNTs. The dangling bonds at the CNT ends were saturated with hydrogen atoms, giving rise to the length of 15.6 Å and 14.8 Å for the (7,0) CNT and (4,4) CNT, respectively. The CNTs lengths are reasonably large to provide a sufficient contact area with NMPs. The numbers of each type of atoms in each structure are listed in Table 4.1.

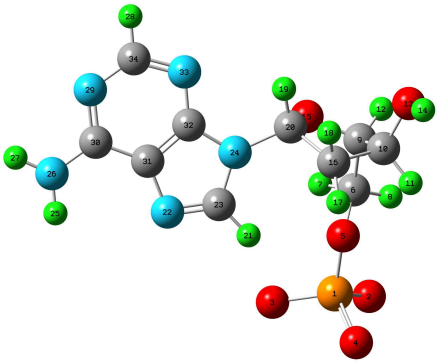

(a) AMP

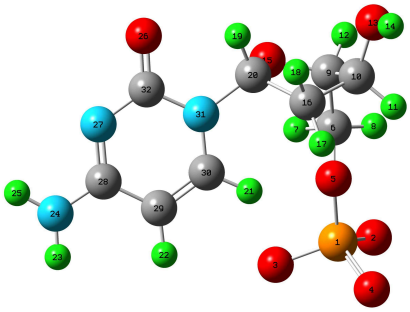

(b) CMP

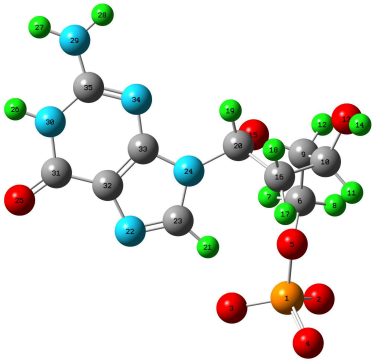

(c) GMP

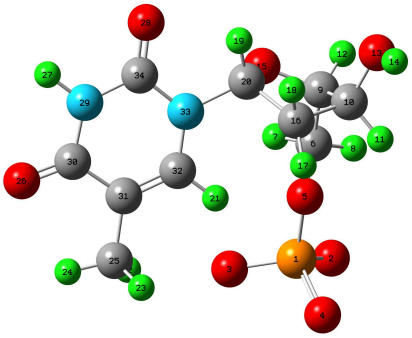

(d) TMP

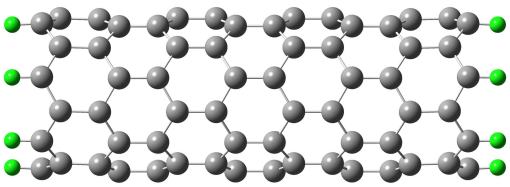

(e) (7,0) CNT

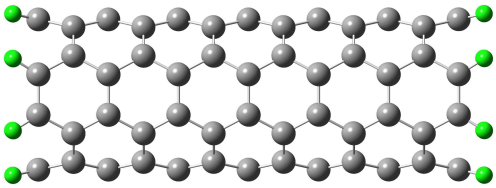

(f) (4,4) CNT

Figure 4.1: Molecular structures of NMPs and CNTs simulated in this work. Atoms in the NMPs are numbered in (a)-(d) to facilitate later discussion on binding structure.

Table 4.1: Numbers of each type of atoms in NMPs and CNTs

	C	H	N	O	P
AMP	10	12	5	6	1
CMP	9	12	3	7	1
GMP	10	12	5	7	1
TMP	10	13	2	8	1
(4,4) CNT	104	16	-	-	-
(7,0) CNT	112	14	-	-	-

NMP-CNT hybrids were assembled by placing the NMPs above the CNT surface. In each system, the nucleobase in the NMP was placed above the CNT surface so that the plane of pyrimidine ring was parallel to a plane defined from a hexagonal ring of carbon atoms on the CNT. Such an orientation was chosen based on previous studies where nucleobases were shown to prefer parallel orientation with respect to the CNT surface in order to maximize the π-π stacking interactions [36, 38, 40, 50, 51]. The separation between NMP and CNT in the initial configuration was set to be 3.2 Å which is close to the optimal distance between nucleobases and CNT reported in previous studies [26, 28, 36, 40, 52]. It is recognized that even with the nucleobase placed parallel to the CNT surface, many initial configurations can be defined, and different initial configurations may result in different optimized structures and BEs. Unfortunately, since our simulated systems are quite large, it is not practical to perform an extensive search to determine the configuration that leads to the most stable structure. Therefore, one initial configuration was chosen for each NMP-CNT system based on our knowledge of what structure might be close to an energy minimum. For the (7,0) CNT, the initial configuration was based on our previous work [40] where a sys-

tematic search was performed to determine the initial configurations that lead to the most stable structures for the corresponding nucleobase-CNT system. For the (4,4) CNT, each NMP was placed above the CNT surface such that the pyrimidine ring in the NMP was aligned with a hexagonal carbon ring on the CNT. The initial configurations for all eight systems are presented in the Appendix B (Figures B.1 and B.2).

To include the effect of an electrolyte solution, the NMP-CNT hybrids were solvated in explicit water and placed in the center of a box with dimensions of $3 \times 2.4 \times 2\ nm^3$ generated using Gromacs [53, 54]. Each of the eight systems simulated in this work include 386 water molecules, which makes the density of water in those model systems to be close to the density of bulk water i.e., 1 g/cm^3. Due to the net negative charge on NMPs, two Na^+ cations were added to the solution to neutralize the system. The location of ions was chosen randomly.

4.2.2 QM:MM method

QM:MM scheme is a relatively new class of methods in which different regions of a molecular system are modelled using different levels of theory i.e., QM and MM levels. ONIOM (our own n-layered integrated molecular orbital and molecular mechanics) is one of the QM:MM methods which can be used to simulate a molecular system with a reasonable computational cost. In an ONIOM simulation, the molecular system is partitioned into different regions and the energy of the entire system can be expressed as Equation 4.1 in which "Real" and "Model" refers to the entire system and the QM region, respectively. ”High” and ”low” refer to the level of theory which are respectively QM and MM.

$$E^{ONIOM} = E^{Model,High} + E^{Real,low} - E^{Model,low} \tag{4.1}$$

The ONIOM method as implemented in Gaussian 09 [55] was used to carry out our simulations. Each system consists of a QM layer and a MM layer. Because there may be charge transfer between the NMP and CNT and this may play an important role in their interaction, both entities were considered in the QM region. Due to the large number of water molecules and the unlikely charge transfer with the NMP and CNT, all water molecules and two cations were treated classically in the MM layer. Therefore, there is no covalent bond between QM and MM regions. Figure 4.2 shows the AMP-(7,0) CNT hybrid in the solution.

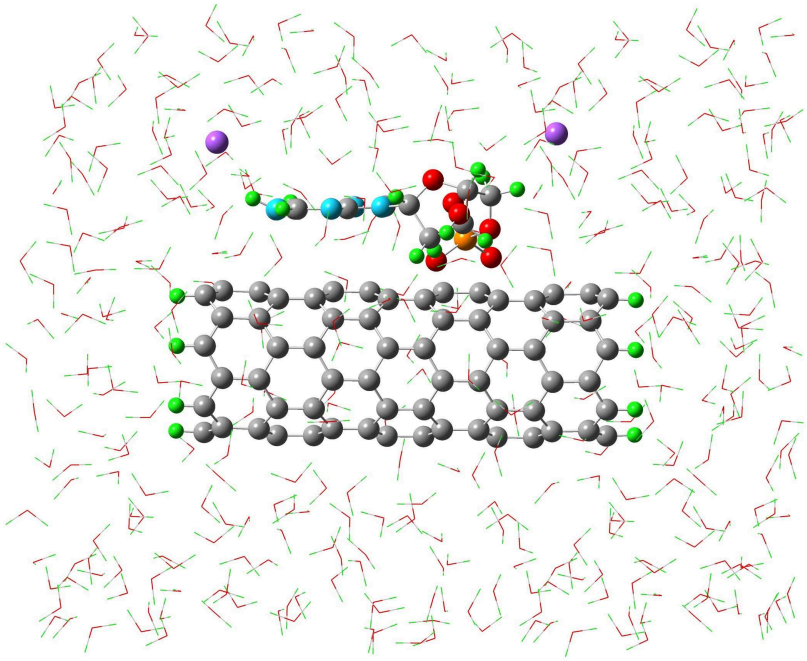

Figure 4.2: The ONIOM representation of the solvated AMP-(7,0) CNT hybrid. The two Na^+ ions are colored purple.

To perform the ONIOM simulation, appropriate methods need to be chosen for the MM and QM regions. For the MM calculations, the Amber force-field (FF) which is widely used to study the biological systems at an atomistic level was employed. It has been shown that the Amber FF can be even more accurate than some of the semi-empirical QM methods for such systems [56, 57]. The TIP3P model for water molecules was used.

For the QM calculation, a wide variety of methods with different levels of complexity and accuracy have been used to study molecular interactions involving nucleobases and nucleotides [22–40, 42, 43, 52, 58–60]. These methods

include *ab initio* methods (HF, MP2 and CCSD(T)), DFT and semi-empirical methods, among which DFT has been most widely used due to its relatively low computational cost compared with high level *ab initio* methods and high accuracy compared with semi-empirical methods. It is worth pointing out that dispersion forces, which are universal and among the most important interactions in molecular systems, were poorly treated in many DFT approaches. For the binding of nucleotides to CNT, dispersion can be important in determining the binding structure and BE since it is believed that $\pi - \pi$ stacking plays a crucial role in the binding. A number of dispersion-corrected methods has been proposed [57, 61–68]. Minnesota density functionals (including M05, M05-2X, M06, M06-L, M06-2X, and M06-HF), Grimme's functionals (B97-D, DFT-D2, and DFT-D3) [69–71], TS [72], vdW-DF [62], vdW-DF2 [73], and B3LYP-DCP [74] are among the dispersion-corrected methods within DFT that have been used to study $\pi - \pi$ interacting systems. M06-2X functional developed by Truhlar's group has shown good performance in several studies where vdW interaction was important [35, 52, 57, 60]. To evaluate the suitability of M06-2X functional in modeling our system, we performed a benchmark study with different basis sets. Individual nucleobases, i.e. adenine (A), cytosine (C), guanine (G), thymine (T) and uracil (U), shown respectively in Figure 4.3(a) to Figure 4.3(e), are considered to interact with a benzene ring shown in 4.3(f). We chose the nucleobase-benzene systems for two reasons: first, it is similar to nucleotide-CNT systems in the sense that the interaction is governed by $\pi - \pi$ stacking; and second, results of BE obtained from high level calculations (CCSD(T) method) are available in literature for the nucleobase-benzene system [57] which allows for the assessment of the M06-2X results.

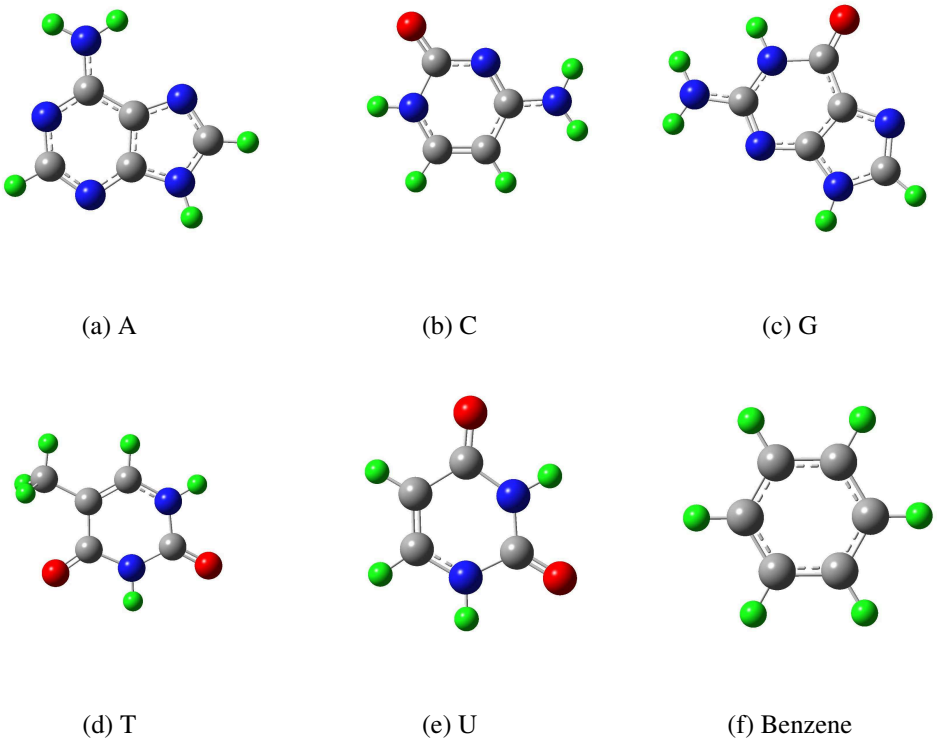

(a) A (b) C (c) G

(d) T (e) U (f) Benzene

Figure 4.3: Molecular structures of the nucleobases and benzene for the benchmarking study.

Configurations for the nucleobase-benzene systems were adopted from the work of [57]. Single-point energy calculations were performed for the individual nucleobases and benzene as well as their hybrids. The BE between nucleobases and benzene is then calculated as follows:

$$BE = |E^{\,Nucleobase-Benzene} - E^{\,Nucleobase} - E^{\,Benzene}| \tag{4.2}$$

where $E^{\,Nucleobase-Benzene}$ is the energy of the hybrid, $E^{\,Nucleobase}$ is the energy of the nucleobase and $E^{\,Benzene}$ is the energy of the benzene. Several different basis

sets were used to test their accuracy. These calculations were conducted using the default "fine grid" in Gaussian. Since it has been reported that M0-family functionals may have grid size dependency, we examined the effect of grid size by evaluating the BEs at M06-2X/6-31G(d) and M06-2X/6-31+G(d,p) levels using ultra fine grid. Table 4.2 shows the BE values obtained using M06-2X and the corresponding relative errors (in the parenthesis) compared to the BEs obtained using CCSD(T).

Table 4.2: BEs (kJ/mol) and relative errors (% in the parenthesis) obtained using M06-2X method compared with CCSD(T) [57] results

Basis Set	A	G	C	T	U
6-31G(d)	24.8 (6.4)	25.6 (1.2)	20.6 (0.0)	24.6 (0.4)	21.4 (1.0)
6-31G(d) (Ultra fine grid)	24.7 (6.0)	25.6 (1.2)	20.6 (0.0)	24.6 (0.4)	21.5 (0.9)
6-31G(d,p)	24.8 (6.4)	25.7 (1.6)	20.7 (0.5)	24.7 (0.8)	21.5 (0.9)
6-31+G(d,p)	24.4 (4.7)	26.2 (3.6)	21.3 (3.3)	25.0 (2.0)	21.6 (0.5)
6-31+G(d,p) (Ultra fine grid)	24.2 (3.9)	26.2 (3.6)	21.3 (3.3)	25.0 (2.0)	21.6 (0.5)
cc-pVDZ	26.3 (12.9)	27.3 (7.9)	21.5 (4.4)	25.0 (2.0)	21.8 (0.5)

It can be seen that the relative errors are quite small except for A-benzene evaluated using cc-pVDZ. In addition, the 6-31G(d) basis set performs well compared with the other basis sets we tested. Our results also show that except for A-benzene and U-benzene systems, grid size has no effect on BEs. Even for those two systems, using ultra fine grid only made a slight difference to the BE. Therefore, to achieve a balance between accuracy and computational efficiency, we chose M06-2X/6-31G(d) with fine grid to perform the QM calculation for our NMP-CNT systems.

4.2.3 Simulation Procedure

All individual NMPs and CNTs were first optimized at M06-2X/6-31G(d) level in vacuum. All atoms were free to relax during this optimization. This step provides appropriate initial structures for the QM:MM simulation in solution. After the optimization in vacuum, Resp charges [75] were evaluated for each NMP and CNT. This was done by single-point energy calculations at HF/6-31G(d) level using Gaussian, followed by Resp charge calculation using AmberTools [76]. Partial atomic charges for the two CNTs are presented in Appendix B (Figure B.3). It should be pointed out that the initial atomic charges in the NMPs and CNTs are different from those in the final optimized structures since the NMPs and CNTs were treated at the QM level in the QM:MM simulations.

The individually relaxed NMP and CNT were assembled and solvated to construct the initial configuration for the QM: MM simulation, as described in Section 4.2.1. Each solvated NMP-CNT hybrids was subjected to a two-step geometry optimization. First, a pure MM optimization was performed in which all atoms were free to move, with the purpose of relaxing atoms especially water molecules and reducing large forces in the system. Amber FF and Resp charges determined from the simulation in vacuum were used in this step. The structure obtained from the MM optimization was then subjected to an ONIOM optimization at M06-2X/6-31G(d):Amber level, where carbon atoms in CNTs were frozen to reduce the computation time.

In order to evaluate the BE between the NMPs and CNTs, two additional simulations were performed, one in which individual CNTs were optimized in water, and the other where individual NMPs were optimized in water in presence of the

two ions. The same two-step optimization procedure was followed for these two simulations. The numbers of water molecules in these two simulations were chosen such that they add up to the same as the number of water molecules in the NMP-CNT hybrid simulation (see details below).

4.2.4 Data analysis

The BE between NMP and CNT was calculated for each of the QM:MM model simulated above, according to the following equation:

$$BE = |E^{NMP-CNT} - E^{NMP} - E^{CNT}| \tag{4.3}$$

where $E^{NMP-CNT}$ is the energy of the optimized hybrid, E^{NMP} is the energy of the relaxed NMPs and E^{CNT} is the energy of the relaxed CNT, all evaluated in presence of solution. Unlike past simulations in vacuum, the BE calculation in the presence of solution is not trivial because of the solute-solvent interactions. In addition, due to the limitations of the ONIOM simulation, applying periodic boundary condition (PBC) was not possible [55], and hence free surfaces exist on the periphery of the simulation box. To include the solute-solvent interactions in the calculation of all energy terms in Equation 4.3, the 386 water molecules in the NMP-CNT hybrid simulation were partitioned into the individual NMP and CNT systems: each CNT was solvated in pure water while each NMP was solvated in water along with the two Na^+ ions.

As pointed out earlier, the lack of PBC introduces free surfaces around the water box, and the surface area of the box in the NMP-CNT hybrid simulation

is not equal to the sum of surface areas of the boxes in the individual NMP and CNT simulations. It is well known that water molecules on the surface have different properties compared with the interior ones, due to the different hydrogen bonding network around surface and interior molecules. It has been shown that at room temperature, on average each bulk water molecule forms 3.59 hydrogen bonds [77], while each surface water molecule forms $\sim$2 hydrogen bonds [78, 79]. One result of this is the high surface tension water possesses. Therefore, the change in surface area can contribute an artificial term in the BE calculated from Equation 4.3. To correct this, the BE from Equation 4.3 was modified to eliminate the effect of the free exterior surfaces. Specifically, the changes in surface energy was calculated in Equation 4.4.

$$\Delta E = |\gamma \Delta S| \tag{4.4}$$

where γ is the surface tension of water (0.072 N/m [80]) and ΔS is the change in exterior surface area calculated from

$$\Delta S = S^{NMP-CNT} - S^{NMP} - S^{CNT} \tag{4.5}$$

where $S^{NMP-CNT}$ is the surface area of water box of the optimized hybrid, S^{NMP} and S^{CNT} are respectively the surface areas of the water boxes for the optimized NMPs and CNT. To determine those surface areas, all oxygen atoms of water molecules were used to define a set of points, and a tetrahedral 3 dimensional mesh

was created based on those points (see Figure B.4 of the Appendix B). The exterior surface of the meshed region was defined to be S and subsequently calculated. The energy correction evaluated in Equation 4.4 was deducted from the BE calculated in Equation 4.3 and presented in the results section for the BEs between NMPs and CNT. It should be pointed out upon binding, some water molecules are released from around the solutes into the bulk. As a result, the water surface surrounding the NMP-CNT hybrid also has a different area compared with the total surface area around the individual NMPs and CNTs. However, the energy associated with water release should be considered in the BE, as water release provides one driving force for the binding process. Hence, correction of BE was only performed for water molecules on the outer surface of the simulation boxes.

4.3 Results

4.3.1 Structural analysis

Figure 4.4 shows the optimized structures for the eight systems simulated in this study (with water and ion removed for clarity; images with water and ion are given in Figure B.3 of the Appendix B). In almost all cases (except the GMP-(7,0) CNT system), the nucleobases tend to have parallel orientation with respect to the CNT surface, which was observed in almost all past simulations on nucleobase-CNT binding [26, 28, 38, 42, 51]. Therefore, the presence of phosphate group and sugar ring does not cause strong interruption to the parallel orientation of nucleobases relative to CNT surface, which has also been reported by Wang and Ceulemans in their simulation for the physisorption of DNA nucleoside on zigzag and armchair

CNTs [42]. In Figure 4.4, the sugar ring in all NMPs exhibits a perpendicular orientation relative to the nucleobase; which was observed in the relaxed NMPs in vacuum and such configuration did not change upon binding to CNT. Overall, little deformation of the internal structure was found during the binding process.

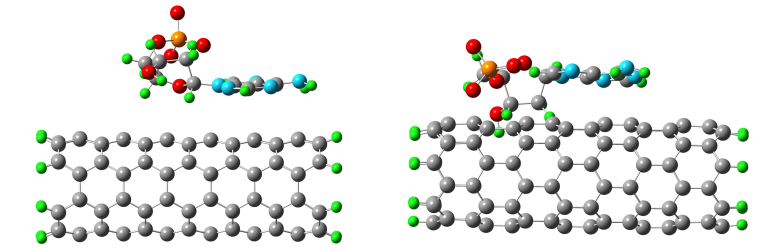

(a) AMP-(4,4) CNT (b) AMP-(7,0) CNT

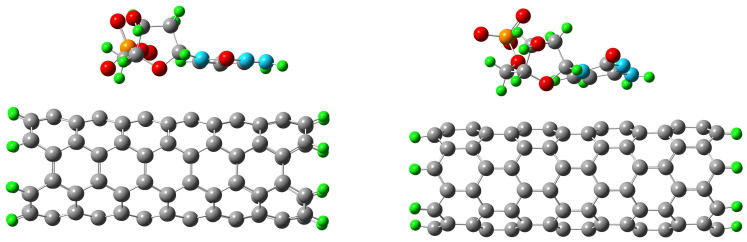

(c) CMP-(4,4) CNT (d) CMP-(7,0) CNT

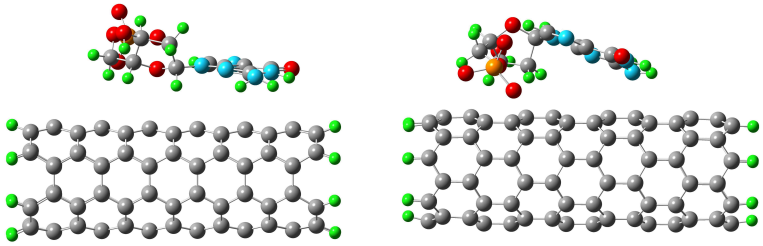

(e) GMP-(4,4) CNT (f) GMP-(7,0) CNT

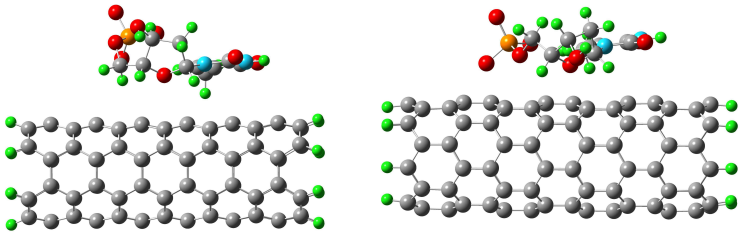

(g) TMP-(4,4) CNT (h) TMP-(7,0) CNT

Figure 4.4: Optimized NMP-CNT structures: (a) AMP-(4,4) CNT, (b) AMP-(7,0) CNT, (c) CMP-(4,4) CNT, (d) CMP-(7,0) CNT, (e) GMP-(4,4) CNT, (f) GMP-(7,0) CNT, (g) TMP-(4,4) CNT, (h) TMP-(7,0) CNT; water molecules and ions are not shown for clarity.

To further explore the location of NMP atoms relative to the CNT, the separation distance between each atom of NMPs and CNT surface in all optimized structures was calculated and shown in Figure 4.5. In each subfigure, the horizontal axis shows the atom number in the NMP and the vertical axis shows the separation distance of the atoms from the CNT surface. The separation was obtained by first calculating the distance from each atom to the CNT axis and then subtracting from it the radius of the CNT. The two series of data in each plot, presented with different symbols, correspond to the two CNTs. The ranges of the separation distance obtained for AMP, CMP, GMP and TMP adsorbed on the (4,4) CNT are respectively [2.30, 7.66] Å, [2.07, 6.08] Å, [2.09, 7.00] Å, and [2.22, 6.05] Å. The corresponding ranges for the (7,0) CNT are respectively [1.73, 4.95] Å, [1.98, 6.06] Å, [2.12, 5.00] Å, and [1.95, 5.55] Å.

In each NMP, No. 1-5 refer to the atoms in the phosphate group (1: phosphorous; 2 to 5: the four oxygens connected to phosphorous), No. 6 to 20 represent atoms on sugar ring, and the rest of the atoms belong to nucleobases, with the last six being the six atoms in the pyrimidine ring). The detailed numbering can be found in Figure 4.1. It can be seen from Figure 4.5 that atoms in the phosphate groups are generally located farther from the CNT surface. This is consistent with the hydrophilic properties of phosphate groups in DNA, namely that the DNA backbone tends to expose itself to the solution to maximize contact with water [81]. On the other hand, the six atoms in the pyrimidine ring of NMPs (29-34 in AMP and TMP, 27-32 in CMP, and 30-35 in GMP) are generally located at a distance of $\sim$3 Å from the CNT, which confirms the parallel orientation of nucleobases in NMPs relative to the CNT surface.

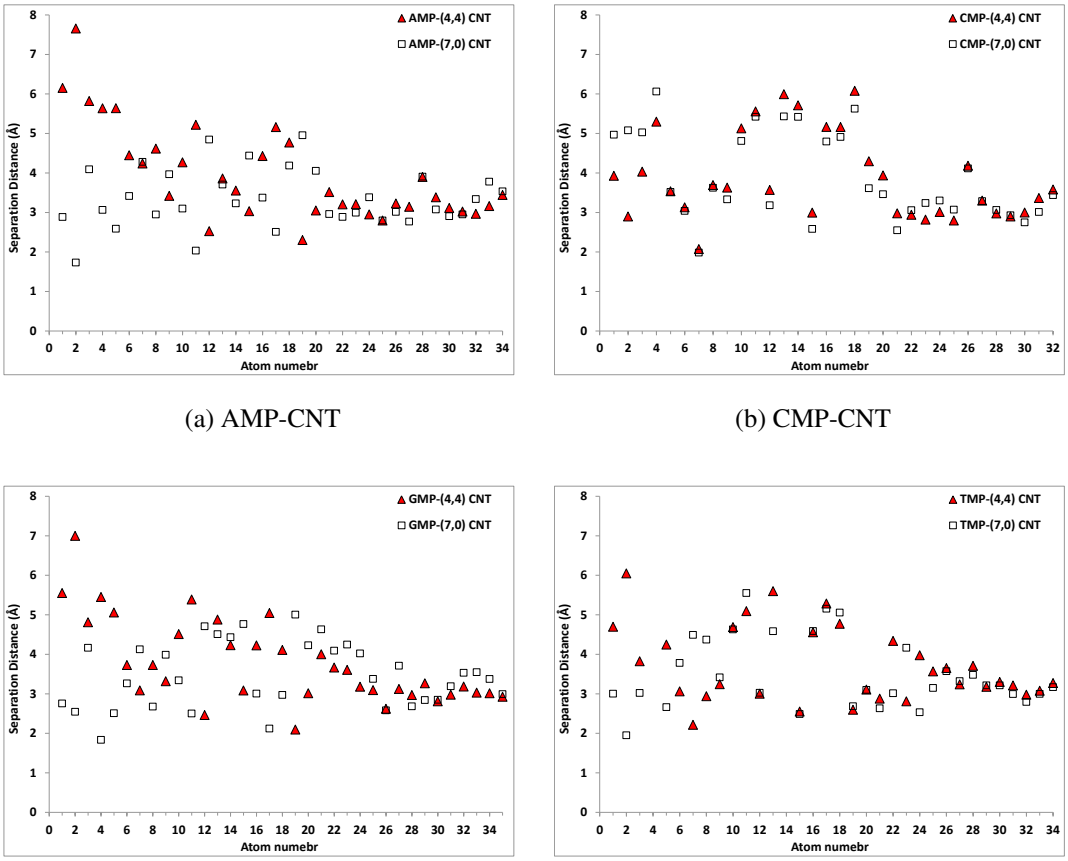

(a) AMP-CNT

(b) CMP-CNT

(c) GMP-CNT

(d) TMP-CNT

Figure 4.5: Separation distance between NMP atoms and CNT surface: (a) AMP-CNT, (b) CMP-CNT, (c) GMP-CNT, (d) TMP-CNT; results for NMP-(4,4) CNT and NMP-(7,0) CNT hybrids are respectively indicated by △ and □ symbols.

4.3.2 Binding Energy

BEs between the NMPs and CNTs evaluated based on the method described in Section 4.2.4 are presented in Table 4.3. It is recognized that there may be an inaccuracy associated with the calculation of surface area S in Equation 4.5. Using the initial structure of the NMP-CNT systems as a benchmark, the error was estimated to be around 2-17%. This may result in 2-25 kJ/mol error in the BEs, which

is still much smaller than the values of the BE in Table 4.3 and hence acceptable. The BE values vary from 146.60 to 503.43 kJ/mol, which are relatively larger than past reported energy of binding of nucleobase or nucleotide with CNT or graphene. For the nucleobase-CNT systems, a wide range of BE values covering 5.79 to 115.78 kJ/mol have been reported, depending on the specific system studied and the method chosen to do the optimization and calculation [41]. Compared with the many works on nucleobase-CNT binding, there are only a few studies on the binding of nucleotides with CNT. For instance, the BE between two connected AMPs on CNTs with the chiralities of (7,0) and (4,4) in vacuum was determined to be respectively 337.70 and 303.93 kJ/mol by Wang and Ceulemans [42]. Given the fact that two connected AMPs were modelled in that work, the BE for a single AMP physisorbed on the CNTs is expected to be around 150-170 kJ/mol, which is comparable to our result for AMP on (4,4) CNT, but smaller than our result for AMP on (7,0) CNT. To the best of our knowledge, the only work on the binding of NMPs with CNT in solution was performed by Frischknecht and Martin, in which the BE was evaluated using molecular dynamics. The BE for a NMP-(6,0) CNT system was determined to vary from 17.99 to 28.87 kJ/mol, depending on the type of NMP and salt concentration, which is considerably smaller compared with our results [14]. Even for the binding of NMPs with graphene which usually possess larger BE compared with CNTs due to larger contact area, smaller BEs (89.73-115.78 kJ/mol) have been reported in vacuum [43].

Table 4.3: BE (kJ/mol) between NMP and CNT in solution and contribution of water release (kJ/mol) (in parenthesis)

NMP	(4,4) CNT	(7,0) CNT
AMP	146.60 (27.91)	459.99 (104.58)
CMP	249.13 (163.98)	406.58 (112.81)
GMP	410.96 (118.17)	448.96 (126.46)
TMP	332.43 (153.77)	503.43 (99.87)

Several reasons might have contributed to the relatively large BEs found in our study. The first is the inclusion of solution and the energy associated with water release. Before binding, the CNT and the NMP are each solvated with certain number of water molecules around it. Upon the physisorption, some water molecules are released into the bulk. As each water molecule forms more hydrogen bonds in the bulk, such water release can contribute to lowering the energy of the system. In fact, water release has been recognized as an important mechanism in the biomolecular binding [82–84]. Using the same approach employed to evaluate the energy due to change in exterior surface area (See Section 4.2.4), we estimated the contribution of water release in the BE and presented it in Table 4.3. Clearly, this contribution is large and is on the order of the BE values. Even though solution was included in some of the previous studies on nucleobase-CNT binding [14, 17, 28, 51, 85], a continuum model for the solution was typically adopted to estimate the solvation energy, which is probably unable to accurately predict the contribution of water release in the BE.

Secondly, NMPs are charged in this study while all past studies except the work of Frischknecht and Martin [14] studied neutral nucelobases or nucleotides. It has been shown that charged molecules can bind stronger compared with their neutral counterparts [86–89]. For instance, the adsorption of CO_2, CH_4, and H_2 on Boron Nitride (BN) nanosheets and nanotubes with neutral, $1e^-$, and $2e^-$ charged states was investigated [86]. The BE between the negatively charged BN nanostructures and the three molecules was reported to be higher compared with the neutral ones, especially for CO_2 molecule. Also, the BE of the hydrogen molecule, H_2, on a doubly charged fullerene, C_{60}^{2+}, was shown to be higher than the value for neutral and singly charged fullerenes [88, 89]. In addition, compared with the past works on nucleobase-CNT binding, the presence of sugar ring and phosphate group can considerably enhance the vdW interactions between NMPs and CNT. According to the results for the separation distance in Figure 4.5, although the phosphate group tends to be solvated in solution, some atoms in the sugar ring and phosphate groups do have similar separation from the CNT surface compared to the nucleobase atoms. These atoms contribute to the vdW attraction between NMP and CNT, leading to larger BE than nucleobase-CNT binding. As for the work of Frischknecht and Martin, even though the study was performed in solution with the presence of charged NMP and ions, CHARMM force-field was used which could not capture the redistribution of electronic charges upon binding. More importantly, the BE calculation was based on the difference between NMP-CNT energy when they are close and the corresponding energy when the NMP and CNT are separated with a spring force. This force was not excluded from their calculations and might be the source of the relatively low BEs compared with results of Wang and Ceulemans [42] and our results.

According to the results in Table 4.3, for the (4,4) CNT the BEs of the four different NMPs follow the order of GMP>TMP>CMP>AMP, while the order for the (7,0) CNT is different, being TMP>AMP>GMP>CMP. Two important factors in determining the order of the BE for $\pi - \pi$ interaction systems are the size and orientation of the molecule. In our study, GMP has the largest size since it contains the highest number of atoms (35) while CMP possess smallest (32). AMP and TMP each contains 34 atoms. The BE results show that GMP has highest BE among the four NMPs for the (4,4) CNT, but it is not the case for the (7,0) CNT. The optimized structure for the GMP-(7,0) CNT (Figure 4(f)) indicates that the nucleobase in GMP is not as parallel as in the other systems which is likely the reason for its smaller BE to the (7,0) CNT compared with TMP and AMP. Although AMP and TMP have the same number of atoms, TMP tends to have higher BE to the CNTs. For the interaction with the (4,4) CNT, the adsorbed TMP is closer to the CNT surface than the adsorbed AMP: the range of separation distance between TMP and the (4,4) CNT is [2.22, 6.05] Å while it is [2.30, 7.66] Å for the AMP. This explains why AMP has smaller BE than TMP and even CMP ([2.07, 6.08] Å from the CNT). For the interaction with the (7,0) CNT, no visible difference in the nucleotide-CNT separation can be observed for AMP and TMP, the cause for the small difference (<10%) in their BE requires further investigation. It is worth mentioning that very different orders for the BE have been reported in the past studies, where the dominant majority focusing on the interaction of nucleobases with CNT in vacuum (See Ref. [41]), although G has been mostly found to bind to CNT more strongly compared with the other nucleobases possibly due to its larger size. For example, Umadevi and Sastry used ONIOM approach at M06-2X:AM1 level to study interactions between nucleobases and arm-

chair CNTs in vacuum [60]. Atoms in the nucleobases and the "reacting atoms" of CNTs were modeled as the high layer using M06-2X/6-31G(d), although it was not clearly explained what carbon atoms were considered to be reacting. The remaining atoms in CNT were considered as the low layer using semi-empirical AM1. The order of the BE between nucleobases and a (4,4) CNT was determined to be T>G∼C>A, but it changed to G>T>A>C when an additional single-point energy calculation using B3LYP-D method was performed.

Comparing the two different CNTs, BEs for NMP-(7,0) CNT hybrids are in general found to be larger than the ones for the NMP-(4,4) CNT hybrids. This difference shows that two CNTs with very similar diameter and hence similar contact areas may interact differently with the same NMP, due to their different chiralities. Chirality dependence of CNT properties has been previously shown to be important in the dispersion and separation of CNTs [8, 9]. Specifically, in the experiment by Zheng et al. [8], it was discovered that single-stranded DNA (ssDNA) can bind to CNT in an aqueous environment and form a hybrid structure where the ssDNA helically wraps around the CNT. The hybrids can be easily dispersed and subsequently separated, using ion exchange chromatography, according to the chirality of the CNT. In addition, both dispersion and separation of CNTs was found to depend on the sequence of the DNA. Our model showed that different nucleobases and CNT chiralities give rise to different BEs, which may affect the stability of the ssDNA-CNT hybrids in the experiments.

4.3.3 Limitation and future perspective

The present work is an attempt to more appropriately model the interactions between NMPs and CNT by combining QM and MM approaches. The model has several merits compared with past studies. Firstly, unlike past studies which focused on nucleobase-CNT binding, the current model includes the charged phosphate group and sugar ring, present in real DNA polymer binding with CNT. Secondly, while past studies usually consider nucleobase-CNT hybrids in vacuum, the current model contains an explicit solution and ions, which does exist in practical applications [8, 9] and can play an important role in the binding. Furthermore, the QM:MM scheme adopted to simulate the binding provides a balance between computational efficiency and accuracy in capturing electronic distribution. In fact, our model contains the largest number of atoms among all available QM and QM:MM simulations on nucleobase/nulceotide-CNT binding. On the other hand, it is important to point out the limitations of this study. First of all, CNTs simulated in this work are short with hydrogen atoms at the two ends. The free edges can introduce some effects on the BE values as well as separation distances. The non-zero partial charges at the edge carbons and hydrogens may also lead to stronger interaction with water compared with infinitely long tube. Application of PBC not only can remove the influence of free edges, but can also more precisely describe electronic properties of CNT. To the best of our knowledge, there is no hybrid QM:MM method available that can include PBC in charged systems. One way to overcome this problem might be using QM approaches with plane wave basis sets in the QM:MM framework. This area of research is being explored to improve the simulation of charged systems using QM:MM methods.

Secondly, each geometry optimization in this study was started with a single initial configuration. It has been shown that initial configuration can affect the optimized structures and results of BE [40]. Performing a potential energy scan (PES) and geometry optimization together can be a solution, however it needs more computational time and resources. Furthermore, only neutral pH was considered in the simulations. Different pH value can lead to different deprotonation states of the phosphate group, which can in turn affect the binding. This is an interesting area to be explored in the future. Lastly, only two neutralizing cations were included in our simulations. Different salt concentrations (number of ions) may also affect the results, which was shown by Frischknecht and Martin [14]. It is worth studying the effect of screening ions, which is especially important if one is to better understanding how the DNA-CNT interaction changes upon addition of salt under the experimental conditions [8].

4.4 Conclusion

A QM:MM model was developed to study the physisorption of nucleotides on CNT surfaces in solution. The nucleotides and CNTs were modeled at the QM level, while the aqueous environment was modelled at the MM level through explicit water molecules and ions. Optimized binding structures were obtained from ONIOM simulations and BEs were calculated from the optimized structures. Our results revealed strong physisorption of nucleotides on CNTs, with the BE in the range of 146.60 to 503.43 kJ/mol for the (4,4) and (7,0) CNTs. The relatively large BE, compared with past studies on nucleobase-CNT binding in vacuum, could be due to the larger size of nucleotides compared with nucleobase, the charges on

the nucleotides, and the inclusion of solution which causes the release of water molecules upon hybridization.

References

[1] S. Iijima, "Helical microtubules of graphitic carbon," *Nature*, vol. 354, pp. 56–58, 1991.

[2] R. Saito, G. Dresselhaus, and M. Dresselhaus, *Physical Properties of Carbon Nanotube*. Imperial College Press, 1998.

[3] R. Singh, D. Pantarotto, D. McCarthy, O. Chaloin, J. Hoebeke, C. D. Partidos, J.-P. Briand, M. Prato, A. Bianco, and K. Kostarelos, "Binding and Condensation of Plasmid DNA onto Functionalized Carbon Nanotubes: Toward the Construction of Nanotube-Based Gene Delivery Vectors," *Journal of the American Chemical Society*, vol. 127, no. 12, pp. 4388–4396, 2005.

[4] C. Hu, Y. Zhang, G. Bao, Y. Zhang, M. Liu, and Z. L. Wang, "DNA Functionalized Single-Walled Carbon Nanotubes for Electrochemical Detection," *The Journal of Physical Chemistry B*, vol. 109, no. 43, pp. 20072–20076, 2005.

[5] Y. Ma, S. R. Ali, A. S. Dodoo, and H. He, "Enhanced Sensitivity for Biosensors: Multiple Functions of DNA-Wrapped Single-Walled Carbon Nanotubes in Self-Doped Polyaniline Nanocomposites," *The Journal of Physical Chemistry B*, vol. 110, no. 33, pp. 16359–16365, 2006.

[6] P. He and M. Bayachou, "Layer-by-Layer Fabrication and Characterization

of DNA-Wrapped Single-Walled Carbon Nanotube Particles," *Langmuir*, vol. 21, no. 13, pp. 6086–6092, 2005.

[7] Y. Xu, P. E. Pehrsson, L. Chen, R. Zhang, and W. Zhao, "Double-Stranded DNA Single-Walled Carbon Nanotube Hybrids for Optical Hydrogen Peroxide and Glucose Sensing," *The Journal of Physical Chemistry C*, vol. 111, no. 24, pp. 8638–8643, 2007.

[8] M. Zheng, A. Jagota, E. D. Semke, B. A. Diner, R. S. Mclean, S. R. Lustig, R. E. Richardson, and N. G. Tassi, "DNA-assisted dispersion and separation of carbon nanotubes," *Nat Mater*, vol. 2, no. 5, pp. 338–342, 2003.

[9] M. Zheng, A. Jagota, M. S. Strano, A. P. Santos, P. Barone, S. G. Chou, B. A. Diner, M. S. Dresselhaus, R. S. Mclean, G. B. Onoa, G. G. Samsonidze, E. D. Semke, M. Usrey, and D. J. Walls, "Structure-Based Carbon Nanotube Sorting by Sequence-Dependent DNA Assembly," *Science*, vol. 302, no. 5650, pp. 1545–1548, 2003.

[10] G. F. Schneider, S. W. Kowalczyk, V. E. Calado, G. Pandraud, H. W. Zandbergen, L. M. K. Vandersypen, and C. Dekker, "DNA Translocation through Graphene Nanopores," *Nano Letters*, vol. 10, no. 8, pp. 3163–3167, 2010.

[11] H. W. C. Postma, "Rapid Sequencing of Individual DNA Molecules in Graphene Nanogaps," *Nano Letters*, vol. 10, no. 2, pp. 420–425, 2010.

[12] D. B. Wells, M. Belkin, J. Comer, and A. Aksimentiev, "Assessing Graphene Nanopores for Sequencing DNA," *Nano Letters*, vol. 12, no. 8, pp. 4117–4123, 2012.

[13] C. Merchant and M. Drndić, "Graphene nanopore devices for dna sensing," in *Nanopore-Based Technology* (M. E. Gracheva, ed.), vol. 870 of *Methods in Molecular Biology*, pp. 211–226, Humana Press, 2012.

[14] A. L. Frischknecht and M. G. Martin, "Simulation of the adsorption of nucleotide monophosphates on carbon nanotubes in aqueous solution," *The Journal of Physical Chemistry C*, vol. 112, no. 16, pp. 6271–6278, 2008.

[15] R. R. Johnson, A. T. C. Johnson, and M. L. Klein, "Probing the Structure of DNA-Carbon Nanotube Hybrids with Molecular Dynamics," *Nano Letters*, vol. 8, no. 1, pp. 69–75, 2008.

[16] R. R. Johnson, A. T. C. Johnson, and M. L. Klein, "The Nature of DNA-Base–Carbon-Nanotube Interactions," *Small*, vol. 6, no. 1, pp. 31–34, 2010.

[17] W. Lv, "The adsorption of DNA bases on neutral and charged (8, 8) carbon-nanotubes," *Chemical Physics Letters*, vol. 514, no. 4–6, pp. 311 – 316, 2011.

[18] A. K. Manna and S. K. Pati, "Theoretical understanding of single-stranded DNA assisted dispersion of graphene," *J. Mater. Chem. B*, vol. 1, pp. 91–100, 2013.

[19] M. L. Mayo, Z. Q. Chen, and S. V. Kilina, "Computational studies of nucleotide selectivity in dna–carbon nanotube hybrids," *The Journal of Physical Chemistry Letters*, vol. 3, no. 19, pp. 2790–2797, 2012.

[20] S. Neihsial, G. Periyasamy, P. K. Samanta, and S. K. Pati, "Understanding the Binding Mechanism of Various Chiral SWCNTs and ssDNA: A Com-

putational Study," *The Journal of Physical Chemistry B*, vol. 116, no. 51, pp. 14754–14759, 2012.

[21] Z. Xiao, X. Wang, X. Xu, H. Zhang, Y. Li, and Y. Wang, "Base- and Structure-Dependent DNA Dinucleotide–Carbon Nanotube Interactions: Molecular Dynamics Simulations and Thermodynamic Analysis," *The Journal of Physical Chemistry C*, vol. 115, no. 44, pp. 21546–21558, 2011.

[22] S. Gowtham, R. H. Scheicher, R. Ahuja, R. Pandey, and S. P. Karna, "Physisorption of nucleobases on graphene: Density-functional calculations," *Phys. Rev. B*, vol. 76, p. 033401, 2007.

[23] S. Gowtham, R. H. Scheicher, R. Pandey, S. P. Karna, and R. Ahuja, "First-principles study of physisorption of nucleic acid bases on small-diameter carbon nanotubes," *Nanotechnology*, vol. 19, no. 12, p. 125701, 2008.

[24] S. Meng, P. Maragakis, C. Papaloukas, and E. Kaxiras, "DNA Nucleoside Interaction and Identification with Carbon Nanotubes," *Nano Letters*, vol. 7, no. 1, pp. 45–50, 2007.

[25] S. Meng, W. L. Wang, P. Maragakis, and E. Kaxiras, "Determination of DNA-Base Orientation on Carbon Nanotubes through Directional Optical Absorbance," *Nano Letters*, vol. 7, no. 8, pp. 2312–2316, 2007.

[26] Y. V. Shtogun, L. M. Woods, and G. I. Dovbeshko, "Adsorption of Adenine and Thymine and Their Radicals on Single-Wall Carbon Nanotubes," *The Journal of Physical Chemistry C*, vol. 111, no. 49, pp. 18174–18181, 2007.

[27] Y. Wang and Y. Bu, "Noncovalent Interactions between Cytosine and

SWCNT," *The Journal of Physical Chemistry B*, vol. 111, no. 23, pp. 6520–6526, 2007.

[28] Y. Wang, "Theoretical Evidence for the Stronger Ability of Thymine to Disperse SWCNT than Cytosine and Adenine: Self-Stacking of DNA Bases vs Their Cross-Stacking with SWCNT," *The Journal of Physical Chemistry C*, vol. 112, no. 37, pp. 14297–14305, 2008.

[29] F. Ortmann, W. G. Schmidt, and F. Bechstedt, "Attracted by Long-Range Electron Correlation: Adenine on Graphite," *Phys. Rev. Lett.*, vol. 95, p. 186101, 2005.

[30] K. Berland, S. D. Chakarova-Käck, V. R. Cooper, D. C. Langreth, and E. Schröder, "A van der Waals density functional study of adenine on graphene: single-molecular adsorption and overlayer binding," *Journal of Physics: Condensed Matter*, vol. 23, no. 13, p. 135001, 2011.

[31] J. Antony and S. Grimme, "Structures and interaction energies of stacked graphene-nucleobase complexes," *Phys. Chem. Chem. Phys.*, vol. 10, pp. 2722–2729, 2008.

[32] S. Panigrahi, A. Bhattacharya, S. Banerjee, and D. Bhattacharyya, "Interaction of Nucleobases with Wrinkled Graphene Surface: Dispersion Corrected DFT and AFM Studies," *The Journal of Physical Chemistry C*, vol. 116, no. 7, pp. 4374–4379, 2012.

[33] D. Le, A. Kara, E. Schröder, P. Hyldgaard, and T. S. Rahman, "Physisorption of nucleobases on graphene: a comparative van der Waals study," *Journal of Physics: Condensed Matter*, vol. 24, no. 42, p. 424210, 2012.

[34] Y. Cho, S. K. Min, J. Yun, W. Y. Kim, A. Tkatchenko, and K. S. Kim, "Noncovalent Interactions of DNA Bases with Naphthalene and Graphene," *Journal of Chemical Theory and Computation*, vol. 9, no. 0, pp. 2090–2096, 2013.

[35] H. Vovusha, S. Sanyal, and B. Sanyal, "Interaction of nucleobases and aromatic amino acids with graphene oxide and graphene flakes," *The Journal of Physical Chemistry Letters*, vol. 4, no. 21, pp. 3710–3718, 2013.

[36] S. Stepanian, M. Karachevtsev, A. Glamazda, V. Karachevtsev, and L. Adamowicz, "Stacking interaction of cytosine with carbon nanotubes: MP2, DFT and Raman spectroscopy study," *Chemical Physics Letters*, vol. 459, no. 1–6, pp. 153–158, 2008.

[37] M. Shukla, M. Dubey, E. Zakar, R. Namburu, Z. Czyznikowska, and J. Leszczynski, "Interaction of nucleic acid bases with single-walled carbon nanotube," *Chemical Physics Letters*, vol. 480, no. 4–6, pp. 269–272, 2009.

[38] B. Akdim, R. Pachter, P. N. Day, S. S. Kim, and R. R. Naik, "On modeling biomolecular–surface nonbonded interactions: application to nucleobase adsorption on single-wall carbon nanotube surfaces," *Nanotechnology*, vol. 23, no. 16, p. 165703, 2012.

[39] A. Sarmah and R. K. Roy, "Understanding the interaction of nucleobases with chiral semiconducting single-walled carbon nanotubes: An alternative theoretical approach based on density functional reactivity theory," *The Journal of Physical Chemistry C*, vol. 117, no. 41, pp. 21539–21550, 2013.

[40] M. Chehel Amirani, T. Tang, and J. Cuervo, "Quantum mechanical treatment of binding energy between DNA nucleobases and carbon nanotube: A DFT analysis," *Physica E: Low-dimensional Systems and Nanostructures*, vol. 54, pp. 65–71, 2013.

[41] M. Chehel Amirani and T. Tang, "Binding of nucleobases with graphene and carbon nanotube: a review of computational studies," *Journal of Biomolecular Structure and Dynamics*, pp. 1–31, 2014.

[42] H. Wang and A. Ceulemans, "Physisorption of adenine DNA nucleosides on zigzag and armchair single-walled carbon nanotubes: A first-principles study," *Phys. Rev. B*, vol. 79, p. 195419, 2009.

[43] A. N. Enyashin, S. Gemming, and G. Seifert, "DNA-wrapped carbon nanotubes," *Nanotechnology*, vol. 18, no. 24, p. 245702, 2007.

[44] A. Lehninger, D. Nelson, and M. Cox, *Lehninger Principles of Biochemistry*. W. H. Freeman, 2005.

[45] G. M. Blackburn, M. J. Gait, D. Loakes, and D. M. Williams, eds., *Nucleic Acids in Chemistry and Biology*. The Royal Society of Chemistry, 2006.

[46] D. Ebbing and S. Gammon, *General Chemistry: Media Enhanced Edition*. Cengage Learning, 2007.

[47] M. Madigan, D. Clark, D. Stahl, and J. Martinko, *Brock Biology of Microorganisms 13th Edition:*. Benjamin Cummings, 2010.

[48] A. Wong and G. Wu, "Selective binding of monovalent cations to the stacking g-quartet structure formed by guanosine 5'-monophosphate: A solid-

state nmr study," *Journal of the American Chemical Society*, vol. 125, no. 45, pp. 13895–13905, 2003.

[49] D. M. Boghaei and M. Gharagozlou, "Charge transfer complexes of adenosine-5ı-monophosphate and cytidine-5ı-monophosphate with water-soluble cobalt(ii) schiff base complexes in aqueous solution," *Spectrochimica Acta Part A: Molecular and Biomolecular Spectroscopy*, vol. 63, no. 1, pp. 139 – 148, 2006.

[50] N. Varghese, U. Mogera, A. Govindaraj, A. Das, P. K. Maiti, A. K. Sood, and C. N. R. Rao, "Binding of DNA Nucleobases and Nucleosides with Graphene," *ChemPhysChem*, vol. 10, no. 1, pp. 206–210, 2009.

[51] A. Das, A. Sood, P. K. Maiti, M. Das, R. Varadarajan, and C. Rao, "Binding of nucleobases with single-walled carbon nanotubes: Theory and experiment," *Chemical Physics Letters*, vol. 453, no. 4–6, pp. 266–273, 2008.

[52] A. Ramraj, I. H. Hillier, M. A. Vincent, and N. A. Burton, "Assessment of approximate quantum chemical methods for calculating the interaction energy of nucleic acid bases with graphene and carbon nanotubes," *Chemical Physics Letters*, vol. 484, no. 4–6, pp. 295–298, 2010.

[53] H. Berendsen, D. van der Spoel, and R. van Drunen, "Gromacs: A message-passing parallel molecular dynamics implementation," *Computer Physics Communications*, vol. 91, no. 1–3, pp. 43 – 56, 1995.

[54] E. Lindahl, B. Hess, and D. van der Spoel, "Gromacs 3.0: a package for molecular simulation and trajectory analysis," *Molecular modeling annual*, vol. 7, no. 8, pp. 306–317, 2001.

[55] M. J. Frisch, G. W. Trucks, H. B. Schlegel, G. E. Scuseria, M. A. Robb, J. R. Cheeseman, G. Scalmani, V. Barone, B. Mennucci, G. A. Petersson, H. Nakatsuji, M. Caricato, X. Li, H. P. Hratchian, A. F. Izmaylov, J. Bloino, G. Zheng, J. L. Sonnenberg, M. Hada, M. Ehara, K. Toyota, R. Fukuda, J. Hasegawa, M. Ishida, T. Nakajima, Y. Honda, O. Kitao, H. Nakai, T. Vreven, J. J. A. Montgomery, J. E. Peralta, F. Ogliaro, M. Bearpark, J. J. Heyd, E. Brothers, K. N. Kudin, V. N. Staroverov, R. Kobayashi, J. Normand, K. Raghavachari, A. Rendell, J. C. Burant, S. S. Iyengar, J. Tomasi, M. Cossi, N. Rega, J. M. Millam, M. Klene, J. E. Knox, J. B. Cross, V. Bakken, C. Adamo, J. Jaramillo, R. Gomperts, R. E. Stratmann, O. Yazyev, A. J. Austin, R. Cammi, C. Pomelli, J. W. Ochterski, R. L. Martin, K. Morokuma, V. G. Zakrzewski, G. A. Voth, P. Salvador, J. J. Dannenberg, S. Dapprich, A. D. Daniels, Ö. Farkas, J. B. Foresman, J. V. Ortiz, J. Cioslowski, and D. J. Fox, "Gaussian 09 Revision A.1." Gaussian Inc. Wallingford CT 2009.

[56] L. R. Rutledge, H. F. Durst, and S. D. Wetmore, "Evidence for Stabilization of DNA/RNA Protein Complexes Arising from Nucleobase Amino Acid Stacking and T-Shaped Interactions," *Journal of Chemical Theory and Computation*, vol. 5, no. 5, pp. 1400–1410, 2009.

[57] L. R. Rutledge and S. D. Wetmore, "The assessment of density functionals for DNAprotein stacked and T-shaped complexes," *Canadian Journal of Chemistry*, vol. 88, no. 8, pp. 815–830, 2010.

[58] S. Chandra Shekar and R. S. Swathi, "Stability of nucleobases and base pairs

adsorbed on graphyne and graphdiyne," *The Journal of Physical Chemistry C*, vol. 118, no. 8, pp. 4516–4528, 2014.

[59] J.-H. Lee, Y.-K. Choi, H.-J. Kim, R. H. Scheicher, and J.-H. Cho, "Physisorption of DNA Nucleobases on h-BN and Graphene: vdW-Corrected DFT Calculations," *The Journal of Physical Chemistry C*, vol. 117, no. 26, pp. 13435–13441, 2013.

[60] D. Umadevi and G. N. Sastry, "Quantum Mechanical Study of Physisorption of Nucleobases on Carbon Materials: Graphene versus Carbon Nanotubes," *The Journal of Physical Chemistry Letters*, vol. 2, no. 13, pp. 1572–1576, 2011.

[61] E. R. Johnson, R. A. Wolkow, and G. A. DiLabio, "Application of 25 density functionals to dispersion-bound homomolecular dimers," *Chemical Physics Letters*, vol. 394, no. 4–6, pp. 334–338, 2004.

[62] M. Dion, H. Rydberg, E. Schröder, D. C. Langreth, and B. I. Lundqvist, "Van der Waals Density Functional for General Geometries," *Phys. Rev. Lett.*, vol. 92, p. 246401, 2004.

[63] E. G. Hohenstein, S. T. Chill, and C. D. Sherrill, "Assessment of the Performance of the M055-2X and M06-2X Exchange-Correlation Functionals for Noncovalent Interactions in Biomolecules," *Journal of Chemical Theory and Computation*, vol. 4, no. 12, pp. 1996–2000, 2008.

[64] Y. Zhao and D. G. Truhlar, "Density functionals with broad applicability in chemistry," *Accounts of Chemical Research*, vol. 41, no. 2, pp. 157–167, 2008.

[65] E. R. Johnson, I. D. Mackie, and G. A. DiLabio, "Dispersion interactions in density-functional theory," *Journal of Physical Organic Chemistry*, vol. 22, no. 12, pp. 1127–1135, 2009.

[66] Y. Zhao and D. G. Truhlar, "Applications and validations of the Minnesota density functionals," *Chemical Physics Letters*, vol. 502, no. 1–3, pp. 1–13, 2011.

[67] S. Grimme, "Density functional theory with London dispersion corrections," *Wiley Interdisciplinary Reviews: Computational Molecular Science*, vol. 1, no. 2, pp. 211–228, 2011.

[68] S. Ehrlich, J. Moellmann, and S. Grimme, "Dispersion-Corrected Density Functional Theory for Aromatic Interactions in Complex Systems," *Accounts of Chemical Research*, vol. 46, no. 4, pp. 916–926, 2013.

[69] S. Grimme, "Semiempirical GGA-type density functional constructed with a long-range dispersion correction," *Journal of Computational Chemistry*, vol. 27, no. 15, pp. 1787–1799, 2006.

[70] S. Grimme, J. Antony, S. Ehrlich, and H. Krieg, "A consistent and accurate ab initio parametrization of density functional dispersion correction (DFT-D) for the 94 elements H-Pu," *The Journal of Chemical Physics*, vol. 132, no. 15, p. 154104, 2010.

[71] S. Grimme, S. Ehrlich, and L. Goerigk, "Effect of the damping function in dispersion corrected density functional theory," *Journal of Computational Chemistry*, vol. 32, no. 7, pp. 1456–1465, 2011.

[72] A. Tkatchenko and M. Scheffler, "Accurate Molecular Van Der Waals Interactions from Ground-State Electron Density and Free-Atom Reference Data," *Phys. Rev. Lett.*, vol. 102, p. 073005, 2009.

[73] K. Lee, É. D. Murray, L. Kong, B. I. Lundqvist, and D. C. Langreth, "Higher-accuracy van der Waals density functional," *Phys. Rev. B*, vol. 82, p. 081101, 2010.

[74] E. Torres and G. A. DiLabio, "A (nearly) universally applicable method for modeling noncovalent interactions using b3lyp," *The Journal of Physical Chemistry Letters*, vol. 3, no. 13, pp. 1738–1744, 2012.

[75] C. I. Bayly, P. Cieplak, W. Cornell, and P. A. Kollman, "A well-behaved electrostatic potential based method using charge restraints for deriving atomic charges: the resp model," *The Journal of Physical Chemistry*, vol. 97, no. 40, pp. 10269–10280, 1993.

[76] D. Case, T. Darden, T. C. III, C. Simmerling, J. Wang, R. Duke, R. Luo, R. Walker, W. Zhang, K. Merz, B. Roberts, S. Hayik, A. Roitberg, G. Seabra, J. Swails, A. GÖtz, I. Kolossváry, K. Wong, F. Paesani, J. Vanicek, R. Wolf, J. Liu, X. Wu, S. Brozell, T. Steinbrecher, H. Gohlke, Q. Cai, X. Ye, J. Wang, M. Hsieh, G. Cui, D. Roe, D. Mathews, M. Seetin, R. Salomon-Ferrer, C. Sagui, V. Babin, T. Luchko, S. Gusarov, A. Kovalenko, and P. Kollman, "AmberTools12." University of California, San Francisco 2012.

[77] W. L. Jorgensen and J. D. Madura, "Temperature and size dependence for monte carlo simulations of tip4p water," *Molecular Physics*, vol. 56, no. 6, pp. 1381–1392, 1985.

[78] E. A. Raymond, T. L. Tarbuck, M. G. Brown, and G. L. Richmond, "Hydrogen-bonding interactions at the vapor/water interface investigated by vibrational sum-frequency spectroscopy of hod/h2o/d2o mixtures and molecular dynamics simulations," *The Journal of Physical Chemistry B*, vol. 107, no. 2, pp. 546–556, 2003.

[79] P. Liu, E. Harder, and B. J. Berne, "Hydrogen-bond dynamics in the air-water interface," *The Journal of Physical Chemistry B*, vol. 109, no. 7, pp. 2949–2955, 2005.

[80] N. B. Vargaftik, B. N. Volkov, and L. D. Voljak, "International tables of the surface tension of water," *Journal of Physical and Chemical Reference Data*, vol. 12, no. 3, pp. 817–820, 1983.

[81] T. Premkumar and K. Geckeler, *Materials Science of DNA*. CRC Press, 2011.

[82] J.-H. Ha, R. S. Spolar, and M. R. Jr, "Role of the hydrophobic effect in stability of site-specific protein-dna complexes," *Journal of Molecular Biology*, vol. 209, no. 4, pp. 801 – 816, 1989.

[83] B. Jayaram and T. Jain, "The role of water in protein-dna recognition," *Annual Review of Biophysics and Biomolecular Structure*, vol. 33, no. 1, pp. 343–361, 2004.

[84] B. Jayaram, K. McConnell, S. B. Dixit, A. Das, and D. L. Beveridge, "Free-energy component analysis of 40 protein–dna complexes: A consensus view on the thermodynamics of binding at the molecular level," *Journal of Computational Chemistry*, vol. 23, no. 1, pp. 1–14, 2002.

[85] T. Yamazaki and H. Fenniri, "Imaging carbon nanotube interaction with nucleobases in water using the statistical mechanical theory of molecular liquids," *The Journal of Physical Chemistry C*, vol. 116, no. 28, pp. 15087–15092, 2012.

[86] Q. Sun, Z. Li, D. J. Searles, Y. Chen, G. M. Lu, and A. Du, "Charge-controlled switchable co2 capture on boron nitride nanomaterials," *Journal of the American Chemical Society*, vol. 135, no. 22, pp. 8246–8253, 2013.

[87] Q. Sun, M. Wang, Z. Li, Y. Ma, and A. Du, "{CO2} capture and gas separation on boron carbon nanotubes," *Chemical Physics Letters*, vol. 575, no. 0, pp. 59 – 66, 2013.

[88] M. Yoon, S. Yang, E. Wang, and Z. Zhang, "Charged fullerenes as high-capacity hydrogen storage media," *Nano Letters*, vol. 7, no. 9, pp. 2578–2583, 2007.

[89] A. Kaiser, C. Leidlmair, P. Bartl, S. Zottl, S. Denifl, A. Mauracher, M. Probst, P. Scheier, and O. Echt, "Adsorption of hydrogen on neutral and charged fullerene: Experiment and theory," *The Journal of Chemical Physics*, vol. 138, no. 7, pp. 1–13, 2013.

Chapter 5

Electrostatics of DNA Nucleotides-Carbon Nanotube Hybrids[1]

5.1 Introduction

Hybrids formed by DNA and carbon nanotubes (CNTs) have attracted much attention in recent years due to their interesting properties and useful applications [1–7]. Dispersion and separation of CNTs using single stranded DNA (ssDNA) is one such application. Due to the hydrophobic nature of CNT, its dispersion in water is difficult and bundled CNTs are usually formed in aqueous solution [8]. Some methods have been proposed to increase the solubility, but they may alter some of CNT's properties at the same time. For example, shortening CNTs using

[1]Reprinted from Nanoscale, Morteza Chehel Amirani & Tian Tang "Electrostatics of DNA Nucleotides-Carbon Nanotube Hybrids Evaluated From QM:MM Simulations", Reproduced by permission of The Royal Society of Chemistry. DOI: 10.1039/C5NR03665H

acids can increase their solubility, but meanwhile this reduces the aspect ratio of the CNTs [9, 10]. In addition to the poor solubility, separation of CNTs according to their chirality is another challenge in their synthesis, which is critical in electronic applications where the CNT's electric properties play an important role. In an experiment by Zheng *et al.* [1], ssDNA was found to helically wrap around the CNT and form a hybrid structure in an electrolyte solution. The negatively charged phosphate groups in the ssDNA backbone caused the hybrids to repel, leading to a stable solution of dispersed hybrids. Separation of the CNTs into metallic and semiconducting types was subsequently achieved using the method of ion exchange chromatography (IEC). In the IEC, the negatively charged hybrids were adsorbed on the positively charged IEC column. With increasing salt concentration, it was found the ssDNA-metallic CNT hybrids generally desorb earlier from the column than the ssDNA-semiconducting CNT hybrids, allowing for their separation. The separation was shown to strongly depend on the ssDNA sequence [11, 12]. More recently, separation of semiconducting CNTs with the same diameter but different chiralities (e.g. (9,1) and (6,5)) has been successfully carried out [13, 14].

Several attempts have been put forward in order to understand the mechanism of the separation phenomenon. Zheng *et al.* proposed that ssDNA sequence and electronic properties of the CNT influence the surface charge of the CNT hybrid [1]. Based on a free energy formulation [15], they predicted ssDNA-metallic CNT to possess less surface charge and hence less binding strength to the IEC column than the ssDNA-semiconducting CNT, if the same ssDNA is used. Khripin *et al.* evaluated the mobility of poly$(GT)_{30}$ ssDNA-CNT hybrids using capillary electrophoresis (CE) technique [16]. With the measured mobility and making

use of the Poisson-Boltzmann (PB) equation and electric double layer formulation [17], they obtained different average charge densities for ssDNA-(6,5) CNT and ssDNA-CNT (7,5) hybrids: -6.0 e/nm for the former and -6.8 e/nm for the latter. They also performed molecular dynamics (MD) simulations to obtain optimized structure of the ssDNA on different CNTs. Based on the wrapping angle, the charge of the hybrid per unit length of the CNT was determined to be -5.8 e/nm and -6.2 e/nm, respectively for ssDNA-(6,5) CNT and ssDNA-CNT (7,5) hybrids. Although these values were in good agreement with those calculated based on CE experiments, due to the nature of the MD simulation (fixed atomic partial charges) the charge transfer between DNA and CNT upon hybridization was not taken into account. In another study using replica exchange MD (REMD), Roxbury *et al.* determined the charge density to be 4.5-6.0 e/nm for a hybrid in which the same (6,5) CNT was wrapped by an ssDNA with the sequence being $(TAT)_4$ [18]; the reported range, instead of a single value, was due to different number of strands (1 to 4) simulated in their work .

While the above studies focused on determining the charge of the hybrid, others attempted to understand the mechanism of separation by examining the electric field of the hybrid. The observation that ssDNA-CNT hybrids with different CNT chiralities elute at different time implies that the strength of electrostatic interaction between the hybrid and the IEC column depends on the electronic response of the CNT. Motivated by this, several studies have been performed to explore the electric field of a charged entity near an electronically responsive media [15, 19–23]. The electrostatic potential of a line of charges in an electrolyte solution near a metallic, dielectric or semiconducting half space was analytically solved using PB theory by Tang *et al.* [19], which was shown to strongly depend on the nature

of the half-space. Malysheva *et al.* presented an analytical solution for the electrostatic potential of a more complicated system which contained a charged wall (representing IEC) and a hybrid consisting of a charged polyelectrolyte (representing DNA) and an electronically responsive cylinder (representing CNT), both embedded in an electrolyte solution [21]. Using the electrostatic potential, they determined the binding force between the wall and the hybrid and showed that the presence of a grounded metallic cylinder reduced the magnitude of the electric field of the polyelectrolyte and resulted in a smaller binding force compared with the polyelectrolyte hybridized with a neutral dielectric cylinder. More recently, Malysheva *et al.* employed the one-dimensional density of state of CNT [24] and the Debye-Hückel equation [25] to evaluate the electrostatic potential of the hybrid [26]. As an approximation, the DNA charges were smeared out onto a cylindrical surface with the same axis as the CNT. The metallic CNT was shown to possess larger induced charge compared with the semiconducting one which resulted in smaller magnitudes of total charge and electrostatic potential for the hybrid, consistent with their previous work. Using a semi-empirical tight binding method, Rotkin and Snyder indicated that DNA charges induced an electron density on CNT surface and changed its electronic structure [27]. They showed that the electrostatic potential of an ssDNA on a (7,0) CNT surface was approximately half of the corresponding value if no CNT was involved [28]. Although the above studies were useful in qualitatively describing the electric field of the hybrid, they were based on several assumptions including simplified geometries to represent DNA and CNT. Furthermore, the DNA sequence which was shown to be very important in the experiments was not taken into account in those studies.

At a much smaller scale, a series of quantum mechanics (QM) simulations

have been also performed to model the DNA-CNT hybrids; however, the focus of those studies was mainly on the structure and energy of binding [29–54]. To the best of our knowledge, there has not been any work at the atomistic level (using QM or even classical molecular mechanics (MM) simulations) to study the electrostatics of the DNA-CNT hybrids due to the complexity of the problem. Classical MM approaches can be used to simulate relatively large DNA-CNT hybrids in solution, however they can neither accurately describe the CNT's electronic structure nor distinguish the CNTs according to their chiralities. To capture CNT's electronic properties as well as the charge transfer upon hybridization, using QM approaches to model DNA and CNT is inevitable; however, the usability of atomistic QM methods is limited by the size of the system.

As the first attempt to study electrostatics of the ssDNA-CNT hybrid at the atomistic level, in this work, we perform a simulation to determine the electrostatic potential of a DNA nucleotide hybridized with a CNT in presence of explicit water and ions. The nucleotide, as a building block of DNA, is expected to capture the charged nature of the DNA backbone, while keeping the amount of computation manageable. A combined QM:MM approach was employed in order to take into account the electron redistribution upon nucleotide-CNT binding, as well as to include the effect of electrolyte solution. In Section 5.2, computational details are described. Results of the electrostatic potential and charge transfer calculations are presented in Section 5.3 and conclusions are given Section 5.4.

5.2 Simulation details

In total, eight systems were simulated in this work, using a QM:MM scheme developed in our previous work [55]. Readers can refer to Ref. [55] for details of the method. Four DNA nucleoside monophosphates (NMPs) were considered in this study: adenosine 5'-monophosphates (AMP), cytidine 5'-monophosphates (CMP), guanosine 5'-monophosphates (GMP), and thymidine 5'-monophosphates (TMP). The corresponding molecular structure of the NMPs is shown in Fig. 5.1(a)-(d). Each NMP carries a charge of -2 due to the presence of two negatively charged oxygen atoms in its phosphate group [56–58]. Two CNTs (Fig. 5.1(e) and 5.1(f)) with different chiralities, (7,0) and (4,4), but similar length (respectively 15.6 and 14.8 Å) and diameter (respectively 5.48 and 5.42 Å) were considered to interact with the NMPs. Since applying periodic boundary condition (PBC) was not possible due to the limitations of the QM:MM approach [59], hydrogen atoms were used to saturate the dangling bonds at the CNT ends. For each system, using Gromacs [60], a water box with dimensions of $3 \times 2.4 \times 2\ nm^3$ was created and the NMP-CNT hybrid was solvated inside the box. In addition, we added two Na^+ cations, by random placement, to the solution so that each simulation system is charge neutral.

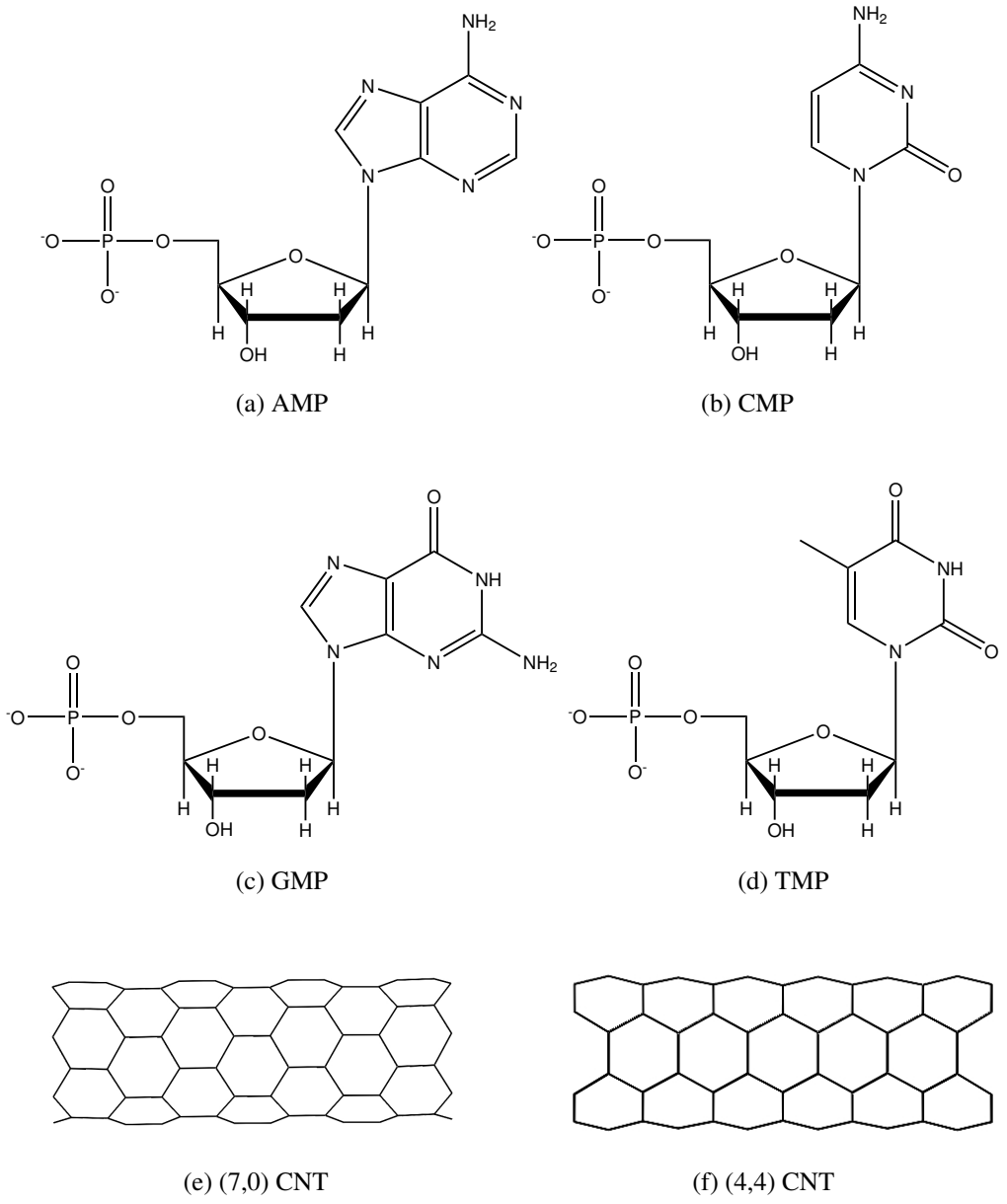

(a) AMP (b) CMP

(c) GMP (d) TMP

(e) (7,0) CNT (f) (4,4) CNT

Figure 5.1: Molecular structures of NMPs and CNTs simulated in this work.

The simulations were performed using ONIOM approach in Gaussian 09 [59]. A QM region and an MM region were defined for each simulated systems. The QM region contains all atoms in the CNT and NMP while the rest of the atoms

i.e., all water molecules and the two cations were considered in the MM region. To perform the ONIOM simulation, we chose density functional theory (DFT) along with M06-2X functional for the QM calculations and Amber force-field for the MM calculations. Each system was optimized according to the following procedures, as described in detail in Ref. [55]:

1. Individual NMP and CNT were optimized in vacuum using DFT with M06-2X functional and the basis set of 6-31G(d). Partial atomic charges (based of restrained electrostatic potential (Resp) [61] method) were calculated for the individually optimized NMP and CNT using AmberTools [62].

2. The simulation system was constructed using the relaxed NMP and CNT as well as water and Na^+ cations. It was then subjected to an MM optimization, using the partial charges obtained from step 1.

3. An ONIOM optimization was performed for the relaxed structures obtained from step 2.

4. Electrostatic potential and charge transfer were evaluated for the optimized hybrids obtained from step 3. The details of the calculations are explained below.

Electrostatic potential, ϕ, was obtained directly from the QM:MM simulations and evaluated at three dimensional grid points in the space surrounding the NMP-CNT hybrid. As pointed out in the introduction, ssDNA-CNT hybrids with different CNT chiralities appear to have different strengths of attraction to the IEC, that is, they likely have different electrostatic potential at the location of the IEC. Therefore, we are interested in the electrostatic potential of the hybrid in its encompassing cylindrical region and will use the cylindrical coordinate shown in Fig. 5.2 (optimized AMP-(4,4) CNT hybrid as an example) to analyze the results. In this coordinate, the CNT axis is set to be the Z-axis. The origin of the coor-

dinate system is defined as the projection of the NMP's center of mass (COM) onto the Z-axis. Y-axis is set to be the axis passing through the NMP's COM and the origin, and X-axis is perpendicular to both Y and Z axes (See Fig. 5.2(b)). The polar coordinates, r and θ, are defined in the $X-Y$ plane where r is the radial distance from the origin and θ is the counterclockwise angle measured from the X-axis. In addition, it was found that the largest separation distance between all NMP atoms and the CNT axis was $\sim$10 Å. Since in the IEC experiment, the surface of the IEC column is expected be located near the hybrid, the range of the radial coordinate, r, was chosen to be between 12 Å and 15 Å throughout the chapter. The Z coordinate was varied from -20 Å to 20 Å which is large enough to cover the length of the CNT. Finally, θ is varied from 0° to 360°.

For the charge transfer, we first employed the Resp approach to calculate the atomic partial charges on the NMP and CNT atoms, as well as on the two Na^+ ions. The Resp scheme was chosen because it generates atomic partial charges at atom centers to reproduce the electrostatic potential, hence is consistent with the electrostatic potential calculations in this work. Water molecules were removed from the molecular model in the charge transfer calculation due to computational limitations [62]. Instead, we used the conductor-like polarizable continuum model (CPCM) [63] which is the most commonly employed implicit model for the solution. Since the initial net charge in each NMP is -2, the charge transfer was determined as the $\delta = q-(-2)$, where q is the final net charge of the NMP. Positive δ corresponds to electron transfer from NMP to CNT.

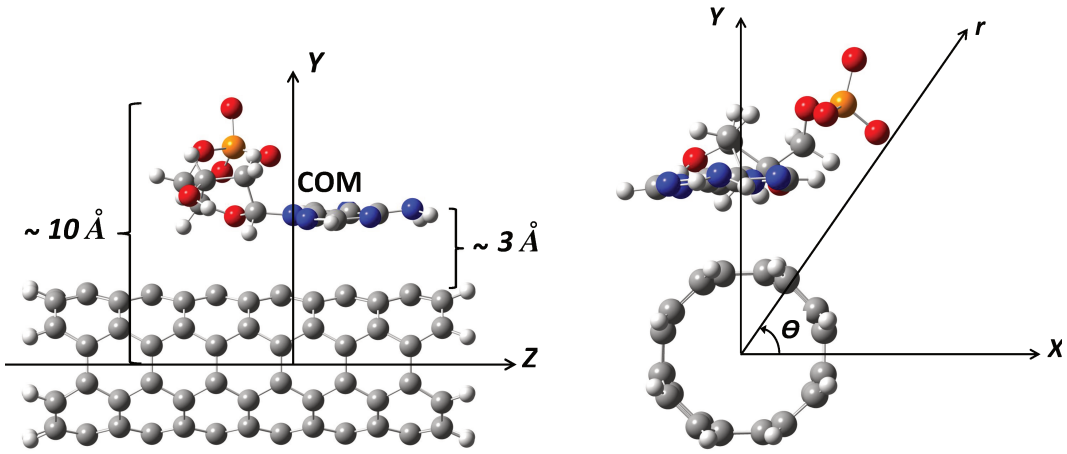

(a) (b)

Figure 5.2: The representation of the cylindrical coordinate (using AMP-(4,4) CNT hybrid): a. Side view; b. Front view. COM marks the center of mass of the AMP.

5.3 Results and discussion

5.3.1 Electrostatic Potential

The final optimized structure for the AMP-(4,4) CNT hybrid is shown in Fig. 5.2 where the water and ions are not shown for the purpose of clarity. Similar final configurations were obtained for the rest of the NMP-CNT hybrids. More specifically, nucleobases possessed a parallel orientation with respect to the CNT surface with a separation distance of ∼3 Å while the phosphate group tends to expose itself to the solution phase. Distributions of the electrostatic potential for the AMP-(4,4) CNT hybrid at the radial distance of 15 Å are shown in Fig. C.1 (The corresponding distributions for all the eight systems are compared in Fig.

C.1 of the Appendix C). In these plots, the electrostatic potential is depicted versus Z (CNT axis) and θ axes, and its magnitude is highlighted by the color. While all values are negative due to the negative charges on the NMPs, the blue and red regions respectively correspond to the most and least negative values.

For all systems, a valley-shaped distribution for the electrostatic potential, ϕ, is obtained. The minimum value of ϕ present in each system (located in the valley and colored blue), ϕ_{min}, corresponds to the lowest electrostatic potential at the radial distance of r =15 Å. The θ and Z coordinates at ϕ_{min} are about 90° and 0, respectively. In other words, at r =15 Å, $\phi_{min} = \phi(\theta =\sim 90^{\circ}, Z =\sim 0)$, which is a location on this cylindrical surface relatively close to the phosphate group of NMPs (see Fig. 5.2). This is expected due to the concentration of the negative charge in the phosphate group. The location of ϕ_{min} is important because if an external charged entity (such as the IEC column) is present, it will have the strongest interaction with the hybrid where the minimum electrostatic potential is found. The magnitude of ϕ_{min} is also of significance since it measures the strength of interaction, and more generally is an indication for the molecular reactivity in biological systems [64–66].

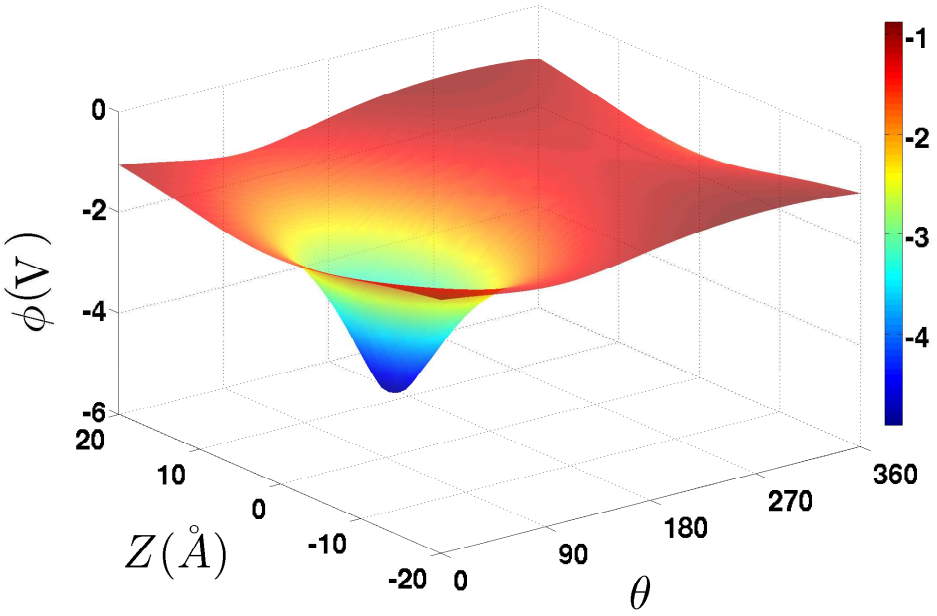

Figure 5.3: Distribution of the electrostatic potential (ϕ) for AMP-(4,4) CNT hybrid as a function of Z and θ. The radial distance is fixed at r=15 Å.

Similar distributions of ϕ for smaller radial distances, i.e., 12 Å $< r <$15 Å , was also obtained. More specifically, at a given r a minimum was found in the vicinity of the phosphate group in all eight systems. To examine ϕ_{min} in detail, we obtain ϕ_{min} at each radial distance and plot it as a function of r in Fig. 5.4. Different curves in Fig. 5.4 correspond to different simulated systems, and they all show a similar trend of ϕ_{min} versus r. Specifically, each curve starts with the most negative value of ϕ_{min} at $r =$12 Å , gradually increases with r, and shows the trend of converging to zero as r tends to infinity. More negative ϕ_{min} is obtained for smaller values of r because the potential is evaluated at points closer to the negatively charged zone of the NMP. The minimum value of the electrostatic potential on the molecular surface of the isolated nucleobases in vacuum

was determined by Pullman *et al.* to be -2.25, -1.34, -1.99, and -1.23 V, respectively for guanine, adenine, cytosine, and thymine [65]. For the nucleotides, more negative values for the minimum electrostatic potential was reported due to the inclusion of the negatively charged phosphate group [66]. Pullman and Pullman studied the electrostatic potential of dimethylphosphate (with a net charge of -1) as a model to represent the phosphate group in DNA. The minimum electrostatic potential was reported to be -8.67 V at a distance of 1.05 Å from the anionic oxygen bound to the phosphors in a plane defined by the phosphorous and two anionic oxygen atoms [64]. Considering all NMP-CNT systems, the range of ϕ_{min} is [-10.30,-4.28] V at r =12 Å and [-4.90, -2.95] V at r =15 Å, which is similar in magnitude to the ϕ_{min} of dimethylphosphate. More direct comparison cannot be made between the electrostatic potential of the NMP-CNT hybrids and that of the dimethylphosphate for several reasons. Firstly, the dimethylphosphate had a net charge of -1 while each of the NMPs we simulated has a net charge of -2. Secondly, the dimethylphosphate was isolated while our NMPs are under the influence of the CNT. In addition, the dimethylphosphate was located in vacuum while our hybrids were solvated. The highly polar solvent (water) and the ions can create a screening effect for the electrostatic field. Also, the electrostatic potential in Ref. [64] was evaluated at a distance of 1.05 Å from the anionic oxygen, while the electrostatic potential in our systems was evaluated at larger distances from the two anionic oxygen atoms.

Despite the qualitative similarity in the dependence of ϕ_{min} on r, quantitatively, ϕ_{min} is quite different for different NMP-CNT hybrids. At any given r, the absolute value of ϕ_{min} follows the order, from small to large, of TMP-(7,0) CNT, AMP-(7,0) CNT, GMP-(7,0) CNT, CMP-(4,4) CNT, TMP-(4,4) CNT, CMP-(7,0)

CNT, GMP-(4,4) CNT, and AMP-(4,4) CNT. Clearly, the electrostatic potential of the hybrids strongly depends on the chirality of the CNT as well as the type of nucleobase in the NMP.

First let us consider the effect of CNT. Except for CMP, NMP-(4,4) CNT hybrids generates stronger electrostatic potential compared with the NMP-(7,0) CNT hybrids. For example, ϕ_{min} at $r = 12$ is -4.39, -7.10, -4.79, and -4.28 V, respectively for AMP, CMP, GMP, and TMP adsorbed to the (7,0) CNT. For the hybrids formed by NMPs and the (4,4) CNT, ϕ_{min}(r=12 Å) is -10.30, -5.41, -8.93, and -6.13 V, respectively for AMP, CMP, GMP, and TMP. Although the two CNTs possess similar length and diameter, their different chiralities lead to very different electrostatic potentials when they interact with the NMPs. To the best of our knowledge, there is no work at an atomistic level to study the electrostatic potential of the hybrid. In the continuum-based study of Malysheva *et al.*, it was shown that a ssDNA-metallic CNT hybrid generates smaller magnitudes of electrostatic potential compared with a ssDNA-semiconducting CNT hybrid [26] which would predict easier elution of ssDNA-metallic CNT hybrids observed in early IEC experiments [1, 11]. The stronger electrostatic potential we found from our simulations for (4,4) CNT, which is seemingly contradicting to the earlier studies [1, 11], may be first due to the fact that the CNTs in this study have finite lengths (caused by the incapability of including PBC within the QM:MM scheme [59]) and hence may not truly reflect the metallic/semiconducting properties of long CNTs. To explore why NMP-(4,4) CNT hybrids generates stronger electrostatic potential, we calculated the separation distance between the NMP atoms and the CNT surface. It was found that except for CMP, the phosphate group in the NMP-(7,0) CNT hybrids is located closer to the CNT compared with

that in the NMP-(4,4) CNT hybrids [55]. In other words, the (7,0) CNT binds more tightly with the NMPs compared with the (4,4) CNT (with the exception of CMP), which is also confirmed by examining the atomic separations and binding energy (see Ref. [55] for detailed results of the binding energy calculations as well as binding structures). The stronger binding can lead to stronger charge transfer (as will be demonstrated in the next section) from the NMP to the CNT, and the wider distribution of charges in space (as compared to concentrated charge at the phosphate group) can cause reduction in the magnitude of electrostatic potential. In other words, the electrostatic field of the hybrid may not be only influenced by the electronic property of the CNT, but also by their binding strength and structure. It should be mentioned that some experiments revealed that semiconducting CNTs were more weakly adsorbed to the IEC and eluted earlier compared with metallic CNTs [14] which implied the complexity of the DNA-CNT interactions.

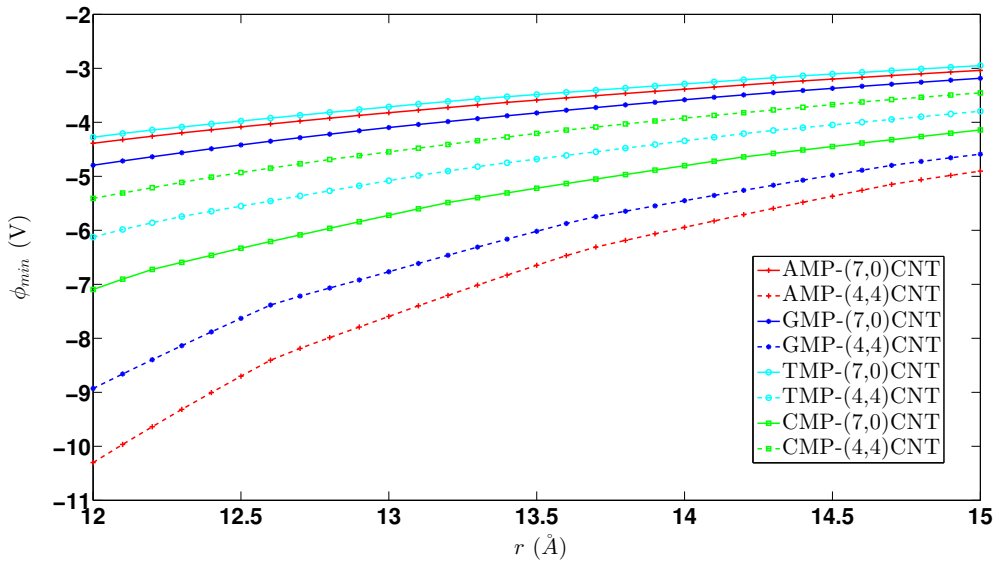

Figure 5.4: Minimum of the electrostatic potential, $\phi_{min}(r)$, for different simulated systems. At each radial distance r, the electrostatic potential is calculated as a function of Z and θ (e.g. see Figure 3), and the minimum value is reported as $\phi_{min}(r)$.

In addition to the influence from the CNTs, the electrostatic potential of the hybrid is also affected by the type of nucleobase in the NMP. When the absolute value of ϕ_{min} is ranked according to the NMP, the order is CMP>GMP∼AMP∼TMP for the NMP-(7,0) CNT hybrids and AMP>GMP>TMP>CMP for the NMP-(4,4) CNT hybrids. The different orders of ϕ_{min} for the two CNTs suggests that the types of CNT and NMP have coupled roles in determining the electrostatic potential of the hybrids. To further explore this, we defined the difference in minimum electrostatic potential, $\Delta\phi_{min}$, presented in equation 5.1.

$$\Delta\phi_{min}(r) = |\phi_{min}^{(7,0)\ CNT}(r) - \phi_{min}^{(4,4)\ CNT}(r)| \tag{5.1}$$

For each NMP, $\Delta\phi_{min}$ was evaluated at each r in the range of 12 Å to 15 Å and is shown in Fig. 5.5. According to the figure, $\Delta\phi_{min}$ decays as r becomes larger and is expected to converge to zero as r tends to infinity, since ϕ_{min} approaches zero in all systems (see Fig. 5.4). Interestingly, for all values of r, $\Delta\phi_{min}$ for AMP and GMP are considerably larger than that for CMP and TMP. For instance, for almost all r, $\Delta\phi_{min}$ of GMP is more than twice that of TMP and CMP, and $\Delta\phi_{min}$ from AMP is more than three times larger. This implies that the type of nucleobase in the NMPs remarkably influence the electrostatic potential of the hybrid, although all NMPs carry the same amount of negative charge and have the sugar ring and phosphate group in common. Quantitatively, $\Delta\phi_{min}$ is a measure on the easiness of distinguishing the two types of CNTs. The significantly larger $\Delta\phi_{min}$ caused by AMP and GMP suggests that the two CNTs can be more easily differentiated and potentially separated with these two types of NMPs. In the separation of CNT using ssDNA in the IEC, it has been shown that the separation is very sensitive to the DNA sequence [11]. Although the simulations here do not involve DNA polymer, our results for $\Delta\phi_{min}$ can provide some clues on why the separation depends on the type and sequence of nucleotides.

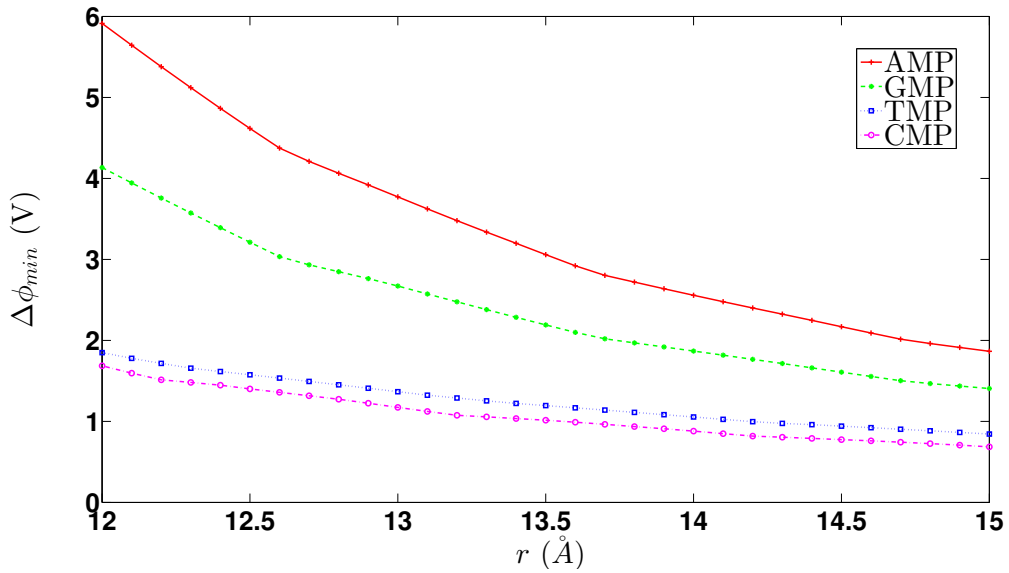

Figure 5.5: Difference in the minimum electrostatic potential between NMP-(4,4) CNT hybrid and NMP-(7,0) CNT hybrid. Each minimum electrostatic potential is evaluated at a given distance *r* from the CNT axis.

5.3.2 Charge Transfer

Final partial atomic charges of the nucleotides and CNTs for all eight systems are presented in the Appendix C (Figure C.2 and Figure C.3). The charge transfer, δ, between each NMP and CNT was calculated and is presented in Table 5.1. For two of the hybrids, AMP-(4,4) CNT and GMP-(4,4) CNT, the adsorption took place without noticeable charge transfer. In the other six hybrids, a partial electronic charge was transferred from the NMP to the CNT and hence the CNT became negatively charged upon the hybridization. In these six systems, δ ranges from 0.08 to 0.65 e: it is similar (around 0.1 e) for the CMP-(4,4) CNT, TMP-(4,4) CNT, AMP-(7,0) CNT, and CMP-(7,0) CNT; while for GMP and TMP adsorbed on the (4,4) CNT, δ is considerably large (around 0.6 e).

Unlike the lack of reports on the electrostatic potential in the literature, the

charge transfer between the nucleotide/nucleobase and CNT has been reported in some of the past studies, all based on using QM approaches. For instance, Shukla *et al.* determined the charge transfer to be 0.02-0.04 *e* from DNA nucleobases to a (7,0) CNT using DFT (M05-2X functional) and Mulliken approach [49]. Using DFT(LDA) and Bader analysis, Gowtham *et al.* showed that a small amount of electric charge, 0.05 and 0.08 *e*, was transferred respectively from adenine and guanine to a (5,0) CNT [31]. Das *et al.* studied the adsorption of DNA nucleobases onto a (5,5) CNT using Mulliken population and showed that the charges were only redistributed among the atoms without any net charge transfer between nucleobases and the CNT [67]. Clearly, the charge transfer between DNA nucleobases and CNT are essentially negligible, due to the absence of the charged phosphate group. Enyashin *et al.*, using self consistent charge density-functional based tight-binding method (SCC-DFTB), reported 0.2-0.4 *e* charge transfer from a PolyC-DNA to CNTs with the chiralities of (8,2) and (7,4), and less than 0.05 *e* for CNTs with the chiraliteis of (5,5), (7,3), (8,0), and (10,0) [47].Considering that the hybrids involved polymer DNA, the charge transfer is still insignificant. This is because although the phosphate groups were included, they were not deprotonated and hence the DNAs simulated were neutral. The only work where the charge transfer was found to be significant is by Wang and Ceulemans, who evaluated the charge transfer for two connected AMPs adsorbed on CNTs using Mulliken approach [35]. The simulations were also performed in vacuum and the two connected AMPs were charge neutral. Charge transfer of 0.85 and 0.56 *e* was found, respectively for (7,0) and (4,4) CNTs, but in contrast to all other studies, the direction of the transfer was from the CNT to the AMPs, which is not yet understood.

It should be pointed out that the charge transfer calculations are quite sensitive to the choice of the QM approach as well as the charge calculation scheme. It has been shown that very different results for the charge transfer in the biological systems may be obtained based on different selections of the QM and charge calculation methods [68]. It is well known that the Mulliken charge scheme, although most widely used due to its simplicity, poorly describes the molecular properties especially the electrostatic potential [69]. On the other hand, Resp approach, employed in our study, is known to accurately reproduce the electrostatic potential of the molecular systems. Our finding that hybrids with (7,0) CNT generally have larger charge transfer compared with the (4,4) CNT is consistent with the electrostatic potential results discussed in Section 5.3.1, and both can be explained in terms of the tightness of the binding. As mentioned earlier, the NMPs are more tightly bound to the (7,0) CNT compared with the (4,4) CNT [55], which may facilitate the charge transfer between the two entities, and this is evidence by the data shown in Table 5.1. The correlation between binding strength and charge transfer was also reported by Lu *et al.*, who showed that the physisorption of naphthalene, anthracene, and tetracyanoquinodimethane (TCNQ) on a (6,6) CNT was in general stronger compared with those on a (10,0) CNT, which was accompanied by higher charge transfer to the (6,6) CNT [70]. On the other hand, for the NMPs adsorbed onto the same CNT, the order of the charge transfer is more complex, and cannot be explained by the tightness of binding alone. For example, for the (4,4) CNT, the energy of binding for the four NMPs was found to follow the order of GMP>TMP>CMP>AMP [55]. The corresponding order for the charge transfer is CMP>TMP>GMP$\sim$AMP. For the (7,0) CNT, the order of the energy of binding was shown to be TMP>AMP>GMP>CMP [55] while the order for

the charge transfer is GMP>TMP>CMP>AMP. One possible explanation might be the position and orientation of the NMPs relative to the CNT. It is well known that the potential energy surface (PES) for nucleobase-CNT hybrids is shallow with many possible local minima [32, 33, 54], which is likely also true for the NMP-CNT hybrids. These local minima can correspond to the similar binding energy but different configurations of the NMPs relative to the CNT, which can result in different charge transfers. Leenaerts *et al.* evaluated the energy of binding and charge transfer upon the adsorption of H_2O, NH_3, CO, NO_2, and NO on graphene. They showed that different relative configurations (adsorption site and orientation) of the adsorbed molecules may result in the same energy of binding, but completely different values of the charge transfer [71].

Table 5.1: Charge transfer (e) between NMPs and CNTs

	AMP	CMP	GMP	TMP
(4,4) CNT	~ 0	0.10	~ 0	0.08
(7,0) CNT	0.12	0.15	0.65	0.54

Compared with past works in literature, the present work adopted an atomistic QM:MM approach and evaluated the electrostatic potential generated by the NMP-CNT hybrid for the first time. An electrolytic environment was introduced, which has two consequences: the charged NMPs as well as the polar medium around the hybrids. This was never done in previous QM studies, but is essential and better mimics the conditions in most experiments involving these hybrids (e.g., the CNT separation experiments using IEC). The presence of solution is im-

portant to the properties of the hybrids including binding structure and strength, as well as electrostatic potential. For instance, the contribution of water release to the binding energy between NMPs and CNTs has been shown to be considerable [55]. The polarization of the CNT by the NMPs and the solution was taken into account so as to produce accurate electron density, which is not possible with classical MM or continuum approaches. Therefore, our work is an important step toward more comprehensive modeling of the DNA-CNT hybrids.

Despite these merits, several limitations, caused by the current limitations in computational capacity and methodology, should be addressed. First, applying PBC or simulating a relatively long CNT is essential in order to precisely resemble the electronic properties of the bulk CNT. Second, a larger number of nucleotides should be included in order to resemble a long DNA interacting with the CNT. Presence of a longer piece of DNA may introduce other influential factors in its interactions with CNTs. For instance, it has been shown that the wrapping angle which is affected by the length of the ssDNA plays an important role in the properties of the hybrid [15]. In addition, only two Na^+ cations were considered in this work to just neutralize the system. Different type and concentrations of salt may affect the properties of the hybrids, as it has been shown that the number of ions affects the energy of binding between NMPs and a (6,0) CNT [56]. The effect on the electrostatic potential and charge transfer requires a series of separate simulations with different salt types and concentrations. Last, the explicit water molecules were replaced by a continuum model in the charge transfer calculations which may reduce the accuracy of the partial atomic charge calculation. It is important to develop computationally affordable QM:MM methods to reduce the aforementioned limitations in order to more precisely study the properties of the

ssDNA-CNT hybrids.

5.4 Conclusions

Using a QM:MM method, the electrostatic potential and charge transfer was evaluated for the hybrids formed by DNA nucleotides and CNTs in aqueous solution. It is the first model that included QM description of the CNT and nucleotide under the influence of the electrolytic environment, and explicitly calculated electrostatic potential from atomic simulations. It is shown that the electrostatic potential of the hybrid in its vicinity strongly depends on the type of nucleotide and the chirality of the CNT. At the same distance from the CNT axis, the NMP-(4,4) CNT hybrids were found to generate stronger electrostatic potential compared with the NMP-(7,0) CNT hybrids. Atomic charge calculations also showed stronger charge transfer from the NMP to the CNT in the case of (7,0) CNT. Compared with our previous findings where NMPs were shown to generally bind tighter to the (7,0) CNT compared with the (4,4) CNT, these results suggest the electrostatics of the DNA-CNT hybrids may be influenced by the tightness of the binding. AMP and GMP were found to produce larger difference in electrostatic potential when they bind to the two types of tubes, indicating their better capability of distinguishing the two CNTs.

References

[1] M. Zheng, A. Jagota, E. D. Semke, B. A. Diner, R. S. Mclean, S. R. Lustig, R. E. Richardson, and N. G. Tassi, “DNA-assisted dispersion and separation

of carbon nanotubes," *Nat Mater*, vol. 2, no. 5, pp. 338–342, 2003.

[2] C. Dwyer, M. Guthold, M. Falvo, S. Washburn, R. Superfine, and D. Erie, "DNA-functionalized single-walled carbon nanotubes," *Nanotechnology*, vol. 13, no. 5, p. 601, 2002.

[3] S. R. Shin, C. K. Lee, I. S. So, J. H. Jeon, T. M. Kang, C. W. Kee, S. I. Kim, G. M. Spinks, G. G. Wallace, and S. J. Kim, "DNA-Wrapped Single-Walled Carbon Nanotube Hybrid Fibers for supercapacitors and Artificial Muscles," *Advanced Materials*, vol. 20, no. 3, pp. 466–470, 2008.

[4] C. M. Arnett, C. P. Marsh, C. R. Welch, M. S. Strano, J.-H. Han, J. H. Gray, and T. A. Carlson, "Enzyme-Mediated Assimilation of DNA-Functionalized Single-Walled Carbon Nanotubes," *Langmuir*, vol. 26, no. 2, pp. 613–617, 2010.

[5] R. Yang, Z. Tang, J. Yan, H. Kang, Y. Kim, Z. Zhu, and W. Tan, "Noncovalent Assembly of Carbon Nanotubes and Single-Stranded DNA: An Effective Sensing Platform for Probing Biomolecular Interactions," *Analytical Chemistry*, vol. 80, no. 19, pp. 7408–7413, 2008.

[6] H. Wang, N. B. Muren, D. Ordinario, A. A. Gorodetsky, J. K. Barton, and C. Nuckolls, "Transducing methyltransferase activity into electrical signals in a carbon nanotube-DNA device," *Chem. Sci.*, vol. 3, pp. 62–65, 2012.

[7] S. Kilina, D. A. Yarotski, A. A. Talin, S. Tretiak, A. J. Taylor, and A. V. Balatsky, "Unveiling Stability Criteria of DNA-Carbon Nanotubes Constructs by Scanning Tunneling Microscopy and Computational Modeling," *Journal of Drug Delivery*, vol. 2011, 2011.

[8] M. Bratcher, B. Gersten, H. Ji, and J. Mays, "Study in the dispersion of carbon nanotubes," in *Symposium Z – Making Functional Materials with Nanotubes*, vol. 706 of *MRS Proceedings*, 2001.

[9] M. N. Tchoul, W. T. Ford, G. Lolli, D. E. Resasco, and S. Arepalli, "Effect of mild nitric acid oxidation on dispersability, size, and structure of single-walled carbon nanotubes," *Chemistry of Materials*, vol. 19, no. 23, pp. 5765–5772, 2007.

[10] A. Rinzler, J. Liu, H. Dai, P. Nikolaev, C. Huffman, F. Rodriguez-Macias, P. Boul, A. Lu, D. Heymann, D. Colbert, R. Lee, J. Fischer, A. Rao, P. Eklund, and R. Smalley, "Large-scale purification of single-wall carbon nanotubes: process, product, and characterization," *Applied Physics A*, vol. 67, no. 1, pp. 29–37, 1998.

[11] M. Zheng, A. Jagota, M. S. Strano, A. P. Santos, P. Barone, S. G. Chou, B. A. Diner, M. S. Dresselhaus, R. S. Mclean, G. B. Onoa, G. G. Samsonidze, E. D. Semke, M. Usrey, and D. J. Walls, "Structure-Based Carbon Nanotube Sorting by Sequence-Dependent DNA Assembly," *Science*, vol. 302, no. 5650, pp. 1545–1548, 2003.

[12] X. Tu and M. Zheng, "A DNA-based approach to the carbon nanotube sorting problem," *Nano Research*, vol. 1, pp. 185–194, 2008.

[13] M. Zheng and E. D. Semke, "Enrichment of single chirality carbon nanotubes," *Journal of the American Chemical Society*, vol. 129, no. 19, pp. 6084–6085, 2007.

[14] X. Tu, S. Manohar, A. Jagota, and M. Zheng, "DNA sequence motifs for structure-specific recognition and separation of carbon nanotubes," *Nat Mater*, vol. 460, no. 7252, pp. 250–253, 2009.

[15] S. R. Lustig, A. Jagota, C. Khripin, and M. Zheng, "Theory of Structure-Based Carbon Nanotube Separations by Ion-Exchange Chromatography of DNA/CNT Hybrids," *The Journal of Physical Chemistry B*, vol. 109, no. 7, pp. 2559–2566, 2005.

[16] C. Y. Khripin, S. Manohar, M. Zheng, and A. Jagota, "Measurement of electrostatic properties of dna-carbon nanotube hybrids by capillary electrophoresis," *The Journal of Physical Chemistry C*, vol. 113, no. 31, pp. 13616–13621, 2009.

[17] S. O. Zur, "Theorie der elektrolytischen doppelschicht," *Electrochem*, vol. 30, pp. 508–16, 1924.

[18] D. Roxbury, A. Jagota, and J. Mittal, "Structural Characteristics of Oligomeric DNA Strands Adsorbed onto Single-Walled Carbon Nanotubes," *The Journal of Physical Chemistry B*, vol. 117, no. 1, pp. 132–140, 2013.

[19] T. Tang, C.-Y. Hui, and A. Jagota, "Line of charges in electrolyte solution near a half-space: Ii. electric field of a single charge," *Journal of Colloid and Interface Science*, vol. 299, no. 2, pp. 572 – 579, 2006.

[20] O. Malysheva, T. Tang, and P. Schiavone, "Adhesion between a charged particle in an electrolyte solution and a charged substrate: Electrostatic and van der waals interactions," *Journal of Colloid and Interface Science*, vol. 327, no. 1, pp. 251 – 260, 2008.

[21] O. Malysheva, T. Tang, and P. Schiavone, "Binding Force Between a Charged Wall and a Complex Formed by a Polyelectrolyte and an Electronically Responsive Cylinder," *The Journal of Adhesion*, vol. 87, no. 3, pp. 251–271, 2011.

[22] M. Zheng, K. Eom, and C. Ke, "Calculations of the resonant response of carbon nanotubes to binding of DNA," *Journal of Physics D: Applied Physics*, vol. 42, no. 14, 2009.

[23] C. Sun and T. Tang, "Structure of a polyelectrolyte around an electronically responsive cylinder," *Journal of Colloid and Interface Science*, vol. 338, no. 1, pp. 276 – 283, 2009.

[24] J. W. Mintmire and C. T. White, "Universal density of states for carbon nanotubes," *Phys. Rev. Lett.*, vol. 81, pp. 2506–2509, 1998.

[25] W. Russel, D. Saville, and W. Schowalter, *Colloidal Dispersions*. Cambridge Monographs on Mechanics, Cambridge University Press, 1992.

[26] O. Malysheva, T. Tang, and P. Schiavone, "A model for carbon nanotube–dna hybrid using one-dimensional density of states," *Journal of Colloid and Interface Science*, vol. 380, no. 1, pp. 25 – 33, 2012.

[27] S. V. Rotkin and S. E. Snyder, *Theory of Electronic and Optical Properties of DNA–SWNT Hybrids*, pp. 23–51. Wiley-VCH Verlag GmbH & Co. KGaA, 2010.

[28] S. Snyder and S. Rotkin, "Polarization component of cohesion energy in

single-wall carbon nanotube-dna complexes," *JETP Letters*, vol. 84, no. 6, pp. 348–351, 2006.

[29] M. Chehel Amirani and T. Tang, "Binding of nucleobases with graphene and carbon nanotube: a review of computational studies," *Journal of Biomolecular Structure and Dynamics*, pp. 1–31, 2014.

[30] S. Gowtham, R. H. Scheicher, R. Ahuja, R. Pandey, and S. P. Karna, "Physisorption of nucleobases on graphene: Density-functional calculations," *Phys. Rev. B*, vol. 76, p. 033401, 2007.

[31] S. Gowtham, R. H. Scheicher, R. Pandey, S. P. Karna, and R. Ahuja, "First-principles study of physisorption of nucleic acid bases on small-diameter carbon nanotubes," *Nanotechnology*, vol. 19, no. 12, p. 125701, 2008.

[32] S. Meng, P. Maragakis, C. Papaloukas, and E. Kaxiras, "DNA Nucleoside Interaction and Identification with Carbon Nanotubes," *Nano Letters*, vol. 7, no. 1, pp. 45–50, 2007.

[33] S. Meng, W. L. Wang, P. Maragakis, and E. Kaxiras, "Determination of DNA-Base Orientation on Carbon Nanotubes through Directional Optical Absorbance," *Nano Letters*, vol. 7, no. 8, pp. 2312–2316, 2007.

[34] Y. V. Shtogun, L. M. Woods, and G. I. Dovbeshko, "Adsorption of Adenine and Thymine and Their Radicals on Single-Wall Carbon Nanotubes," *The Journal of Physical Chemistry C*, vol. 111, no. 49, pp. 18174–18181, 2007.

[35] H. Wang and A. Ceulemans, "Physisorption of adenine DNA nucleosides

on zigzag and armchair single-walled carbon nanotubes: A first-principles study," *Phys. Rev. B*, vol. 79, p. 195419, 2009.

[36] Y. Wang and Y. Bu, "Noncovalent Interactions between Cytosine and SWCNT," *The Journal of Physical Chemistry B*, vol. 111, no. 23, pp. 6520–6526, 2007.

[37] Y. Wang, "Theoretical Evidence for the Stronger Ability of Thymine to Disperse SWCNT than Cytosine and Adenine: Self-Stacking of DNA Bases vs Their Cross-Stacking with SWCNT," *The Journal of Physical Chemistry C*, vol. 112, no. 37, pp. 14297–14305, 2008.

[38] F. Ortmann, W. G. Schmidt, and F. Bechstedt, "Attracted by Long-Range Electron Correlation: Adenine on Graphite," *Phys. Rev. Lett.*, vol. 95, p. 186101, 2005.

[39] K. Berland, S. D. Chakarova-Käck, V. R. Cooper, D. C. Langreth, and E. Schröder, "A van der Waals density functional study of adenine on graphene: single-molecular adsorption and overlayer binding," *Journal of Physics: Condensed Matter*, vol. 23, no. 13, p. 135001, 2011.

[40] S. Panigrahi, A. Bhattacharya, S. Banerjee, and D. Bhattacharyya, "Interaction of Nucleobases with Wrinkled Graphene Surface: Dispersion Corrected DFT and AFM Studies," *The Journal of Physical Chemistry C*, vol. 116, no. 7, pp. 4374–4379, 2012.

[41] S. Chandra Shekar and R. S. Swathi, "Stability of nucleobases and base pairs adsorbed on graphyne and graphdiyne," *The Journal of Physical Chemistry C*, vol. 118, no. 8, pp. 4516–4528, 2014.

[42] J. Antony and S. Grimme, "Structures and interaction energies of stacked graphene-nucleobase complexes," *Phys. Chem. Chem. Phys.*, vol. 10, pp. 2722–2729, 2008.

[43] J.-H. Lee, Y.-K. Choi, H.-J. Kim, R. H. Scheicher, and J.-H. Cho, "Physisorption of DNA Nucleobases on h-BN and Graphene: vdW-Corrected DFT Calculations," *The Journal of Physical Chemistry C*, vol. 117, no. 26, pp. 13435–13441, 2013.

[44] D. Le, A. Kara, E. Schröder, P. Hyldgaard, and T. S. Rahman, "Physisorption of nucleobases on graphene: a comparative van der Waals study," *Journal of Physics: Condensed Matter*, vol. 24, no. 42, p. 424210, 2012.

[45] Y. Cho, S. K. Min, J. Yun, W. Y. Kim, A. Tkatchenko, and K. S. Kim, "Noncovalent Interactions of DNA Bases with Naphthalene and Graphene," *Journal of Chemical Theory and Computation*, vol. 9, no. 0, pp. 2090–2096, 2013.

[46] H. Vovusha, S. Sanyal, and B. Sanyal, "Interaction of nucleobases and aromatic amino acids with graphene oxide and graphene flakes," *The Journal of Physical Chemistry Letters*, vol. 4, no. 21, pp. 3710–3718, 2013.

[47] A. N. Enyashin, S. Gemming, and G. Seifert, "DNA-wrapped carbon nanotubes," *Nanotechnology*, vol. 18, no. 24, p. 245702, 2007.

[48] S. Stepanian, M. Karachevtsev, A. Glamazda, V. Karachevtsev, and L. Adamowicz, "Stacking interaction of cytosine with carbon nanotubes: MP2, DFT and Raman spectroscopy study," *Chemical Physics Letters*, vol. 459, no. 1–6, pp. 153–158, 2008.

[49] M. Shukla, M. Dubey, E. Zakar, R. Namburu, Z. Czyznikowska, and J. Leszczynski, "Interaction of nucleic acid bases with single-walled carbon nanotube," *Chemical Physics Letters*, vol. 480, no. 4–6, pp. 269–272, 2009.

[50] B. Akdim, R. Pachter, P. N. Day, S. S. Kim, and R. R. Naik, "On modeling biomolecular–surface nonbonded interactions: application to nucleobase adsorption on single-wall carbon nanotube surfaces," *Nanotechnology*, vol. 23, no. 16, p. 165703, 2012.

[51] A. Ramraj, I. H. Hillier, M. A. Vincent, and N. A. Burton, "Assessment of approximate quantum chemical methods for calculating the interaction energy of nucleic acid bases with graphene and carbon nanotubes," *Chemical Physics Letters*, vol. 484, no. 4–6, pp. 295–298, 2010.

[52] D. Umadevi and G. N. Sastry, "Quantum Mechanical Study of Physisorption of Nucleobases on Carbon Materials: Graphene versus Carbon Nanotubes," *The Journal of Physical Chemistry Letters*, vol. 2, no. 13, pp. 1572–1576, 2011.

[53] A. Sarmah and R. K. Roy, "Understanding the interaction of nucleobases with chiral semiconducting single-walled carbon nanotubes: An alternative theoretical approach based on density functional reactivity theory," *The Journal of Physical Chemistry C*, vol. 117, no. 41, pp. 21539–21550, 2013.

[54] M. Chehel Amirani, T. Tang, and J. Cuervo, "Quantum mechanical treatment of binding energy between DNA nucleobases and carbon nanotube: A DFT

analysis," *Physica E: Low-dimensional Systems and Nanostructures*, vol. 54, pp. 65–71, 2013.

[55] M. Chehel Amirani and T. Tang, "A QM:MM model for the interaction of DNA nucleotides with carbon nanotubes," *Phys. Chem. Chem. Phys.*, vol. 17, pp. 7564–7575, 2015.

[56] A. L. Frischknecht and M. G. Martin, "Simulation of the adsorption of nucleotide monophosphates on carbon nanotubes in aqueous solution," *The Journal of Physical Chemistry C*, vol. 112, no. 16, pp. 6271–6278, 2008.

[57] A. Lehninger, D. Nelson, and M. Cox, *Lehninger Principles of Biochemistry*. W. H. Freeman, 2005.

[58] D. M. Boghaei and M. Gharagozlou, "Charge transfer complexes of adenosine-5′-monophosphate and cytidine-5′-monophosphate with water-soluble cobalt(ii) schiff base complexes in aqueous solution," *Spectrochimica Acta Part A: Molecular and Biomolecular Spectroscopy*, vol. 63, no. 1, pp. 139 – 148, 2006.

[59] M. J. Frisch, G. W. Trucks, H. B. Schlegel, G. E. Scuseria, M. A. Robb, J. R. Cheeseman, G. Scalmani, V. Barone, B. Mennucci, G. A. Petersson, H. Nakatsuji, M. Caricato, X. Li, H. P. Hratchian, A. F. Izmaylov, J. Bloino, G. Zheng, J. L. Sonnenberg, M. Hada, M. Ehara, K. Toyota, R. Fukuda, J. Hasegawa, M. Ishida, T. Nakajima, Y. Honda, O. Kitao, H. Nakai, T. Vreven, J. J. A. Montgomery, J. E. Peralta, F. Ogliaro, M. Bearpark, J. J. Heyd, E. Brothers, K. N. Kudin, V. N. Staroverov, R. Kobayashi, J. Normand, K. Raghavachari, A. Rendell, J. C. Burant, S. S. Iyengar,

J. Tomasi, M. Cossi, N. Rega, J. M. Millam, M. Klene, J. E. Knox, J. B. Cross, V. Bakken, C. Adamo, J. Jaramillo, R. Gomperts, R. E. Stratmann, O. Yazyev, A. J. Austin, R. Cammi, C. Pomelli, J. W. Ochterski, R. L. Martin, K. Morokuma, V. G. Zakrzewski, G. A. Voth, P. Salvador, J. J. Dannenberg, S. Dapprich, A. D. Daniels, Ö. Farkas, J. B. Foresman, J. V. Ortiz, J. Cioslowski, and D. J. Fox, "Gaussian 09 Revision A.1." Gaussian Inc. Wallingford CT 2009.

[60] E. Lindahl, B. Hess, and D. van der Spoel, "Gromacs 3.0: a package for molecular simulation and trajectory analysis," *Molecular modeling annual*, vol. 7, no. 8, pp. 306–317, 2001.

[61] C. I. Bayly, P. Cieplak, W. Cornell, and P. A. Kollman, "A well-behaved electrostatic potential based method using charge restraints for deriving atomic charges: the resp model," *The Journal of Physical Chemistry*, vol. 97, no. 40, pp. 10269–10280, 1993.

[62] D. Case, T. Darden, T. C. III, C. Simmerling, J. Wang, R. Duke, R. Luo, R. Walker, W. Zhang, K. Merz, B. Roberts, S. Hayik, A. Roitberg, G. Seabra, J. Swails, A. GÖtz, I. Kolossváry, K. Wong, F. Paesani, J. Vanicek, R. Wolf, J. Liu, X. Wu, S. Brozell, T. Steinbrecher, H. Gohlke, Q. Cai, X. Ye, J. Wang, M. Hsieh, G. Cui, D. Roe, D. Mathews, M. Seetin, R. Salomon-Ferrer, C. Sagui, V. Babin, T. Luchko, S. Gusarov, A. Kovalenko, and P. Kollman, "AmberTools13." University of California, San Francisco 2012.

[63] V. Barone and M. Cossi, "Quantum calculation of molecular energies and

energy gradients in solution by a conductor solvent model," *The Journal of Physical Chemistry A*, vol. 102, no. 11, pp. 1995–2001, 1998.

[64] A. Pullman and B. Pullman, "Molecular electrostatic potential of the nucleic acids.," *Quarterly Reviews of Biophysics*, vol. 14, no. 3, pp. 289–380, 1981.

[65] A. Pullman, B. Pullman, and R. Lavery, "Molecular electrostatic potential versus field. significance for dna and its constituents.," *Journal of Molecular Structure: THEOCHEM*, vol. 93, no. 0, pp. 85 – 91, 1983. Proceedings of the XIIIth Congress of Theoretical Chemists of Latin Expression.

[66] P. P, L. P. R, and J. K, "Molecular electrostatic potentials: an effective tool for the elucidation of biochemical phenomena.," *Environmental Health Perspectives*, vol. 61, pp. 191–202, 1985.

[67] A. Das, A. Sood, P. K. Maiti, M. Das, R. Varadarajan, and C. Rao, "Binding of nucleobases with single-walled carbon nanotubes: Theory and experiment," *Chemical Physics Letters*, vol. 453, no. 4–6, pp. 266–273, 2008.

[68] A. v. d. Vaart and K. M. Merz, Jr., "Charge transfer in biologically important molecules: comparison of high-level ab initio and semiempirical methods," *International Journal of Quantum Chemistry*, vol. 77, no. 1, pp. 27–43, 2000.

[69] Z. Maksić and J. Ángyán, *Theoretical Treatment of Large Molecules and Their Interactions*. International Series in Heat and Mass Transfer, Springer-Verlag, 1991.

[70] J. Lu, S. Nagase, X. Zhang, D. Wang, M. Ni, Y. Maeda, T. Wakahara,

T. Nakahodo, T. Tsuchiya, T. Akasaka, Z. Gao, D. Yu, H. Ye, W. N. Mei, and Y. Zhou, "Selective interaction of large or charge-transfer aromatic molecules with metallic single-wall carbon nanotubes: Critical role of the molecular size and orientation," *Journal of the American Chemical Society*, vol. 128, no. 15, pp. 5114–5118, 2006.

[71] O. Leenaerts, B. Partoens, and F. M. Peeters, "Adsorption of h_2O, Nh_3, co, No_2, and no on graphene: A first-principles study," *Phys. Rev. B*, vol. 77, p. 125416, 2008.

Chapter 6

Interactions between DNA Nucleotides and Carbon Nanotube: A Molecular Dynamics Study[1]

6.1 Introduction

DNA-Carbon nanotube (CNT) hybrid structure has attracted immense attention in the last ten years. This hybrid structure has shown very interesting properties and potential applications including drug delivery [1–4], cancer detection [5], and CNT processing technologies [6]. Many theoretical studies including molecular dynamics (MD) simulations have been performed to study the role of important parameters including CNT chirality, DNA length and sequence, and solution environment on the interactions of DNA and CNT. However, quantum effects were neglected in those studies. In particular, the partial atomic charges (PAC) on the

[1] A version of this chapter is in preparation for publication.

DNA and the CNT in these MD simulations were based on isolated DNA and CNT optimized in vacuum. Further interactions between DNA and CNT are assumed not to alter these PACs. In Chapter 5, it has been shown that the charge transfer between DNA nucleotides and CNT can be considerable, and the distribution of the PAC on the nucleotides and CNT optimized in an aqueous environment can be very different from the PAC obtained using an individually optimized molecule in vacuum. It is therefore interesting to explore the effect of the redistributed PAC on the behaviors of the nucleotide-CNT hybrids in a dynamic environment, which is the main objective of this Chapter.

The same nucleotide monophosphate (NMP)-CNT hybrids studied in Chapter 4 and 5 are simulated here using classical MD at room temperature. Computational details are described in Section 6.2. Results of NMP-(4,4) CNT and NMP-(7,0) CNT hybrids are presented in Section 6.3 and conclusions are given Section 6.4.

In this study, the adsorption of negatively charged NMPs to two different CNTs with chiralities of (4,4) and (7,7) in solution is investigated. We are mainly interested to determine how the partial atomic charge assignment methods, CNT's chirality, and nucleobase type affect the structural properties of the NMP-CNT system. Computational details are described in Section 6.2. Results of NMP-(4,4) CNT and NMP-(7,0) CNT hybrids are presented in Section 6.3 and conclusions are given Section 6.4.

6.2 Simulation details

Figure 6.1 shows four DNA nucleotides and two CNTs considered in this study. Nucleotides in the form of monophosphates i.e., nucleoside monophosphate (NMP) include adenosine 5'-monophosphates (AMP), cytidine 5'-monophosphates (CMP) , guanosine 5'-monophosphates (GMP) and thymidine 5'-monophosphates (TMP). The two CNTs with the chiralities of (7,0) and (4,4) possess similar diameters (5.48 Å and 5.42 Å) and lengths (15.6 Å and 14.8 Å). The starting geometry for all eight NMP-CNT hybrids were adopted from our previous work [7] where the same hybrids were optimized using a QM:MM approach. The hybrids were then immersed in a $60 \times 60 \times 60\ nm^3$ water box. Two Na^+ cations were also added to the simulation box to neutralize the system since each NMP carries a charge of -2 [8–10].

Two sets of simulations were performed which differ by the way the partial atomic charges were assigned. More specifically, two schemes, namely original charges scheme (OCS) and redistributed charges scheme (RCS) were considered. In OCS, the partial atomic charges are the ones obtained for each isolated NMP and CNT in vacuum. Each of isolated NMPs and CNTs was optimized using a QM approach. The partial atomic charges were then evaluated based on Resp approach using Gaussian [11] and AmberTools [12]. This method is the typical way of assigning atomic partial charges in most MD simulations. On the other hand, in the RCS, the Resp partial atomic charges were obtained after a geometry optimization for the NMP-CNT hybrid using a QM:MM approach in Ref. [7]. Specifically, partial atomic charges are redistributed in both CNT and NMP upon hybridization. Therefore, redistributed partial charges are more realistic to per-

form the MD simulation. Partial atomic charges based on OCS and RCS are respectively presented in Fig. B.3 and Fig. C.2-3.

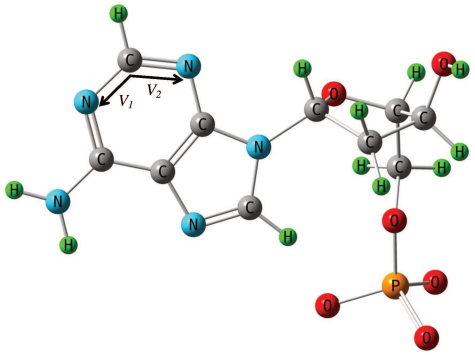

(a) AMP

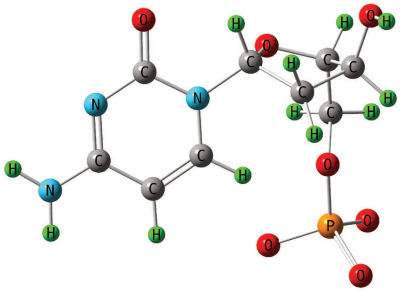

(b) CMP

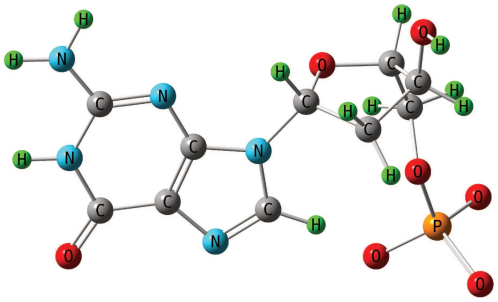

(c) GMP

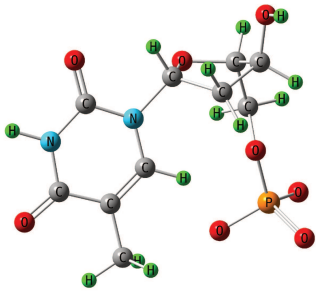

(d) TMP

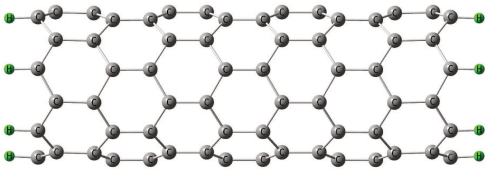

(e) (7,0) CNT

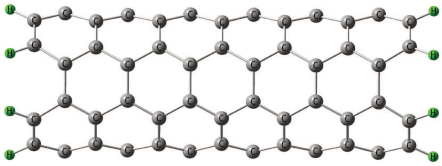

(f) (4,4) CNT

Figure 6.1: Molecular structures of NMPs and CNTs simulated in this work.

Molecular dynamics simulations were carried out based on general Amber force field (GAFF) [13] using Amber 14 package [14]. Each of the eight NMP-CNT systems was simulated in the isothermal-isobaric (NPT) ensemble. The pressure was controlled at 1 bar with the isotropic position scaling scheme. The Langevin dynamics with the collision frequency 1.0 ps^{-1} was employed to control the temperature at 300 K. Periodic boundary conditions (PBC) were applied in all three directions. Particle Mesh Ewald (PME) method with a non-bonded cut off distance of 12 Å for treating long-range electrostatics was used. SHAKE algorithm was applied to constrain bonds involving hydrogen atom. The time step was set to be 2 femtoseconds (fs). Initially, each NMP-CNT hybrid was subjected to an initial energy minimization step where NMP and CNT were kept fixed. A second energy minimization step was performed where all atoms were free to relax. An equilibration step for 200 picoseconds (ps) was then carried out in which the temperature was increased from 0 to 300 K. Finally, the production phase was run for 100 ns. The trajectories were saved at 2 ps intervals for further analysis using AmberTools 14 [12].

To investigate the displacement and orientation of the NMPs with respect to CNTs, three degrees of freedom are chosen to study: the separation distance (d), the horizontal position (h), and the tilting angle (θ). Fig. 6.2 shows a schematic description for d, h, and θ. d is defined as the distance between the nucleobase's center of mass (COM) and the CNT surface and was obtained by first calculating the distance from COM of nucleobase to the CNT axis and then subtracting from it the radius of the CNT. h is defined as the relative position of each NMP with respect to the CNT. To evaluate h, the projection of the nucleobase's COM onto the CNT axis at each time (O_t) was obtained. h is then defined as the position of

O_t relative to C_t, where C_t is the location of the center of the CNT along the axis at each time. Given that the length of the two CNTs are both around 15 Å, h is between ~ -7.5 Å and ~ 7.5 Å if the NMP is located within the length of each CNT. In Fig. 6.2, vector u is the vector connecting O_t and COM and n is the vector perpendicular to the nucleobase plane, where the nucleobase plane is determined by two nitrogen atoms and one carbon atom located in between in each pyrimidine ring of the nucleobase (e.g., see the plane defined by V_1 and V_2 in Fig 6.1(a)). θ is defined as the angle between vectors u and n. When θ is 0 (or 90) degrees, the plane of nucleobase possess respectively a parallel (or perpendicular) orientation with respect to the CNT surface. At the beginning of each simulation, $\cos\theta$ is positive. During the simulations, if $\cos\theta$ becomes negative, it indicates that the nucleobase has flipped compared to its original configuration.

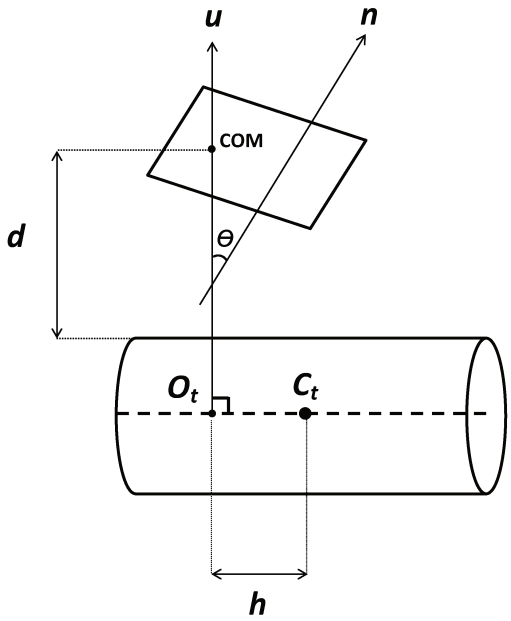

Figure 6.2: Schematic description of d, h, and θ.

6.3 Results and discussion

6.3.1 NMP-(4,4) CNT hybrids

Fig. 6.3 shows the separation distance, d, and horizontal position, h, for the NMP-(4,4) CNT hybrids. Sub-figures in the left and right panels were obtained respectively based on the RCS and OCS.

Let us first look at the results of d, based on the RCS. For AMP, CMP, and GMP, d slightly fluctuates around an average value of $\sim$3 Å for most of the simulation time, indicating those NMPs remain adsorbed to the CNT throughout the simulation course. Only for TMP large fluctuations are found during the time between $\sim$ 30 to 40 ns, with d reaching up to 40 Å. This indicates that the TMP detaches from the CNT surface for approximately 10 ns, reattaches to the CNT and remains adsorbed afterwards. Based on the OCS (see right sub-figures in Fig. 6.3), the variation of d is different since except GMP, all NMPs detaches from the CNT surface for some periods of time. For instance, AMP detaches from the CNT at $\sim$7 ns for a very short period of time and reattaches. At the time of $\sim$35 ns, AMP detaches again for $\sim$5 ns. CMP detaches from the CNT from $\sim$75 ns to $\sim$85 ns while the detachment for TMP occurs at the time between $\sim$76 ns to $\sim$80 ns.

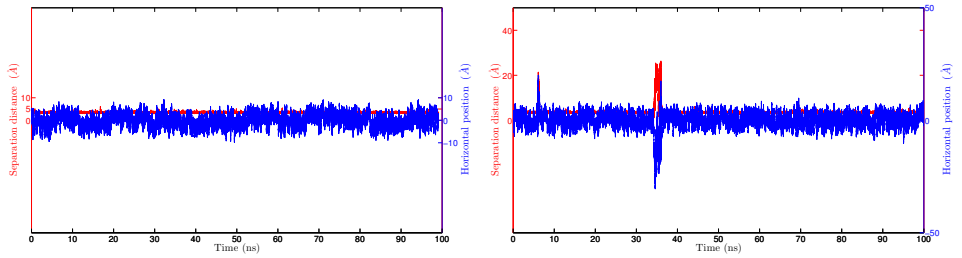

(a) AMP-(4,4) CNT

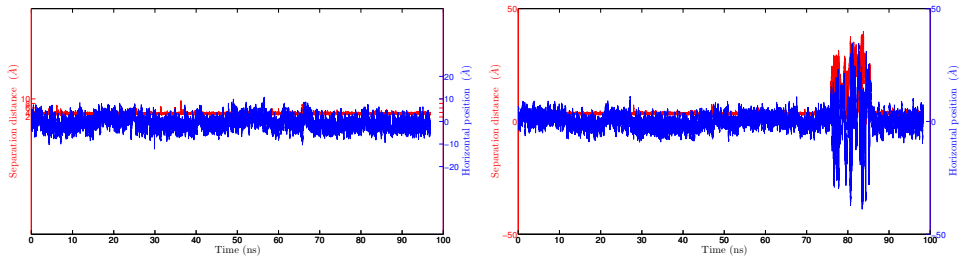

(b) CMP-(4,4) CNT

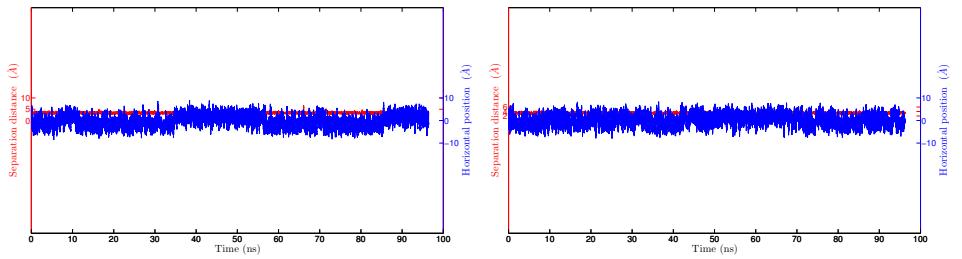

(c) GMP-(4,4) CNT

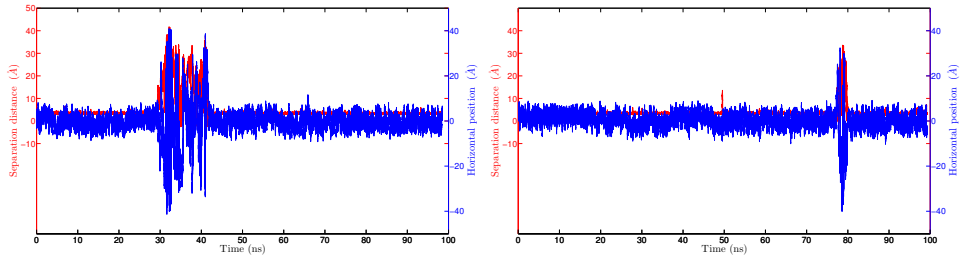

(d) TMP-(4,4) CNT

Figure 6.3: Separation distance and horizontal position between NMPs and (4,4) CNT: (a) AMP-(4,4) CNT, (b) CMP-(4,4) CNT, (c) GMP-(4,4) CNT, and (d) TMP-(4,4) CNT; results for separation distance and horizontal position respectively coloured red and blue. Figures in the left and right panels were obtained respectively based on the RCS and OCS.

The probability distribution of d for all four NMPs based on the RCS and OCS is presented in Fig. 6.4. In all hybrids, the highest peak is present at $d \sim 3$ Å, indicating that the nucleobase in each NMP tends to be located at that separation distance from the CNT surface. Based on the RCS, except for TMP, the probability of d being larger than ~ 5 Å is zero. For TMP, the probability of d being larger than ~ 5 Å is non zero due to the detachment of the TMP from the CNT between 30 ns and 40 ns . Based on the OCS, the probability of d being larger than ~ 5 Å is only zero for GMP. Such probability is also negligible for AMP and TMP compared with that for CMP, since the detachment for AMP and TMP occurs for a much shorter time.

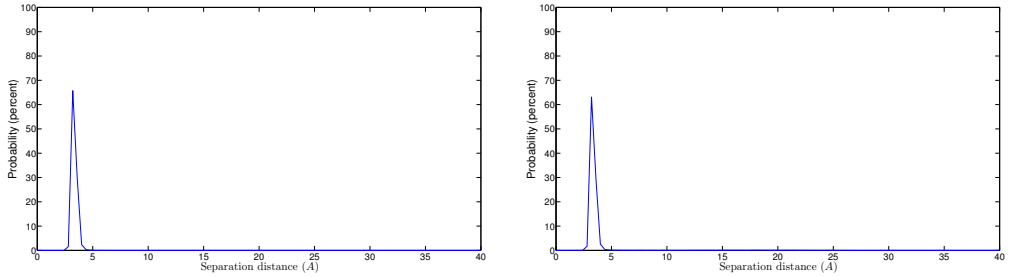

(a) AMP-(4,4) CNT

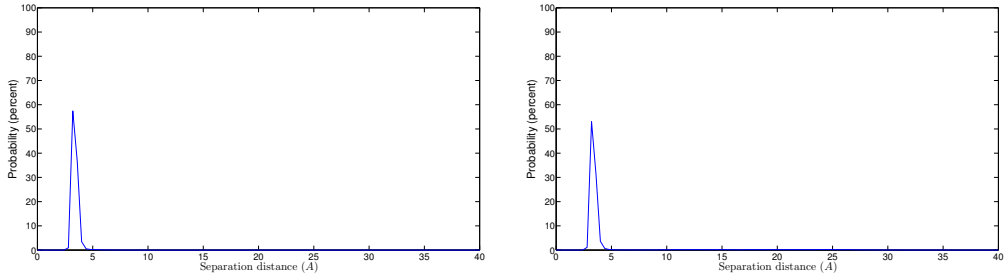

(b) CMP-(4,4) CNT

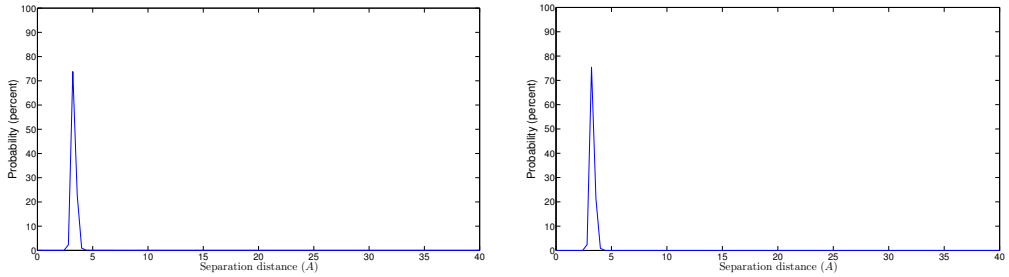

(c) GMP-(4,4) CNT

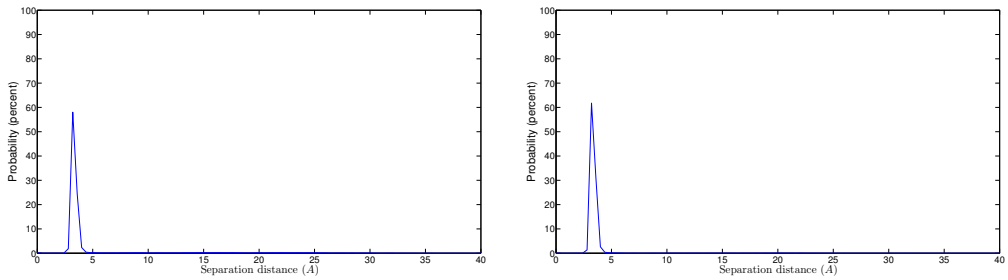

(d) TMP-(4,4) CNT

Figure 6.4: Probability distribution for the separation distance between NMPs and (4,4) CNT: (a) AMP-(4,4) CNT, (b) CMP-(4,4) CNT, (c) GMP-(4,4) CNT, and (d) TMP-(4,4) CNT. Figures in the left and right panels were obtained respectively based on the RCS and OCS.

Compared with the separation distance, the horizontal position exhibits a much more dynamic behaviour in Fig. 6.3. Based on both RCS and OCS, larger fluctuations in h are observed compared with that in d. Furthermore, fluctuations become much larger at the time intervals during which largest fluctuations in d are seen, corresponding to the detachment of NMPs. To investigate the horizontal position of NMPs in more detail, the probability distributions of h is depicted in Fig. 6.5. Sub-figures in the left and right panels were obtained respectively based on the RCS and OCS. Compared with Fig. 6.4, the distribution of h is clearly much wider, consistent with the larger fluctuation in h compared to d (Fig. 6.3). This also indicate that horizontal shift along the CNT axis is a more dominant mode of motion compared with displacement away from the CNT axis. h is mostly found to be between ~ -7.5 Å and 7.5 Å. According to the definition of h presented in Section 6.2, Fig. 6.5 suggests that the nucleobases's COM is mainly located within the length of the CNT while each NMP displaces from one CNT end to the other. In all cases, the highest peak is found at $h = 0$ i.e., the probability of nucleobases's COM to be located in the middle of the CNT is highest while the corresponding probability is lowest near the two CNT ends. In addition, the distribution is nearly symmetric with similar magnitudes in both left and right panels in Fig. 6.5. This implies that there is no preferred direction in which NMPs shift relative to the CNT.

Based on the RCS, the probability of h to be less than -10 Å or greater than 10 Å is zero, except for TMP which is due to its detachment from the CNT at 30 ns to 40 ns. Based on the OCS, the probability of h to be less than -10 Å or greater than 10 Å is non zero for AMP, CMP, and TMP. Such probability is large for CMP compared with AMP and TMP since CMP detaches from the CNT for a longer

time compared with the two NMPs.

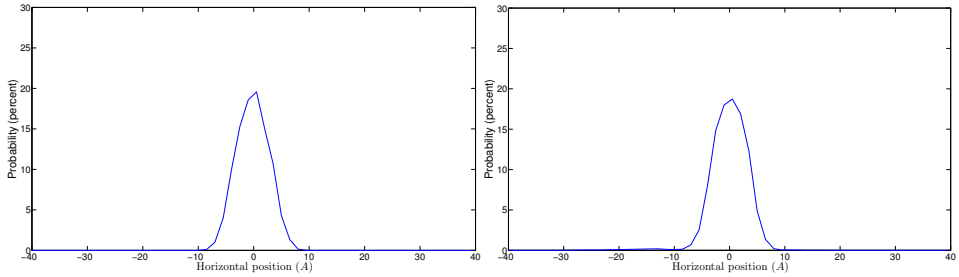

(a) AMP-(4,4) CNT

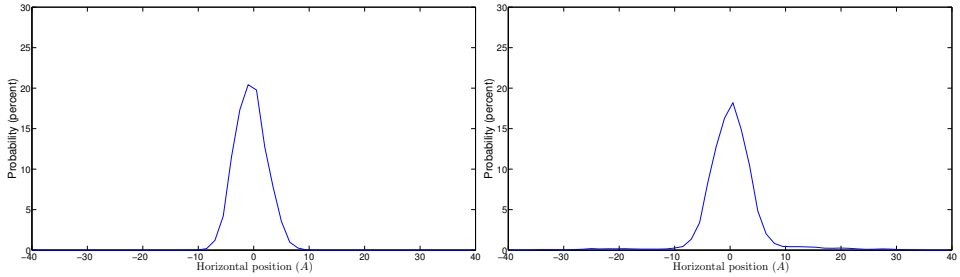

(b) CMP-(4,4) CNT

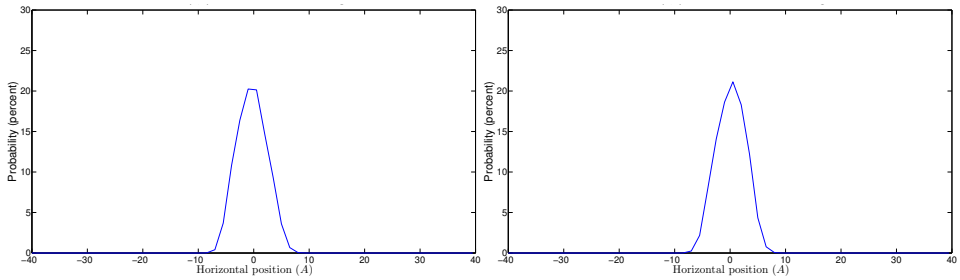

(c) GMP-(4,4) CNT

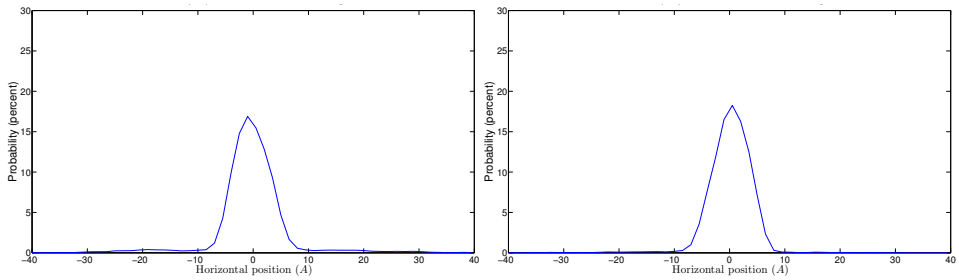

(d) TMP-(4,4) CNT

Figure 6.5: Probability distribution for the horizontal position between NMP and (4,4) CNT: (a) AMP-(4,4) CNT, (b) CMP-(4,4) CNT, (c) GMP-(4,4) CNT, and (d) TMP-(4,4) CNT. Figures in the left and right panels were obtained respectively based on RCS and OCS.

In order to analyze the orientation of the NMPs with respect to the CNT, the probability of $\cos\theta$ for NMP-(4,4) CNT hybrids is presented in Fig. 6.6. Sub-figures in the left and right panels present the results respectively for the RCS and OCS. For all NMPs, the highest peak is found at $\cos\theta$ being ~ 1, which corresponds to the cases where the nucleobase plane in each NMP is parallel with respect to the CNT surface. Based on the RCS, the probability of finding $\cos\theta$ to be negative is zero for all NMPs, except for TMP in which case a secondary peak is found at the probability of $\cos\theta$ being between ~ -0.9 to -1. Such negative values of $\cos\theta$ indicates that the nucleobase plane is flipped with respect to its initial configuration. This is consistent with the results in Fig. 6.3 in which TMP was found to detach from the CNT for ~ 10 ns (Also see plots of $\cos\theta$ versus d in Appendix D.). Based on the OCS, except for GMP, the probability of negative values for $\cos\theta$ is non-zero for all NMPs. Specifically, nucleobases in NMPs (except GMP) flip for some period of time due to the detachment from the CNT, consistent with results in Fig. 6.3. A secondary peak is seen at $\cos\theta$ being between ~ -0.9 to -1 for AMP, CMP, and TMP which is relatively high compared with the results obtained based on the RCS.

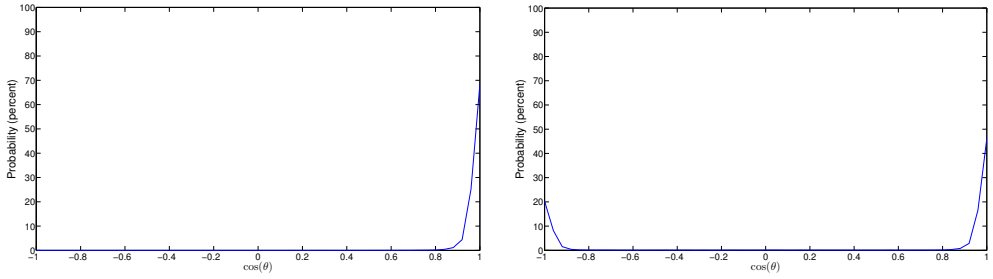

(a) AMP-(4,4) CNT

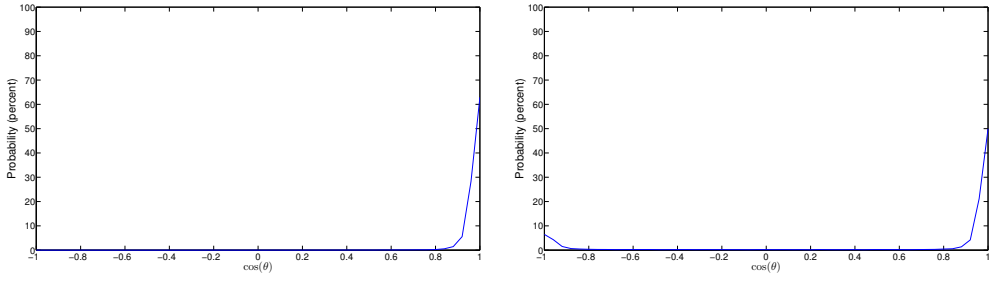

(b) CMP-(4,4)

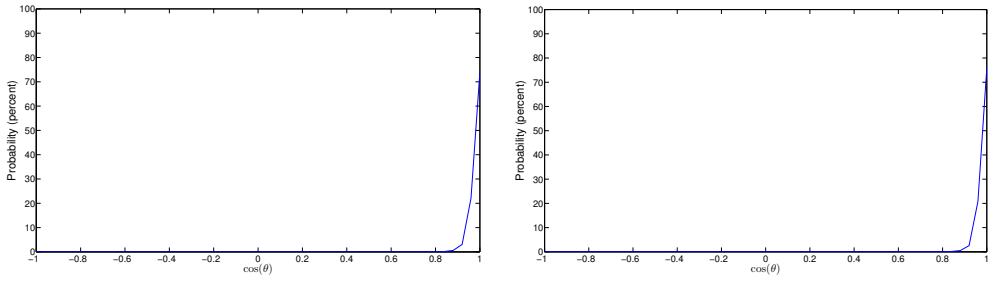

(c) GMP-(4,4)

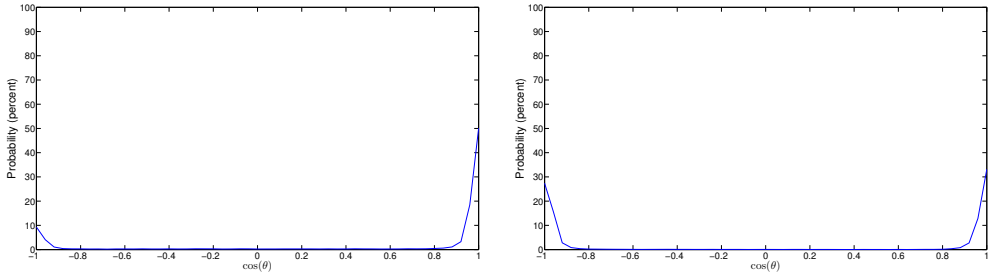

(d) TMP-(4,4)

Figure 6.6: Probability distribution of $\cos\theta$ for: (a) AMP-(4,4) CNT, (b) CMP-(4,4) CNT, (c) GMP-(4,4) CNT, and (d) TMP-(4,4) CNT hybrids. Figures in the left and right panels were obtained respectively based on the RCS and OCS.

The distance between each Na^+ ion and the phosphorous atom (P) in each NMP was also calculated in order to track the displacements of ions in the solution. Fig. 6.7 shows the Na^+-P distance for the NMP-(4,4) CNT hybrids. Results based on the RCS and OCS are respectively shown in the left and right panels. Based on RCS, at each simulation time, at least one of the Na^+ ions was found to be located at a distance of $\sim$ 3 Å from the P atom. For each hybrid, there are instants at which the two ions exchange, namely the attached one is released to the solution while the other ion attaches to the phosphate group. However, results obtained based on the OCS are different as there is $\sim$ 50% of time during which both ions are found at the distance greater than 3 Å. For instance, both ions are far from the TMP for most of the simulation time in the TMP-(4,4) CNT hybrid and one of ions is found bound to the phosphate group only for some short periods of time.

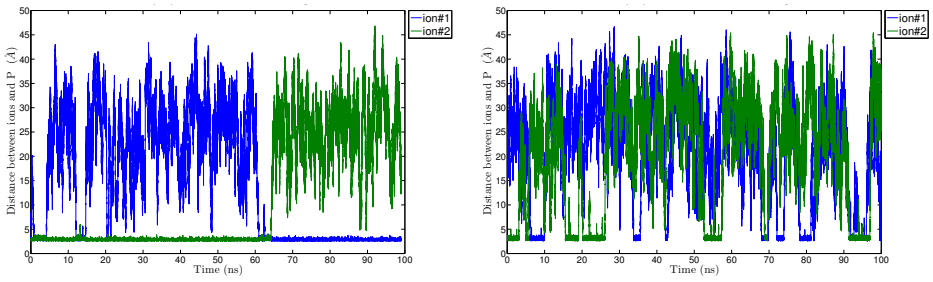

(a) AMP-(4,4) CNT

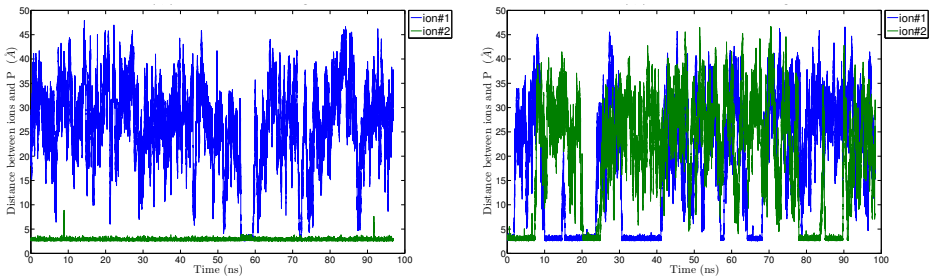

(b) CMP-(4,4) CNT

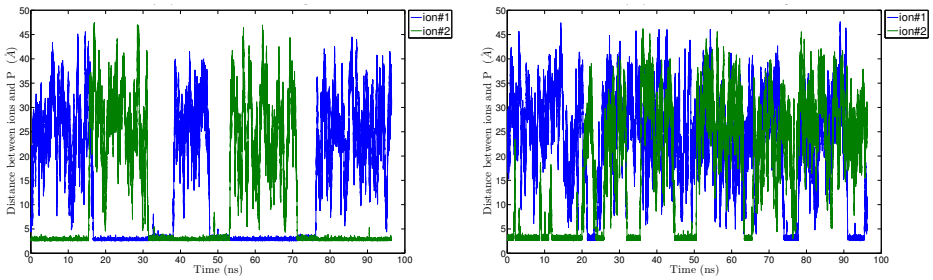

(c) GMP-(4,4) CNT

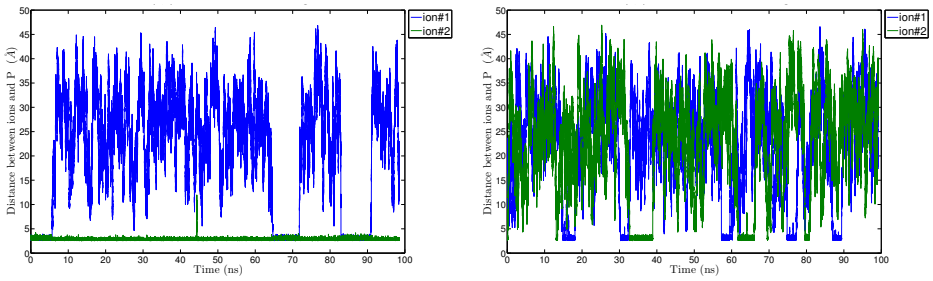

(d) TMP-(4,4) CNT

Figure 6.7: Distance between Na^+ ions and P atom for: (a) AMP-(4,4) CNT, (b) CMP-(4,4) CNT, (c) GMP-(4,4) CNT, and (d) TMP-(4,4) CNT hybrids. Figures in the left and right panels were obtained respectively based on the RCS and OCS.

The three DOFs (d, h, and θ) correspond to the relative motion of NMPs with respect to the CNT. The horizontal displacement, h, was found to be the most significant mode of NMPs' displacement. The probability distribution of h was symmetric i.e., each NMP displaces within the length of the CNT with no preferred direction. NMPs were found to located in the vicinity of the CNT surface; however few transient detachments from were also observed. The orientation of the nucleobase is parallel to the CNT surface (stacked) for the most time, but associated with the transient detachment, unstacking or even flipping for some of the NMPs were present. The dynamic detachments of NMPs from the CNT surface involve large fluctuations in all three DOFs.

The three DOFs were shown to depend on the charge assignment scheme. Specifically, compared with the RCS, more frequent large fluctuations in d and h are found based on the OCS. Furthermore, the probability of finding $\cos\theta$ being negative is higher using the OCS. Such findings implies that NMP-CNT systems are more dynamic if the OCS is employed. One possible reason for such difference caused from different charge schemes is that the charge transfer between NMP and CNT could be large [15]. Hence, the original and redistributed partial atomic charges could be very different, leading to different structural properties of the hybrid. The charge transfer from NMP to the CNT contributes to the higher stability of binding between the two [7]. Therefore, NMP-CNT hybrids are likely more stable based on the RCS compared with the OCS in which the charge transfer was not take into account.

Different charge schemes were also found to have a significant influence on the dynamics of ions in the solution (see Fig.6.7). Specifically, ions were found to be more weakly bound to the NMPs using the OCS. Our charge analysis showed

that the total charge of the phosphate group is more negative (approximately 20%) based on the RCS compared with that based on the OCS [15]. Higher concentration of negative charges on the phosphate group may lead to stronger electrostatic attraction with the positively charged sodium ions and hence less dynamic motions for the ions, as seen in Fig.6.7.

For further discussion below, only the results based on the RCS are considered, as it is more accurate compared with the OCS. NMP-(4,4) CNT hybrids are found to be relatively stable as each NMP remains adsorbed on the CNT surface for most of the simulation time. Only TMP detaches for a short period of time which could be due to relatively smaller molecular mass compared with AMP and GMP. CMP possess smaller molecular mass compared with TMP, however the charge transfer from that to the CNT is slightly larger which may facilitate its stability on a CNT. It should be pointed out that the stability of NMPs on CNT surface depend on several factors including the orientation of NMPs with respect to the CNT, NMP's molecular mass, and charge transfer between NMP and the CNT. Parallel orientation of nucleobase plane with respect to the CNT surface maximizes the non-bonded van der Waals interaction between them and hence the hybrid becomes more stable. In addition, the adsorption of heavier NMPs is less likely disturbed by the thermal fluctuations of the system in MD simulations. For instance, no detachment is observed for GMP which has the largest molecular mass among the four NMPs.

6.3.2 NMP-(7,0) CNT hybrids

Results of d and h for NMP-(7,0) CNT hybrids are shown in Fig. 6.8. Sub-figures in the left and right panels were obtained respectively based on the RCS and OCS. Overall, results are similar to the ones obtained and discussed for the NMP-(4,4) CNT hybrids in the previous section. However, non of the NMPs detaches from the (7,0) CNT surface based on the RCS. The detachment occurs only for two cases: AMP and CMP, if the OCS is employed. AMP is found to detach for $\sim$ 5 ns, while CMP detaches for a shorter period of time. Fig. 6.9 shows the probability distribution of d. Similar to the NMP-(4,4) CNT hybrids, the highest peak is present at $d \sim 3$ Å.

Fig. 6.10 shows the probability distribution of h with the highest peak in the middle, similar to the ones in Fig. 6.5. Probability of h for AMP and CMP based on the OCS differ from the other distributions as non-zero probability is seen for h being less than ~ -10 Å and greater than ~ 10 Å. This is due the detachment of AMP and CMP from the CNT for some period of time.

Probability of $\cos\theta$ is presented in Fig. 6.11. Large peaks of $\cos\theta$ at ~ 1 are indication of the parallel orientation of nucleobases in NMPs with respect to the CNT surface. Distributions for AMP and CMP based on the OCS are different as peaks of $\cos\theta$ at ~ -1 are relatively large due to high probability of those NMPs to detach from the CNT surface for a considerable simulation time.

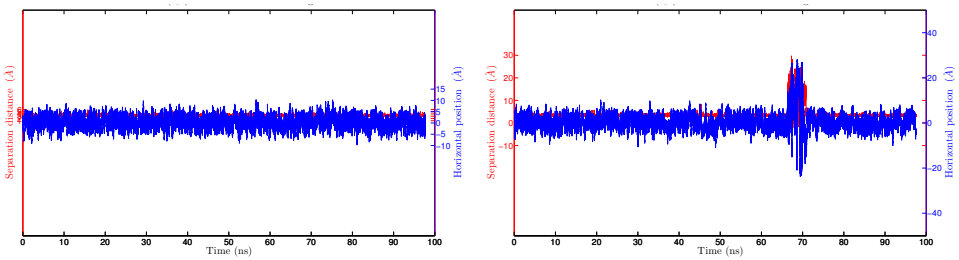

(a) AMP-(7,0) CNT

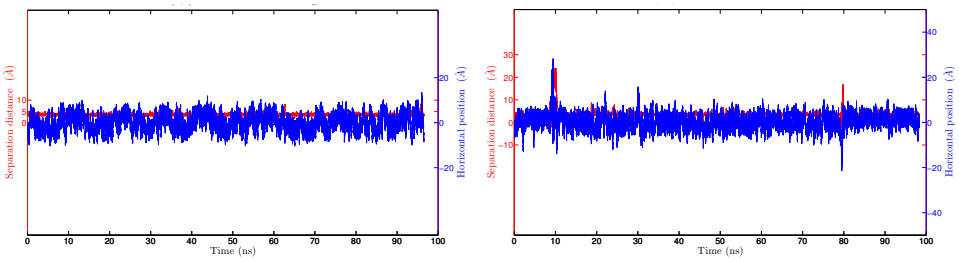

(b) CMP-(7,0) CNT

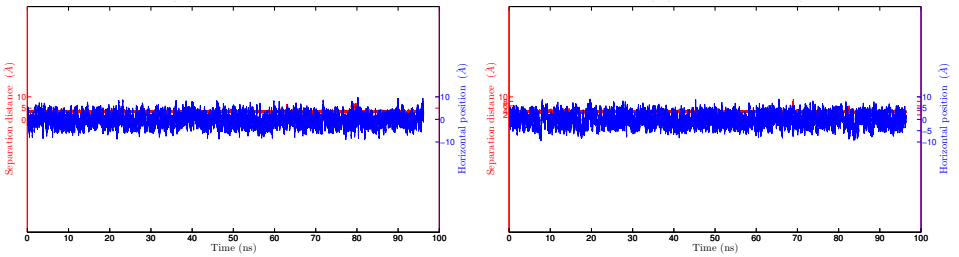

(c) GMP-(7,0) CNT

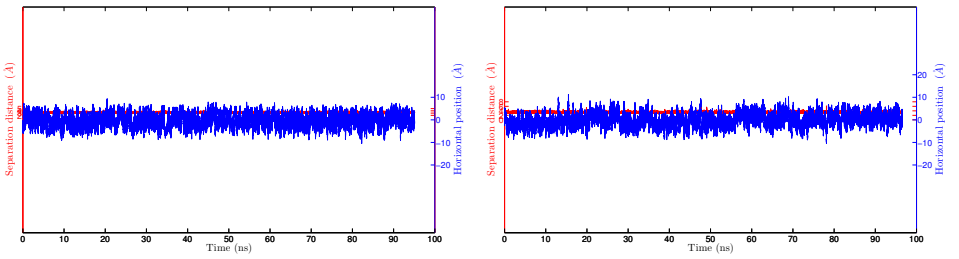

(d) TMP-(7,0) CNT

Figure 6.8: Separation distance and horizontal position between NMPs and (7,0) CNT: (a) AMP-(7,0) CNT, (b) CMP-(7,0) CNT, (c) GMP-(7,0) CNT, and (d) TMP-(7,0) CNT; results for separation distance and horizontal position respectively coloured red and blue. Figures in the left and right panels were obtained respectively based on the RCS and OCS.

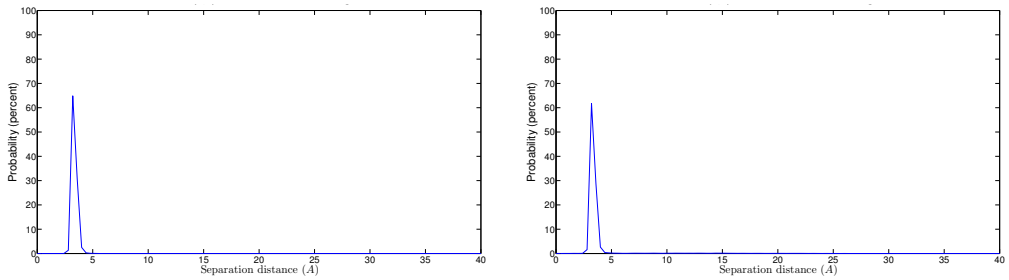

(a) AMP-(7,0) CNT

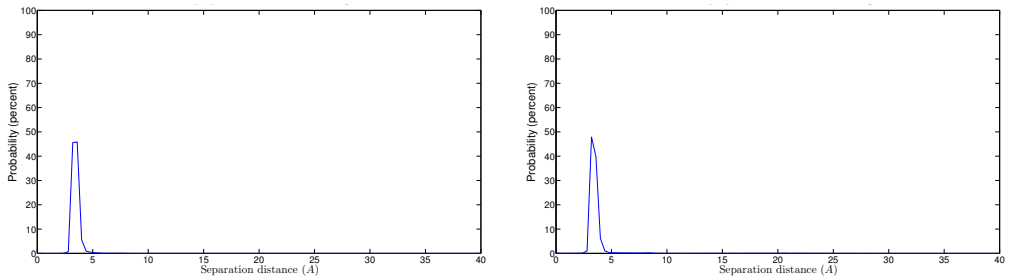

(b) CMP-(7,0) CNT

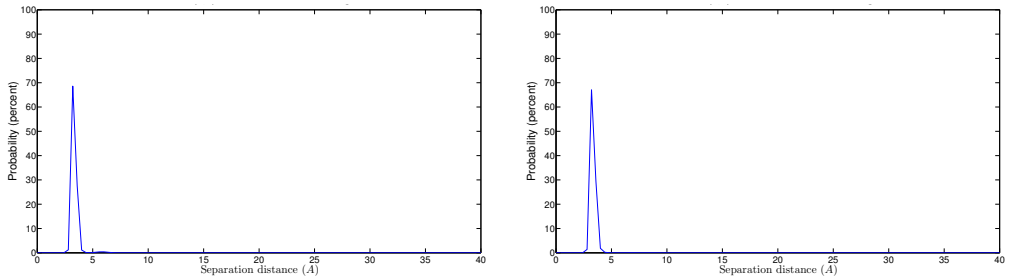

(c) GMP-(7,0) CNT

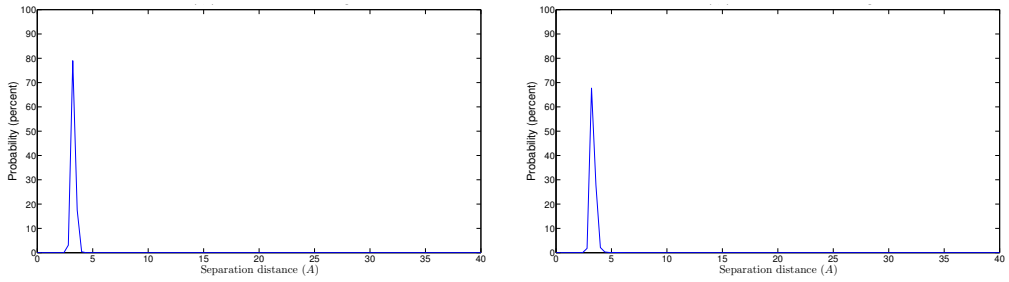

(d) TMP-(7,0) CNT

Figure 6.9: Probability distribution for the separation distance between NMPs and (7,0) CNT: (a) AMP-(7,0) CNT, (b) CMP-(7,0) CNT, (c) GMP-(7,0) CNT, and (d) TMP-(7,0) CNT. Figures in the left and right panels were obtained respectively based on the RCS and OCS.

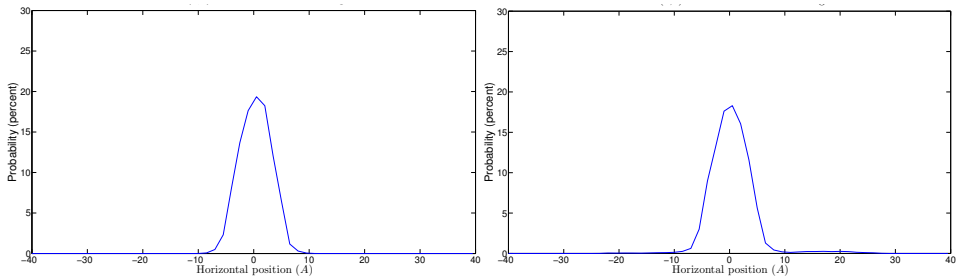

(a) AMP-(7,0) CNT

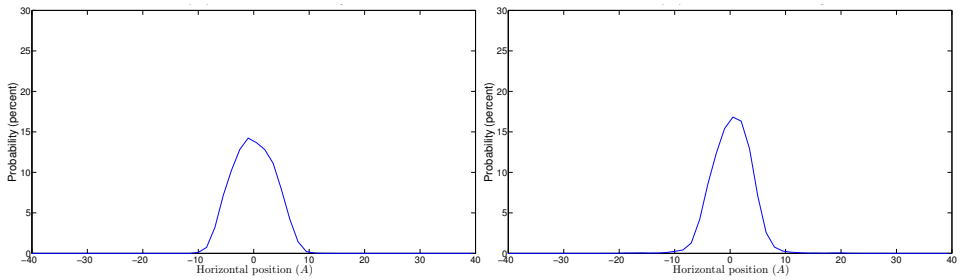

(b) CMP-(7,0) CNT

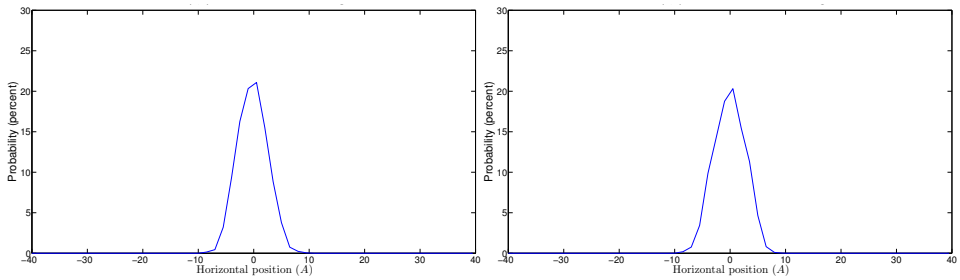

(c) GMP-(7,0) CNT

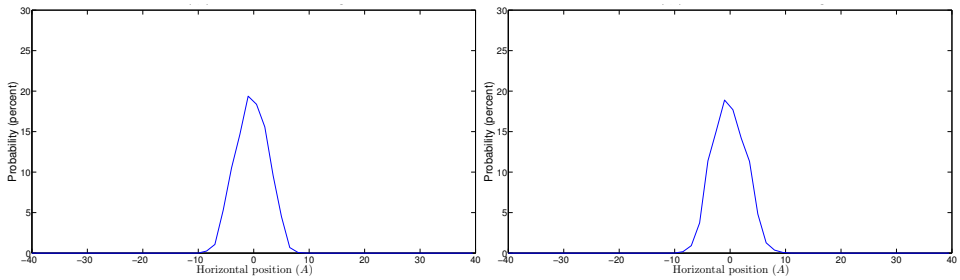

(d) TMP-(7,0) CNT

Figure 6.10: Probability distribution for the horizontal position between NMP and (7,0) CNT: (a) AMP-(7,0) CNT, (b) CMP-(7,0) CNT, (c) GMP-(7,0) CNT, and (d) TMP-(7,0) CNT. Figures in the left and right panels were obtained respectively based on the RCS and OCS.

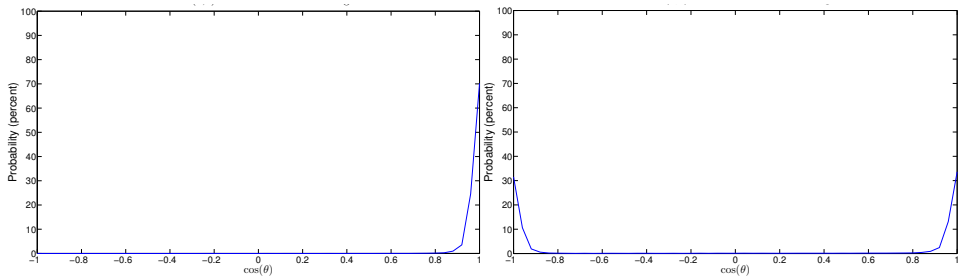

(a) AMP-(7,0) CNT

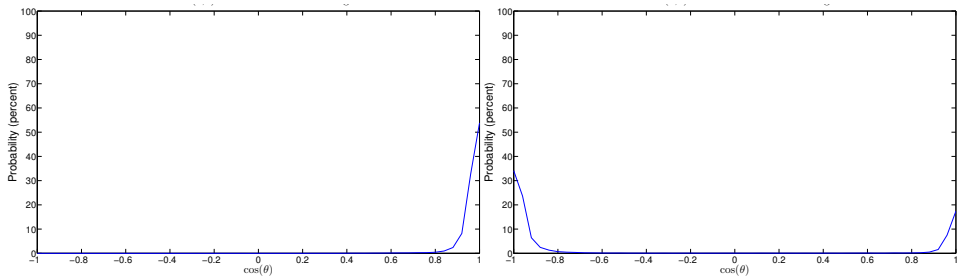

(b) CMP-(7,0)

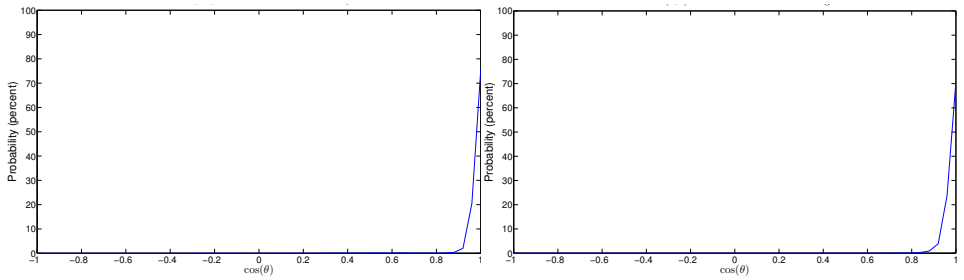

(c) GMP-(7,0)

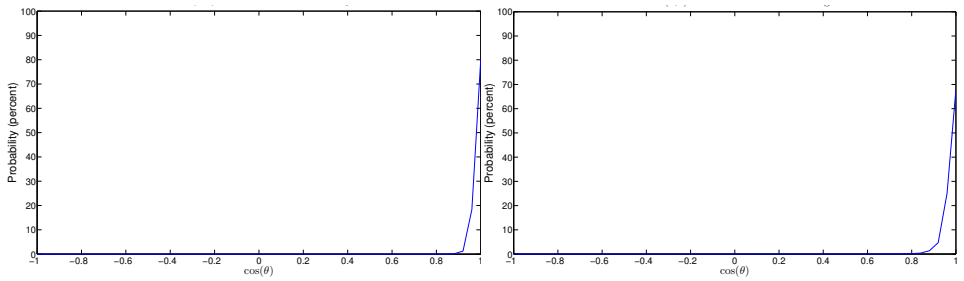

(d) TMP-(7,0)

Figure 6.11: Probability distribution of $\cos\theta$ for: (a) AMP-(7,0) CNT, (b) CMP-(7,0) CNT, (c) GMP-(7,0) CNT, and (d) TMP-(7,0) CNT hybrids. Figures in the left and right panels were obtained respectively based on the RCS and OCS.

Fig. 6.7 shows the distance between each Na^+ ion and the phosphorous atom (P) in each NMP. Based on the RCS, at least one of the ions is located within the distance of $\sim$ 3 Å from the P atom in AMP-(7,0) CNT and TMP-(7,0) CNT hybrids. For CMP-(7,0) CNT and GMP-(7,0) CNT hybrids, there are instants that both ions are located far from the NMP. Based on the OCS, no ions are found near the NMP for some periods of time for all hybrids. Overall, ions are found to be more dynamic based on the OCS, similar to NMP-(4,4) CNT hybrids.

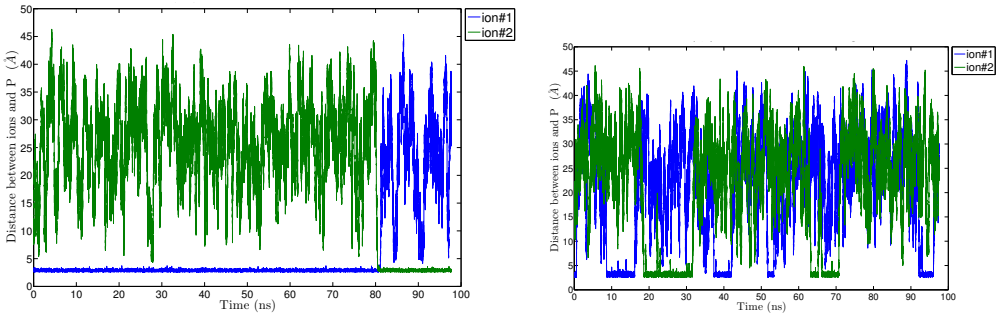

(a) AMP-(7,0) CNT

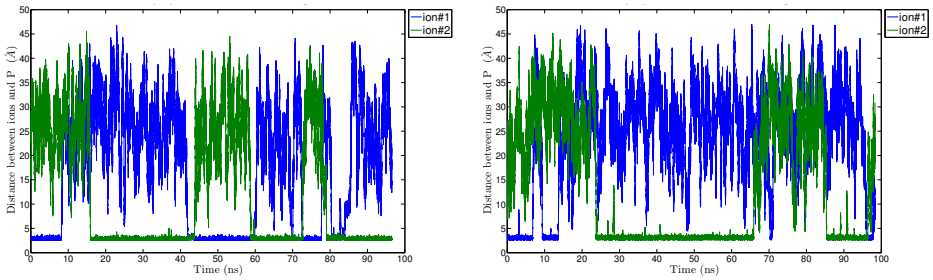

(a) CMP-(7,0) CNT

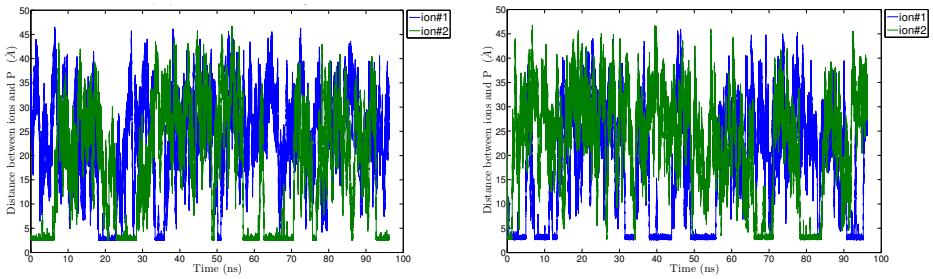

(a) GMP-(7,0) CNT

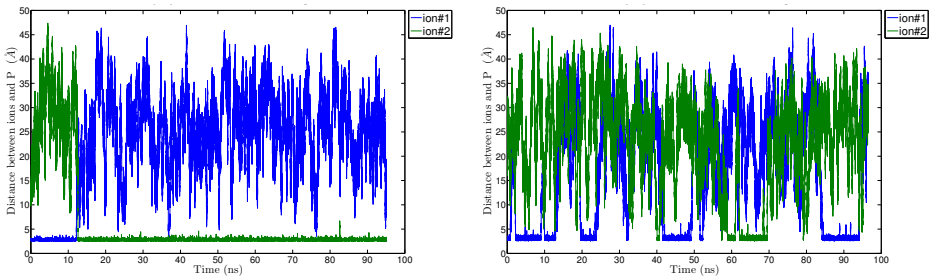

(a) TMP-(7,0) CNT

Figure 6.12: Distance between Na^+ ions and P atom for: (a) AMP-(7,0) CNT, (b) CMP-(7,0) CNT, (c) GMP-(7,0) CNT, and (d) TMP-(7,0) CNT hybrids. Figures in the left and right panels were obtained respectively based on the RCS and OCS.

It is important to study the effect of CNT's chirality on the properties of NMP-CNT hybrids. We only consider the results obtained based on the RCS to compare the results of the NMP-(4,4) CNT and NMP-(7,0) CNT hybrids hereafter. Similar bahavior in d was found for both CNTs indicating NMPs adsorb on both CNTs within similar separation distance. In addition, the probability of h being approximately zero was highest for all NMPs adsorbed on the CNTs indicating that NMPs are mainly found in the middle of each of CNTs. Furthermore, NMPs preferred a parallel orientation with respect to the CNT surface, regardless of the chirality of the CNT.

Despite the above similarities, there are considerable differences due to the difference in CNTs' chiralities. First of all, TMP was found to detach from the (4,4) CNT while it remains adsorbed on the (7,0) CNT. It has been shown that TMP adsorbs more weekly to the (4,4) CNT surface in the absence of dynamics motions [7] i.e., TMP-(4,4) hybrid is less stable compared with TMP-(7,0) CNT hybrid and hence the the detachment from the (4,4) CNT is more likely to take place. Secondly, more frequent exchange of ions are seen in the NMP-(7,0) CNT hybrids especially for CMP and GMP. Also, different from GMP-(4,4) CNT hybrids, no ion is bound to the phosphate group during a considerable simulation time for the GMP-(7,0) CNT hybrid. Except for GMP, the concentration of negative charge in the phosphate group is higher in all NMP-(7,0) CNT hybrids compared with that in NMP-(4,4) CNT hybrids, which may explain why positively charged ions are less likely bound to the GMP in the GMP-(7,0) CNT hybrid.

It should be pointed out that several limitations were present in this study. First of all, although the PACs in the RCS are expected to be more accurate when the NMP and CNT are near their optimized structures, they were assumed to be

fixed during MD simulations in both charge assignment schemes. In reality, PAC can further vary upon displacement of NMPs with respect to CNTs due to the possible charge transfer between them. Future advances in ab initio molecular dynamics [16] and polarizable force fields [17] can eliminate such limitation. Secondly, only two types of CNTs were considered in this study. It is interesting to systematically explore the effect of CNT's chirality by investigating a series of CNTs with different chiralities. In addition, only two Na^+ cations were present in the systems. Different salt type and concentration may affect the properties of NMP-CNT hybrids; for instance Frischknecht and Martin showed that the binding energy between NMP and CNT depends on the salt concentration [9]. Despite those limitations, the findings of this study will shed a light in future attempts to simulate interactions between DNA and CNTs.

6.4 Conclusions

A series of classical molecular dynamics simulations was performed to study the adsorption of DNA nucleotides on two CNTs with different chiralities of (4,4) and (7,0). Our results showed that nucleotides undergoes considerable horizontal shift along the CNTs' axis subjected to a constant separation distance between them. In addition, the nucleobase plane in each NMP tends to posses a parallel orientation with respect to the CNTs surface. Occasional detachment and reattachment of NMPs from CNTs were observed. It was also found that the configurational properties of NMP-CNT hybrids depend on partial atomic charges. Specifically, each NMP-CNT hybrid was more stable if the partial atomic charges were obtained from a quantum mechanical calculation on the same optimized NMP-CNT

hybrid, compared with the typical way of assigning partial charges in molecular dynamics simulations in which the partial charges are determined based on isolated molecules.

References

[1] R. Singh, D. Pantarotto, D. McCarthy, O. Chaloin, J. Hoebeke, C. D. Partidos, J.-P. Briand, M. Prato, A. Bianco, and K. Kostarelos, "Binding and Condensation of Plasmid DNA onto Functionalized Carbon Nanotubes: Toward the Construction of Nanotube-Based Gene Delivery Vectors," *Journal of the American Chemical Society*, vol. 127, no. 12, pp. 4388–4396, 2005.

[2] C. Hu, Y. Zhang, G. Bao, Y. Zhang, M. Liu, and Z. L. Wang, "DNA Functionalized Single-Walled Carbon Nanotubes for Electrochemical Detection," *The Journal of Physical Chemistry B*, vol. 109, no. 43, pp. 20072–20076, 2005.

[3] Y. Ma, S. R. Ali, A. S. Dodoo, and H. He, "Enhanced Sensitivity for Biosensors: Multiple Functions of DNA-Wrapped Single-Walled Carbon Nanotubes in Self-Doped Polyaniline Nanocomposites," *The Journal of Physical Chemistry B*, vol. 110, no. 33, pp. 16359–16365, 2006.

[4] P. He and M. Bayachou, "Layer-by-Layer Fabrication and Characterization of DNA-Wrapped Single-Walled Carbon Nanotube Particles," *Langmuir*, vol. 21, no. 13, pp. 6086–6092, 2005.

[5] S. Wang, R. Wang, P. J. Sellin, and S. Chang, "Carbon nanotube based

dna biosensor for rapid detection of anti-cancer drug of cyclophosphamide," *Current Nanoscience*, vol. 5, no. 3, pp. 312–317, 2009.

[6] M. Zheng, A. Jagota, E. D. Semke, B. A. Diner, R. S. Mclean, S. R. Lustig, R. E. Richardson, and N. G. Tassi, "DNA-assisted dispersion and separation of carbon nanotubes," *Nat Mater*, vol. 2, no. 5, pp. 338–342, 2003.

[7] M. Chehel Amirani and T. Tang, "A QM:MM model for the interaction of DNA nucleotides with carbon nanotubes," *Phys. Chem. Chem. Phys.*, vol. 17, pp. 7564–7575, 2015.

[8] D. M. Boghaei and M. Gharagozlou, "Charge transfer complexes of adenosine-5′-monophosphate and cytidine-5′-monophosphate with water-soluble cobalt(ii) schiff base complexes in aqueous solution," *Spectrochimica Acta Part A: Molecular and Biomolecular Spectroscopy*, vol. 63, no. 1, pp. 139 – 148, 2006.

[9] A. L. Frischknecht and M. G. Martin, "Simulation of the adsorption of nucleotide monophosphates on carbon nanotubes in aqueous solution," *The Journal of Physical Chemistry C*, vol. 112, no. 16, pp. 6271–6278, 2008.

[10] A. Lehninger, D. Nelson, and M. Cox, *Lehninger Principles of Biochemistry*. W. H. Freeman, 2005.

[11] M. J. Frisch, G. W. Trucks, H. B. Schlegel, G. E. Scuseria, M. A. Robb, J. R. Cheeseman, G. Scalmani, V. Barone, B. Mennucci, G. A. Petersson, H. Nakatsuji, M. Caricato, X. Li, H. P. Hratchian, A. F. Izmaylov, J. Bloino, G. Zheng, J. L. Sonnenberg, M. Hada, M. Ehara, K. Toyota, R. Fukuda,

J. Hasegawa, M. Ishida, T. Nakajima, Y. Honda, O. Kitao, H. Nakai, T. Vreven, J. J. A. Montgomery, J. E. Peralta, F. Ogliaro, M. Bearpark, J. J. Heyd, E. Brothers, K. N. Kudin, V. N. Staroverov, R. Kobayashi, J. Normand, K. Raghavachari, A. Rendell, J. C. Burant, S. S. Iyengar, J. Tomasi, M. Cossi, N. Rega, J. M. Millam, M. Klene, J. E. Knox, J. B. Cross, V. Bakken, C. Adamo, J. Jaramillo, R. Gomperts, R. E. Stratmann, O. Yazyev, A. J. Austin, R. Cammi, C. Pomelli, J. W. Ochterski, R. L. Martin, K. Morokuma, V. G. Zakrzewski, G. A. Voth, P. Salvador, J. J. Dannenberg, S. Dapprich, A. D. Daniels, Ö. Farkas, J. B. Foresman, J. V. Ortiz, J. Cioslowski, and D. J. Fox, "Gaussian 09 Revision A.1." Gaussian Inc. Wallingford CT 2009.

[12] D. Case, J. Berryman, R. Betz, D. Cerutti, T. Cheatham, III, T. Darden, R. Duke, T. Giese, H. Gohlke, A. Goetz, N. Homeyer, S. Izadi, P. Janowski, J. Kaus, A. Kovalenko, T. Lee, S. LeGrand, P. Li, T. Luchko, R. Luo, B. Madej, K. Merz, G. Monard, P. Needham, H. Nguyen, H. Nguyen, I. Omelyan, A. Onufriev, D. Roe, A. Roitberg, R. Salomon-Ferrer, C. Simmerling, W. Smith, J. Swails, R. Walker, J. Wang, R. Wolf, X. Wu, D. York, and P. Kollman, "Ambertools 14," 2014. University of California, San Francisco.

[13] J. Wang, R. M. Wolf, J. W. Caldwell, P. A. Kollman, and D. A. Case, "Development and testing of a general amber force field," *Journal of Computational Chemistry*, vol. 25, no. 9, pp. 1157–1174, 2004.

[14] D. Case, J. Berryman, R. Betz, D. Cerutti, T. Cheatham, III, T. Darden, R. Duke, T. Giese, H. Gohlke, A. Goetz, N. Homeyer, S. Izadi, P. Janowski,

J. Kaus, A. Kovalenko, T. Lee, S. LeGrand, P. Li, T. Luchko, R. Luo, B. Madej, K. Merz, G. Monard, P. Needham, H. Nguyen, H. Nguyen, I. Omelyan, A. Onufriev, D. Roe, A. Roitberg, R. Salomon-Ferrer, C. Simmerling, W. Smith, J. Swails, R. Walker, J. Wang, R. Wolf, X. Wu, D. York, and P. Kollman, "Amber 14." AMBER 2015, University of California, San Francisco.

[15] M. Chehel Amirani and T. Tang, "Electrostatics of dna nucleotides-carbon nanotube hybrids evaluated from qm:mm simulations," *Nanoscale*, 2015. Accepted.

[16] R. Car and M. Parrinello, "Unified approach for molecular dynamics and density-functional theory," *Phys. Rev. Lett.*, vol. 55, pp. 2471–2474, 1985.

[17] P. E. M. Lopes, J. Huang, J. Shim, Y. Luo, H. Li, B. Roux, and J. Alexander D. MacKerell, "Polarizable force field for peptides and proteins based on the classical drude oscillator," *Journal of Chemical Theory and Computation*, vol. 9, no. 12, pp. 5430–5449, 2013.

Chapter 7

Conclusions and Future work

7.1 Conclusions

Recent studies on the DNA-CNT hybrid have revealed it as a very promising nano hybrid structure with many appealing applications. Those applications include bio-sensors for cancer detection, CNT dispersion and purification, and drug delivery [1–7]. While experimental studies on this subject are expanding, accurate theoretical models are needed in order to describe the properties of these complicated DNA-CNT hybrids. Such models can be used to predict and customize the chemo-physical properties of the hybrids and facilitate future experimental efforts.

This study is an attempt to improve past theoretical efforts on studying DNA-CNT hybrids in an electrolyte solution. There has been a large gap between theoretical models and experiments due to several limitations in the theoretical studies. Even though simulations at quantum mechanical level can accurately capture the electron distribution in the hybrid, the molecular models were very small and the

hybrids were simulated in vacuum, which lacked the important electrolytic environment present in experiments. Molecular mechanics simulations allowed the increase in length and time scales, but description of the interactions between DNA and CNT was inaccurate. In particular, the electronic structure of the CNT was missing, which is crucial in DNA-assisted CNT separation. The main goal of this study is to reduce those deficiencies by introducing a mixed quantum mechanics:molecular mechanics model along with employing suitable computational methods for such model.

To build the model, a comprehensive critical review of relevant past studies on the interactions of DNA building blocks (nucleobase and nucleotide) with CNT/graphene was first performed. It was shown that there are discrepancies in the theoretical results for the structural properties and strength of binding of DNA nucleobase/nucleotide to CNT/graphene, due to the difference in simulated systems, simulation method and procedure. Important factors and limitations in simulation of DNA-CNT hybrids leading to the existing discrepancies were discussed.

Based on the review study, we adopted the systems and methods of Ref. [8] and studied the binding of DNA nucleobases to a CNT with the chirality of (7,0). Specifically, we calculated the binding energy and separation distance between DNA nucleobases and the CNT in vacuum from the geometry optimization of the hybrid using DFT. It was shown in detail that the initial configuration of nucleobase with respect to the CNT is an important factor and considerably influences the results.

In order to include the electrolyte solution so as to present a more realistic model, mixed quantum mechanics and classical molecular mechanics (QM:MM)

were employed to study the binding of DNA nucleotides with CNTs. To make the problem computationally manageable, explicit water molecules and ions were treated classically using the Amber force field. The DNA nucleotides (all four types) and CNT (two chiralities: (4,4) and (7,0)) were modeled with a validated dispersion-corrected DFT approach, which is essential to accurately describe the interactions between nucleotides and CNT. Optimized binding structures for the hybrids were obtained and binding energies were calculated. Our results showed a strong physisorption of nucleotides on CNTs, compared with past studies on nucleobase-CNT binding in a vacuum. It was pointed out that the contribution from the release of water molecules upon hybridization to the binding energy could be considerable, facilitating the adsorption. Furthermore, dependency of the binding structure and energy on the chirality of the CNT as well as the nucleobase type was shown.

The electrostatic potential and charge transfer for the optimized DNA nucleotide-CNT hybrids were also evaluated. The results suggested that the electrostatic potential of the hybrids depends on the chirality of the CNT which can be used to distinguish CNTs with different chiralities. Also, it was shown that charge transfer from the nucleotides to the (7,0) CNT is larger compared with that for the (4,4) CNT, which correlates with the stronger nucleotide-CNT binding found for the (7,0) CNT.

Finally, a series of classical molecular dynamics simulations were performed for the DNA nucleotide-CNT hybrids. It was revealed that nucleotides adsorb on CNT surface with a nearly constant separation distance while the relative horizontal displacement along the CNTs' axis was considerable. Occasional attachment/reattachment from the CNT surface was also observed. NMP-(7,0) CNT

hybrids were found to be more stable compared with NMP-(4,4) CNT hybrids, consistent with previous findings. In addition, the stability of NMP-CNT hybrids was shown to depend on partial atomic charges. Specifically, atomic charges obtained from our QM:MM simulations for the same NMP-CNT hybrids resulted in more sable hybrids compared with those obtained for isolated NMPs and CNTs.

7.2 Future Work

Our goals in this thesis were to build atomistic-scale models for hybrids formed by DNA nucleobases or nucleotides with CNT using classical and quantum mechanical approaches, to study the properties of such hybrids, and to investigate the effect of nucleobase type, CNT chirality, and inclusion of solution.

Although the work presented here is the first attempt to provide a comprehensive model for the DNA nucleotide-CNT hybrids, there are clear limitations, as mentioned throughout the previous Chapters. Future efforts can be spent to eliminate these limitations and here we point out a few directions in which improvement can be made.

1- It would be more realistic if a piece of DNA is modelled instead on a single nucleotide. It has been shown that the wrapping angle, which will be present only if a relatively large DNA is modelled, has considerable effects on DNA-CNT properties [9]. Although a larger DNA piece requires much more computational resources, it is an essential step in studying DNA-CNT hybrids. Larger DNA will also allow the study on the effect of DNA sequence, which has been shown to influence the structural configuration of DNA on CNT surface [3, 10].

2- It would be very useful to consider longer CNTs. Long CNTs will first

eliminate the edge effects; secondly, more accurate description of the electronic properties of CNT will be provided, if a QM approach is used to simulate the long CNT. Despite notable advances in the computational methods and facilities, simulation of long CNTs is still very challenging. An alternative would be developing QM:MM approaches for periodic systems.

3- Considering a variety of CNTs with different chiralities and hence different electronic properties will be an interesting direction to pursue, as it has been shown that the electronic properties of the CNT are among the most important factors in the separation of CNTs according to their chiralities [9, 11].

4- Effects of salt type and concentration need to be addressed. The increase in salt concentration can not only provide screening for the electric field generated by the DNA-CNT hybrids, but also can affect the binding. Different types of salt have been shown to have different performance in the separation of CNTs according to their chiralities [9, 12], so it would be interesting to explore the mechanisms behind this observation

5- Another extension to this study would be performing a dynamic QM:MM simulation instead of a geometry optimization. Dynamic effects including temperature, pressure, entropy, and other thermodynamic quantities are important to consider in order to make comparison with experiments. Currently, it is not computationally feasible to perform such simulation for large systems, however, it might be doable to employ semi-empirical approaches for DNA-CNT hybrids.

6- Beside the theoretical points mentioned above, on the experimental side, it would be beneficial to perform experiments so that more direct comparison with theoretical results can be made. For instance, instead of DNA polymers, it would be helpful to have experiments on the binding of single nucleobases and

nucleotides to CNT. In addition, experiments on the binding of single DNA nucleotides to different CNTs with different chiralities seem to be necessary to find out how the CNT chirality affect the properties of the hybrids.

References

[1] M. Zheng, A. Jagota, E. D. Semke, B. A. Diner, R. S. Mclean, S. R. Lustig, R. E. Richardson, and N. G. Tassi, "DNA-assisted dispersion and separation of carbon nanotubes," *Nat Mater*, vol. 2, no. 5, pp. 338–342, 2003.

[2] M. Zheng, A. Jagota, M. S. Strano, A. P. Santos, P. Barone, S. G. Chou, B. A. Diner, M. S. Dresselhaus, R. S. Mclean, G. B. Onoa, G. G. Samsonidze, E. D. Semke, M. Usrey, and D. J. Walls, "Structure-Based Carbon Nanotube Sorting by Sequence-Dependent DNA Assembly," *Science*, vol. 302, no. 5650, pp. 1545–1548, 2003.

[3] X. Tu, S. Manohar, A. Jagota, and M. Zheng, "DNA sequence motifs for structure-specific recognition and separation of carbon nanotubes," *Nat Mater*, vol. 460, no. 7252, pp. 250–253, 2009.

[4] P. K. Brahman, R. A. Dar, and K. S. Pitre, "DNA-functionalized electrochemical biosensor for detection of vitamin {B1} using electrochemically treated multiwalled carbon nanotube paste electrode by voltammetric methods ," *Sensors and Actuators B: Chemical*, vol. 177, no. 0, pp. 807 – 812, 2013.

[5] S. Wang, R. Wang, P. J. Sellin, and S. Chang, "Carbon nanotube based

dna biosensor for rapid detection of anti-cancer drug of cyclophosphamide," *Current Nanoscience*, vol. 5, no. 3, pp. 312–317, 2009.

[6] E. Katz and I. Willner, "Biomolecule-Functionalized Carbon Nanotubes: Applications in Nanobioelectronics," *ChemPhysChem*, vol. 5, no. 8, pp. 1084–1104, 2004.

[7] M. Prato, K. Kostarelos, and A. Bianco, "Functionalized Carbon Nanotubes in Drug Design and Discovery," *Accounts of Chemical Research*, vol. 41, no. 1, pp. 60–68, 2008.

[8] M. Shukla, M. Dubey, E. Zakar, R. Namburu, Z. Czyznikowska, and J. Leszczynski, "Interaction of nucleic acid bases with single-walled carbon nanotube," *Chemical Physics Letters*, vol. 480, no. 4–6, pp. 269–272, 2009.

[9] S. R. Lustig, A. Jagota, C. Khripin, and M. Zheng, "Theory of Structure-Based Carbon Nanotube Separations by Ion-Exchange Chromatography of DNA/CNT Hybrids," *The Journal of Physical Chemistry B*, vol. 109, no. 7, pp. 2559–2566, 2005.

[10] D. Roxbury, A. Jagota, and J. Mittal, "Structural Characteristics of Oligomeric DNA Strands Adsorbed onto Single-Walled Carbon Nanotubes," *The Journal of Physical Chemistry B*, vol. 117, no. 1, pp. 132–140, 2013.

[11] X. Tu and M. Zheng, "A DNA-based approach to the carbon nanotube sorting problem," *Nano Research*, vol. 1, pp. 185–194, 2008.

[12] A. L. Frischknecht and M. G. Martin, "Simulation of the adsorption of nucleotide monophosphates on carbon nanotubes in aqueous solution," *The Journal of Physical Chemistry C*, vol. 112, no. 16, pp. 6271–6278, 2008.

References for Chapter 1

[1] M. Zheng, A. Jagota, E. D. Semke, B. A. Diner, R. S. Mclean, S. R. Lustig, R. E. Richardson, and N. G. Tassi, "DNA-assisted dispersion and separation of carbon nanotubes," *Nat Mater*, vol. 2, no. 5, pp. 338–342, 2003.

[2] M. Zheng, A. Jagota, M. S. Strano, A. P. Santos, P. Barone, S. G. Chou, B. A. Diner, M. S. Dresselhaus, R. S. Mclean, G. B. Onoa, G. G. Samsonidze, E. D. Semke, M. Usrey, and D. J. Walls, "Structure-Based Carbon Nanotube Sorting by Sequence-Dependent DNA Assembly," *Science*, vol. 302, no. 5650, pp. 1545–1548, 2003.

[3] X. Tu, S. Manohar, A. Jagota, and M. Zheng, "DNA sequence motifs for structure-specific recognition and separation of carbon nanotubes," *Nat Mater*, vol. 460, no. 7252, pp. 250–253, 2009.

[4] P. K. Brahman, R. A. Dar, and K. S. Pitre, "DNA-functionalized electrochemical biosensor for detection of vitamin {B1} using electrochemically treated multiwalled carbon nanotube paste electrode by voltammetric methods ," *Sensors and Actuators B: Chemical*, vol. 177, no. 0, pp. 807 – 812, 2013.

[5] S. Wang, R. Wang, P. J. Sellin, and S. Chang, "Carbon nanotube based dna biosensor for rapid detection of anti-cancer drug of cyclophosphamide," *Current Nanoscience*, vol. 5, no. 3, pp. 312–317, 2009.

[6] E. Katz and I. Willner, "Biomolecule-Functionalized Carbon Nanotubes: Applications in Nanobioelectronics," *ChemPhysChem*, vol. 5, no. 8, pp. 1084–1104, 2004.

[7] M. Prato, K. Kostarelos, and A. Bianco, "Functionalized Carbon Nanotubes in Drug Design and Discovery," *Accounts of Chemical Research*, vol. 41, no. 1, pp. 60–68, 2008.

References for Chapter 2

[1] S. Iijima, "Helical microtubules of graphitic carbon," *Nature*, vol. 354, pp. 56–58, 1991.

[2] S. Akita, H. Nishijima, Y. Nakayama, F. Tokumasu, and K. Takeyasu, "Carbon nanotube tips for a scanning probe microscope: their fabrication and properties," *Journal of Physics D: Applied Physics*, vol. 32, no. 9, p. 1044, 1999.

[3] R. H. Baughman, A. A. Zakhidov, and W. A. de Heer, "Carbon Nanotubes–the Route Toward Applications," *Science*, vol. 297, no. 5582, pp. 787–792, 2002.

[4] R. H. Baughman, C. Cui, A. A. Zakhidov, Z. Iqbal, J. N. Barisci, G. M. Spinks, G. G. Wallace, A. Mazzoldi, D. De Rossi, A. G. Rinzler, O. Jaschinski, S. Roth, and M. Kertesz, "Carbon Nanotube Actuators," *Science*, vol. 284, no. 5418, pp. 1340–1344, 1999.

[5] T. Zhang, S. Mubeen, N. V. Myung, and M. A. Deshusses, "Recent progress in carbon nanotube-based gas sensors," *Nanotechnology*, vol. 19, no. 33, p. 332001, 2008.

[6] M. Zhang, S. Fang, A. A. Zakhidov, S. B. Lee, A. E. Aliev, C. D. Williams, K. R. Atkinson, and R. H. Baughman, "Strong, Transparent, Multifunctional, Carbon Nanotube Sheets," *Science*, vol. 309, no. 5738, pp. 1215–1219, 2005.

[7] R. Saito, G. Dresselhaus, and M. Dresselhaus, *Physical Properties of Carbon Nanotube*. Imperial College Press, 1998.

[8] A. Krishnan, E. Dujardin, T. W. Ebbesen, P. N. Yianilos, and M. M. J. Treacy, "Young's modulus of single-walled nanotubes," *Phys. Rev. B*, vol. 58, pp. 14013–14019, 1998.

[9] S. Xiao and W. Hou, "Studies of Size Effects on Carbon Nanotubes' Mechanical Properties by Using Different Potential Functions," *Fullerenes, Nanotubes and Carbon Nanostructures*, vol. 14, no. 1, pp. 9–16, 2006.

[10] B. WenXing, Z. ChangChun, and C. WanZhao, "Simulation of Young's modulus of single-walled carbon nanotubes by molecular dynamics," *Physica B: Condensed Matter*, vol. 352, no. 1–4, pp. 156–163, 2004.

[11] M. Meo and M. Rossi, "Prediction of Young's modulus of single wall carbon nanotubes by molecular-mechanics based finite element modelling," *Composites Science and Technology*, vol. 66, no. 11–12, pp. 1597–1605, 2006.

[12] A. M. Marconnet, M. A. Panzer, and K. E. Goodson, "Thermal conduction phenomena in carbon nanotubes and related nanostructured materials," *Rev. Mod. Phys.*, vol. 85, pp. 1295–1326, 2013.

[13] M. S. Dresselhaus, G. Dresselhaus, J. C. Charlier, and E. Hernández, "Electronic, thermal and mechanical properties of carbon nanotubes," *Philosophical Transactions of the Royal Society of London. Series A: Mathematical, Physical and Engineering Sciences*, vol. 362, no. 1823, pp. 2065–2098, 2004.

[14] A. A. Balandin, "Thermal Properties of Graphene, Carbon Nanotubes and Nanostructured Carbon Materials," *Nature Materials*, vol. 10, pp. 569–581, 2011.

[15] H. Hu, Y. Ni, V. Montana, R. C. Haddon, and V. Parpura, "Chemically Functionalized Carbon Nanotubes as Substrates for Neuronal Growth," *Nano Letters*, vol. 4, no. 3, pp. 507–511, 2004.

[16] C. B. Jacobs, M. J. Peairs, and B. J. Venton, "Review: Carbon nanotube based electrochemical sensors for biomolecules," *Analytica Chimica Acta*, vol. 662, no. 2, pp. 105–127, 2010.

[17] C. Dwyer, M. Guthold, M. Falvo, S. Washburn, R. Superfine, and D. Erie, "DNA-functionalized single-walled carbon nanotubes," *Nanotechnology*, vol. 13, no. 5, p. 601, 2002.

[18] K. Balasubramanian and M. Burghard, "Chemically Functionalized Carbon Nanotubes," *Small*, vol. 1, no. 2, pp. 180–192, 2005.

[19] S. Banerjee, T. Hemraj-Benny, and S. S. Wong, "Covalent Surface Chemistry of Single-Walled Carbon Nanotubes," *Advanced Materials*, vol. 17, no. 1, pp. 17–29, 2005.

[20] R. J. Chen, S. Bangsaruntip, K. A. Drouvalakis, N. Wong Shi Kam, M. Shim, Y. Li, W. Kim, P. J. Utz, and H. Dai, "Noncovalent functionalization of carbon nanotubes for highly specific electronic biosensors," *Proceedings of the National Academy of Sciences*, vol. 100, no. 9, pp. 4984–4989, 2003.

[21] M. Zheng, A. Jagota, E. D. Semke, B. A. Diner, R. S. Mclean, S. R. Lustig, R. E. Richardson, and N. G. Tassi, "DNA-assisted dispersion and separation of carbon nanotubes," *Nat Mater*, vol. 2, no. 5, pp. 338–342, 2003.

[22] E. Katz and I. Willner, "Biomolecule-Functionalized Carbon Nanotubes: Applications in Nanobioelectronics," *ChemPhysChem*, vol. 5, no. 8, pp. 1084–1104, 2004.

[23] F. Fang and H. Choi, "Noncovalent self-assembly of carbon nanotube wrapped carbonyl iron particles and their magnetorheology," *Journal of Applied Physics*, vol. 103, no. 7, pp. 07A301–07A301–3, 2008.

[24] H. Gao, Y. Kong, D. Cui, and C. S. Ozkan, "Spontaneous Insertion of DNA Oligonucleotides into Carbon Nanotubes," *Nano Letters*, vol. 3, no. 4, pp. 471–473, 2003.

[25] J. V. Veetil and K. Ye, "Development of Immunosensors Using Carbon Nanotubes," *Biotechnology Progress*, vol. 23, no. 3, pp. 517–531, 2007.

[26] Y.-B. Zhang, M. Kanungo, A. J. Ho, P. Freimuth, D. van der Lelie, M. Chen, S. M. Khamis, S. S. Datta, A. T. C. Johnson, J. A. Misewich, and S. S. Wong, "Functionalized Carbon Nanotubes for Detecting Viral Proteins," *Nano Letters*, vol. 7, no. 10, pp. 3086–3091, 2007.

[27] A. Hirsch, "Functionalization of Single-Walled Carbon Nanotubes," *Angewandte Chemie International Edition*, vol. 41, no. 11, pp. 1853–1859, 2002.

[28] M. S. Strano, C. A. Dyke, M. L. Usrey, P. W. Barone, M. J. Allen, H. Shan, C. Kittrell, R. H. Hauge, J. M. Tour, and R. E. Smalley, "Electronic Structure Control of Single-Walled Carbon Nanotube Functionalization," *Science*, vol. 301, no. 5639, pp. 1519–1522, 2003.

[29] Y. Wang, Z. Iqbal, and S. Mitra, "Microwave-induced rapid chemical functionalization of single-walled carbon nanotubes," *Carbon*, vol. 43, no. 5, pp. 1015–1020, 2005.

[30] Y.-P. Sun, K. Fu, Y. Lin, and W. Huang, "Functionalized Carbon Nanotubes: Properties and Applications," *Accounts of Chemical Research*, vol. 35, no. 12, pp. 1096–1104, 2002.

[31] M. Prato, K. Kostarelos, and A. Bianco, "Functionalized Carbon Nanotubes in Drug Design and Discovery," *Accounts of Chemical Research*, vol. 41, no. 1, pp. 60–68, 2008.

[32] J. L. Bahr and J. M. Tour, "Highly Functionalized Carbon Nanotubes Using in Situ Generated Diazonium Compounds," *Chemistry of Materials*, no. 11, pp. 3823–3824, 2001.

[33] T. Ramanathan, F. T. Fisher, R. S. Ruoff, and L. C. Brinson, "Amino-Functionalized Carbon Nanotubes for Binding to Polymers and Biological Systems," *Chemistry of Materials*, vol. 17, no. 6, pp. 1290–1295, 2005.

[34] J. L. Bahr, J. Yang, D. V. Kosynkin, M. J. Bronikowski, R. E. Smalley, and J. M. Tour, "Functionalization of Carbon Nanotubes by Electrochemical Reduction of Aryl Diazonium Salts: A Bucky Paper Electrode," *Journal of the American Chemical Society*, vol. 123, no. 27, pp. 6536–6542, 2001.

[35] V. Georgakilas, K. Kordatos, M. Prato, D. M. Guldi, M. Holzinger, and A. Hirsch, "Organic Functionalization of Carbon Nanotubes," *Journal of the American Chemical Society*, vol. 124, no. 5, pp. 760–761, 2002.

[36] J. Chen, H. Liu, W. A. Weimer, M. D. Halls, D. H. Waldeck, and G. C. Walker, "Noncovalent Engineering of Carbon Nanotube Surfaces by Rigid, Functional Conjugated Polymers," *Journal of the American Chemical Society*, vol. 124, no. 31, pp. 9034–9035, 2002.

[37] D. Pantarotto, C. D. Partidos, R. GraffH, J. Hoebeke, J.-P. Briand, M. Prato, and A. Bianco, "Synthesis, Structural Characterization, and Immunological Properties of Carbon Nanotubes Functionalized with Peptides," *Journal of the American Chemical Society*, vol. 125, no. 20, pp. 6160–6164, 2003.

[38] Y. Lin, A. M. Rao, B. Sadanadan, E. A. Kenik, and Y.-P. Sun, "Functionalizing Multiple-Walled Carbon Nanotubes with Aminopolymers," *The Journal of Physical Chemistry B*, vol. 106, no. 6, pp. 1294–1298, 2002.

[39] M. Shim, N. W. Shi Kam, R. J. Chen, Y. Li, and H. Dai, "Functionalization of Carbon Nanotubes for Biocompatibility and Biomolecular Recognition," *Nano Letters*, vol. 2, no. 4, pp. 285–288, 2002.

[40] P. Qi, O. Vermesh, M. Grecu, A. Javey, Q. Wang, H. Dai, S. Peng, and K. J. Cho, "Toward Large Arrays of Multiplex Functionalized Carbon Nanotube

Sensors for Highly Sensitive and Selective Molecular Detection," *Nano Letters*, vol. 3, no. 3, pp. 347–351, 2003.

[41] R. Rastogi, N. Dhindsa, C. R. Suri, B. Pant, S. Tripathi, I. Kaur, and L. M. Bharadwaj, "Interfacing of {DNA} with carbon nanotubes for nanodevice applications ," *Materials Chemistry and Physics*, vol. 135, no. 2–3, pp. 268 – 276, 2012.

[42] S. R. Shin, C. K. Lee, I. S. So, J. H. Jeon, T. M. Kang, C. W. Kee, S. I. Kim, G. M. Spinks, G. G. Wallace, and S. J. Kim, "DNA-Wrapped Single-Walled Carbon Nanotube Hybrid Fibers for supercapacitors and Artificial Muscles," *Advanced Materials*, vol. 20, no. 3, pp. 466–470, 2008.

[43] C. M. Arnett, C. P. Marsh, C. R. Welch, M. S. Strano, J.-H. Han, J. H. Gray, and T. A. Carlson, "Enzyme-Mediated Assimilation of DNA-Functionalized Single-Walled Carbon Nanotubes," *Langmuir*, vol. 26, no. 2, pp. 613–617, 2010.

[44] J. N. Barisci, M. Tahhan, G. G. Wallace, S. Badaire, T. Vaugien, M. Maugey, and P. Poulin, "Properties of Carbon Nanotube Fibers Spun from DNA-Stabilized Dispersions," *Advanced Functional Materials*, vol. 14, no. 2, pp. 133–138, 2004.

[45] R. Yang, Z. Tang, J. Yan, H. Kang, Y. Kim, Z. Zhu, and W. Tan, "Non-covalent Assembly of Carbon Nanotubes and Single-Stranded DNA: An Effective Sensing Platform for Probing Biomolecular Interactions," *Analytical Chemistry*, vol. 80, no. 19, pp. 7408–7413, 2008.

[46] K. A. Williams, P. T. M. Veenhuizen, B. G. de la Torre, R. Eritja, and C. Dekker, "Towards DNA-Mediated Self Assembly of Carbon Nanotube Molecular Devices," *AIP Conference Proceedings*, vol. 633, no. 1, pp. 444–448, 2002.

[47] H. Wang, N. B. Muren, D. Ordinario, A. A. Gorodetsky, J. K. Barton, and C. Nuckolls, "Transducing methyltransferase activity into electrical signals in a carbon nanotube-DNA device," *Chem. Sci.*, vol. 3, pp. 62–65, 2012.

[48] P. K. Brahman, R. A. Dar, and K. S. Pitre, "DNA-functionalized electrochemical biosensor for detection of vitamin {B1} using electrochemically treated multiwalled carbon nanotube paste electrode by voltammetric methods ," *Sensors and Actuators B: Chemical*, vol. 177, no. 0, pp. 807 – 812, 2013.

[49] P. Singh, J. Kumar, F. M. Toma, J. Raya, M. Prato, B. Fabre, S. Verma, and A. Bianco, "Synthesis and characterization of nucleobase-carbon nanotube hybrids," *Journal of the American Chemical Society*, vol. 131, no. 37, pp. 13555–13562, 2009.

[50] D. A. Yarotski, S. V. Kilina, A. A. Talin, S. Tretiak, O. V. Prezhdo, A. V. Balatsky, and A. J. Taylor, "Scanning Tunneling Microscopy of DNA-Wrapped Carbon Nanotubes," *Nano Letters*, vol. 9, no. 1, pp. 12–17, 2009.

[51] X. Qiu, C. Y. Khripin, F. Ke, S. C. Howell, and M. Zheng, "Electrostatically Driven Interactions between Hybrid DNA-Carbon Nanotubes," *Phys. Rev. Lett.*, vol. 111, p. 048301, 2013.

[52] S. S. Kim, C. L. Hisey, Z. Kuang, D. A. Comfort, B. L. Farmer, and R. R. Naik, "The effect of single wall carbon nanotube metallicity on genomic DNA-mediated chirality enrichment," *Nanoscale*, vol. 5, pp. 4931–4936, 2013.

[53] R. Singh, D. Pantarotto, D. McCarthy, O. Chaloin, J. Hoebeke, C. D. Partidos, J.-P. Briand, M. Prato, A. Bianco, and K. Kostarelos, "Binding and Condensation of Plasmid DNA onto Functionalized Carbon Nanotubes: Toward the Construction of Nanotube-Based Gene Delivery Vectors," *Journal of the American Chemical Society*, vol. 127, no. 12, pp. 4388–4396, 2005.

[54] C. Hu, Y. Zhang, G. Bao, Y. Zhang, M. Liu, and Z. L. Wang, "DNA Functionalized Single-Walled Carbon Nanotubes for Electrochemical Detection," *The Journal of Physical Chemistry B*, vol. 109, no. 43, pp. 20072–20076, 2005.

[55] Y. Ma, S. R. Ali, A. S. Dodoo, and H. He, "Enhanced Sensitivity for Biosensors: Multiple Functions of DNA-Wrapped Single-Walled Carbon Nanotubes in Self-Doped Polyaniline Nanocomposites," *The Journal of Physical Chemistry B*, vol. 110, no. 33, pp. 16359–16365, 2006.

[56] P. He and M. Bayachou, "Layer-by-Layer Fabrication and Characterization of DNA-Wrapped Single-Walled Carbon Nanotube Particles," *Langmuir*, vol. 21, no. 13, pp. 6086–6092, 2005.

[57] Y. Xu, P. E. Pehrsson, L. Chen, R. Zhang, and W. Zhao, "Double-Stranded DNA Single-Walled Carbon Nanotube Hybrids for Optical Hy-

drogen Peroxide and Glucose Sensing," *The Journal of Physical Chemistry C*, vol. 111, no. 24, pp. 8638–8643, 2007.

[58] M. Zheng, A. Jagota, M. S. Strano, A. P. Santos, P. Barone, S. G. Chou, B. A. Diner, M. S. Dresselhaus, R. S. Mclean, G. B. Onoa, G. G. Samsonidze, E. D. Semke, M. Usrey, and D. J. Walls, "Structure-Based Carbon Nanotube Sorting by Sequence-Dependent DNA Assembly," *Science*, vol. 302, no. 5650, pp. 1545–1548, 2003.

[59] S. Kilina, D. A. Yarotski, A. A. Talin, S. Tretiak, A. J. Taylor, and A. V. Balatsky, "Unveiling Stability Criteria of DNA-Carbon Nanotubes Constructs by Scanning Tunneling Microscopy and Computational Modeling," *Journal of Drug Delivery*, vol. 2011, 2011.

[60] M. Allen, M. Balooch, S. Subbiah, R. Tench, W. Siekhaus, and R. Balhorn, "Scanning Tunneling Microscope Images of Adenine and Thymine at Atomic Resolution," *Scanning Microsc*, vol. 5, no. 3, pp. 625–630, 1991.

[61] W. M. Heckl, D. P. Smith, G. Binnig, H. Klagges, T. W. Hänsch, and J. Maddocks, "Two-Dimensional Ordering of the DNA Base Guanine Observed by Scanning Tunneling Microscopy," *Proc. Natl. Acad. Sci. U. S. A.*, vol. 88, no. 18, pp. 8003–8005, 1991.

[62] N. J. Tao and Z. Shi, "Monolayer Guanine and Adenine on Graphite in NaCl Solution: A Comparative STM and AFM Study," *The Journal of Physical Chemistry*, vol. 98, no. 5, pp. 1464–1471, 1994.

[63] J. E. Freund, M. Edelwirth, P. Kröbel, and W. M. Heckl, "Structure deter-

mination of two-dimensional adenine crystals on graphite," *Phys. Rev. B*, vol. 55, pp. 5394–5397, 1997.

[64] R. Srinivasan, J. Murphy, R. Fainchtein, and N. Pattabiraman, "Electrochemical STM of condensed guanine on graphite ," *Journal of Electroanalytical Chemistry and Interfacial Electrochemistry*, vol. 312, no. 1–2, pp. 293 – 300, 1991.

[65] R. Srinivasan, J. Murphy, and N. Pattabiraman, "STM observations of two-dimensional condensed layers on solid electrodes ," *Ultramicroscopy*, vol. 42–44, Part 1, no. 0, pp. 453 – 459, 1992.

[66] R. Srinivasan and P. Gopalan, "Order and stability of an electrochemically condensed adenine layer on graphite," *The Journal of Physical Chemistry*, vol. 97, no. 34, pp. 8770–8775, 1993.

[67] S. Sowerby, W. Heckl, and G. Petersen, "Chiral symmetry breaking during the self-assembly of monolayers from achiral purine molecules," *Journal of Molecular Evolution*, vol. 43, no. 5, pp. 419–424, 1996.

[68] S. J. Sowerby and G. B. Petersen, "Scanning tunneling microscopy of uracil monolayers self-assembled at the solid|liquid interface ," *Journal of Electroanalytical Chemistry*, vol. 433, no. 1–2, pp. 85 – 90, 1997.

[69] S. Sowerby, M. Edelwirth, and W. Heckl, "Molecular mechanics simulation of uracil adlayers on molybdenum disulfide and graphite surfaces," *Applied Physics A*, vol. 66, no. 1, pp. S649–S653, 1998.

[70] S. J. Sowerby, M. Edelwirth, and W. M. Heckl, "Self-Assembly at the Prebiotic Solid-Liquid Interface: Structures of Self-Assembled Monolayers of Adenine and Guanine Bases Formed on Inorganic Surfaces," *The Journal of Physical Chemistry B*, vol. 102, no. 30, pp. 5914–5922, 1998.

[71] S. Sowerby and W. Heckl, "The Role of Self-Assembled Monolayers of the Purine and Pyrimidine Bases in the Emergence of Life," *Origins of life and evolution of the biosphere*, vol. 28, no. 3, pp. 283–310, 1998.

[72] S. Sowerby, P. Stockwell, W. Heckl, and G. Petersen, "Self-programmable, Self-assembling Two-dimensional Genetic Matter," *Origins of life and evolution of the biosphere*, vol. 30, no. 1, pp. 81–99, 2000.

[73] S. J. Sowerby, C. A. Cohn, W. M. Heckl, and N. G. Holm, "Differential adsorption of nucleic acid bases: Relevance to the origin of life," *Proceedings of the National Academy of Sciences*, vol. 98, no. 3, pp. 820–822, 2001.

[74] T. Uchihashi, T. Okada, Y. Sugawara, K. Yokoyama, and S. Morita, "Self-assembled monolayer of adenine base on graphite studied by noncontact atomic force microscopy," *Phys. Rev. B*, vol. 60, pp. 8309–8313, 1999.

[75] A. Das, A. Sood, P. K. Maiti, M. Das, R. Varadarajan, and C. Rao, "Binding of nucleobases with single-walled carbon nanotubes: Theory and experiment," *Chemical Physics Letters*, vol. 453, no. 4–6, pp. 266–273, 2008.

[76] N. Varghese, U. Mogera, A. Govindaraj, A. Das, P. K. Maiti, A. K. Sood, and C. N. R. Rao, "Binding of DNA Nucleobases and Nucleosides with Graphene," *ChemPhysChem*, vol. 10, no. 1, pp. 206–210, 2009.

[77] J. E. Freund, . PhD thesis, Ludwig-Maximilians-Universität, München, 1998.

[78] S. Gowtham, R. H. Scheicher, R. Ahuja, R. Pandey, and S. P. Karna, "Physisorption of nucleobases on graphene: Density-functional calculations," *Phys. Rev. B*, vol. 76, p. 033401, 2007.

[79] S. Gowtham, R. H. Scheicher, R. Pandey, S. P. Karna, and R. Ahuja, "First-principles study of physisorption of nucleic acid bases on small-diameter carbon nanotubes," *Nanotechnology*, vol. 19, no. 12, p. 125701, 2008.

[80] S. Meng, P. Maragakis, C. Papaloukas, and E. Kaxiras, "DNA Nucleoside Interaction and Identification with Carbon Nanotubes," *Nano Letters*, vol. 7, no. 1, pp. 45–50, 2007.

[81] S. Meng, W. L. Wang, P. Maragakis, and E. Kaxiras, "Determination of DNA-Base Orientation on Carbon Nanotubes through Directional Optical Absorbance," *Nano Letters*, vol. 7, no. 8, pp. 2312–2316, 2007.

[82] Y. V. Shtogun, L. M. Woods, and G. I. Dovbeshko, "Adsorption of Adenine and Thymine and Their Radicals on Single-Wall Carbon Nanotubes," *The Journal of Physical Chemistry C*, vol. 111, no. 49, pp. 18174–18181, 2007.

[83] H. Wang and A. Ceulemans, "Physisorption of adenine DNA nucleosides on zigzag and armchair single-walled carbon nanotubes: A first-principles study," *Phys. Rev. B*, vol. 79, p. 195419, 2009.

[84] Y. Wang and Y. Bu, "Noncovalent Interactions between Cytosine and

SWCNT," *The Journal of Physical Chemistry B*, vol. 111, no. 23, pp. 6520–6526, 2007.

[85] Y. Wang, "Theoretical Evidence for the Stronger Ability of Thymine to Disperse SWCNT than Cytosine and Adenine: Self-Stacking of DNA Bases vs Their Cross-Stacking with SWCNT," *The Journal of Physical Chemistry C*, vol. 112, no. 37, pp. 14297–14305, 2008.

[86] F. Ortmann, W. G. Schmidt, and F. Bechstedt, "Attracted by Long-Range Electron Correlation: Adenine on Graphite," *Phys. Rev. Lett.*, vol. 95, p. 186101, 2005.

[87] K. Berland, S. D. Chakarova-Käck, V. R. Cooper, D. C. Langreth, and E. Schröder, "A van der Waals density functional study of adenine on graphene: single-molecular adsorption and overlayer binding," *Journal of Physics: Condensed Matter*, vol. 23, no. 13, p. 135001, 2011.

[88] S. Panigrahi, A. Bhattacharya, S. Banerjee, and D. Bhattacharyya, "Interaction of Nucleobases with Wrinkled Graphene Surface: Dispersion Corrected DFT and AFM Studies," *The Journal of Physical Chemistry C*, vol. 116, no. 7, pp. 4374–4379, 2012.

[89] S. Chandra Shekar and R. S. Swathi, "Stability of nucleobases and base pairs adsorbed on graphyne and graphdiyne," *The Journal of Physical Chemistry C*, vol. 118, no. 8, pp. 4516–4528, 2014.

[90] J. Antony and S. Grimme, "Structures and interaction energies of stacked graphene-nucleobase complexes," *Phys. Chem. Chem. Phys.*, vol. 10, pp. 2722–2729, 2008.

[91] J.-H. Lee, Y.-K. Choi, H.-J. Kim, R. H. Scheicher, and J.-H. Cho, "Physisorption of DNA Nucleobases on h-BN and Graphene: vdW-Corrected DFT Calculations," *The Journal of Physical Chemistry C*, vol. 117, no. 26, pp. 13435–13441, 2013.

[92] D. Le, A. Kara, E. Schröder, P. Hyldgaard, and T. S. Rahman, "Physisorption of nucleobases on graphene: a comparative van der Waals study," *Journal of Physics: Condensed Matter*, vol. 24, no. 42, p. 424210, 2012.

[93] Y. Cho, S. K. Min, J. Yun, W. Y. Kim, A. Tkatchenko, and K. S. Kim, "Noncovalent Interactions of DNA Bases with Naphthalene and Graphene," *Journal of Chemical Theory and Computation*, vol. 9, no. 0, pp. 2090–2096, 2013.

[94] H. Vovusha, S. Sanyal, and B. Sanyal, "Interaction of nucleobases and aromatic amino acids with graphene oxide and graphene flakes," *The Journal of Physical Chemistry Letters*, vol. 4, no. 21, pp. 3710–3718, 2013.

[95] A. N. Enyashin, S. Gemming, and G. Seifert, "DNA-wrapped carbon nanotubes," *Nanotechnology*, vol. 18, no. 24, p. 245702, 2007.

[96] S. Stepanian, M. Karachevtsev, A. Glamazda, V. Karachevtsev, and L. Adamowicz, "Stacking interaction of cytosine with carbon nanotubes: MP2, DFT and Raman spectroscopy study," *Chemical Physics Letters*, vol. 459, no. 1–6, pp. 153–158, 2008.

[97] M. Shukla, M. Dubey, E. Zakar, R. Namburu, Z. Czyznikowska, and J. Leszczynski, "Interaction of nucleic acid bases with single-walled car-

bon nanotube," *Chemical Physics Letters*, vol. 480, no. 4–6, pp. 269–272, 2009.

[98] B. Akdim, R. Pachter, P. N. Day, S. S. Kim, and R. R. Naik, "On modeling biomolecular–surface nonbonded interactions: application to nucleobase adsorption on single-wall carbon nanotube surfaces," *Nanotechnology*, vol. 23, no. 16, p. 165703, 2012.

[99] A. Ramraj, I. H. Hillier, M. A. Vincent, and N. A. Burton, "Assessment of approximate quantum chemical methods for calculating the interaction energy of nucleic acid bases with graphene and carbon nanotubes," *Chemical Physics Letters*, vol. 484, no. 4–6, pp. 295–298, 2010.

[100] D. Umadevi and G. N. Sastry, "Quantum Mechanical Study of Physisorption of Nucleobases on Carbon Materials: Graphene versus Carbon Nanotubes," *The Journal of Physical Chemistry Letters*, vol. 2, no. 13, pp. 1572–1576, 2011.

[101] A. Sarmah and R. K. Roy, "Understanding the interaction of nucleobases with chiral semiconducting single-walled carbon nanotubes: An alternative theoretical approach based on density functional reactivity theory," *The Journal of Physical Chemistry C*, vol. 117, no. 41, pp. 21539–21550, 2013.

[102] M. Chehel Amirani, T. Tang, and J. Cuervo, "Quantum mechanical treatment of binding energy between DNA nucleobases and carbon nanotube: A DFT analysis," *Physica E: Low-dimensional Systems and Nanostructures*, vol. 54, pp. 65–71, 2013.

[103] A. L. Frischknecht and M. G. Martin, "Simulation of the adsorption of nucleotide monophosphates on carbon nanotubes in aqueous solution," *The Journal of Physical Chemistry C*, vol. 112, no. 16, pp. 6271–6278, 2008.

[104] W. Lv, "The adsorption of DNA bases on neutral and charged (8, 8) carbon-nanotubes," *Chemical Physics Letters*, vol. 514, no. 4–6, pp. 311 – 316, 2011.

[105] Zhao and J. K. Johnson, "Simulation of Adsorption of DNA on Carbon Nanotubes," *Journal of the American Chemical Society*, vol. 129, no. 34, pp. 10438–10445, 2007.

[106] R. R. Johnson, A. T. C. Johnson, and M. L. Klein, "Probing the Structure of DNA-Carbon Nanotube Hybrids with Molecular Dynamics," *Nano Letters*, vol. 8, no. 1, pp. 69–75, 2008.

[107] R. R. Johnson, A. T. C. Johnson, and M. L. Klein, "The Nature of DNA-Base–Carbon-Nanotube Interactions," *Small*, vol. 6, no. 1, pp. 31–34, 2010.

[108] S. Manohar, T. Tang, and A. Jagota, "Structure of Homopolymer DNA-CNT Hybrids," *The Journal of Physical Chemistry C*, vol. 111, no. 48, pp. 17835–17845, 2007.

[109] D. Roxbury, A. Jagota, and J. Mittal, "Sequence-Specific Self-Stitching Motif of Short Single-Stranded DNA on a Single-Walled Carbon Nanotube," *Journal of the American Chemical Society*, vol. 133, no. 34, pp. 13545–13550, 2011.

[110] X. Zhao, "Self-Assembly of DNA Segments on Graphene and Carbon Nanotube Arrays in Aqueous Solution: A Molecular Simulation Study," *The Journal of Physical Chemistry C*, vol. 115, no. 14, pp. 6181–6189, 2011.

[111] Z. Xiao, X. Wang, X. Xu, H. Zhang, Y. Li, and Y. Wang, "Base- and Structure-Dependent DNA Dinucleotide–Carbon Nanotube Interactions: Molecular Dynamics Simulations and Thermodynamic Analysis," *The Journal of Physical Chemistry C*, vol. 115, no. 44, pp. 21546–21558, 2011.

[112] S. Neihsial, G. Periyasamy, P. K. Samanta, and S. K. Pati, "Understanding the Binding Mechanism of Various Chiral SWCNTs and ssDNA: A Computational Study," *The Journal of Physical Chemistry B*, vol. 116, no. 51, pp. 14754–14759, 2012.

[113] D. Roxbury, A. Jagota, and J. Mittal, "Structural Characteristics of Oligomeric DNA Strands Adsorbed onto Single-Walled Carbon Nanotubes," *The Journal of Physical Chemistry B*, vol. 117, no. 1, pp. 132–140, 2013.

[114] A. K. Manna and S. K. Pati, "Theoretical understanding of single-stranded DNA assisted dispersion of graphene," *J. Mater. Chem. B*, vol. 1, pp. 91–100, 2013.

[115] W. Martin, W. Zhu, and G. Krilov, "Simulation Study of Noncovalent Hybridization of Carbon Nanotubes by Single-Stranded DNA in Water," *The Journal of Physical Chemistry B*, vol. 112, no. 50, pp. 16076–16089, 2008.

[116] J. Zou, W. Liang, and S. Zhang, "Coarse-grained molecular dynamics mod-

eling of DNA–carbon nanotube complexes," *International Journal for Numerical Methods in Engineering*, vol. 83, no. 8-9, pp. 968–985, 2010.

[117] T. Yamazaki and H. Fenniri, "Imaging carbon nanotube interaction with nucleobases in water using the statistical mechanical theory of molecular liquids," *The Journal of Physical Chemistry C*, vol. 116, no. 28, pp. 15087–15092, 2012.

[118] O. Malysheva, T. Tang, and P. Schiavone, "Binding Force Between a Charged Wall and a Complex Formed by a Polyelectrolyte and an Electronically Responsive Cylinder," *The Journal of Adhesion*, vol. 87, no. 3, pp. 251–271, 2011.

[119] S. R. Lustig, A. Jagota, C. Khripin, and M. Zheng, "Theory of Structure-Based Carbon Nanotube Separations by Ion-Exchange Chromatography of DNA/CNT Hybrids," *The Journal of Physical Chemistry B*, vol. 109, no. 7, pp. 2559–2566, 2005.

[120] C. Sun and T. Tang, "Structure of a polyelectrolyte around an electronically responsive cylinder," *Journal of Colloid and Interface Science*, vol. 338, no. 1, pp. 276 – 283, 2009.

[121] M. Zheng, K. Eom, and C. Ke, "Calculations of the resonant response of carbon nanotubes to binding of DNA," *Journal of Physics D: Applied Physics*, vol. 42, no. 14, 2009.

[122] P. Debye and E. Hückel, "The theory of electrolytes. i. lowering of freezing point and related phenomena," *Physikalische Zeitschrift*, vol. 24, pp. 185–206, 1923.

[123] M. Edelwirth, J. Freund, S. Sowerby, and W. Heckl, "Molecular mechanics study of hydrogen bonded self-assembled adenine monolayers on graphite ," *Surface Science*, vol. 417, no. 2–3, pp. 201 – 209, 1998.

[124] C. Møller and M. S. Plesset, "Note on an approximation treatment for many-electron systems," *Phys. Rev.*, vol. 46, pp. 618–622, 1934.

[125] M. Head-Gordon, J. A. Pople, and M. J. Frisch, "{MP2} energy evaluation by direct methods," *Chemical Physics Letters*, vol. 153, no. 6, pp. 503 – 506, 1988.

[126] M. J. S. Dewar, E. G. Zoebisch, E. F. Healy, and J. J. P. Stewart, "Development and use of quantum mechanical molecular models. 76. am1: a new general purpose quantum mechanical molecular model," *Journal of the American Chemical Society*, vol. 107, no. 13, pp. 3902–3909, 1985.

[127] J. J. P. Stewart, "Optimization of parameters for semiempirical methods i. method," *Journal of Computational Chemistry*, vol. 10, no. 2, pp. 209–220, 1989.

[128] J. J. P. Stewart, "Optimization of parameters for semiempirical methods ii. applications," *Journal of Computational Chemistry*, vol. 10, no. 2, pp. 221–264, 1989.

[129] J. J. P. Stewart, "Optimization of parameters for semiempirical methods. iii extension of pm3 to be, mg, zn, ga, ge, as, se, cd, in, sn, sb, te, hg, tl, pb, and bi," *Journal of Computational Chemistry*, vol. 12, no. 3, pp. 320–341, 1991.

[130] J. Stewart, "Optimization of parameters for semiempirical methods v: Modification of nddo approximations and application to 70 elements," *Journal of Molecular Modeling*, vol. 13, no. 12, pp. 1173–1213, 2007.

[131] P. Hohenberg and W. Kohn, "Inhomogeneous electron gas," *Phys. Rev.*, vol. 136, pp. B864–B871, 1964.

[132] W. Kohn and L. J. Sham, "Self-consistent equations including exchange and correlation effects," *Phys. Rev.*, vol. 140, pp. A1133–A1138, 1965.

[133] J. P. Perdew, K. Burke, and M. Ernzerhof, "Generalized gradient approximation made simple," *Phys. Rev. Lett.*, vol. 77, pp. 3865–3868, 1996.

[134] E. R. Johnson, R. A. Wolkow, and G. A. DiLabio, "Application of 25 density functionals to dispersion-bound homomolecular dimers," *Chemical Physics Letters*, vol. 394, no. 4–6, pp. 334–338, 2004.

[135] E. R. Johnson, I. D. Mackie, and G. A. DiLabio, "Dispersion interactions in density-functional theory," *Journal of Physical Organic Chemistry*, vol. 22, no. 12, pp. 1127–1135, 2009.

[136] L. R. Rutledge, H. F. Durst, and S. D. Wetmore, "Evidence for Stabilization of DNA/RNA Protein Complexes Arising from Nucleobase Amino Acid Stacking and T-Shaped Interactions," *Journal of Chemical Theory and Computation*, vol. 5, no. 5, pp. 1400–1410, 2009.

[137] L. R. Rutledge and S. D. Wetmore, "The assessment of density functionals for DNAprotein stacked and T-shaped complexes," *Canadian Journal of Chemistry*, vol. 88, no. 8, pp. 815–830, 2010.

[138] Y. Zhao and D. G. Truhlar, "Benchmark databases for nonbonded interactions and their use to test density functional theory," *Journal of Chemical Theory and Computation*, vol. 1, no. 3, pp. 415–432, 2005.

[139] Y. Zhao and D. G. Truhlar, "Applications and validations of the Minnesota density functionals," *Chemical Physics Letters*, vol. 502, no. 1–3, pp. 1–13, 2011.

[140] E. Meijer and M. Sprik, "A density-functional study of the intermolecular interactions of benzene," *Journal of Chemical Physics*, vol. 105, no. 19, pp. 8684–8689, 1996.

[141] A. Tkatchenko and M. Scheffler, "Accurate Molecular Van Der Waals Interactions from Ground-State Electron Density and Free-Atom Reference Data," *Phys. Rev. Lett.*, vol. 102, p. 073005, 2009.

[142] S. Grimme, "Accurate description of van der Waals complexes by density functional theory including empirical corrections," *Journal of Computational Chemistry*, vol. 25, no. 12, pp. 1463–1473, 2004.

[143] S. Grimme, "Semiempirical GGA-type density functional constructed with a long-range dispersion correction," *Journal of Computational Chemistry*, vol. 27, no. 15, pp. 1787–1799, 2006.

[144] S. Grimme, J. Antony, S. Ehrlich, and H. Krieg, "A consistent and accurate ab initio parametrization of density functional dispersion correction (DFT-D) for the 94 elements H-Pu," *The Journal of Chemical Physics*, vol. 132, no. 15, p. 154104, 2010.

[145] S. Ehrlich, J. Moellmann, and S. Grimme, "Dispersion-Corrected Density Functional Theory for Aromatic Interactions in Complex Systems," *Accounts of Chemical Research*, vol. 46, no. 4, pp. 916–926, 2013.

[146] S. Grimme and M. Steinmetz, "Effects of London dispersion correction in density functional theory on the structures of organic molecules in the gas phase," *Phys. Chem. Chem. Phys.*, pp. 16031–16042, 2013.

[147] S. Grimme, "Density functional theory with London dispersion corrections," *Wiley Interdisciplinary Reviews: Computational Molecular Science*, vol. 1, no. 2, pp. 211–228, 2011.

[148] J. Gräfenstein and D. Cremer, "An efficient algorithm for the density-functional theory treatment of dispersion interactions.," *Journal of Chemical Physics*, vol. 130, no. 12, p. 124105, 2009.

[149] J. Seponer, J. Leszczynski, and P. Hobza, "Base stacking in cytosine dimer. A comparison of correlated ab initio calculations with three empirical potential models and density functional theory calculations," *Journal of Computational Chemistry*, vol. 17, no. 7, pp. 841–850, 1996.

[150] N. Kurita and H. Sekino, "Ab initio and {DFT} studies for accurate description of van der Waals interaction between He atoms," *Chemical Physics Letters*, vol. 348, no. 1–2, pp. 139–146, 2001.

[151] M. Dion, H. Rydberg, E. Schröder, D. C. Langreth, and B. I. Lundqvist, "Van der Waals Density Functional for General Geometries," *Phys. Rev. Lett.*, vol. 92, p. 246401, 2004.

[152] P. Jurečka, J. Černý, P. Hobza, and D. R. Salahub, "Density functional theory augmented with an empirical dispersion term. Interaction energies and geometries of 80 noncovalent complexes compared with ab initio quantum mechanics calculations.," *Journal of Computational Chemistry*, vol. 28, no. 2, pp. 555–569, 2007.

[153] O. A. von Lilienfeld, I. Tavernelli, U. Rothlisberger, and D. Sebastiani, "Optimization of Effective Atom Centered Potentials for London Dispersion Forces in Density Functional Theory," *Phys. Rev. Lett.*, vol. 93, p. 153004, 2004.

[154] S. Kristyán and P. Pulay, "Can (semi)local density functional theory account for the London dispersion forces?," *Chemical Physics Letters*, vol. 229, no. 3, pp. 175–180, 1994.

[155] R. O. Jones and O. Gunnarsson, "The density functional formalism, its applications and prospects," *Rev. Mod. Phys.*, vol. 61, pp. 689–746, 1989.

[156] N. Park, S. Lim, G. Kim, and S.-H. Jhi, "Calculation of Hydrogen Physisorption Affinity to Graphene Species with Ab-Intio and Density-Functional Methods ," *Journal of the Korean Physical Society*, vol. 53, no. 23, pp. 691–694, 2008.

[157] A. Tkatchenko, J. Robert A. DiStasio, M. Head-Gordon, and M. Scheffler, "Dispersion-corrected M[o-slash]ller–Plesset second-order perturbation theory," *The Journal of Chemical Physics*, vol. 131, no. 9, p. 094106, 2009.

[158] P. Hobza, H. L. Selzle, and E. W. Schlag, "Potential Energy Surface for the Benzene Dimer. Results of ab Initio CCSD(T) Calculations Show Two Nearly Isoenergetic Structures: T-Shaped and Parallel-Displaced," *The Journal of Physical Chemistry*, vol. 100, no. 48, pp. 18790–18794, 1996.

[159] S. Tsuzuki, T. Uchimaru, K. Matsumura, M. Mikami, and K. Tanabe, "Effects of the higher electron correlation correction on the calculated intermolecular interaction energies of benzene and naphthalene dimers: comparison between {MP2} and CCSD(T) calculations," *Chemical Physics Letters*, vol. 319, no. 5–6, pp. 547–554, 2000.

[160] R. L. Jaffe and G. D. Smith, "A quantum chemistry study of benzene dimer," *The Journal of Chemical Physics*, vol. 105, no. 7, pp. 2780–2788, 1996.

[161] B. Brooks, R. Bruccoleri, D. Olafson, D. States, S. Swaminathan, and M. Karplus, "Charmm: A program for macromolecular energy, minimization, and dynamics calculations," *Journal of Computational Chemistry*, vol. 4, pp. 187–217, 1983.

[162] A. MacKerel Jr., C. Brooks III, L. Nilsson, B. Roux, Y. Won, and M. Karplus, *CHARMM: The Energy Function and Its Parameterization with an Overview of the Program*, vol. 1 of *The Encyclopedia of Computational Chemistry*, pp. 271–277. John Wiley & Sons: Chichester, 1998.

[163] J. H. Walther, R. Jaffe, T. Halicioglu, and P. Koumoutsakos, "Carbon nanotubes in water: Structural characteristics and energetics," *The Journal of Physical Chemistry B*, vol. 105, no. 41, pp. 9980–9987, 2001.

[164] V. Barone and M. Cossi, "Quantum calculation of molecular energies and energy gradients in solution by a conductor solvent model," *The Journal of Physical Chemistry A*, vol. 102, no. 11, pp. 1995–2001, 1998.

[165] E. G. Hohenstein, S. T. Chill, and C. D. Sherrill, "Assessment of the Performance of the M055-2X and M06-2X Exchange-Correlation Functionals for Noncovalent Interactions in Biomolecules," *Journal of Chemical Theory and Computation*, vol. 4, no. 12, pp. 1996–2000, 2008.

[166] Y. Zhao and D. G. Truhlar, "Density functionals with broad applicability in chemistry," *Accounts of Chemical Research*, vol. 41, no. 2, pp. 157–167, 2008.

[167] Y. Zhao, N. E. Schultz, and D. G. Truhlar, "Exchange-correlation functional with broad accuracy for metallic and nonmetallic compounds, kinetics, and noncovalent interactions," *The Journal of Chemical Physics*, vol. 123, no. 16, pp. 1–4, 2005.

[168] Y. Zhao, N. E. Schultz, and D. G. Truhlar, "Design of density functionals by combining the method of constraint satisfaction with parametrization for thermochemistry, thermochemical kinetics, and noncovalent interactions," *Journal of Chemical Theory and Computation*, vol. 2, no. 2, pp. 364–382, 2006.

[169] Y. Zhao and D. Truhlar, "The M06 suite of density functionals for main group thermochemistry, thermochemical kinetics, noncovalent interactions, excited states, and transition elements: two new functionals and systematic

testing of four M06-class functionals and 12 other functionals," *Theoretical Chemistry Accounts*, vol. 120, no. 1-3, pp. 215–241, 2008.

[170] Y. Zhao and D. G. Truhlar, "Density Functional for Spectroscopy: No Long-Range Self-Interaction Error, Good Performance for Rydberg and Charge-Transfer States, and Better Performance on Average than B3LYP for Ground States," *The Journal of Physical Chemistry A*, vol. 110, no. 49, pp. 13126–13130, 2006.

[171] Y. Zhao and D. G. Truhlar, "A new local density functional for main-group thermochemistry, transition metal bonding, thermochemical kinetics, and noncovalent interactions," *The Journal of Chemical Physics*, vol. 125, no. 19, p. 194101, 2006.

[172] S. Grimme, S. Ehrlich, and L. Goerigk, "Effect of the damping function in dispersion corrected density functional theory," *Journal of Computational Chemistry*, vol. 32, no. 7, pp. 1456–1465, 2011.

[173] K. Lee, É. D. Murray, L. Kong, B. I. Lundqvist, and D. C. Langreth, "Higher-accuracy van der Waals density functional," *Phys. Rev. B*, vol. 82, p. 081101, 2010.

[174] E. Torres and G. A. DiLabio, "A (nearly) universally applicable method for modeling noncovalent interactions using b3lyp," *The Journal of Physical Chemistry Letters*, vol. 3, no. 13, pp. 1738–1744, 2012.

[175] J. P. Perdew and Y. Wang, "Accurate and simple analytic representation of the electron-gas correlation energy," *Phys. Rev. B*, vol. 45, pp. 13244–13249, 1992.

[176] T. Okada, T. Abe, and M. Kaneko, "Historical overview and fundamental aspects of molecular catalysts for energy conversion," in *Molecular Catalysts for Energy Conversion* (T. Okada and M. Kaneko, eds.), vol. 111 of *Springer Series in Materials Science*, pp. 1–36, Springer Berlin Heidelberg, 2009.

[177] M. Hasegawa and K. Nishidate, "Semiempirical approach to the energetics of interlayer binding in graphite," *Phys. Rev. B*, vol. 70, p. 205431, 2004.

[178] J. c. v. Klimeš, D. R. Bowler, and A. Michaelides, "Van der waals density functionals applied to solids," *Phys. Rev. B*, vol. 83, p. 195131, 2011.

[179] M. S. Gordon, L. Slipchenko, H. Li, and J. H. Jensen, "Chapter 10 the effective fragment potential: A general method for predicting intermolecular interactions," vol. 3 of *Annual Reports in Computational Chemistry*, pp. 177 – 193, Elsevier, 2007.

[180] W. D. Cornell, P. Cieplak, C. I. Bayly, I. R. Gould, K. M. Merz, D. M. Ferguson, D. C. Spellmeyer, T. Fox, J. W. Caldwell, and P. A. Kollman, "A second generation force field for the simulation of proteins, nucleic acids, and organic molecules," *Journal of the American Chemical Society*, vol. 117, no. 19, pp. 5179–5197, 1995.

[181] S. L. Mayo, B. D. Olafson, and W. A. Goddard, "Dreiding: a generic force field for molecular simulations," *The Journal of Physical Chemistry*, vol. 94, no. 26, pp. 8897–8909, 1990.

[182] A. K. Rappe, C. J. Casewit, K. S. Colwell, W. A. Goddard, and W. M. Skiff, "UFF, a full periodic table force field for molecular mechanics and

molecular dynamics simulations," *Journal of the American Chemical Society*, vol. 114, no. 25, pp. 10024–10035, 1992.

[183] M. G. Martin, "Comparison of the AMBER, CHARMM, COMPASS, GROMOS, OPLS, TraPPE and UFF force fields for prediction of vapor–liquid coexistence curves and liquid densities ," *Fluid Phase Equilibria*, vol. 248, no. 1, pp. 50 – 55, 2006.

[184] K. Brameld, S. Dasgupta, and W. A. Goddard, "Distance dependent hydrogen bond potentials for nucleic acid base pairs from ab initio quantum mechanical calculations (lmp2/cc-pvtz)," *The Journal of Physical Chemistry B*, vol. 101, no. 24, pp. 4851–4859, 1997.

[185] T. Werder, J. H. Walther, R. L. Jaffe, T. Halicioglu, and P. Koumoutsakos, "On the water-carbon interaction for use in molecular dynamics simulations of graphite and carbon nanotubes," *The Journal of Physical Chemistry B*, vol. 107, no. 6, pp. 1345–1352, 2003.

[186] F. Hirata, ed., *Molecular Theory of Solvation*, vol. 24 of *Understanding Chemical Reactivity*. Springer, 2003.

[187] G. Hummer, J. Rasaiah, and J. Noworyta, "Water conduction through the hydrophobic channel of a carbon nanotube.," *Nature*, vol. 414, no. 6860, p. 188, 2001.

[188] F. Tournus and J.-C. Charlier, "*Ab initio* study of benzene adsorption on carbon nanotubes," *Phys. Rev. B*, vol. 71, p. 165421, 2005.

[189] L. Goerigk and S. Grimme, "A thorough benchmark of density functional

methods for general main group thermochemistry, kinetics, and noncovalent interactions," *Phys. Chem. Chem. Phys.*, vol. 13, pp. 6670–6688, 2011.

[190] H. Iikura, T. Tsuneda, T. Yanai, and K. Hirao, "A long-range correction scheme for generalized-gradient-approximation exchange functionals," *The Journal of Chemical Physics*, vol. 115, no. 8, pp. 3540–3544, 2001.

[191] S. A. Petrosyan, A. A. Rigos, and T. A. Arias, "Joint density-funationl theory: Ab initio study of cr2o3 surface chemistry in solution," *The Journal of Physical Chemistry B*, vol. 109, no. 32, pp. 15436–15444, 2005.

[192] D. Roxbury, S. Manohar, and A. Jagota, "Molecular Simulation of DNA β-Sheet and β-Barrel Structures on Graphite and Carbon Nanotubes," *The Journal of Physical Chemistry C*, vol. 114, no. 31, pp. 13267–13276, 2010.

[193] A. J. Patil, J. L. Vickery, T. B. Scott, and S. Mann, "Aqueous Stabilization and Self-Assembly of Graphene Sheets into Layered Bio-Nanocomposites using DNA," *Advanced Materials*, vol. 21, no. 31, pp. 3159–3164, 2009.

[194] T. Premkumar and K. E. Geckeler, "Graphene–DNA hybrid materials: Assembly, applications, and prospects ," *Progress in Polymer Science*, vol. 37, no. 4, pp. 515 – 529, 2012. Topical Issue on Polymer Physics.

[195] F. Albertorio, M. E. Hughes, J. A. Golovchenko, and D. Branton, "Base dependent DNA–carbon nanotube interactions: activation enthalpies and assembly–disassembly control," *Nanotechnology*, vol. 20, no. 39, p. 395101, 2009.

[196] A. Shankar, A. Jagota, and J. Mittal, "DNA Base Dimers Are Stabilized

by Hydrogen-Bonding Interactions Including Non-Watson–Crick Pairing Near Graphite Surfaces," *The Journal of Physical Chemistry B*, vol. 116, no. 40, pp. 12088–12094, 2012.

[197] A. v. d. Vaart and K. M. Merz, Jr., "Charge transfer in biologically important molecules: comparison of high-level ab initio and semiempirical methods," *International Journal of Quantum Chemistry*, vol. 77, no. 1, pp. 27–43, 2000.

References for Chapter 3

[1] S. Iijima, "Helical microtubules of graphitic carbon," *Nature*, vol. 354, pp. 56–58, 1991.

[2] A. Jorio, G. Dresselhaus, and M. S. Dresselhaus, *Carbon Nanotubes: Advanced Topics in the Synthesis, Structure, Properties and Applications*. , Springer, 2008.

[3] R. H. Baughman, A. A. Zakhidov, and W. A. de Heer, "Carbon Nanotubes–the Route Toward Applications," *Science*, vol. 297, no. 5582, pp. 787–792, 2002.

[4] S. B. Sinnott and R. Andrews, "Carbon Nanotubes: Synthesis, Properties, and Applications," *Critical Reviews in Solid State and Materials Sciences*, vol. 26, no. 3, pp. 145–249, 2001.

[5] J. Prasek, J. Drbohlavova, J. Chomoucka, J. Hubalek, O. Jasek, V. Adam,

and R. Kizek, "Methods for carbon nanotubes synthesis-review," *Journal of Materials Chemistry*, vol. 21, pp. 15872–15884, 2011.

[6] M. Zheng, A. Jagota, E. D. Semke, B. A. Diner, R. S. Mclean, S. R. Lustig, R. E. Richardson, and N. G. Tassi, "DNA-assisted dispersion and separation of carbon nanotubes," *Nat Mater*, vol. 2, no. 5, pp. 338–342, 2003.

[7] X. Tu, S. Manohar, A. Jagota, and M. Zheng, "DNA sequence motifs for structure-specific recognition and separation of carbon nanotubes," *Nature Materials*, vol. 460, no. 7252, pp. 250–253, 2009.

[8] M. Zheng, A. Jagota, M. S. Strano, A. P. Santos, P. Barone, S. G. Chou, B. A. Diner, M. S. Dresselhaus, R. S. Mclean, G. B. Onoa, G. G. Samsonidze, E. D. Semke, M. Usrey, and D. J. Walls, "Structure-Based Carbon Nanotube Sorting by Sequence-Dependent DNA Assembly," *Science*, vol. 302, no. 5650, pp. 1545–1548, 2003.

[9] X. Tu and M. Zheng, "A DNA-based approach to the carbon nanotube sorting problem," *Nano Research*, vol. 1, pp. 185–194, 2008.

[10] O. Malysheva, T. Tang, and P. Schiavone, "Binding Force Between a Charged Wall and a Complex Formed by a Polyelectrolyte and an Electronically Responsive Cylinder," *The Journal of Adhesion*, vol. 87, no. 3, pp. 251–271, 2011.

[11] C. Sun and T. Tang, "Structure of a polyelectrolyte around an electronically responsive cylinder," *Journal of Colloid and Interface Science*, vol. 338, no. 1, pp. 276 – 283, 2009.

[12] S. R. Lustig, A. Jagota, C. Khripin, and M. Zheng, "Theory of Structure-Based Carbon Nanotube Separations by Ion-Exchange Chromatography of DNA/CNT Hybrids," *The Journal of Physical Chemistry B*, vol. 109, no. 7, pp. 2559–2566, 2005.

[13] M. Zheng, K. Eom, and C. Ke, "Calculations of the resonant response of carbon nanotubes to binding of DNA," *Journal of Physics D: Applied Physics*, vol. 42, no. 14, 2009.

[14] S. Manohar, T. Tang, and A. Jagota, "Structure of Homopolymer DNA-CNT Hybrids," *The Journal of Physical Chemistry C*, vol. 111, no. 48, pp. 17835–17845, 2007.

[15] D. Roxbury, A. Jagota, and J. Mittal, "Sequence-Specific Self-Stitching Motif of Short Single-Stranded DNA on a Single-Walled Carbon Nanotube," *Journal of the American Chemical Society*, vol. 133, no. 34, pp. 13545–13550, 2011.

[16] S. Gowtham, R. H. Scheicher, R. Ahuja, R. Pandey, and S. P. Karna, "Physisorption of nucleobases on graphene: Density-functional calculations," *Phys. Rev. B*, vol. 76, p. 033401, 2007.

[17] J. Antony and S. Grimme, "Structures and interaction energies of stacked graphene-nucleobase complexes," *Phys. Chem. Chem. Phys.*, vol. 10, pp. 2722–2729, 2008.

[18] S. Panigrahi, A. Bhattacharya, S. Banerjee, and D. Bhattacharyya, "Interaction of Nucleobases with Wrinkled Graphene Surface: Dispersion Corrected

DFT and AFM Studies," *The Journal of Physical Chemistry C*, vol. 116, no. 7, pp. 4374–4379, 2012.

[19] S. Gowtham, R. H. Scheicher, R. Pandey, S. P. Karna, and R. Ahuja, "First-principles study of physisorption of nucleic acid bases on small-diameter carbon nanotubes," *Nanotechnology*, vol. 19, no. 12, p. 125701, 2008.

[20] Y. Wang, "Theoretical Evidence for the Stronger Ability of Thymine to Disperse SWCNT than Cytosine and Adenine: Self-Stacking of DNA Bases vs Their Cross-Stacking with SWCNT," *The Journal of Physical Chemistry C*, vol. 112, no. 37, pp. 14297–14305, 2008.

[21] A. Das, A. Sood, P. K. Maiti, M. Das, R. Varadarajan, and C. Rao, "Binding of nucleobases with single-walled carbon nanotubes: Theory and experiment," *Chemical Physics Letters*, vol. 453, no. 4–6, pp. 266–273, 2008.

[22] M. Shukla, M. Dubey, E. Zakar, R. Namburu, Z. Czyznikowska, and J. Leszczynski, "Interaction of nucleic acid bases with single-walled carbon nanotube," *Chemical Physics Letters*, vol. 480, no. 4–6, pp. 269–272, 2009.

[23] A. Ramraj, I. H. Hillier, M. A. Vincent, and N. A. Burton, "Assessment of approximate quantum chemical methods for calculating the interaction energy of nucleic acid bases with graphene and carbon nanotubes," *Chemical Physics Letters*, vol. 484, no. 4–6, pp. 295–298, 2010.

[24] D. Umadevi and G. N. Sastry, "Quantum Mechanical Study of Physisorption of Nucleobases on Carbon Materials: Graphene versus Carbon Nanotubes,"

The Journal of Physical Chemistry Letters, vol. 2, no. 13, pp. 1572–1576, 2011.

[25] B. Akdim, R. Pachter, P. N. Day, S. S. Kim, and R. R. Naik, "On modeling biomolecular–surface nonbonded interactions: application to nucleobase adsorption on single-wall carbon nanotube surfaces," *Nanotechnology*, vol. 23, no. 16, p. 165703, 2012.

[26] E. J. Meijer and M. Sprik, "A density-functional study of the intermolecular interactions of benzene," *The Journal of Chemical Physics*, vol. 105, no. 19, pp. 8684–8689, 1996.

[27] D. Le, A. Kara, E. Schröder, P. Hyldgaard, and T. S. Rahman, "Physisorption of nucleobases on graphene: a comparative van der Waals study," *Journal of Physics: Condensed Matter*, vol. 24, no. 42, p. 424210, 2012.

[28] A. Tkatchenko and M. Scheffler, "Accurate Molecular Van Der Waals Interactions from Ground-State Electron Density and Free-Atom Reference Data," *Phys. Rev. Lett.*, vol. 102, p. 073005, 2009.

[29] M. Dion, H. Rydberg, E. Schröder, D. C. Langreth, and B. I. Lundqvist, "Van der Waals Density Functional for General Geometries," *Phys. Rev. Lett.*, vol. 92, p. 246401, 2004.

[30] K. Lee, É. D. Murray, L. Kong, B. I. Lundqvist, and D. C. Langreth, "Higher-accuracy van der Waals density functional," *Phys. Rev. B*, vol. 82, p. 081101, 2010.

[31] S. Grimme, "Semiempirical GGA-type density functional constructed with

a long-range dispersion correction," *Journal of Computational Chemistry*, vol. 27, no. 15, pp. 1787–1799, 2006.

[32] S. Grimme, J. Antony, S. Ehrlich, and H. Krieg, "A consistent and accurate ab initio parametrization of density functional dispersion correction (DFT-D) for the 94 elements H-Pu," *The Journal of Chemical Physics*, vol. 132, no. 15, p. 154104, 2010.

[33] E. R. Johnson, R. A. Wolkow, and G. A. DiLabio, "Application of 25 density functionals to dispersion-bound homomolecular dimers," *Chemical Physics Letters*, vol. 394, no. 4–6, pp. 334–338, 2004.

[34] E. R. Johnson, I. D. Mackie, and G. A. DiLabio, "Dispersion interactions in density-functional theory," *Journal of Physical Organic Chemistry*, vol. 22, no. 12, pp. 1127–1135, 2009.

[35] Y. Zhao, N. E. Schultz, and D. G. Truhlar, "Design of density functionals by combining the method of constraint satisfaction with parametrization for thermochemistry, thermochemical kinetics, and noncovalent interactions," *Journal of Chemical Theory and Computation*, vol. 2, no. 2, pp. 364–382, 2006.

[36] Y. V. Shtogun, L. M. Woods, and G. I. Dovbeshko, "Adsorption of Adenine and Thymine and Their Radicals on Single-Wall Carbon Nanotubes," *The Journal of Physical Chemistry C*, vol. 111, no. 49, pp. 18174–18181, 2007.

[37] S. Stepanian, M. Karachevtsev, A. Glamazda, V. Karachevtsev, and L. Adamowicz, "Stacking interaction of cytosine with carbon nanotubes:

MP2, DFT and Raman spectroscopy study," *Chemical Physics Letters*, vol. 459, no. 1–6, pp. 153–158, 2008.

[38] Y. Zhao and D. G. Truhlar, "Density Functionals with Broad Applicability in Chemistry," *Accounts of Chemical Research*, vol. 41, no. 2, pp. 157–167, 2008.

[39] Y. Zhao and D. G. Truhlar, "Applications and validations of the Minnesota density functionals," *Chemical Physics Letters*, vol. 502, no. 1–3, pp. 1 – 13, 2011.

[40] M. J. Frisch, G. W. Trucks, H. B. Schlegel, G. E. Scuseria, M. A. Robb, J. R. Cheeseman, G. Scalmani, V. Barone, B. Mennucci, G. A. Petersson, H. Nakatsuji, M. Caricato, X. Li, H. P. Hratchian, A. F. Izmaylov, J. Bloino, G. Zheng, J. L. Sonnenberg, M. Hada, M. Ehara, K. Toyota, R. Fukuda, J. Hasegawa, M. Ishida, T. Nakajima, Y. Honda, O. Kitao, H. Nakai, T. Vreven, J. J. A. Montgomery, J. E. Peralta, F. Ogliaro, M. Bearpark, J. J. Heyd, E. Brothers, K. N. Kudin, V. N. Staroverov, R. Kobayashi, J. Normand, K. Raghavachari, A. Rendell, J. C. Burant, S. S. Iyengar, J. Tomasi, M. Cossi, N. Rega, J. M. Millam, M. Klene, J. E. Knox, J. B. Cross, V. Bakken, C. Adamo, J. Jaramillo, R. Gomperts, R. E. Stratmann, O. Yazyev, A. J. Austin, R. Cammi, C. Pomelli, J. W. Ochterski, R. L. Martin, K. Morokuma, V. G. Zakrzewski, G. A. Voth, P. Salvador, J. J. Dannenberg, S. Dapprich, A. D. Daniels, Ö. Farkas, J. B. Foresman, J. V. Ortiz, J. Cioslowski, and D. J. Fox, "Gaussian 09 Revision A.1." Gaussian Inc. Wallingford CT 2009.

[41] J. E. Freund, M. Edelwirth, P. Kröbel, and W. M. Heckl, "Structure determination of two-dimensional adenine crystals on graphite," *Phys. Rev. B*, vol. 55, pp. 5394–5397, 1997.

[42] R. Srinivasan and P. Gopalan, "Order and stability of an electrochemically condensed adenine layer on graphite," *The Journal of Physical Chemistry*, vol. 97, no. 34, pp. 8770–8775, 1993.

[43] M. Santosh, S. Panigrahi, D. Bhattacharyya, A. K. Sood, and P. K. Maiti, "Unzipping and binding of small interfering RNA with single walled carbon nanotube: A platform for small interfering RNA delivery," *The Journal of Chemical Physics*, vol. 136, no. 6, p. 065106, 2012.

[44] S. J. Sowerby, C. A. Cohn, W. M. Heckl, and N. G. Holm, "Differential adsorption of nucleic acid bases: Relevance to the origin of life," *Proceedings of the National Academy of Sciences*, vol. 98, no. 3, pp. 820–822, 2001.

[45] N. Varghese, U. Mogera, A. Govindaraj, A. Das, P. K. Maiti, A. K. Sood, and C. N. R. Rao, "Binding of DNA Nucleobases and Nucleosides with Graphene," *ChemPhysChem*, vol. 10, no. 1, pp. 206–210, 2009.

[46] L. R. Rutledge and S. D. Wetmore, "The assessment of density functionals for DNAprotein stacked and T-shaped complexes," *Canadian Journal of Chemistry*, vol. 88, no. 8, pp. 815–830, 2010.

References for Chapter 4

[1] S. Iijima, "Helical microtubules of graphitic carbon," *Nature*, vol. 354, pp. 56–58, 1991.

[2] R. Saito, G. Dresselhaus, and M. Dresselhaus, *Physical Properties of Carbon Nanotube*. Imperial College Press, 1998.

[3] R. Singh, D. Pantarotto, D. McCarthy, O. Chaloin, J. Hoebeke, C. D. Partidos, J.-P. Briand, M. Prato, A. Bianco, and K. Kostarelos, "Binding and Condensation of Plasmid DNA onto Functionalized Carbon Nanotubes: Toward the Construction of Nanotube-Based Gene Delivery Vectors," *Journal of the American Chemical Society*, vol. 127, no. 12, pp. 4388–4396, 2005.

[4] C. Hu, Y. Zhang, G. Bao, Y. Zhang, M. Liu, and Z. L. Wang, "DNA Functionalized Single-Walled Carbon Nanotubes for Electrochemical Detection," *The Journal of Physical Chemistry B*, vol. 109, no. 43, pp. 20072–20076, 2005.

[5] Y. Ma, S. R. Ali, A. S. Dodoo, and H. He, "Enhanced Sensitivity for Biosensors: Multiple Functions of DNA-Wrapped Single-Walled Carbon Nanotubes in Self-Doped Polyaniline Nanocomposites," *The Journal of Physical Chemistry B*, vol. 110, no. 33, pp. 16359–16365, 2006.

[6] P. He and M. Bayachou, "Layer-by-Layer Fabrication and Characterization of DNA-Wrapped Single-Walled Carbon Nanotube Particles," *Langmuir*, vol. 21, no. 13, pp. 6086–6092, 2005.

[7] Y. Xu, P. E. Pehrsson, L. Chen, R. Zhang, and W. Zhao, "Double-Stranded

DNA Single-Walled Carbon Nanotube Hybrids for Optical Hydrogen Peroxide and Glucose Sensing," *The Journal of Physical Chemistry C*, vol. 111, no. 24, pp. 8638–8643, 2007.

[8] M. Zheng, A. Jagota, E. D. Semke, B. A. Diner, R. S. Mclean, S. R. Lustig, R. E. Richardson, and N. G. Tassi, "DNA-assisted dispersion and separation of carbon nanotubes," *Nat Mater*, vol. 2, no. 5, pp. 338–342, 2003.

[9] M. Zheng, A. Jagota, M. S. Strano, A. P. Santos, P. Barone, S. G. Chou, B. A. Diner, M. S. Dresselhaus, R. S. Mclean, G. B. Onoa, G. G. Samsonidze, E. D. Semke, M. Usrey, and D. J. Walls, "Structure-Based Carbon Nanotube Sorting by Sequence-Dependent DNA Assembly," *Science*, vol. 302, no. 5650, pp. 1545–1548, 2003.

[10] G. F. Schneider, S. W. Kowalczyk, V. E. Calado, G. Pandraud, H. W. Zandbergen, L. M. K. Vandersypen, and C. Dekker, "DNA Translocation through Graphene Nanopores," *Nano Letters*, vol. 10, no. 8, pp. 3163–3167, 2010.

[11] H. W. C. Postma, "Rapid Sequencing of Individual DNA Molecules in Graphene Nanogaps," *Nano Letters*, vol. 10, no. 2, pp. 420–425, 2010.

[12] D. B. Wells, M. Belkin, J. Comer, and A. Aksimentiev, "Assessing Graphene Nanopores for Sequencing DNA," *Nano Letters*, vol. 12, no. 8, pp. 4117–4123, 2012.

[13] C. Merchant and M. Drndić, "Graphene nanopore devices for dna sensing," in *Nanopore-Based Technology* (M. E. Gracheva, ed.), vol. 870 of *Methods in Molecular Biology*, pp. 211–226, Humana Press, 2012.

[14] A. L. Frischknecht and M. G. Martin, "Simulation of the adsorption of nucleotide monophosphates on carbon nanotubes in aqueous solution," *The Journal of Physical Chemistry C*, vol. 112, no. 16, pp. 6271–6278, 2008.

[15] R. R. Johnson, A. T. C. Johnson, and M. L. Klein, "Probing the Structure of DNA-Carbon Nanotube Hybrids with Molecular Dynamics," *Nano Letters*, vol. 8, no. 1, pp. 69–75, 2008.

[16] R. R. Johnson, A. T. C. Johnson, and M. L. Klein, "The Nature of DNA-Base–Carbon-Nanotube Interactions," *Small*, vol. 6, no. 1, pp. 31–34, 2010.

[17] W. Lv, "The adsorption of DNA bases on neutral and charged (8, 8) carbon-nanotubes," *Chemical Physics Letters*, vol. 514, no. 4–6, pp. 311 – 316, 2011.

[18] A. K. Manna and S. K. Pati, "Theoretical understanding of single-stranded DNA assisted dispersion of graphene," *J. Mater. Chem. B*, vol. 1, pp. 91–100, 2013.

[19] M. L. Mayo, Z. Q. Chen, and S. V. Kilina, "Computational studies of nucleotide selectivity in dna–carbon nanotube hybrids," *The Journal of Physical Chemistry Letters*, vol. 3, no. 19, pp. 2790–2797, 2012.

[20] S. Neihsial, G. Periyasamy, P. K. Samanta, and S. K. Pati, "Understanding the Binding Mechanism of Various Chiral SWCNTs and ssDNA: A Computational Study," *The Journal of Physical Chemistry B*, vol. 116, no. 51, pp. 14754–14759, 2012.

[21] Z. Xiao, X. Wang, X. Xu, H. Zhang, Y. Li, and Y. Wang, "Base- and

Structure-Dependent DNA Dinucleotide–Carbon Nanotube Interactions: Molecular Dynamics Simulations and Thermodynamic Analysis," *The Journal of Physical Chemistry C*, vol. 115, no. 44, pp. 21546–21558, 2011.

[22] S. Gowtham, R. H. Scheicher, R. Ahuja, R. Pandey, and S. P. Karna, "Physisorption of nucleobases on graphene: Density-functional calculations," *Phys. Rev. B*, vol. 76, p. 033401, 2007.

[23] S. Gowtham, R. H. Scheicher, R. Pandey, S. P. Karna, and R. Ahuja, "First-principles study of physisorption of nucleic acid bases on small-diameter carbon nanotubes," *Nanotechnology*, vol. 19, no. 12, p. 125701, 2008.

[24] S. Meng, P. Maragakis, C. Papaloukas, and E. Kaxiras, "DNA Nucleoside Interaction and Identification with Carbon Nanotubes," *Nano Letters*, vol. 7, no. 1, pp. 45–50, 2007.

[25] S. Meng, W. L. Wang, P. Maragakis, and E. Kaxiras, "Determination of DNA-Base Orientation on Carbon Nanotubes through Directional Optical Absorbance," *Nano Letters*, vol. 7, no. 8, pp. 2312–2316, 2007.

[26] Y. V. Shtogun, L. M. Woods, and G. I. Dovbeshko, "Adsorption of Adenine and Thymine and Their Radicals on Single-Wall Carbon Nanotubes," *The Journal of Physical Chemistry C*, vol. 111, no. 49, pp. 18174–18181, 2007.

[27] Y. Wang and Y. Bu, "Noncovalent Interactions between Cytosine and SWCNT," *The Journal of Physical Chemistry B*, vol. 111, no. 23, pp. 6520–6526, 2007.

[28] Y. Wang, "Theoretical Evidence for the Stronger Ability of Thymine to Disperse SWCNT than Cytosine and Adenine: Self-Stacking of DNA Bases vs Their Cross-Stacking with SWCNT," *The Journal of Physical Chemistry C*, vol. 112, no. 37, pp. 14297–14305, 2008.

[29] F. Ortmann, W. G. Schmidt, and F. Bechstedt, "Attracted by Long-Range Electron Correlation: Adenine on Graphite," *Phys. Rev. Lett.*, vol. 95, p. 186101, 2005.

[30] K. Berland, S. D. Chakarova-Käck, V. R. Cooper, D. C. Langreth, and E. Schröder, "A van der Waals density functional study of adenine on graphene: single-molecular adsorption and overlayer binding," *Journal of Physics: Condensed Matter*, vol. 23, no. 13, p. 135001, 2011.

[31] J. Antony and S. Grimme, "Structures and interaction energies of stacked graphene-nucleobase complexes," *Phys. Chem. Chem. Phys.*, vol. 10, pp. 2722–2729, 2008.

[32] S. Panigrahi, A. Bhattacharya, S. Banerjee, and D. Bhattacharyya, "Interaction of Nucleobases with Wrinkled Graphene Surface: Dispersion Corrected DFT and AFM Studies," *The Journal of Physical Chemistry C*, vol. 116, no. 7, pp. 4374–4379, 2012.

[33] D. Le, A. Kara, E. Schröder, P. Hyldgaard, and T. S. Rahman, "Physisorption of nucleobases on graphene: a comparative van der Waals study," *Journal of Physics: Condensed Matter*, vol. 24, no. 42, p. 424210, 2012.

[34] Y. Cho, S. K. Min, J. Yun, W. Y. Kim, A. Tkatchenko, and K. S. Kim, "Noncovalent Interactions of DNA Bases with Naphthalene and Graphene," *Jour-*

nal of Chemical Theory and Computation, vol. 9, no. 0, pp. 2090–2096, 2013.

[35] H. Vovusha, S. Sanyal, and B. Sanyal, "Interaction of nucleobases and aromatic amino acids with graphene oxide and graphene flakes," *The Journal of Physical Chemistry Letters*, vol. 4, no. 21, pp. 3710–3718, 2013.

[36] S. Stepanian, M. Karachevtsev, A. Glamazda, V. Karachevtsev, and L. Adamowicz, "Stacking interaction of cytosine with carbon nanotubes: MP2, DFT and Raman spectroscopy study," *Chemical Physics Letters*, vol. 459, no. 1–6, pp. 153–158, 2008.

[37] M. Shukla, M. Dubey, E. Zakar, R. Namburu, Z. Czyznikowska, and J. Leszczynski, "Interaction of nucleic acid bases with single-walled carbon nanotube," *Chemical Physics Letters*, vol. 480, no. 4–6, pp. 269–272, 2009.

[38] B. Akdim, R. Pachter, P. N. Day, S. S. Kim, and R. R. Naik, "On modeling biomolecular–surface nonbonded interactions: application to nucleobase adsorption on single-wall carbon nanotube surfaces," *Nanotechnology*, vol. 23, no. 16, p. 165703, 2012.

[39] A. Sarmah and R. K. Roy, "Understanding the interaction of nucleobases with chiral semiconducting single-walled carbon nanotubes: An alternative theoretical approach based on density functional reactivity theory," *The Journal of Physical Chemistry C*, vol. 117, no. 41, pp. 21539–21550, 2013.

[40] M. Chehel Amirani, T. Tang, and J. Cuervo, "Quantum mechanical treatment of binding energy between DNA nucleobases and carbon nanotube: A DFT

analysis," *Physica E: Low-dimensional Systems and Nanostructures*, vol. 54, pp. 65–71, 2013.

[41] M. Chehel Amirani and T. Tang, "Binding of nucleobases with graphene and carbon nanotube: a review of computational studies," *Journal of Biomolecular Structure and Dynamics*, pp. 1–31, 2014.

[42] H. Wang and A. Ceulemans, "Physisorption of adenine DNA nucleosides on zigzag and armchair single-walled carbon nanotubes: A first-principles study," *Phys. Rev. B*, vol. 79, p. 195419, 2009.

[43] A. N. Enyashin, S. Gemming, and G. Seifert, "DNA-wrapped carbon nanotubes," *Nanotechnology*, vol. 18, no. 24, p. 245702, 2007.

[44] A. Lehninger, D. Nelson, and M. Cox, *Lehninger Principles of Biochemistry*. W. H. Freeman, 2005.

[45] G. M. Blackburn, M. J. Gait, D. Loakes, and D. M. Williams, eds., *Nucleic Acids in Chemistry and Biology*. The Royal Society of Chemistry, 2006.

[46] D. Ebbing and S. Gammon, *General Chemistry: Media Enhanced Edition*. Cengage Learning, 2007.

[47] M. Madigan, D. Clark, D. Stahl, and J. Martinko, *Brock Biology of Microorganisms 13th Edition:*. Benjamin Cummings, 2010.

[48] A. Wong and G. Wu, "Selective binding of monovalent cations to the stacking g-quartet structure formed by guanosine 5'-monophosphate: A solid-state nmr study," *Journal of the American Chemical Society*, vol. 125, no. 45, pp. 13895–13905, 2003.

[49] D. M. Boghaei and M. Gharagozlou, "Charge transfer complexes of adenosine-5′-monophosphate and cytidine-5′-monophosphate with water-soluble cobalt(ii) schiff base complexes in aqueous solution," *Spectrochimica Acta Part A: Molecular and Biomolecular Spectroscopy*, vol. 63, no. 1, pp. 139 – 148, 2006.

[50] N. Varghese, U. Mogera, A. Govindaraj, A. Das, P. K. Maiti, A. K. Sood, and C. N. R. Rao, "Binding of DNA Nucleobases and Nucleosides with Graphene," *ChemPhysChem*, vol. 10, no. 1, pp. 206–210, 2009.

[51] A. Das, A. Sood, P. K. Maiti, M. Das, R. Varadarajan, and C. Rao, "Binding of nucleobases with single-walled carbon nanotubes: Theory and experiment," *Chemical Physics Letters*, vol. 453, no. 4–6, pp. 266–273, 2008.

[52] A. Ramraj, I. H. Hillier, M. A. Vincent, and N. A. Burton, "Assessment of approximate quantum chemical methods for calculating the interaction energy of nucleic acid bases with graphene and carbon nanotubes," *Chemical Physics Letters*, vol. 484, no. 4–6, pp. 295–298, 2010.

[53] H. Berendsen, D. van der Spoel, and R. van Drunen, "Gromacs: A message-passing parallel molecular dynamics implementation," *Computer Physics Communications*, vol. 91, no. 1–3, pp. 43 – 56, 1995.

[54] E. Lindahl, B. Hess, and D. van der Spoel, "Gromacs 3.0: a package for molecular simulation and trajectory analysis," *Molecular modeling annual*, vol. 7, no. 8, pp. 306–317, 2001.

[55] M. J. Frisch, G. W. Trucks, H. B. Schlegel, G. E. Scuseria, M. A. Robb, J. R. Cheeseman, G. Scalmani, V. Barone, B. Mennucci, G. A. Petersson,

H. Nakatsuji, M. Caricato, X. Li, H. P. Hratchian, A. F. Izmaylov, J. Bloino, G. Zheng, J. L. Sonnenberg, M. Hada, M. Ehara, K. Toyota, R. Fukuda, J. Hasegawa, M. Ishida, T. Nakajima, Y. Honda, O. Kitao, H. Nakai, T. Vreven, J. J. A. Montgomery, J. E. Peralta, F. Ogliaro, M. Bearpark, J. J. Heyd, E. Brothers, K. N. Kudin, V. N. Staroverov, R. Kobayashi, J. Normand, K. Raghavachari, A. Rendell, J. C. Burant, S. S. Iyengar, J. Tomasi, M. Cossi, N. Rega, J. M. Millam, M. Klene, J. E. Knox, J. B. Cross, V. Bakken, C. Adamo, J. Jaramillo, R. Gomperts, R. E. Stratmann, O. Yazyev, A. J. Austin, R. Cammi, C. Pomelli, J. W. Ochterski, R. L. Martin, K. Morokuma, V. G. Zakrzewski, G. A. Voth, P. Salvador, J. J. Dannenberg, S. Dapprich, A. D. Daniels, Ö. Farkas, J. B. Foresman, J. V. Ortiz, J. Cioslowski, and D. J. Fox, "Gaussian 09 Revision A.1." Gaussian Inc. Wallingford CT 2009.

[56] L. R. Rutledge, H. F. Durst, and S. D. Wetmore, "Evidence for Stabilization of DNA/RNA Protein Complexes Arising from Nucleobase Amino Acid Stacking and T-Shaped Interactions," *Journal of Chemical Theory and Computation*, vol. 5, no. 5, pp. 1400–1410, 2009.

[57] L. R. Rutledge and S. D. Wetmore, "The assessment of density functionals for DNAprotein stacked and T-shaped complexes," *Canadian Journal of Chemistry*, vol. 88, no. 8, pp. 815–830, 2010.

[58] S. Chandra Shekar and R. S. Swathi, "Stability of nucleobases and base pairs adsorbed on graphyne and graphdiyne," *The Journal of Physical Chemistry C*, vol. 118, no. 8, pp. 4516–4528, 2014.

[59] J.-H. Lee, Y.-K. Choi, H.-J. Kim, R. H. Scheicher, and J.-H. Cho, "Physisorption of DNA Nucleobases on h-BN and Graphene: vdW-Corrected DFT Calculations," *The Journal of Physical Chemistry C*, vol. 117, no. 26, pp. 13435–13441, 2013.

[60] D. Umadevi and G. N. Sastry, "Quantum Mechanical Study of Physisorption of Nucleobases on Carbon Materials: Graphene versus Carbon Nanotubes," *The Journal of Physical Chemistry Letters*, vol. 2, no. 13, pp. 1572–1576, 2011.

[61] E. R. Johnson, R. A. Wolkow, and G. A. DiLabio, "Application of 25 density functionals to dispersion-bound homomolecular dimers," *Chemical Physics Letters*, vol. 394, no. 4–6, pp. 334–338, 2004.

[62] M. Dion, H. Rydberg, E. Schröder, D. C. Langreth, and B. I. Lundqvist, "Van der Waals Density Functional for General Geometries," *Phys. Rev. Lett.*, vol. 92, p. 246401, 2004.

[63] E. G. Hohenstein, S. T. Chill, and C. D. Sherrill, "Assessment of the Performance of the M055-2X and M06-2X Exchange-Correlation Functionals for Noncovalent Interactions in Biomolecules," *Journal of Chemical Theory and Computation*, vol. 4, no. 12, pp. 1996–2000, 2008.

[64] Y. Zhao and D. G. Truhlar, "Density functionals with broad applicability in chemistry," *Accounts of Chemical Research*, vol. 41, no. 2, pp. 157–167, 2008.

[65] E. R. Johnson, I. D. Mackie, and G. A. DiLabio, "Dispersion interactions in

density-functional theory," *Journal of Physical Organic Chemistry*, vol. 22, no. 12, pp. 1127–1135, 2009.

[66] Y. Zhao and D. G. Truhlar, "Applications and validations of the Minnesota density functionals," *Chemical Physics Letters*, vol. 502, no. 1–3, pp. 1–13, 2011.

[67] S. Grimme, "Density functional theory with London dispersion corrections," *Wiley Interdisciplinary Reviews: Computational Molecular Science*, vol. 1, no. 2, pp. 211–228, 2011.

[68] S. Ehrlich, J. Moellmann, and S. Grimme, "Dispersion-Corrected Density Functional Theory for Aromatic Interactions in Complex Systems," *Accounts of Chemical Research*, vol. 46, no. 4, pp. 916–926, 2013.

[69] S. Grimme, "Semiempirical GGA-type density functional constructed with a long-range dispersion correction," *Journal of Computational Chemistry*, vol. 27, no. 15, pp. 1787–1799, 2006.

[70] S. Grimme, J. Antony, S. Ehrlich, and H. Krieg, "A consistent and accurate ab initio parametrization of density functional dispersion correction (DFT-D) for the 94 elements H-Pu," *The Journal of Chemical Physics*, vol. 132, no. 15, p. 154104, 2010.

[71] S. Grimme, S. Ehrlich, and L. Goerigk, "Effect of the damping function in dispersion corrected density functional theory," *Journal of Computational Chemistry*, vol. 32, no. 7, pp. 1456–1465, 2011.

[72] A. Tkatchenko and M. Scheffler, "Accurate Molecular Van Der Waals Interactions from Ground-State Electron Density and Free-Atom Reference Data," *Phys. Rev. Lett.*, vol. 102, p. 073005, 2009.

[73] K. Lee, É. D. Murray, L. Kong, B. I. Lundqvist, and D. C. Langreth, "Higher-accuracy van der Waals density functional," *Phys. Rev. B*, vol. 82, p. 081101, 2010.

[74] E. Torres and G. A. DiLabio, "A (nearly) universally applicable method for modeling noncovalent interactions using b3lyp," *The Journal of Physical Chemistry Letters*, vol. 3, no. 13, pp. 1738–1744, 2012.

[75] C. I. Bayly, P. Cieplak, W. Cornell, and P. A. Kollman, "A well-behaved electrostatic potential based method using charge restraints for deriving atomic charges: the resp model," *The Journal of Physical Chemistry*, vol. 97, no. 40, pp. 10269–10280, 1993.

[76] D. Case, T. Darden, T. C. III, C. Simmerling, J. Wang, R. Duke, R. Luo, R. Walker, W. Zhang, K. Merz, B. Roberts, S. Hayik, A. Roitberg, G. Seabra, J. Swails, A. GÖtz, I. Kolossváry, K. Wong, F. Paesani, J. Vanicek, R. Wolf, J. Liu, X. Wu, S. Brozell, T. Steinbrecher, H. Gohlke, Q. Cai, X. Ye, J. Wang, M. Hsieh, G. Cui, D. Roe, D. Mathews, M. Seetin, R. Salomon-Ferrer, C. Sagui, V. Babin, T. Luchko, S. Gusarov, A. Kovalenko, and P. Kollman, "AmberTools12." University of California, San Francisco 2012.

[77] W. L. Jorgensen and J. D. Madura, "Temperature and size dependence for monte carlo simulations of tip4p water," *Molecular Physics*, vol. 56, no. 6, pp. 1381–1392, 1985.

[78] E. A. Raymond, T. L. Tarbuck, M. G. Brown, and G. L. Richmond, "Hydrogen-bonding interactions at the vapor/water interface investigated by vibrational sum-frequency spectroscopy of hod/h2o/d2o mixtures and molecular dynamics simulations," *The Journal of Physical Chemistry B*, vol. 107, no. 2, pp. 546–556, 2003.

[79] P. Liu, E. Harder, and B. J. Berne, "Hydrogen-bond dynamics in the air-water interface," *The Journal of Physical Chemistry B*, vol. 109, no. 7, pp. 2949–2955, 2005.

[80] N. B. Vargaftik, B. N. Volkov, and L. D. Voljak, "International tables of the surface tension of water," *Journal of Physical and Chemical Reference Data*, vol. 12, no. 3, pp. 817–820, 1983.

[81] T. Premkumar and K. Geckeler, *Materials Science of DNA*. CRC Press, 2011.

[82] J.-H. Ha, R. S. Spolar, and M. R. Jr, "Role of the hydrophobic effect in stability of site-specific protein-dna complexes," *Journal of Molecular Biology*, vol. 209, no. 4, pp. 801 – 816, 1989.

[83] B. Jayaram and T. Jain, "The role of water in protein-dna recognition," *Annual Review of Biophysics and Biomolecular Structure*, vol. 33, no. 1, pp. 343–361, 2004.

[84] B. Jayaram, K. McConnell, S. B. Dixit, A. Das, and D. L. Beveridge, "Free-energy component analysis of 40 protein–dna complexes: A consensus view on the thermodynamics of binding at the molecular level," *Journal of Computational Chemistry*, vol. 23, no. 1, pp. 1–14, 2002.

[85] T. Yamazaki and H. Fenniri, "Imaging carbon nanotube interaction with nucleobases in water using the statistical mechanical theory of molecular liquids," *The Journal of Physical Chemistry C*, vol. 116, no. 28, pp. 15087–15092, 2012.

[86] Q. Sun, Z. Li, D. J. Searles, Y. Chen, G. M. Lu, and A. Du, "Charge-controlled switchable co2 capture on boron nitride nanomaterials," *Journal of the American Chemical Society*, vol. 135, no. 22, pp. 8246–8253, 2013.

[87] Q. Sun, M. Wang, Z. Li, Y. Ma, and A. Du, "{CO2} capture and gas separation on boron carbon nanotubes," *Chemical Physics Letters*, vol. 575, no. 0, pp. 59 – 66, 2013.

[88] M. Yoon, S. Yang, E. Wang, and Z. Zhang, "Charged fullerenes as high-capacity hydrogen storage media," *Nano Letters*, vol. 7, no. 9, pp. 2578–2583, 2007.

[89] A. Kaiser, C. Leidlmair, P. Bartl, S. Zottl, S. Denifl, A. Mauracher, M. Probst, P. Scheier, and O. Echt, "Adsorption of hydrogen on neutral and charged fullerene: Experiment and theory," *The Journal of Chemical Physics*, vol. 138, no. 7, pp. 1–13, 2013.

References for Chapter 5

[1] M. Zheng, A. Jagota, E. D. Semke, B. A. Diner, R. S. Mclean, S. R. Lustig, R. E. Richardson, and N. G. Tassi, "DNA-assisted dispersion and separation of carbon nanotubes," *Nat Mater*, vol. 2, no. 5, pp. 338–342, 2003.

[2] C. Dwyer, M. Guthold, M. Falvo, S. Washburn, R. Superfine, and D. Erie, "DNA-functionalized single-walled carbon nanotubes," *Nanotechnology*, vol. 13, no. 5, p. 601, 2002.

[3] S. R. Shin, C. K. Lee, I. S. So, J. H. Jeon, T. M. Kang, C. W. Kee, S. I. Kim, G. M. Spinks, G. G. Wallace, and S. J. Kim, "DNA-Wrapped Single-Walled Carbon Nanotube Hybrid Fibers for supercapacitors and Artificial Muscles," *Advanced Materials*, vol. 20, no. 3, pp. 466–470, 2008.

[4] C. M. Arnett, C. P. Marsh, C. R. Welch, M. S. Strano, J.-H. Han, J. H. Gray, and T. A. Carlson, "Enzyme-Mediated Assimilation of DNA-Functionalized Single-Walled Carbon Nanotubes," *Langmuir*, vol. 26, no. 2, pp. 613–617, 2010.

[5] R. Yang, Z. Tang, J. Yan, H. Kang, Y. Kim, Z. Zhu, and W. Tan, "Noncovalent Assembly of Carbon Nanotubes and Single-Stranded DNA: An Effective Sensing Platform for Probing Biomolecular Interactions," *Analytical Chemistry*, vol. 80, no. 19, pp. 7408–7413, 2008.

[6] H. Wang, N. B. Muren, D. Ordinario, A. A. Gorodetsky, J. K. Barton, and C. Nuckolls, "Transducing methyltransferase activity into electrical signals in a carbon nanotube-DNA device," *Chem. Sci.*, vol. 3, pp. 62–65, 2012.

[7] S. Kilina, D. A. Yarotski, A. A. Talin, S. Tretiak, A. J. Taylor, and A. V. Balatsky, "Unveiling Stability Criteria of DNA-Carbon Nanotubes Constructs by Scanning Tunneling Microscopy and Computational Modeling," *Journal of Drug Delivery*, vol. 2011, 2011.

[8] M. Bratcher, B. Gersten, H. Ji, and J. Mays, "Study in the dispersion of carbon nanotubes," in *Symposium Z – Making Functional Materials with Nanotubes*, vol. 706 of *MRS Proceedings*, 2001.

[9] M. N. Tchoul, W. T. Ford, G. Lolli, D. E. Resasco, and S. Arepalli, "Effect of mild nitric acid oxidation on dispersability, size, and structure of single-walled carbon nanotubes," *Chemistry of Materials*, vol. 19, no. 23, pp. 5765–5772, 2007.

[10] A. Rinzler, J. Liu, H. Dai, P. Nikolaev, C. Huffman, F. Rodriguez-Macias, P. Boul, A. Lu, D. Heymann, D. Colbert, R. Lee, J. Fischer, A. Rao, P. Eklund, and R. Smalley, "Large-scale purification of single-wall carbon nanotubes: process, product, and characterization," *Applied Physics A*, vol. 67, no. 1, pp. 29–37, 1998.

[11] M. Zheng, A. Jagota, M. S. Strano, A. P. Santos, P. Barone, S. G. Chou, B. A. Diner, M. S. Dresselhaus, R. S. Mclean, G. B. Onoa, G. G. Samsonidze, E. D. Semke, M. Usrey, and D. J. Walls, "Structure-Based Carbon Nanotube Sorting by Sequence-Dependent DNA Assembly," *Science*, vol. 302, no. 5650, pp. 1545–1548, 2003.

[12] X. Tu and M. Zheng, "A DNA-based approach to the carbon nanotube sorting problem," *Nano Research*, vol. 1, pp. 185–194, 2008.

[13] M. Zheng and E. D. Semke, "Enrichment of single chirality carbon nanotubes," *Journal of the American Chemical Society*, vol. 129, no. 19, pp. 6084–6085, 2007.

[14] X. Tu, S. Manohar, A. Jagota, and M. Zheng, "DNA sequence motifs for structure-specific recognition and separation of carbon nanotubes," *Nat Mater*, vol. 460, no. 7252, pp. 250–253, 2009.

[15] S. R. Lustig, A. Jagota, C. Khripin, and M. Zheng, "Theory of Structure-Based Carbon Nanotube Separations by Ion-Exchange Chromatography of DNA/CNT Hybrids," *The Journal of Physical Chemistry B*, vol. 109, no. 7, pp. 2559–2566, 2005.

[16] C. Y. Khripin, S. Manohar, M. Zheng, and A. Jagota, "Measurement of electrostatic properties of dna-carbon nanotube hybrids by capillary electrophoresis," *The Journal of Physical Chemistry C*, vol. 113, no. 31, pp. 13616–13621, 2009.

[17] S. O. Zur, "Theorie der elektrolytischen doppelschicht," *Electrochem*, vol. 30, pp. 508–16, 1924.

[18] D. Roxbury, A. Jagota, and J. Mittal, "Structural Characteristics of Oligomeric DNA Strands Adsorbed onto Single-Walled Carbon Nanotubes," *The Journal of Physical Chemistry B*, vol. 117, no. 1, pp. 132–140, 2013.

[19] T. Tang, C.-Y. Hui, and A. Jagota, "Line of charges in electrolyte solution near a half-space: Ii. electric field of a single charge," *Journal of Colloid and Interface Science*, vol. 299, no. 2, pp. 572 – 579, 2006.

[20] O. Malysheva, T. Tang, and P. Schiavone, "Adhesion between a charged particle in an electrolyte solution and a charged substrate: Electrostatic and van der waals interactions," *Journal of Colloid and Interface Science*, vol. 327, no. 1, pp. 251 – 260, 2008.

[21] O. Malysheva, T. Tang, and P. Schiavone, "Binding Force Between a Charged Wall and a Complex Formed by a Polyelectrolyte and an Electronically Responsive Cylinder," *The Journal of Adhesion*, vol. 87, no. 3, pp. 251–271, 2011.

[22] M. Zheng, K. Eom, and C. Ke, "Calculations of the resonant response of carbon nanotubes to binding of DNA," *Journal of Physics D: Applied Physics*, vol. 42, no. 14, 2009.

[23] C. Sun and T. Tang, "Structure of a polyelectrolyte around an electronically responsive cylinder," *Journal of Colloid and Interface Science*, vol. 338, no. 1, pp. 276 – 283, 2009.

[24] J. W. Mintmire and C. T. White, "Universal density of states for carbon nanotubes," *Phys. Rev. Lett.*, vol. 81, pp. 2506–2509, 1998.

[25] W. Russel, D. Saville, and W. Schowalter, *Colloidal Dispersions*. Cambridge Monographs on Mechanics, Cambridge University Press, 1992.

[26] O. Malysheva, T. Tang, and P. Schiavone, "A model for carbon nanotube–dna hybrid using one-dimensional density of states," *Journal of Colloid and Interface Science*, vol. 380, no. 1, pp. 25 – 33, 2012.

[27] S. V. Rotkin and S. E. Snyder, *Theory of Electronic and Optical Properties of DNA–SWNT Hybrids*, pp. 23–51. Wiley-VCH Verlag GmbH & Co. KGaA, 2010.

[28] S. Snyder and S. Rotkin, "Polarization component of cohesion energy in

single-wall carbon nanotube-dna complexes," *JETP Letters*, vol. 84, no. 6, pp. 348–351, 2006.

[29] M. Chehel Amirani and T. Tang, "Binding of nucleobases with graphene and carbon nanotube: a review of computational studies," *Journal of Biomolecular Structure and Dynamics*, pp. 1–31, 2014.

[30] S. Gowtham, R. H. Scheicher, R. Ahuja, R. Pandey, and S. P. Karna, "Physisorption of nucleobases on graphene: Density-functional calculations," *Phys. Rev. B*, vol. 76, p. 033401, 2007.

[31] S. Gowtham, R. H. Scheicher, R. Pandey, S. P. Karna, and R. Ahuja, "First-principles study of physisorption of nucleic acid bases on small-diameter carbon nanotubes," *Nanotechnology*, vol. 19, no. 12, p. 125701, 2008.

[32] S. Meng, P. Maragakis, C. Papaloukas, and E. Kaxiras, "DNA Nucleoside Interaction and Identification with Carbon Nanotubes," *Nano Letters*, vol. 7, no. 1, pp. 45–50, 2007.

[33] S. Meng, W. L. Wang, P. Maragakis, and E. Kaxiras, "Determination of DNA-Base Orientation on Carbon Nanotubes through Directional Optical Absorbance," *Nano Letters*, vol. 7, no. 8, pp. 2312–2316, 2007.

[34] Y. V. Shtogun, L. M. Woods, and G. I. Dovbeshko, "Adsorption of Adenine and Thymine and Their Radicals on Single-Wall Carbon Nanotubes," *The Journal of Physical Chemistry C*, vol. 111, no. 49, pp. 18174–18181, 2007.

[35] H. Wang and A. Ceulemans, "Physisorption of adenine DNA nucleosides

on zigzag and armchair single-walled carbon nanotubes: A first-principles study," *Phys. Rev. B*, vol. 79, p. 195419, 2009.

[36] Y. Wang and Y. Bu, "Noncovalent Interactions between Cytosine and SWCNT," *The Journal of Physical Chemistry B*, vol. 111, no. 23, pp. 6520–6526, 2007.

[37] Y. Wang, "Theoretical Evidence for the Stronger Ability of Thymine to Disperse SWCNT than Cytosine and Adenine: Self-Stacking of DNA Bases vs Their Cross-Stacking with SWCNT," *The Journal of Physical Chemistry C*, vol. 112, no. 37, pp. 14297–14305, 2008.

[38] F. Ortmann, W. G. Schmidt, and F. Bechstedt, "Attracted by Long-Range Electron Correlation: Adenine on Graphite," *Phys. Rev. Lett.*, vol. 95, p. 186101, 2005.

[39] K. Berland, S. D. Chakarova-Käck, V. R. Cooper, D. C. Langreth, and E. Schröder, "A van der Waals density functional study of adenine on graphene: single-molecular adsorption and overlayer binding," *Journal of Physics: Condensed Matter*, vol. 23, no. 13, p. 135001, 2011.

[40] S. Panigrahi, A. Bhattacharya, S. Banerjee, and D. Bhattacharyya, "Interaction of Nucleobases with Wrinkled Graphene Surface: Dispersion Corrected DFT and AFM Studies," *The Journal of Physical Chemistry C*, vol. 116, no. 7, pp. 4374–4379, 2012.

[41] S. Chandra Shekar and R. S. Swathi, "Stability of nucleobases and base pairs adsorbed on graphyne and graphdiyne," *The Journal of Physical Chemistry C*, vol. 118, no. 8, pp. 4516–4528, 2014.

[42] J. Antony and S. Grimme, "Structures and interaction energies of stacked graphene-nucleobase complexes," *Phys. Chem. Chem. Phys.*, vol. 10, pp. 2722–2729, 2008.

[43] J.-H. Lee, Y.-K. Choi, H.-J. Kim, R. H. Scheicher, and J.-H. Cho, "Physisorption of DNA Nucleobases on h-BN and Graphene: vdW-Corrected DFT Calculations," *The Journal of Physical Chemistry C*, vol. 117, no. 26, pp. 13435–13441, 2013.

[44] D. Le, A. Kara, E. Schröder, P. Hyldgaard, and T. S. Rahman, "Physisorption of nucleobases on graphene: a comparative van der Waals study," *Journal of Physics: Condensed Matter*, vol. 24, no. 42, p. 424210, 2012.

[45] Y. Cho, S. K. Min, J. Yun, W. Y. Kim, A. Tkatchenko, and K. S. Kim, "Noncovalent Interactions of DNA Bases with Naphthalene and Graphene," *Journal of Chemical Theory and Computation*, vol. 9, no. 0, pp. 2090–2096, 2013.

[46] H. Vovusha, S. Sanyal, and B. Sanyal, "Interaction of nucleobases and aromatic amino acids with graphene oxide and graphene flakes," *The Journal of Physical Chemistry Letters*, vol. 4, no. 21, pp. 3710–3718, 2013.

[47] A. N. Enyashin, S. Gemming, and G. Seifert, "DNA-wrapped carbon nanotubes," *Nanotechnology*, vol. 18, no. 24, p. 245702, 2007.

[48] S. Stepanian, M. Karachevtsev, A. Glamazda, V. Karachevtsev, and L. Adamowicz, "Stacking interaction of cytosine with carbon nanotubes: MP2, DFT and Raman spectroscopy study," *Chemical Physics Letters*, vol. 459, no. 1–6, pp. 153–158, 2008.

[49] M. Shukla, M. Dubey, E. Zakar, R. Namburu, Z. Czyznikowska, and J. Leszczynski, "Interaction of nucleic acid bases with single-walled carbon nanotube," *Chemical Physics Letters*, vol. 480, no. 4–6, pp. 269–272, 2009.

[50] B. Akdim, R. Pachter, P. N. Day, S. S. Kim, and R. R. Naik, "On modeling biomolecular–surface nonbonded interactions: application to nucleobase adsorption on single-wall carbon nanotube surfaces," *Nanotechnology*, vol. 23, no. 16, p. 165703, 2012.

[51] A. Ramraj, I. H. Hillier, M. A. Vincent, and N. A. Burton, "Assessment of approximate quantum chemical methods for calculating the interaction energy of nucleic acid bases with graphene and carbon nanotubes," *Chemical Physics Letters*, vol. 484, no. 4–6, pp. 295–298, 2010.

[52] D. Umadevi and G. N. Sastry, "Quantum Mechanical Study of Physisorption of Nucleobases on Carbon Materials: Graphene versus Carbon Nanotubes," *The Journal of Physical Chemistry Letters*, vol. 2, no. 13, pp. 1572–1576, 2011.

[53] A. Sarmah and R. K. Roy, "Understanding the interaction of nucleobases with chiral semiconducting single-walled carbon nanotubes: An alternative theoretical approach based on density functional reactivity theory," *The Journal of Physical Chemistry C*, vol. 117, no. 41, pp. 21539–21550, 2013.

[54] M. Chehel Amirani, T. Tang, and J. Cuervo, "Quantum mechanical treatment of binding energy between DNA nucleobases and carbon nanotube: A DFT

analysis," *Physica E: Low-dimensional Systems and Nanostructures*, vol. 54, pp. 65–71, 2013.

[55] M. Chehel Amirani and T. Tang, "A QM:MM model for the interaction of DNA nucleotides with carbon nanotubes," *Phys. Chem. Chem. Phys.*, vol. 17, pp. 7564–7575, 2015.

[56] A. L. Frischknecht and M. G. Martin, "Simulation of the adsorption of nucleotide monophosphates on carbon nanotubes in aqueous solution," *The Journal of Physical Chemistry C*, vol. 112, no. 16, pp. 6271–6278, 2008.

[57] A. Lehninger, D. Nelson, and M. Cox, *Lehninger Principles of Biochemistry*. W. H. Freeman, 2005.

[58] D. M. Boghaei and M. Gharagozlou, "Charge transfer complexes of adenosine-5′-monophosphate and cytidine-5′-monophosphate with water-soluble cobalt(ii) schiff base complexes in aqueous solution," *Spectrochimica Acta Part A: Molecular and Biomolecular Spectroscopy*, vol. 63, no. 1, pp. 139 – 148, 2006.

[59] M. J. Frisch, G. W. Trucks, H. B. Schlegel, G. E. Scuseria, M. A. Robb, J. R. Cheeseman, G. Scalmani, V. Barone, B. Mennucci, G. A. Petersson, H. Nakatsuji, M. Caricato, X. Li, H. P. Hratchian, A. F. Izmaylov, J. Bloino, G. Zheng, J. L. Sonnenberg, M. Hada, M. Ehara, K. Toyota, R. Fukuda, J. Hasegawa, M. Ishida, T. Nakajima, Y. Honda, O. Kitao, H. Nakai, T. Vreven, J. J. A. Montgomery, J. E. Peralta, F. Ogliaro, M. Bearpark, J. J. Heyd, E. Brothers, K. N. Kudin, V. N. Staroverov, R. Kobayashi, J. Normand, K. Raghavachari, A. Rendell, J. C. Burant, S. S. Iyengar,

J. Tomasi, M. Cossi, N. Rega, J. M. Millam, M. Klene, J. E. Knox, J. B. Cross, V. Bakken, C. Adamo, J. Jaramillo, R. Gomperts, R. E. Stratmann, O. Yazyev, A. J. Austin, R. Cammi, C. Pomelli, J. W. Ochterski, R. L. Martin, K. Morokuma, V. G. Zakrzewski, G. A. Voth, P. Salvador, J. J. Dannenberg, S. Dapprich, A. D. Daniels, Ö. Farkas, J. B. Foresman, J. V. Ortiz, J. Cioslowski, and D. J. Fox, "Gaussian 09 Revision A.1." Gaussian Inc. Wallingford CT 2009.

[60] E. Lindahl, B. Hess, and D. van der Spoel, "Gromacs 3.0: a package for molecular simulation and trajectory analysis," *Molecular modeling annual*, vol. 7, no. 8, pp. 306–317, 2001.

[61] C. I. Bayly, P. Cieplak, W. Cornell, and P. A. Kollman, "A well-behaved electrostatic potential based method using charge restraints for deriving atomic charges: the resp model," *The Journal of Physical Chemistry*, vol. 97, no. 40, pp. 10269–10280, 1993.

[62] D. Case, T. Darden, T. C. III, C. Simmerling, J. Wang, R. Duke, R. Luo, R. Walker, W. Zhang, K. Merz, B. Roberts, S. Hayik, A. Roitberg, G. Seabra, J. Swails, A. GÖtz, I. Kolossváry, K. Wong, F. Paesani, J. Vanicek, R. Wolf, J. Liu, X. Wu, S. Brozell, T. Steinbrecher, H. Gohlke, Q. Cai, X. Ye, J. Wang, M. Hsieh, G. Cui, D. Roe, D. Mathews, M. Seetin, R. Salomon-Ferrer, C. Sagui, V. Babin, T. Luchko, S. Gusarov, A. Kovalenko, and P. Kollman, "AmberTools13." University of California, San Francisco 2012.

[63] V. Barone and M. Cossi, "Quantum calculation of molecular energies and

energy gradients in solution by a conductor solvent model," *The Journal of Physical Chemistry A*, vol. 102, no. 11, pp. 1995–2001, 1998.

[64] A. Pullman and B. Pullman, "Molecular electrostatic potential of the nucleic acids.," *Quarterly Reviews of Biophysics*, vol. 14, no. 3, pp. 289–380, 1981.

[65] A. Pullman, B. Pullman, and R. Lavery, "Molecular electrostatic potential versus field. significance for dna and its constituents.," *Journal of Molecular Structure: THEOCHEM*, vol. 93, no. 0, pp. 85 – 91, 1983. Proceedings of the XIIIth Congress of Theoretical Chemists of Latin Expression.

[66] P. P, L. P. R, and J. K, "Molecular electrostatic potentials: an effective tool for the elucidation of biochemical phenomena.," *Environmental Health Perspectives*, vol. 61, pp. 191–202, 1985.

[67] A. Das, A. Sood, P. K. Maiti, M. Das, R. Varadarajan, and C. Rao, "Binding of nucleobases with single-walled carbon nanotubes: Theory and experiment," *Chemical Physics Letters*, vol. 453, no. 4–6, pp. 266–273, 2008.

[68] A. v. d. Vaart and K. M. Merz, Jr., "Charge transfer in biologically important molecules: comparison of high-level ab initio and semiempirical methods," *International Journal of Quantum Chemistry*, vol. 77, no. 1, pp. 27–43, 2000.

[69] Z. Maksić and J. Ángyán, *Theoretical Treatment of Large Molecules and Their Interactions*. International Series in Heat and Mass Transfer, Springer-Verlag, 1991.

[70] J. Lu, S. Nagase, X. Zhang, D. Wang, M. Ni, Y. Maeda, T. Wakahara,

T. Nakahodo, T. Tsuchiya, T. Akasaka, Z. Gao, D. Yu, H. Ye, W. N. Mei, and Y. Zhou, "Selective interaction of large or charge-transfer aromatic molecules with metallic single-wall carbon nanotubes: Critical role of the molecular size and orientation," *Journal of the American Chemical Society*, vol. 128, no. 15, pp. 5114–5118, 2006.

[71] O. Leenaerts, B. Partoens, and F. M. Peeters, "Adsorption of h_2O, Nh_3, co, No_2, and no on graphene: A first-principles study," *Phys. Rev. B*, vol. 77, p. 125416, 2008.

References for Chapter 6

[1] R. Singh, D. Pantarotto, D. McCarthy, O. Chaloin, J. Hoebeke, C. D. Partidos, J.-P. Briand, M. Prato, A. Bianco, and K. Kostarelos, "Binding and Condensation of Plasmid DNA onto Functionalized Carbon Nanotubes: Toward the Construction of Nanotube-Based Gene Delivery Vectors," *Journal of the American Chemical Society*, vol. 127, no. 12, pp. 4388–4396, 2005.

[2] C. Hu, Y. Zhang, G. Bao, Y. Zhang, M. Liu, and Z. L. Wang, "DNA Functionalized Single-Walled Carbon Nanotubes for Electrochemical Detection," *The Journal of Physical Chemistry B*, vol. 109, no. 43, pp. 20072–20076, 2005.

[3] Y. Ma, S. R. Ali, A. S. Dodoo, and H. He, "Enhanced Sensitivity for Biosensors: Multiple Functions of DNA-Wrapped Single-Walled Carbon Nanotubes in Self-Doped Polyaniline Nanocomposites," *The Journal of Physical Chemistry B*, vol. 110, no. 33, pp. 16359–16365, 2006.

[4] P. He and M. Bayachou, "Layer-by-Layer Fabrication and Characterization of DNA-Wrapped Single-Walled Carbon Nanotube Particles," *Langmuir*, vol. 21, no. 13, pp. 6086–6092, 2005.

[5] S. Wang, R. Wang, P. J. Sellin, and S. Chang, "Carbon nanotube based dna biosensor for rapid detection of anti-cancer drug of cyclophosphamide," *Current Nanoscience*, vol. 5, no. 3, pp. 312–317, 2009.

[6] M. Zheng, A. Jagota, E. D. Semke, B. A. Diner, R. S. Mclean, S. R. Lustig, R. E. Richardson, and N. G. Tassi, "DNA-assisted dispersion and separation of carbon nanotubes," *Nat Mater*, vol. 2, no. 5, pp. 338–342, 2003.

[7] M. Chehel Amirani and T. Tang, "A QM:MM model for the interaction of DNA nucleotides with carbon nanotubes," *Phys. Chem. Chem. Phys.*, vol. 17, pp. 7564–7575, 2015.

[8] D. M. Boghaei and M. Gharagozlou, "Charge transfer complexes of adenosine-5′-monophosphate and cytidine-5′-monophosphate with water-soluble cobalt(ii) schiff base complexes in aqueous solution," *Spectrochimica Acta Part A: Molecular and Biomolecular Spectroscopy*, vol. 63, no. 1, pp. 139 – 148, 2006.

[9] A. L. Frischknecht and M. G. Martin, "Simulation of the adsorption of nucleotide monophosphates on carbon nanotubes in aqueous solution," *The Journal of Physical Chemistry C*, vol. 112, no. 16, pp. 6271–6278, 2008.

[10] A. Lehninger, D. Nelson, and M. Cox, *Lehninger Principles of Biochemistry*. W. H. Freeman, 2005.

[11] M. J. Frisch, G. W. Trucks, H. B. Schlegel, G. E. Scuseria, M. A. Robb, J. R. Cheeseman, G. Scalmani, V. Barone, B. Mennucci, G. A. Petersson, H. Nakatsuji, M. Caricato, X. Li, H. P. Hratchian, A. F. Izmaylov, J. Bloino, G. Zheng, J. L. Sonnenberg, M. Hada, M. Ehara, K. Toyota, R. Fukuda, J. Hasegawa, M. Ishida, T. Nakajima, Y. Honda, O. Kitao, H. Nakai, T. Vreven, J. J. A. Montgomery, J. E. Peralta, F. Ogliaro, M. Bearpark, J. J. Heyd, E. Brothers, K. N. Kudin, V. N. Staroverov, R. Kobayashi, J. Normand, K. Raghavachari, A. Rendell, J. C. Burant, S. S. Iyengar, J. Tomasi, M. Cossi, N. Rega, J. M. Millam, M. Klene, J. E. Knox, J. B. Cross, V. Bakken, C. Adamo, J. Jaramillo, R. Gomperts, R. E. Stratmann, O. Yazyev, A. J. Austin, R. Cammi, C. Pomelli, J. W. Ochterski, R. L. Martin, K. Morokuma, V. G. Zakrzewski, G. A. Voth, P. Salvador, J. J. Dannenberg, S. Dapprich, A. D. Daniels, Ö. Farkas, J. B. Foresman, J. V. Ortiz, J. Cioslowski, and D. J. Fox, "Gaussian 09 Revision A.1." Gaussian Inc. Wallingford CT 2009.

[12] D. Case, J. Berryman, R. Betz, D. Cerutti, T. Cheatham, III, T. Darden, R. Duke, T. Giese, H. Gohlke, A. Goetz, N. Homeyer, S. Izadi, P. Janowski, J. Kaus, A. Kovalenko, T. Lee, S. LeGrand, P. Li, T. Luchko, R. Luo, B. Madej, K. Merz, G. Monard, P. Needham, H. Nguyen, H. Nguyen, I. Omelyan, A. Onufriev, D. Roe, A. Roitberg, R. Salomon-Ferrer, C. Simmerling, W. Smith, J. Swails, R. Walker, J. Wang, R. Wolf, X. Wu, D. York, and P. Kollman, "Ambertools 14," 2014. University of California, San Francisco.

[13] J. Wang, R. M. Wolf, J. W. Caldwell, P. A. Kollman, and D. A. Case, "Devel-

opment and testing of a general amber force field," *Journal of Computational Chemistry*, vol. 25, no. 9, pp. 1157–1174, 2004.

[14] D. Case, J. Berryman, R. Betz, D. Cerutti, T. Cheatham, III, T. Darden, R. Duke, T. Giese, H. Gohlke, A. Goetz, N. Homeyer, S. Izadi, P. Janowski, J. Kaus, A. Kovalenko, T. Lee, S. LeGrand, P. Li, T. Luchko, R. Luo, B. Madej, K. Merz, G. Monard, P. Needham, H. Nguyen, H. Nguyen, I. Omelyan, A. Onufriev, D. Roe, A. Roitberg, R. Salomon-Ferrer, C. Simmerling, W. Smith, J. Swails, R. Walker, J. Wang, R. Wolf, X. Wu, D. York, and P. Kollman, "Amber 14." AMBER 2015, University of California, San Francisco.

[15] M. Chehel Amirani and T. Tang, "Electrostatics of dna nucleotides-carbon nanotube hybrids evaluated from qm:mm simulations," *Nanoscale*, 2015. Accepted.

[16] R. Car and M. Parrinello, "Unified approach for molecular dynamics and density-functional theory," *Phys. Rev. Lett.*, vol. 55, pp. 2471–2474, 1985.

[17] P. E. M. Lopes, J. Huang, J. Shim, Y. Luo, H. Li, B. Roux, and J. Alexander D. MacKerell, "Polarizable force field for peptides and proteins based on the classical drude oscillator," *Journal of Chemical Theory and Computation*, vol. 9, no. 12, pp. 5430–5449, 2013.

References for Chapter 7

[1] M. Zheng, A. Jagota, E. D. Semke, B. A. Diner, R. S. Mclean, S. R. Lustig, R. E. Richardson, and N. G. Tassi, "DNA-assisted dispersion and separation of carbon nanotubes," *Nat Mater*, vol. 2, no. 5, pp. 338–342, 2003.

[2] M. Zheng, A. Jagota, M. S. Strano, A. P. Santos, P. Barone, S. G. Chou, B. A. Diner, M. S. Dresselhaus, R. S. Mclean, G. B. Onoa, G. G. Samsonidze, E. D. Semke, M. Usrey, and D. J. Walls, "Structure-Based Carbon Nanotube Sorting by Sequence-Dependent DNA Assembly," *Science*, vol. 302, no. 5650, pp. 1545–1548, 2003.

[3] X. Tu, S. Manohar, A. Jagota, and M. Zheng, "DNA sequence motifs for structure-specific recognition and separation of carbon nanotubes," *Nat Mater*, vol. 460, no. 7252, pp. 250–253, 2009.

[4] P. K. Brahman, R. A. Dar, and K. S. Pitre, "DNA-functionalized electrochemical biosensor for detection of vitamin {B1} using electrochemically treated multiwalled carbon nanotube paste electrode by voltammetric methods ," *Sensors and Actuators B: Chemical*, vol. 177, no. 0, pp. 807 – 812, 2013.

[5] S. Wang, R. Wang, P. J. Sellin, and S. Chang, "Carbon nanotube based dna biosensor for rapid detection of anti-cancer drug of cyclophosphamide," *Current Nanoscience*, vol. 5, no. 3, pp. 312–317, 2009.

[6] E. Katz and I. Willner, "Biomolecule-Functionalized Carbon Nanotubes:

Applications in Nanobioelectronics," *ChemPhysChem*, vol. 5, no. 8, pp. 1084–1104, 2004.

[7] M. Prato, K. Kostarelos, and A. Bianco, "Functionalized Carbon Nanotubes in Drug Design and Discovery," *Accounts of Chemical Research*, vol. 41, no. 1, pp. 60–68, 2008.

[8] M. Shukla, M. Dubey, E. Zakar, R. Namburu, Z. Czyznikowska, and J. Leszczynski, "Interaction of nucleic acid bases with single-walled carbon nanotube," *Chemical Physics Letters*, vol. 480, no. 4–6, pp. 269–272, 2009.

[9] S. R. Lustig, A. Jagota, C. Khripin, and M. Zheng, "Theory of Structure-Based Carbon Nanotube Separations by Ion-Exchange Chromatography of DNA/CNT Hybrids," *The Journal of Physical Chemistry B*, vol. 109, no. 7, pp. 2559–2566, 2005.

[10] D. Roxbury, A. Jagota, and J. Mittal, "Structural Characteristics of Oligomeric DNA Strands Adsorbed onto Single-Walled Carbon Nanotubes," *The Journal of Physical Chemistry B*, vol. 117, no. 1, pp. 132–140, 2013.

[11] X. Tu and M. Zheng, "A DNA-based approach to the carbon nanotube sorting problem," *Nano Research*, vol. 1, pp. 185–194, 2008.

[12] A. L. Frischknecht and M. G. Martin, "Simulation of the adsorption of nucleotide monophosphates on carbon nanotubes in aqueous solution," *The Journal of Physical Chemistry C*, vol. 112, no. 16, pp. 6271–6278, 2008.

Appendix A

Supplementary figures for Chapter 3

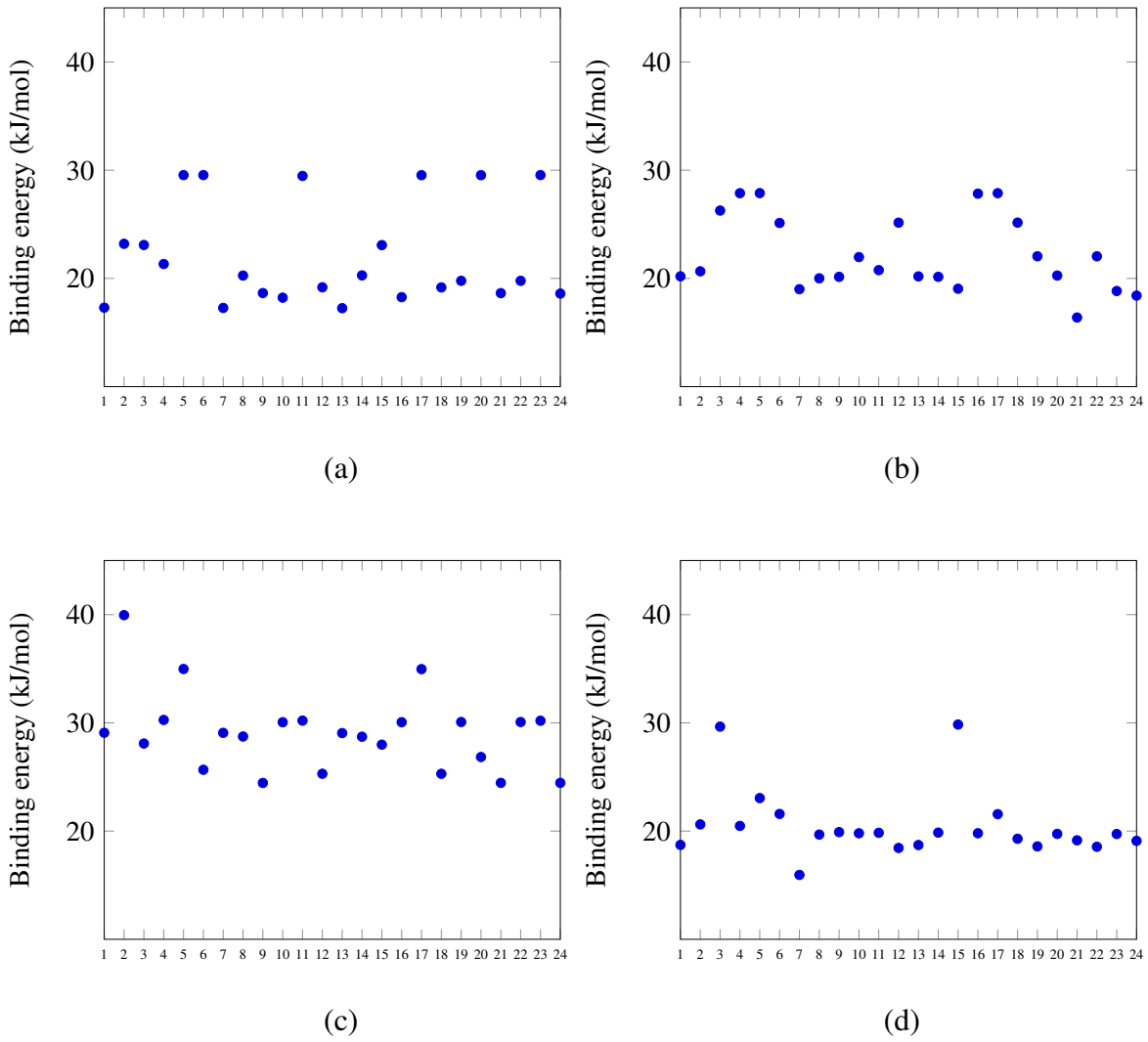

Figure A.1: Binding energies for: (a) A-CNT, (b) C-CNT, (c) G-CNT, and (d) T-CNT obtained from 24 simulations for each hybrid. Horizontal axis in each subfigure represents the indices for the 24 initial configurations.

Appendix B

Supplementary figures for Chapter 4

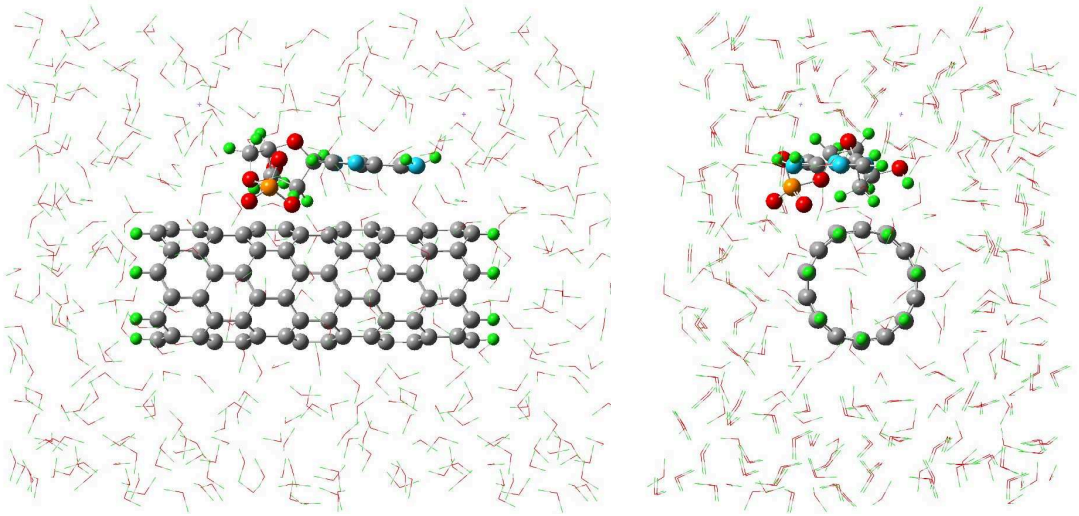

(a)

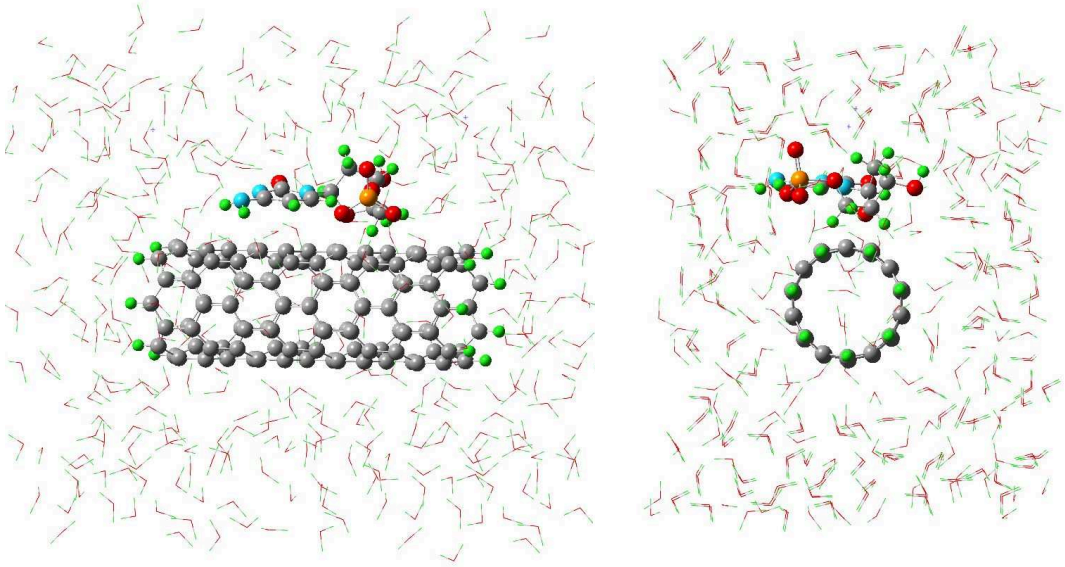

(b)

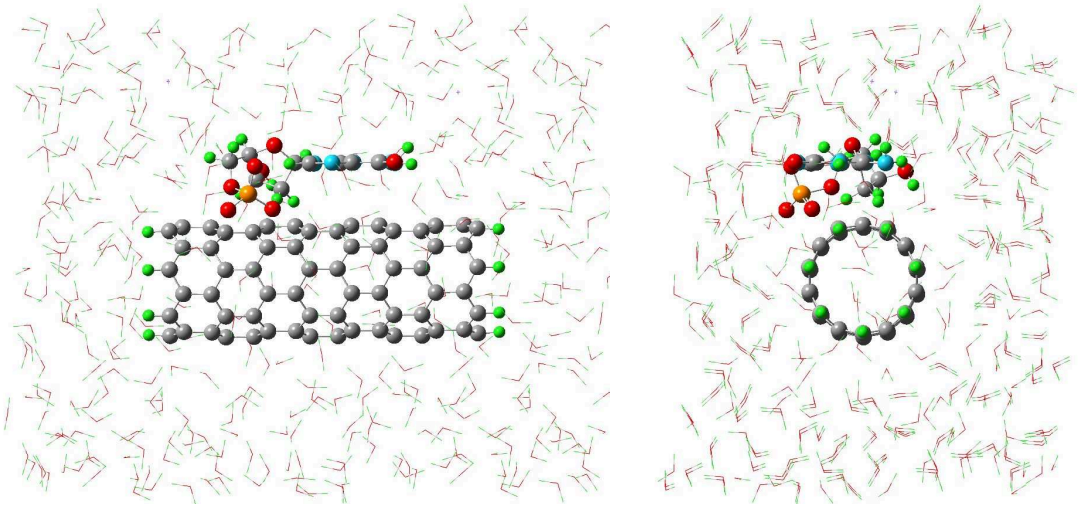

(c)

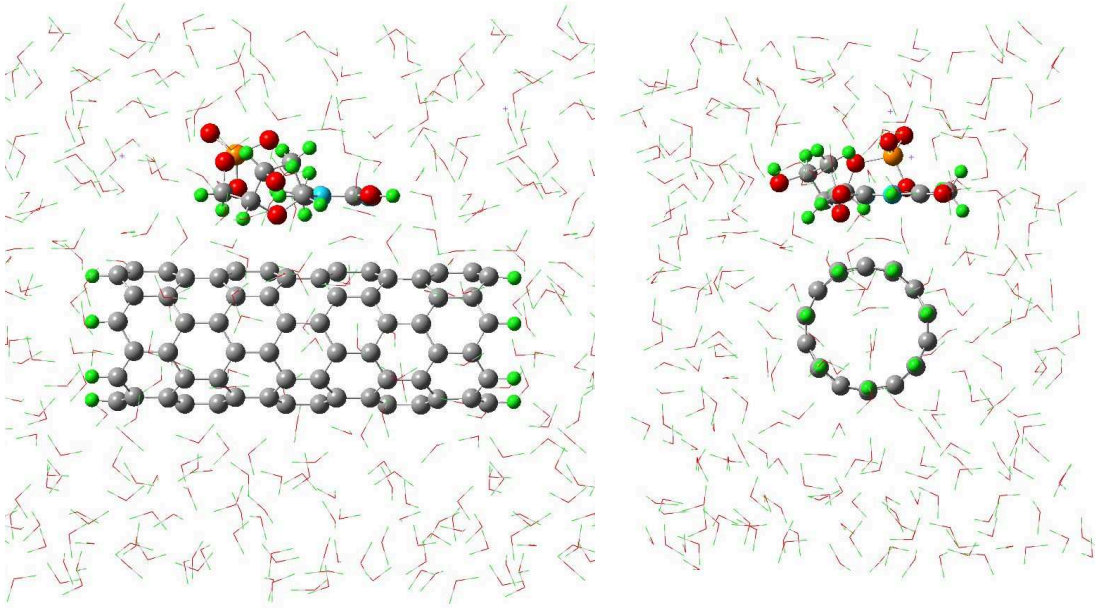

(d)

Figure B.1: Initial configuration of NMP-CNT systems in solution: (a) AMP-(7,0) CNT, (b) CMP-(7,0) CNT, (c) GMP-(7,0) CNT, and (d) TMP-(7,0) CNT; left and right figures are receptively front and side view.

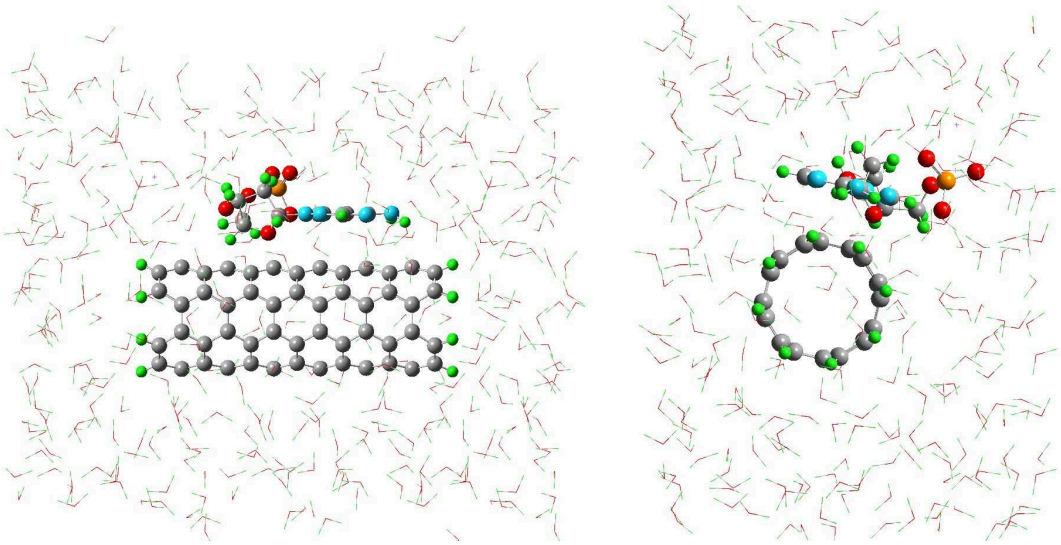

(a)

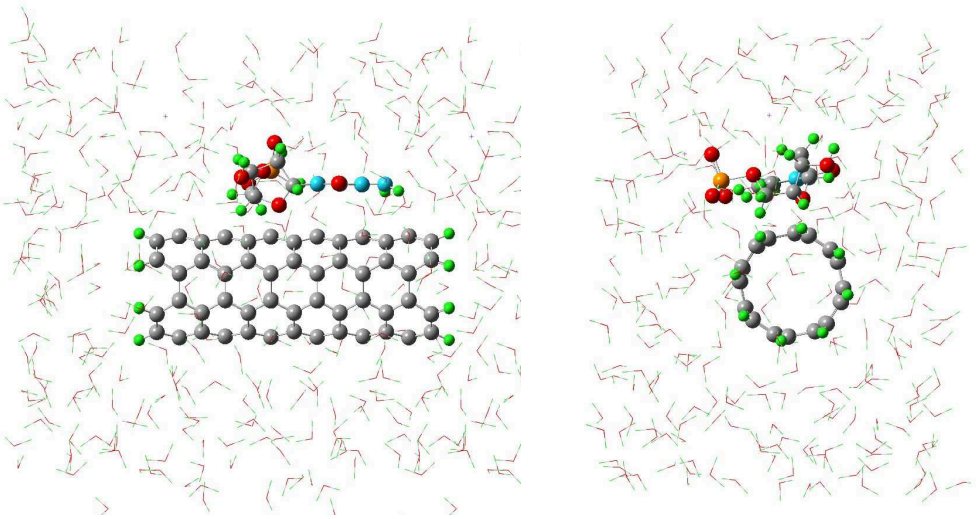

(b)

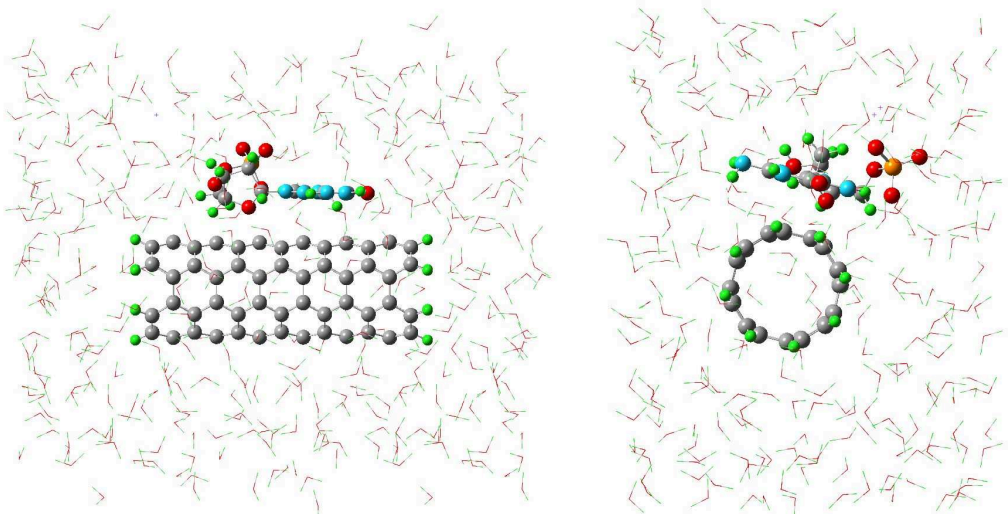

(c)

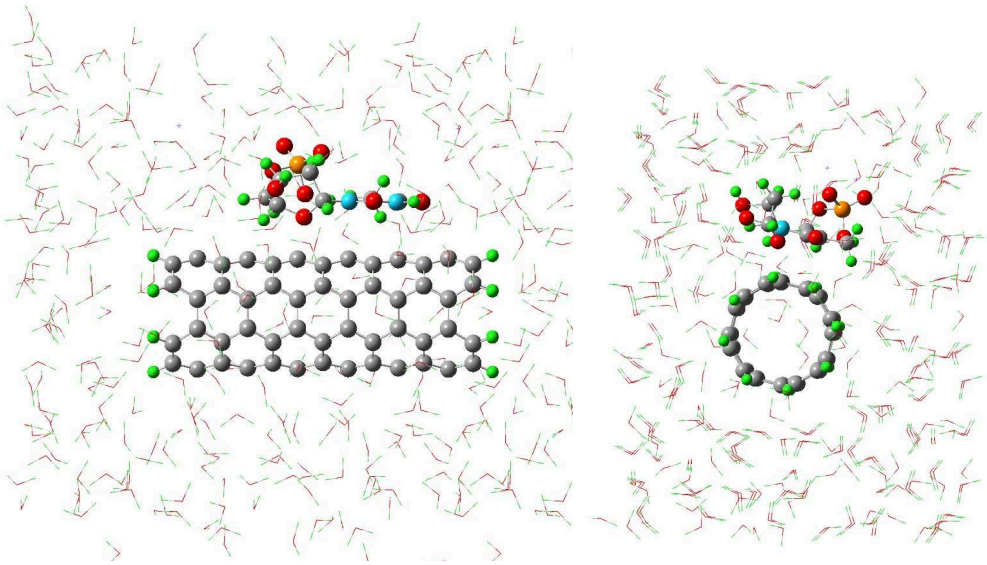

(d)

Figure B.2: Initial configuration of NMP-CNT systems in solution: (a) AMP-(4,4) CNT, (b) CMP-(4,4) CNT, (c) GMP-(4,4) CNT, and (d) TMP-(4,4) CNT; left and right figures are receptively front and side view.

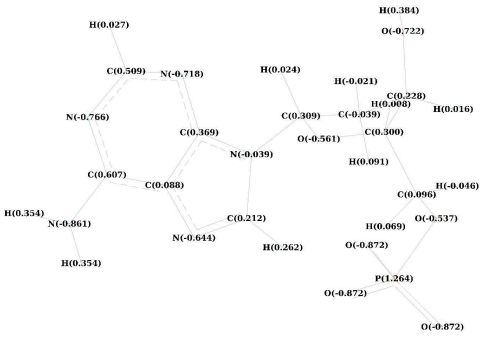
H(0.384)
O(-0.722)
H(0.027)
C(0.509)
N(-0.718)
H(0.024)
H(-0.021)
C(0.228)
H(0.008)
H(0.016)
N(-0.766)
C(0.309)
C(-0.039)
C(0.369)
O(-0.561)
C(0.300)
N(-0.039)
H(0.091)
C(0.607)
C(0.088)
C(0.096)
H(-0.046)
H(0.354)
N(-0.861)
C(0.212)
O(-0.537)
H(0.069)
N(-0.644)
H(0.262)
O(-0.872)
H(0.354)
P(1.264)
O(-0.872)
O(-0.872)

(a)

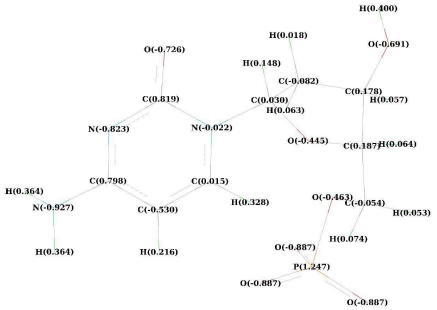
H(0.400)
O(-0.691)
H(0.018)
O(-0.726)
H(0.148)
C(-0.082)
C(0.178)
H(0.057)
C(0.819)
C(0.030)
H(0.063)
N(-0.823)
N(-0.022)
O(-0.445)
C(0.187)
H(0.064)
C(0.798)
C(0.015)
H(0.364)
O(-0.463)
C(-0.054)
N(-0.927)
C(-0.530)
H(0.328)
H(0.053)
H(0.364)
H(0.216)
H(0.074)
O(-0.887)
P(1.247)
O(-0.887)
O(-0.887)

(b)

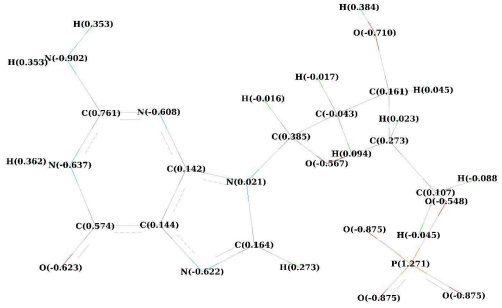
H(0.384)
O(-0.710)
H(0.353)
N(-0.902)
H(0.353)
H(-0.017)
C(0.161)
H(0.045)
H(-0.016)
C(0.761)
N(-0.608)
C(-0.043)
H(0.023)
C(0.385)
C(0.273)
H(0.094)
H(0.362)
N(-0.637)
O(-0.567)
C(0.142)
N(0.021)
H(-0.088
C(0.107)
O(-0.548)
C(0.574)
C(0.144)
O(-0.875)
H(-0.045)
C(0.164)
O(-0.623)
N(-0.622)
H(0.273)
P(1.271)
O(-0.875)
O(-0.875)

(c)

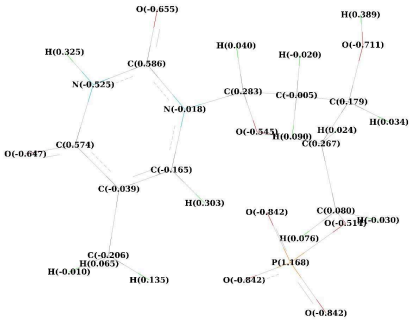
O(-0.655)
H(0.389)
H(0.325)
C(0.586)
H(0.040)
H(-0.020)
O(-0.711)
N(-0.525)
C(0.283)
C(-0.005)
C(0.179)
N(-0.018)
H(0.034)
O(-0.545)
H(0.090)
H(0.024)
C(0.267)
C(0.574)
O(-0.647)
C(-0.165)
C(-0.039)
H(0.303)
O(-0.842)
C(0.080)
O(-0.531)
H(-0.030)
H(0.076)
C(-0.206)
H(0.065)
P(1.168)
H(-0.010)
H(0.135)
O(-0.842)
O(-0.842)

(d)

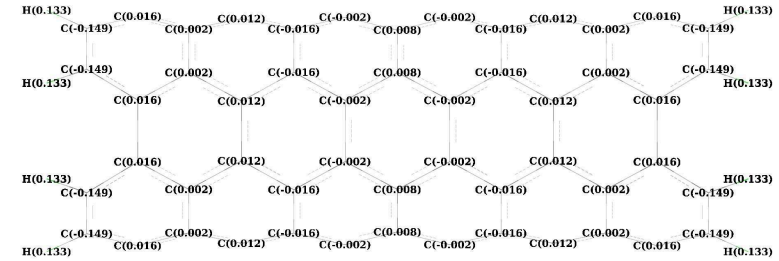

(e)

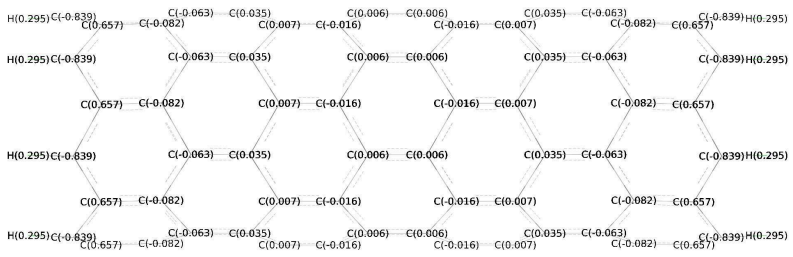

(f)

Figure B.3: Atomic partial charges: (a) AMP, (b) CMP, (c) GMP, (d) TMP, (e) (4,4) CNT, and (f) (7,0) CNT.

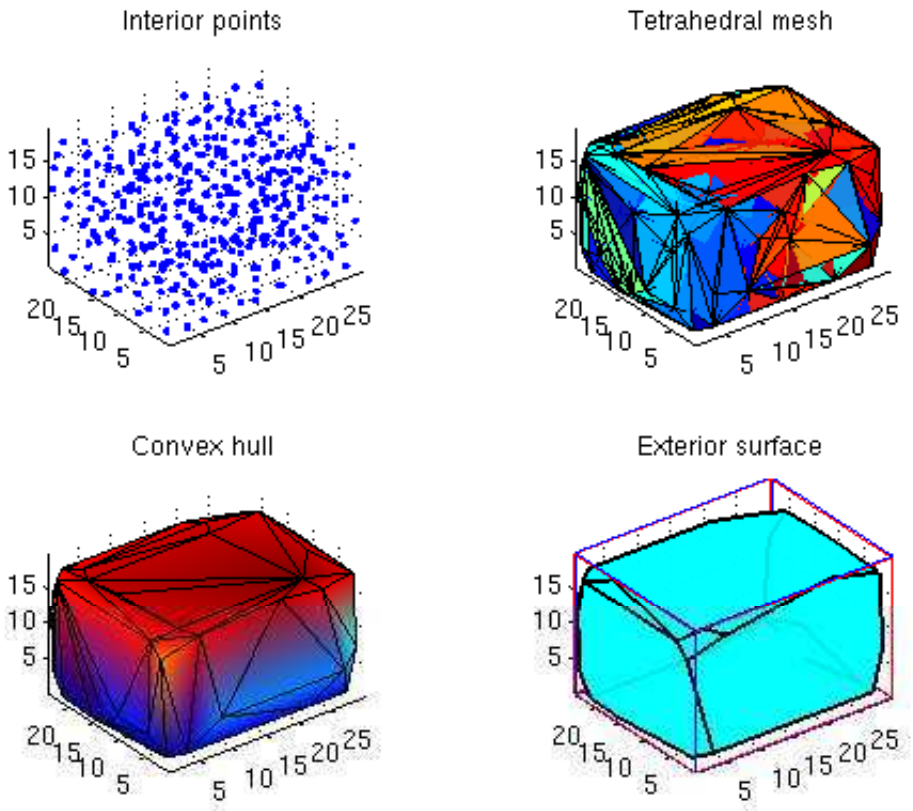

Figure B.4: Interior points, 3D mesh (Tetrahedral mesh), exterior mesh (Convex hull), and exterior surface for AMP-(4,4) CNT hybrid.

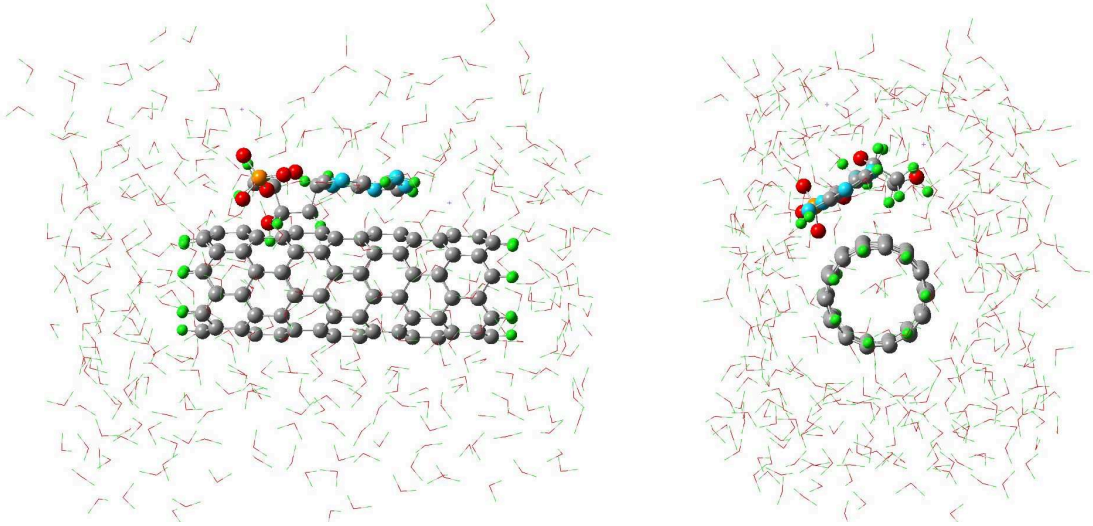

(a)

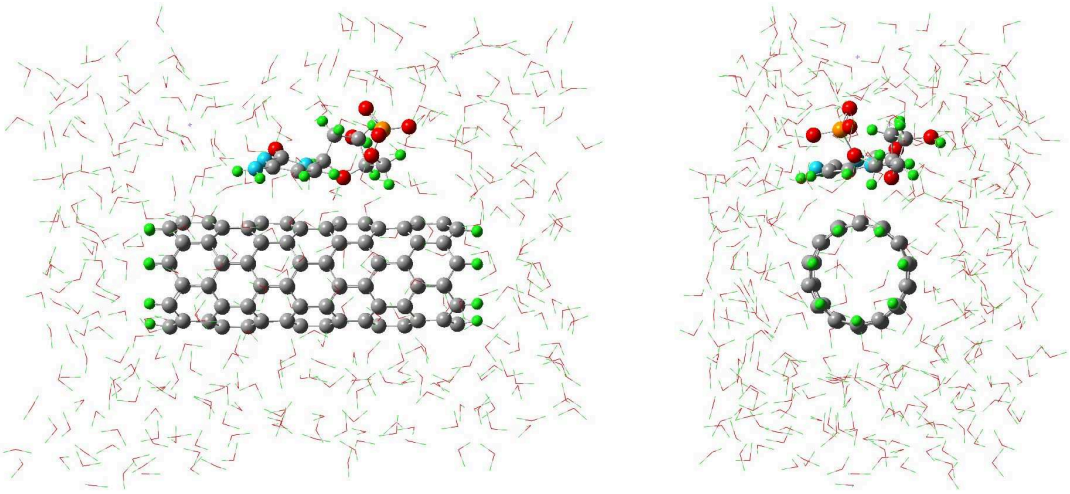

(b)

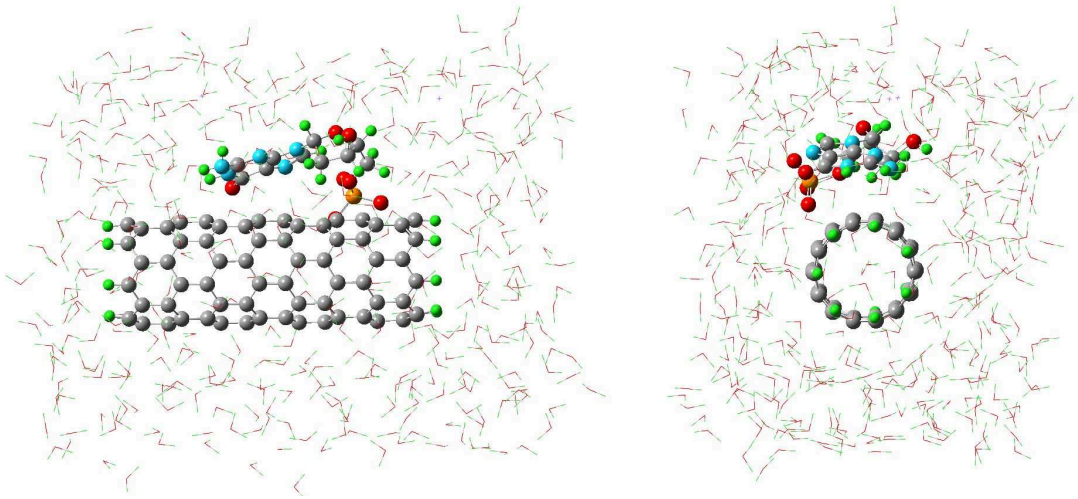

(c)

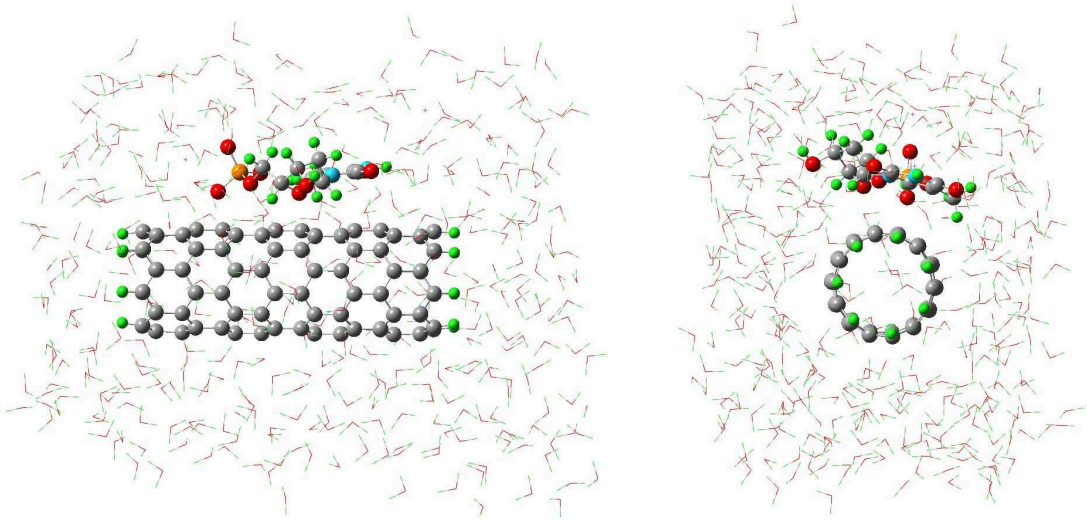

(d)

Figure B.5: Final optimized configuration of NMP-CNT systems in solution: (a) AMP-(7,0) CNT, (b) CMP-(7,0) CNT, (c) GMP-(7,0) CNT, and (d) TMP-(7,0) CNT; left and right figures are respectively front and side view.

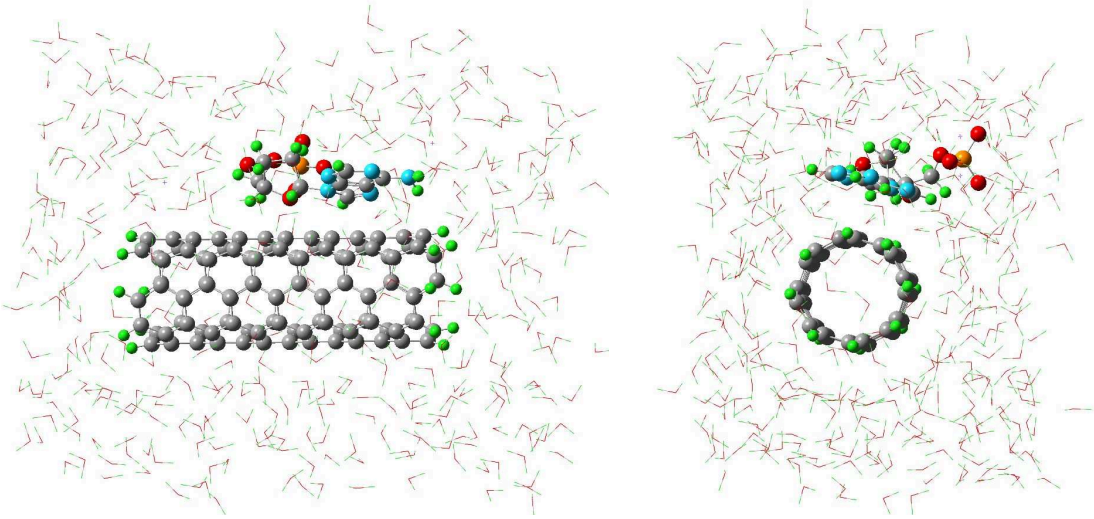

(a)

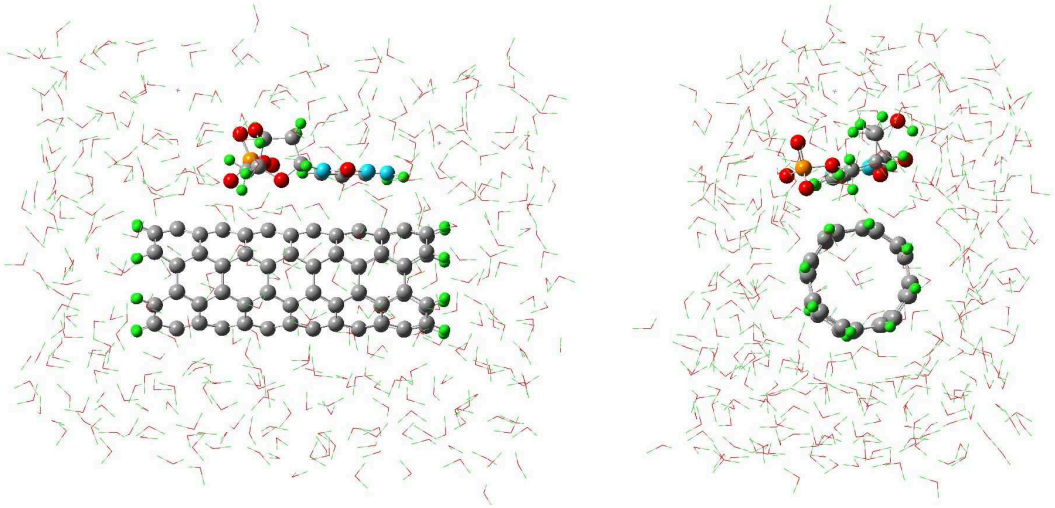

(b)

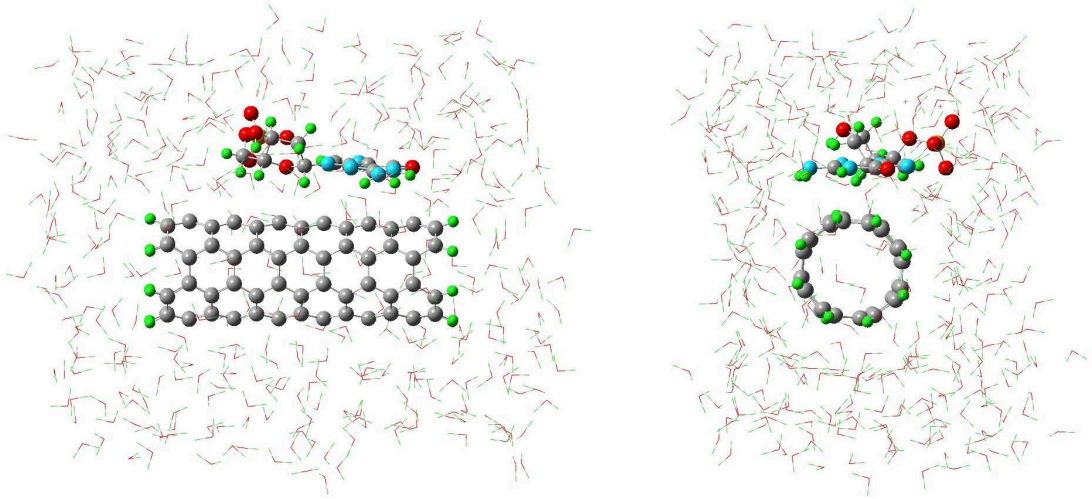

(c)

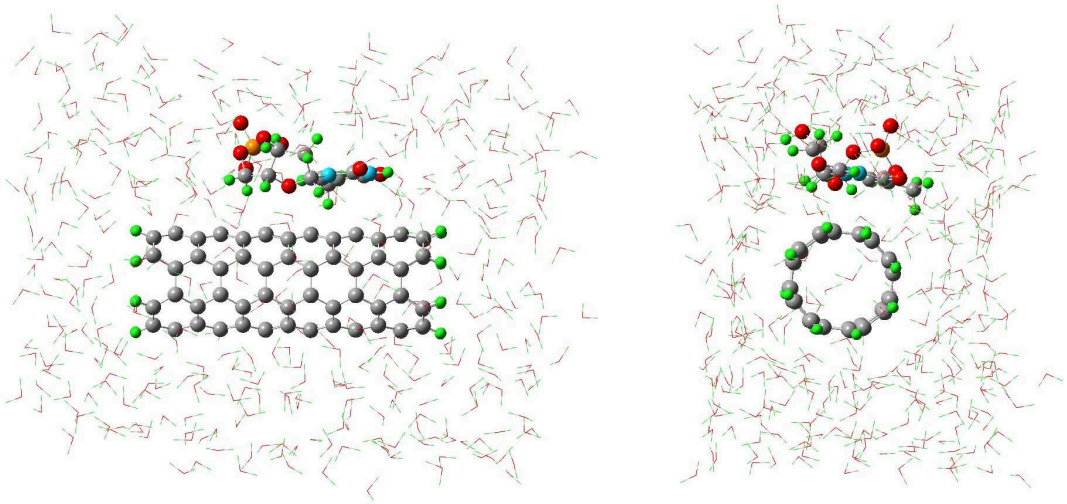

(d)

Figure B.6: Final optimized configuration of NMP-CNT systems in solution: (a) AMP-(4,4) CNT, (b) CMP-(4,4) CNT, (c) GMP-(4,4) CNT, and (d) TMP-(4,4) CNT; left and right figures are respectively front and side view.

Appendix C

Supplementary figures for Chapter 5

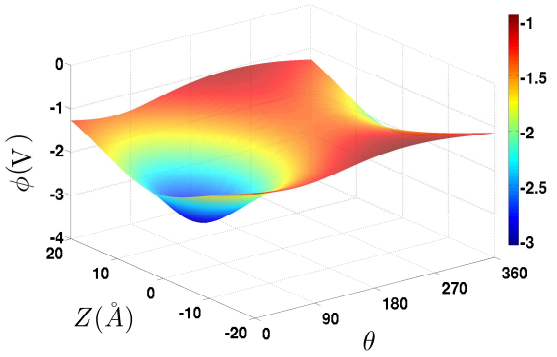

(a) AMP-(7,0) CNT

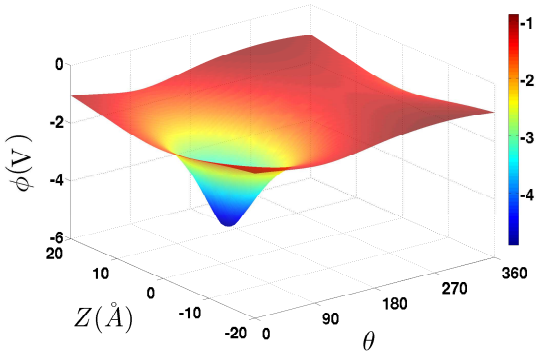

(b) AMP-(4,4)CNT

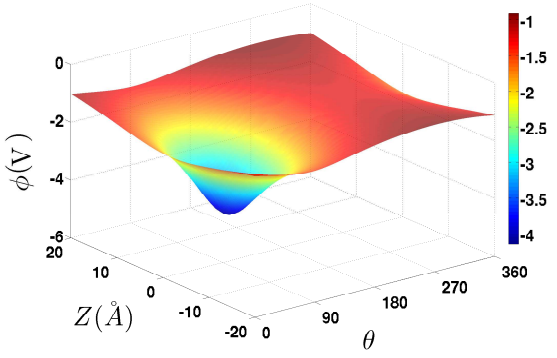

(c) CMP-(7,0) CNT

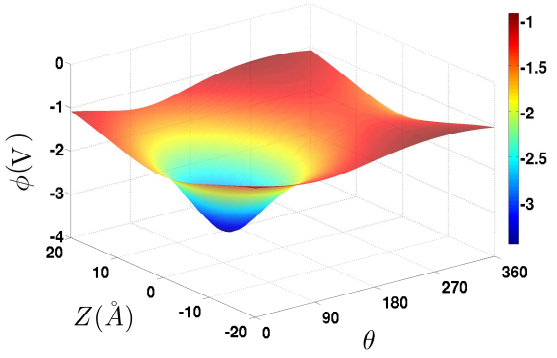

(d) CMP-(4,4)CNT

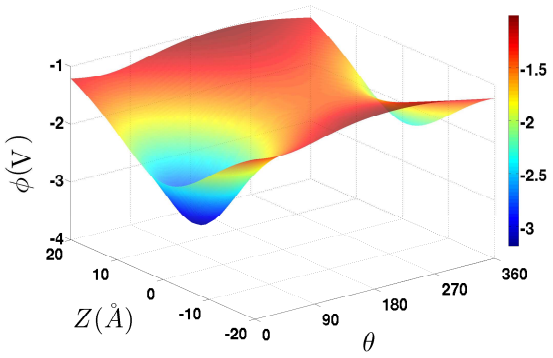

(e) GMP-(7,0) CNT

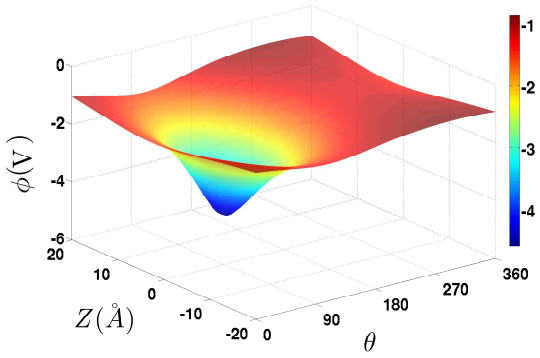

(f) GMP-(4,4) CNT

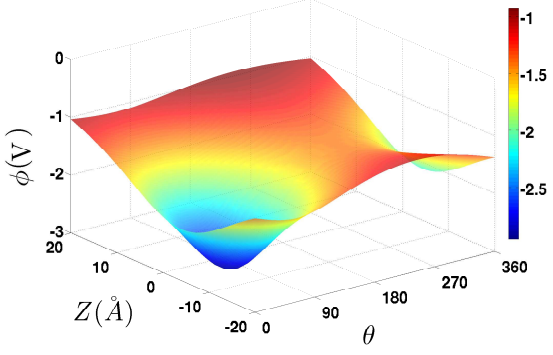

(g) TMP-(7,0) CNT

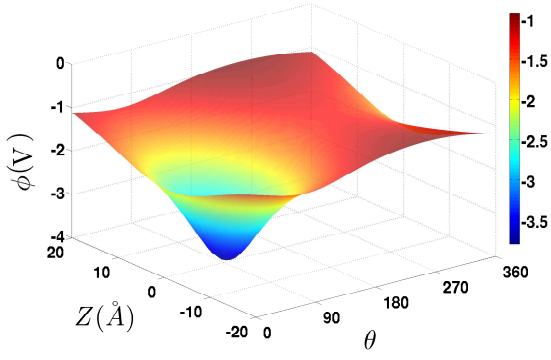

(h) TMP-(4,4) CNT

Figure C.1: Distribution of the electrostatic potential ϕ as a function of Z and θ. The radial distance is fixed at r=15 Å.

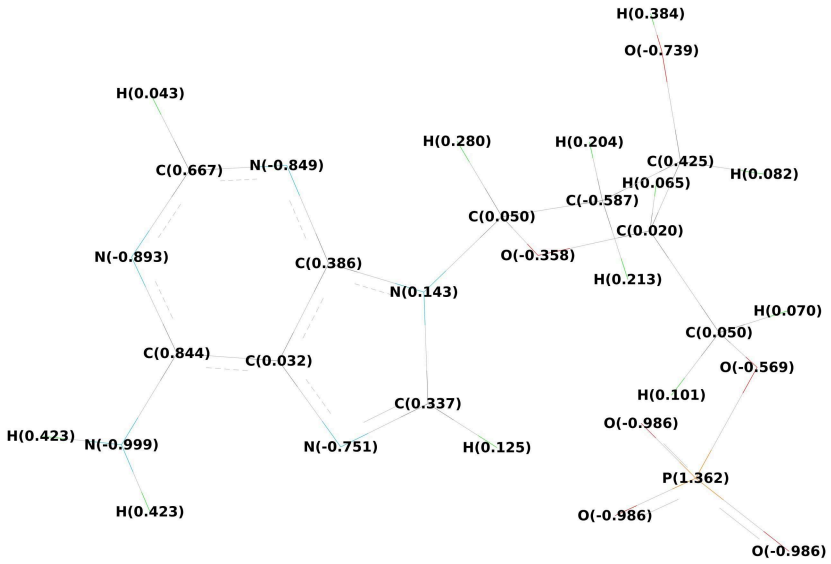
H(0.384)
O(-0.739)
H(0.043)
H(0.280)
H(0.204)
C(0.667)
N(-0.849)
C(0.425)
H(0.082)
H(0.065)
C(-0.587)
C(0.050)
C(0.020)
N(-0.893)
C(0.386)
O(-0.358)
H(0.213)
N(0.143)
H(0.070)
C(0.050)
C(0.844)
C(0.032)
O(-0.569)
H(0.101)
C(0.337)
O(-0.986)
H(0.423)
N(-0.999)
N(-0.751)
H(0.125)
P(1.362)
H(0.423)
O(-0.986)
O(-0.986)

(a)

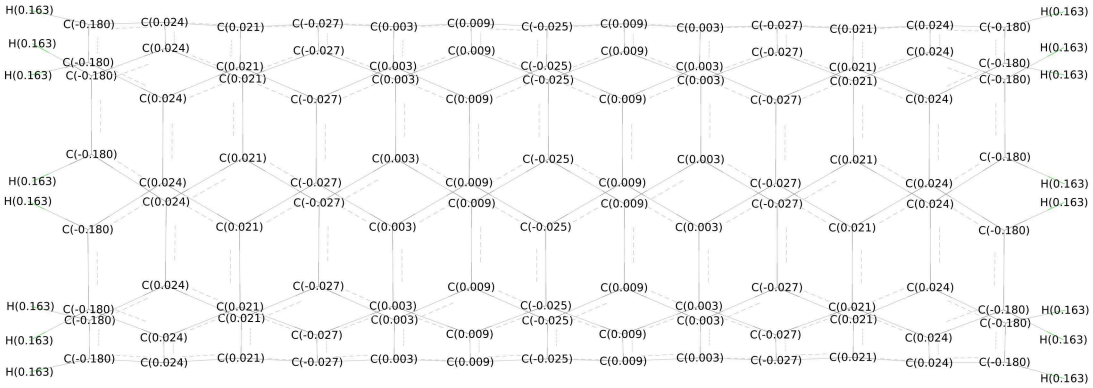

(b)

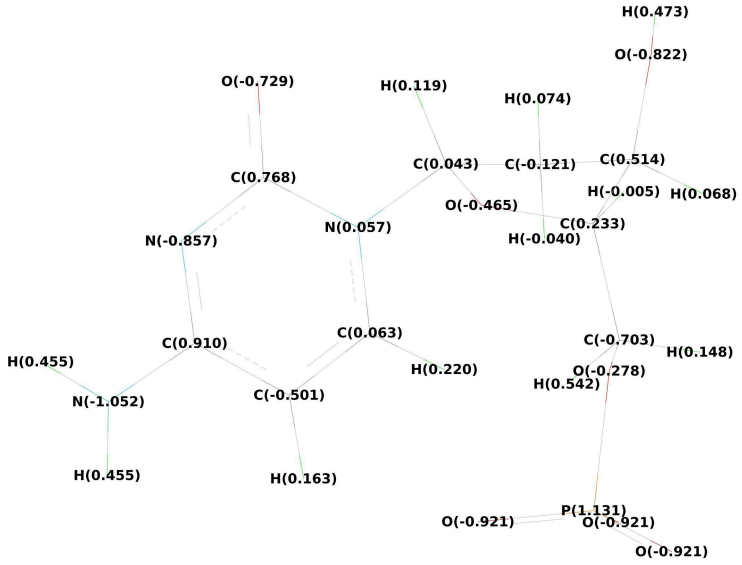
H(0.473)
O(-0.822)
O(-0.729)
H(0.119)
H(0.074)
C(0.043)
C(-0.121)
C(0.514)
C(0.768)
H(-0.005)
H(0.068)
O(-0.465)
C(0.233)
N(-0.857)
N(0.057)
H(-0.040)
C(0.910)
C(0.063)
C(-0.703)
H(0.148)
H(0.455)
H(0.220)
O(-0.278)
H(0.542)
N(-1.052)
C(-0.501)
H(0.455)
H(0.163)
P(1.131)
O(-0.921)
O(-0.921)
O(-0.921)

(c)

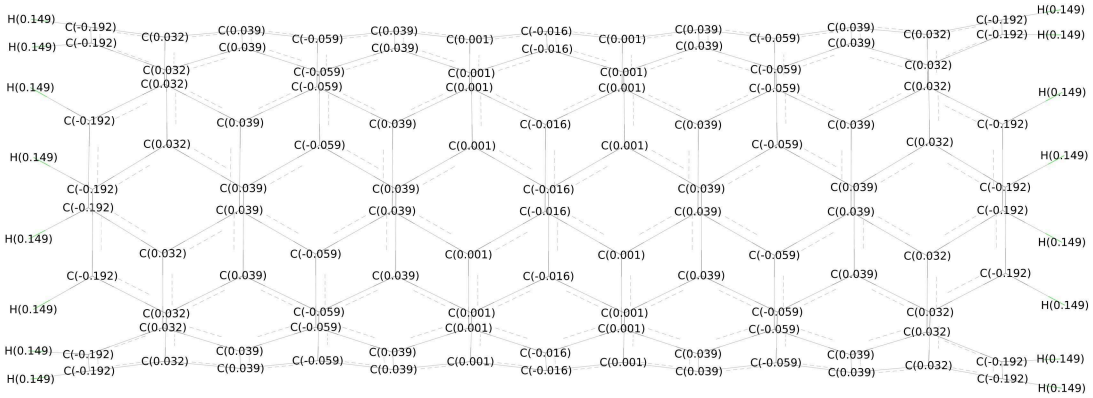

(d)

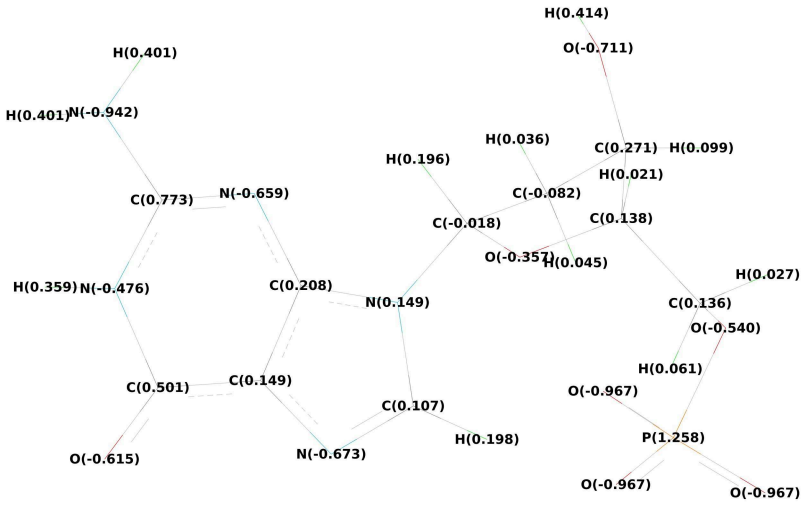
H(0.414)
O(-0.711)
H(0.401)
H(0.401)
N(-0.942)
H(0.036)
C(0.271)
H(0.099)
H(0.196)
H(0.021)
C(0.773)
N(-0.659)
C(-0.082)
C(-0.018)
C(0.138)
O(-0.357)
H(0.045)
H(0.027)
H(0.359)
N(-0.476)
C(0.208)
N(0.149)
C(0.136)
O(-0.540)
H(0.061)
C(0.501)
C(0.149)
O(-0.967)
C(0.107)
H(0.198)
P(1.258)
O(-0.615)
N(-0.673)
O(-0.967)
O(-0.967)

(e)

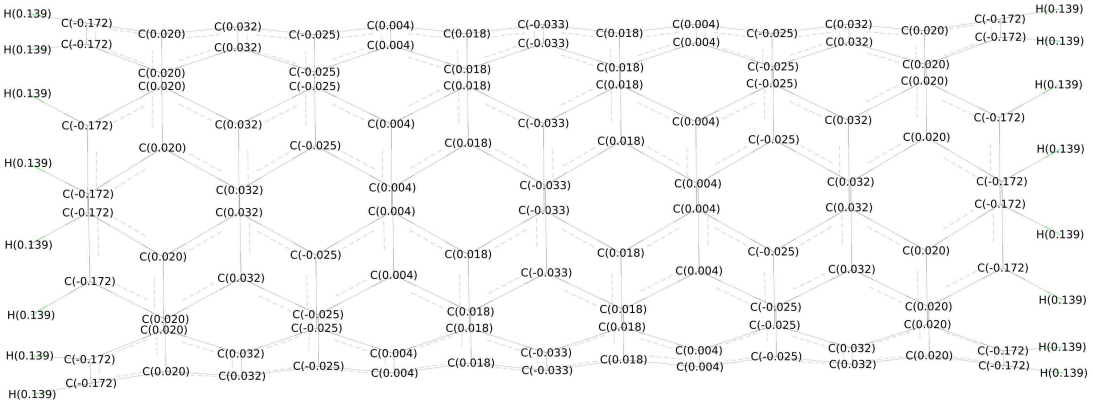

(f)

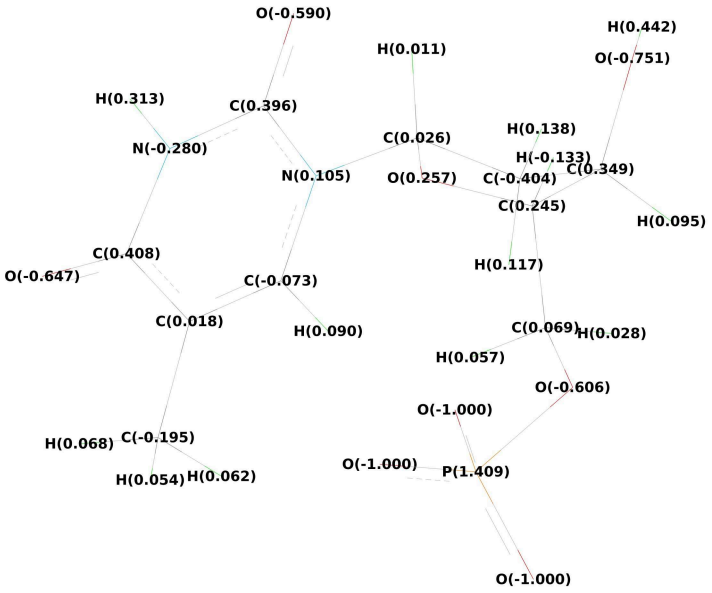

(g)

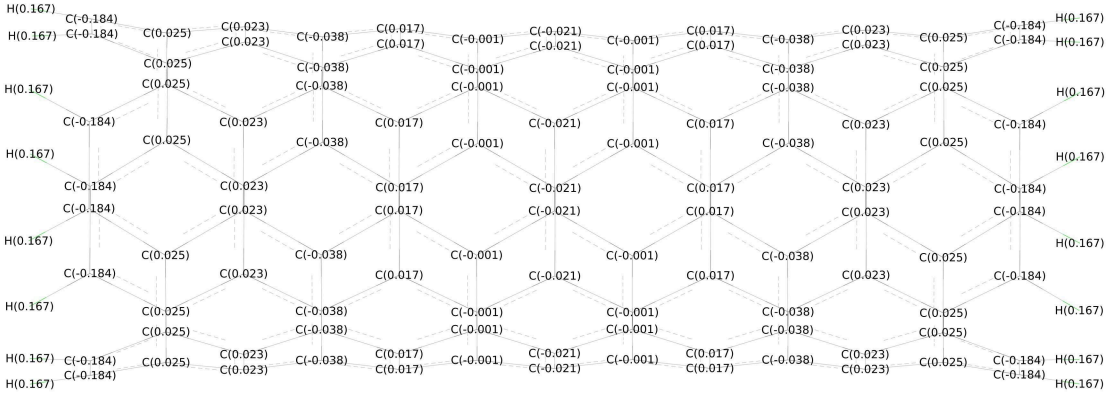

(h)

Figure C.2: Atomic partial charges for: (a) AMP in AMP-(4,4) CNT hybrid, (b) (4,4) CNT in AMP-(4,4) CNT hybrid, (c) CMP in CMP-(4,4) CNT hybrid, (d) (4,4) CNT in CMP-(4,4) CNT hybrid, (e) GMP in GMP-(4,4) CNT hybrid, (f) (4,4) CNT in GMP-(4,4) CNT hybrid, (g) TMP in TMP-(4,4) CNT hybrid, and (h) (4,4) CNT in TMP-(4,4) CNT hybrid. Charges were calculated for the optimized structures using resp approach.

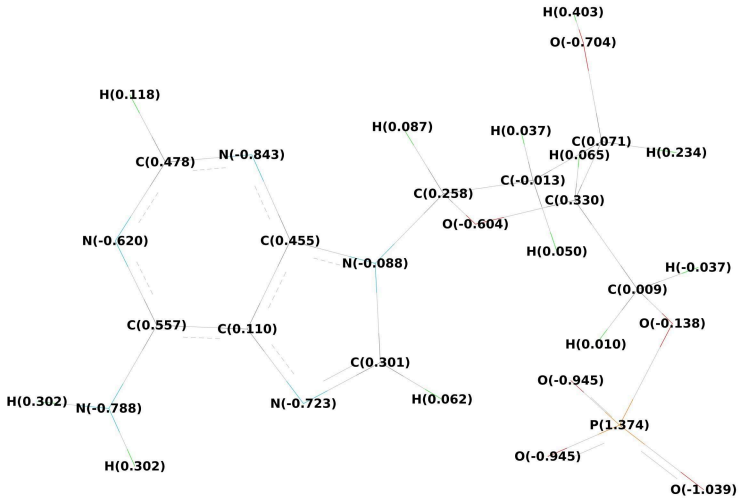
H(0.403)
O(-0.704)
H(0.118)
H(0.087)
H(0.037)
C(0.071)
H(0.065)
H(0.234)
C(0.478)
N(-0.843)
C(-0.013)
C(0.258)
C(0.330)
O(-0.604)
N(-0.620)
C(0.455)
H(0.050)
N(-0.088)
H(-0.037)
C(0.009)
C(0.557)
C(0.110)
O(-0.138)
H(0.010)
C(0.301)
O(-0.945)
H(0.302)
N(-0.788)
N(-0.723)
H(0.062)
P(1.374)
O(-0.945)
H(0.302)
O(-1.039)

(a)

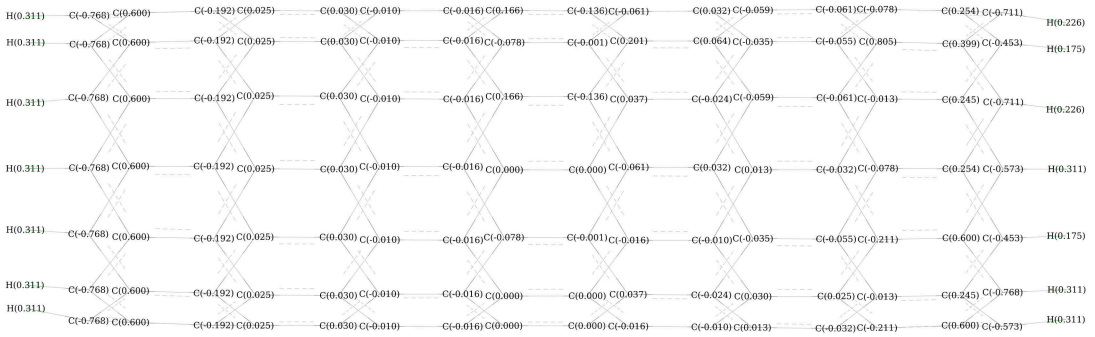

(b)

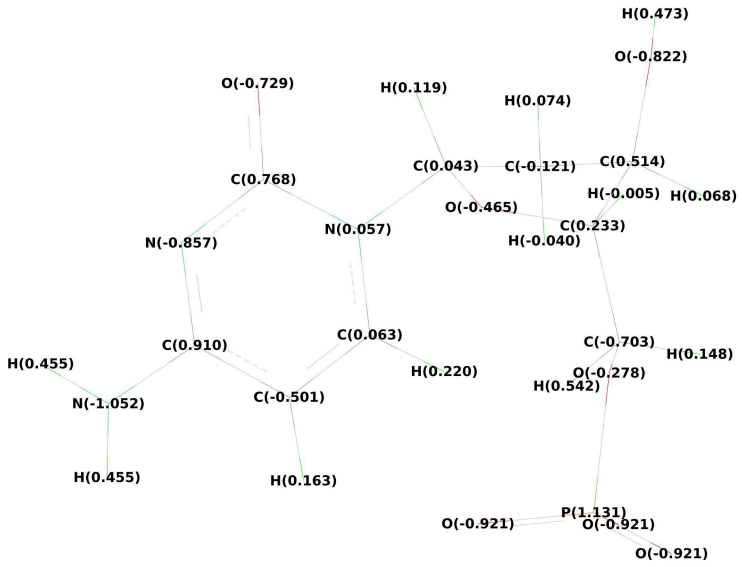
H(0.473)
O(-0.822)
O(-0.729)
H(0.119)
H(0.074)
C(0.043)
C(-0.121)
C(0.514)
C(0.768)
H(-0.005)
H(0.068)
O(-0.465)
C(0.233)
N(0.057)
N(-0.857)
H(-0.040)
C(0.063)
C(0.910)
C(-0.703)
H(0.148)
H(0.455)
H(0.220)
O(-0.278)
H(0.542)
C(-0.501)
N(-1.052)
H(0.455)
H(0.163)
P(1.131)
O(-0.921)
O(-0.921)
O(-0.921)

(c)

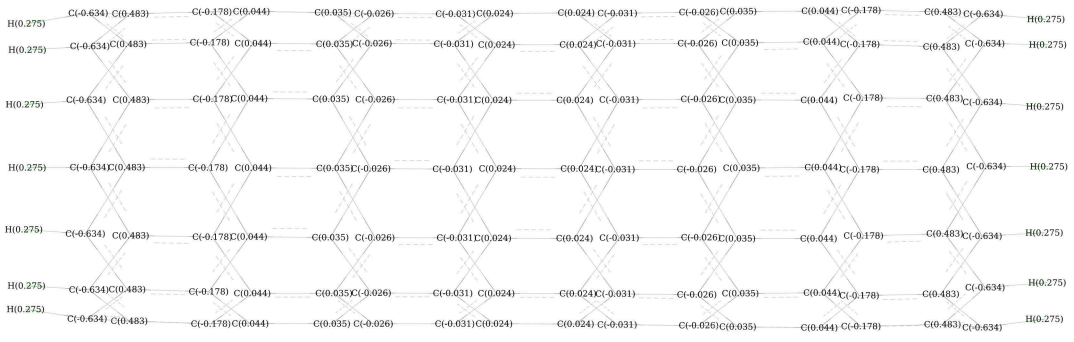

(d)

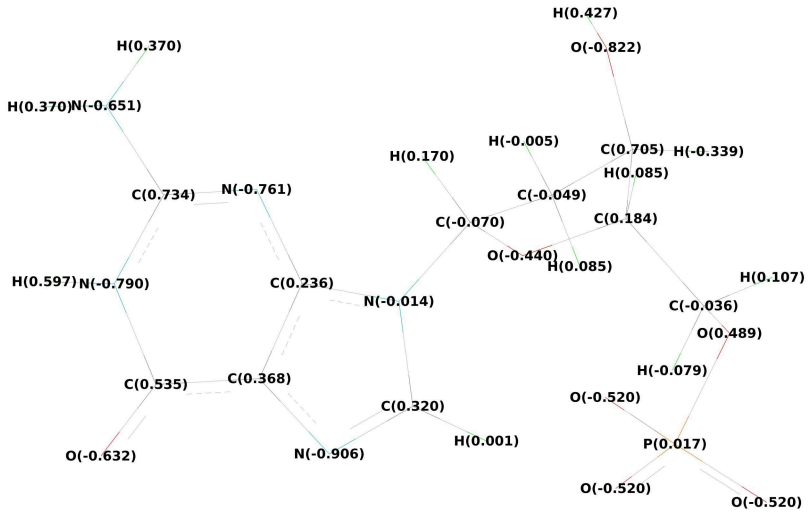
H(0.427)
O(-0.822)
H(0.370)
H(0.370)
N(-0.651)
H(-0.005)
C(0.705)
H(-0.339)
H(0.170)
H(0.085)
C(0.734)
N(-0.761)
C(-0.049)
C(-0.070)
C(0.184)
O(-0.440)
H(0.085)
H(0.597)
N(-0.790)
C(0.236)
N(-0.014)
H(0.107)
C(-0.036)
O(0.489)
H(-0.079)
C(0.535)
C(0.368)
O(-0.520)
C(0.320)
H(0.001)
P(0.017)
O(-0.632)
N(-0.906)
O(-0.520)
O(-0.520)

(e)

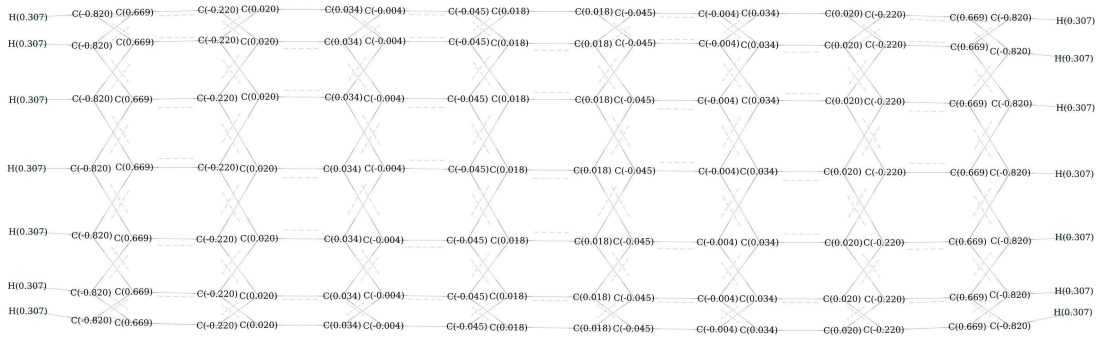

(f)

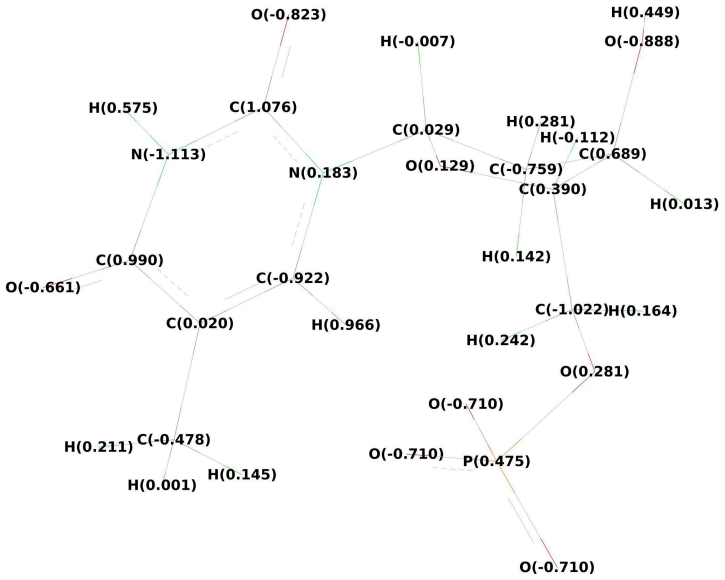

(g)

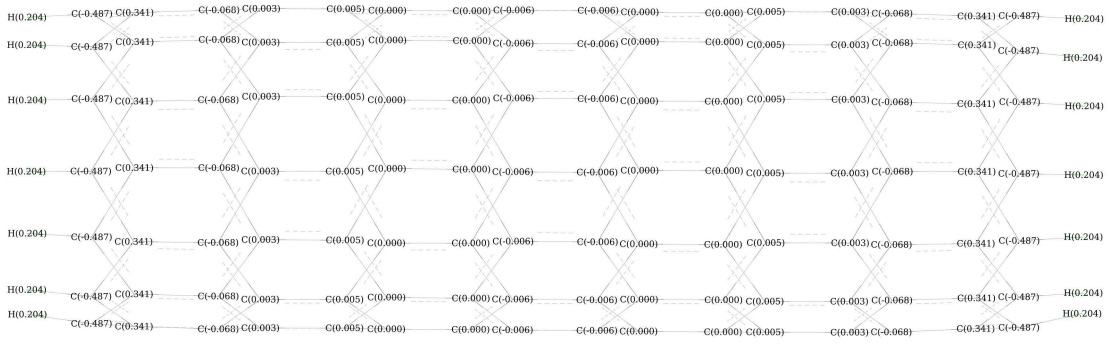

(h)

Figure C.3: Atomic partial charges for: (a) AMP in AMP-(7,0) CNT hybrid, (b) (7,0) CNT in AMP-(7,0) CNT hybrid, (c) CMP in CMP-(7,0) CNT hybrid, (d) (7,0) CNT in CMP-(7,0) CNT hybrid, (e) GMP in GMP-(7,0) CNT hybrid, (f) (7,0) CNT in GMP-(7,0) CNT hybrid, (g) TMP in TMP-(7,0) CNT hybrid, and (h) (7,0) CNT in TMP-(7,0) CNT hybrid. Charges were calculated for the optimized structures using resp approach.

Appendix D

Supplementary figures for Chapter 6

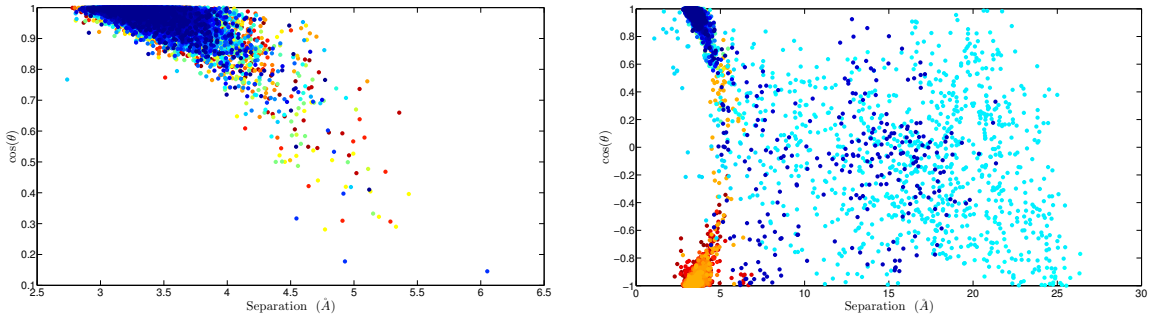

(a) AMP-(4,4) CNT

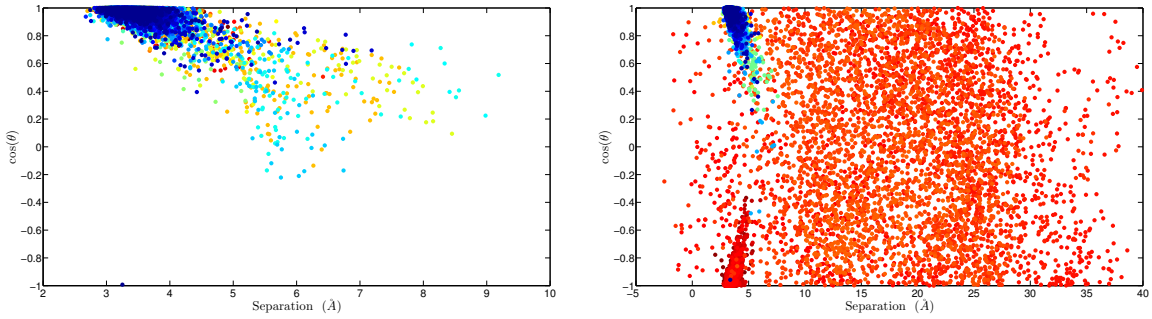

(b) CMP-(4,4) CNT

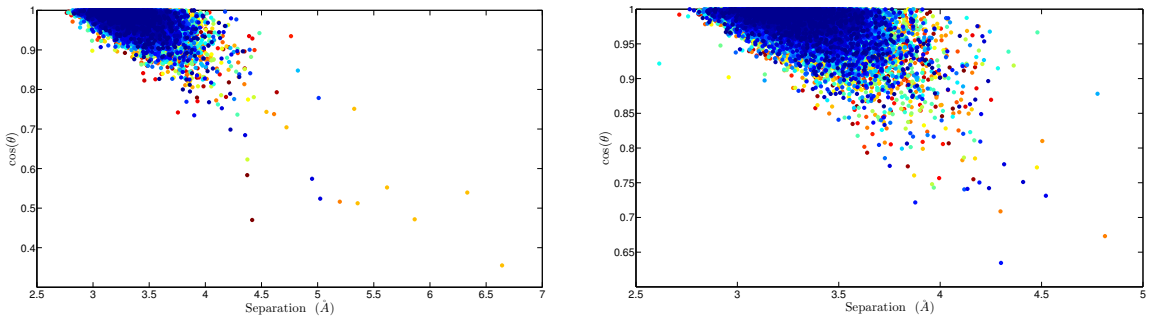

(c) GMP-(4,4) CNT

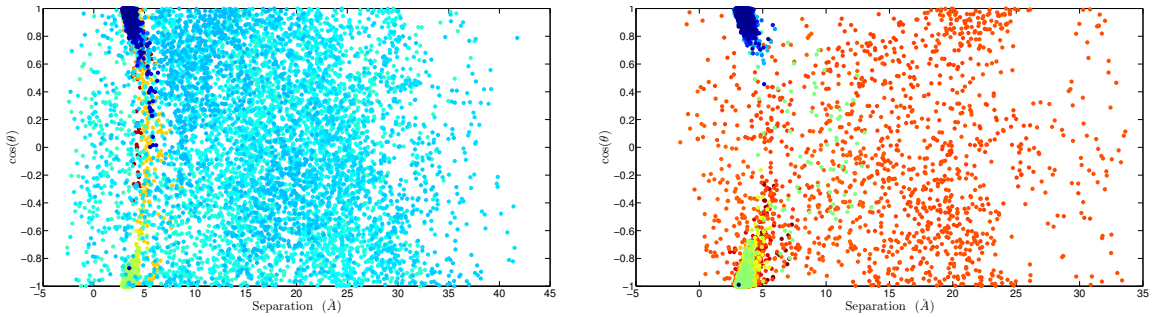

(d) TMP-(4,4) CNT

Figure D.1: Tilting angle versus separation distance for NMP-(4,4) CNT hybrids: (a) AMP-(4,4) CNT, (b) CMP-(4,4) CNT, (c) GMP-(4,4) CNT, and (d) TMP-(4,4) CNT. Color ranging from blue to red represents the time evolution from 0 to $\sim$ 100 ns. Figures in the left and right panels were obtained respectively based on the RCS and OCS.

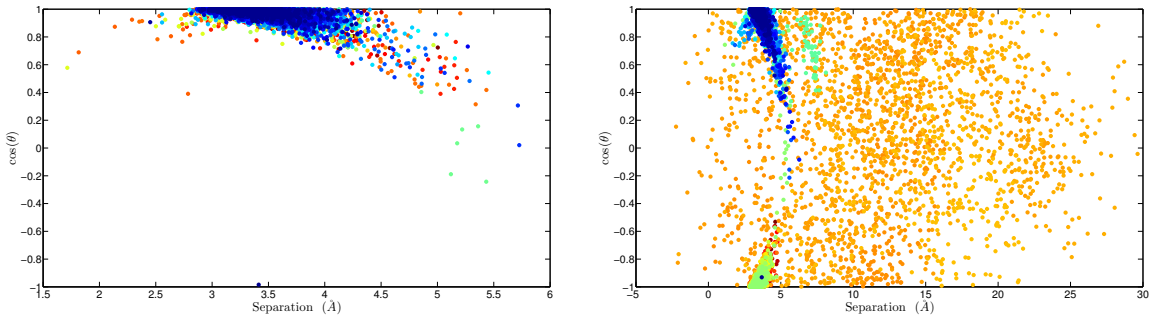

(a) AMP-(7,0) CNT

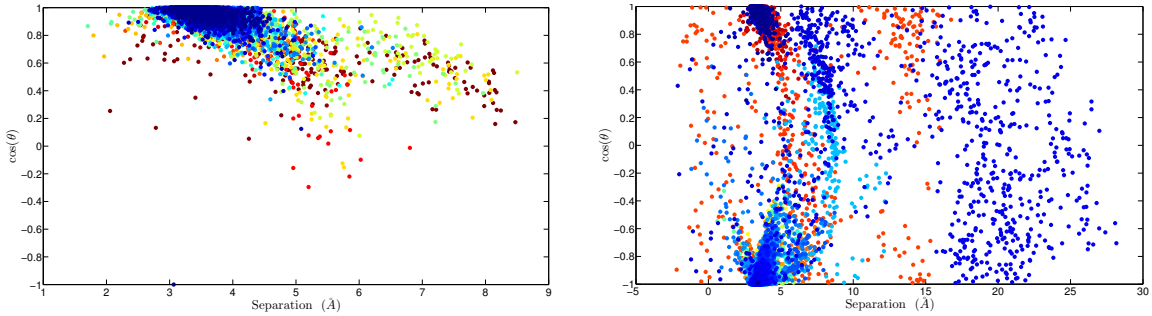

(b) CMP-(7,0) CNT

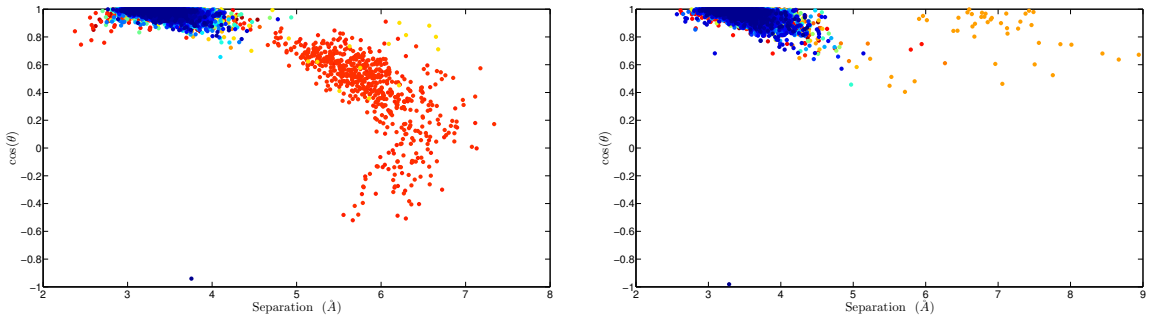

(c) GMP-(7,0) CNT

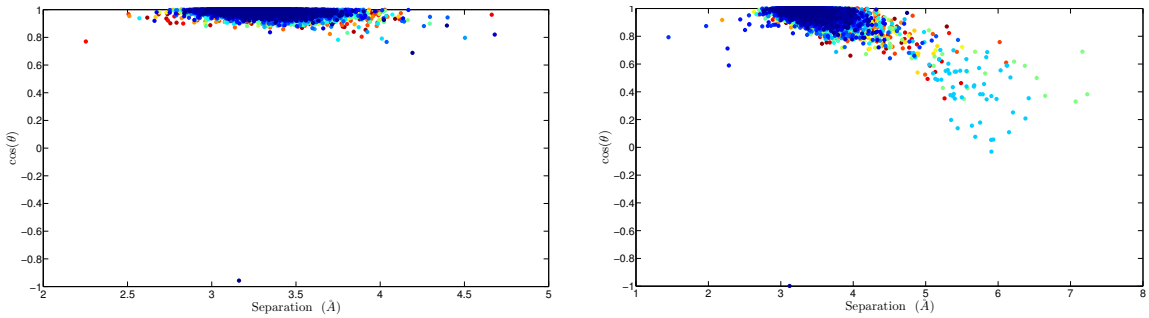

(d) TMP-(7,0) CNT

Figure D.2: Tilting angle versus separation distance for NMP-(7,0) CNT hybrids: (a) AMP-(7,0) CNT, (b) CMP-(7,0) CNT, (c) GMP-(7,0) CNT, and (d) TMP-(7,0) CNT. Color ranging from blue to red represents the time evolution from 0 to $\sim$ 100 ns. Figures in the left and right panels were obtained respectively based on the RCS and OCS.